THE STRUCTURE, PROPERTIES AND POLYMORPHISM

OF

POLY (HEXAMETHYLENE TEREPHTHALATE)

A Thesis presented to the

VICTORIA UNIVERSITY OF MANCHESTER

for the Degree

of

DOCTOR OF PHILOSOPHY

by

BUTHAINA ALAADIN IBRAHIM

Department of Pure and Applied Physics
The University of Manchester
Institute of Science and Technology

JUNE, 1980

To my parents,

husband and

our son, Omar

ACKNOWLEDGEMENTS

My sincere thanks are expressed mainly to my supervisor, Dr. I. H. Hall, for his continued assistance and understanding during the course of this work. I would also like to thank Dr. C. J. E. Kempster for his advice on the Weissenberg photographs.

My thanks are also extended to Professor R. H. Peters and Dr. R. H. Still of the Department of Polymer and Fibre Science for the preparation of 6GT in their laboratories and making the equipment available. My thanks are extended also to Mr. S. K. Dawber for his help and advice in spinning.

I am grateful to Dr. M. Pickering of the S.R.C. Daresbury Laboratories for the scanning of X-ray films and preparing the contour maps. I would like to thank Mr. J. Z. Neisser for making the program of intensity measurement available and his co-operation, and to Mr. F. Kirkman for his help with the X-ray generators and production of the photographs. My thanks are also extended to Mr. W. Hughes for his help.

My special thanks to Mrs. S. Westland for typing the thesis.

I wish to express my thanks and gratitude to Mr. & Mrs. F. Bowden for their kindness and great care of my son.

My grateful thanks and appreciation are extended to Naji A. Halim for his encouragement and unfailing assistance throughout this work.

I would like to express my sincere thanks to my husband Mutaz for his encouragement, understanding and unending help with the correction of the manuscript and the preparation of the thesis.

Finally, I would like to express my thanks to the Government of the Republic of Iraq for providing me with a scholarship, without which this work would not have been possible.

ABSTRACT

Melt-spun fibres and cast films of poly (hexa-methylene terephthalate) - 6GT - were produced to investigate the polymorphism, to determine the unit cell and crystal structure and also to study the mechanical and thermal properties. For these purposes, X-ray (wide-angle and small-angle) cameras, a differential scanning calorimeter (DSC-2), an Instron tensile tester and a scanning electron microscope were used.

This polymer crystallises in three different forms; the first, designated α, dominates in highly drawn fibres; the second, designated β, dominates upon annealing fibres at about 150°C, and the third, designated γ, is found only in cast films. The unit cell of each form was determined; the α-form is monoclinic with a = 9.06Å, b = 17.24 Å, c = 15.51 Å, α = 127.3°, β = 90.0° and γ = 90.0°, the β-form is triclinic with a = 4.75 Å, b = 6.23 Å, c = 15.68 Å, α = 55.7°, β = 116.0° and γ = 118.8°, and the γ-form is also triclinic with a = 10.56 Å, b = 5.05 Å, c = 15.51 Å, α = 126.2°, β = 98.7°and γ = 95.3°. The chain conformation of the β-form was determined.

Usually, the as-spun fibres have more than one crystal form at room temperature, the proportion of which depends on the take-up velocity; the proportion of α-form increases with the take-up velocity. The effect of drawing and annealing on the crystal structure was studied; irreversible transitions from β- to -α and also from α- to -β were found to occur upon drawing and annealing respectively. In view of these transitions, it is suggested that the α-form comprises extended chain crystals, whereas, those of β are chain folded. The mechanical and thermal properties were also investigated and interpreted according to the afore-mentioned suggestion and, thus, a relationship between the polymorphism of 6GT and its properties has been established.

CONTENTS

CHAPTER ONE

INTRODUCTION

A series of polymers having the structural formula:

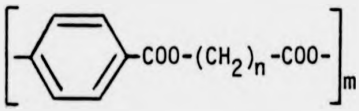

is known as poly [n(methylene terephthalate)] and abbreviated n-GT. One member of this series is poly (hexamethylene terephthalate) chosen as the polymer under investigation in this work. The best known member is 2GT poly (ethylene terephthalate) which has been extensively studied and commercially produced.

The series has been investigated by several workers whose studies have been concerned mainly with the physical properties and crystal structure of the different members. The earliest investigations involved comparisons of the melting points, the glass transition temperature and the crystallographic repeat unit length[1-4]. From these investigations, it has been found that even values of n tend to produce polymers having higher crystallinity, much higher nucleating density and higher crystalline melting points than those of odd n-values; also the higher the methylene group, the longer is the chemical repeat unit length.

Furthermore, Jakeways et al[5] and Ward et al[6] have investigated the mechanical properties of oriented fibres of 2GT, 3GT and 4GT for different molecular weights and draw ratios. They concluded that the differences in the properties and stress-strain curves are due to different crystal structure for these polymers.

The crystal structure of 2-[7], 3-[8,9], 4-[10-13] and 5GT[14] have been determined, as have the unit cell parameters of 6-[3,4,15] and 10GT[3,4]. These studies have shown that for 2GT the chain is near its fully extended conformation (98%), with the methylene bond trans.

For 3GT, the contracted conformation (76%) has been found with the methylene bonds gauche-gauche. In oriented fibres of 4GT and 5GT, the polymer chain normally crystallises in a contracted conformation (α-form) with the chain repeat length extended to 86% and 84% respectively. Under tension, this contracted form is transformed into more extended form (β-form). In 4GT, the α-form is regained on relaxation but in 5GT, the β-form can be retained in the relaxed fibre by annealing under tension.

Bateman et al[4] have reported that the crystal structure of 2GT, 6GT and 10GT are similar, since they undergo no changes with different temperatures up to their melting points. On the other hand, in their work on 6GT, they observed several weak X-ray reflections which could not fit the unit cell derived from the principal reflections. These weak reflections have been attributed to the existence of another form of crystal structure.

Schenk[16] and Ghaffar[17] have found the measured density of 6GT bulk polymer to be between 1.235 and 1.24 gm/cm^3, while the density calculated from the unit cell dimensions, published by Bateman et al, was found to be 1.14 gm/cm^3. The unit cell density is unlikely to be less than that of the bulk material, because molecules in the non-crystalline material are likely to be less densely packed than in the crystal. Schenk has given two explanations for this discrepancy: one is that of error in the unit cell parameters published by Bateman et al, while the other is the existence of two crystal forms of 6GT. The latter is indicated by the X-ray diffraction patterns which show a change in the relative intensity of the rings for the untreated sample (melt crystallised) and for one annealed at $80^{o}C$. Schenk has also reported that the X-ray diffraction pattern for powder precipitated from solution is

completely different from either of those found above.

Joly et al[15] have reported another unit cell for 6GT. The density calculated from its parameters was reported to be 1.335 gm/cm^3. In these investigations, neither the weak reflections observed by Bateman were reported nor was the possibility of another crystal structure mentioned.

The repeat unit length of 6GT has been reported by Goodman[1], Bateman et al[4], Gilbert[2] and Joly et al[15] to be about 15.5Å, which indicate that the chain conformation is fully extended to 97%. The information available in the literature is that 6GT is very well crystallised with a glass transition temperature around room temperature[17,18] and the melting point is about 155^{o}C.

The existence of more than one crystal structure has not yet been confirmed, and no investigation of conditions favouring particular structures has been made. Neither has the structure of any form been determined. The aim of this work is to investigate the existence of more than one crystal form, the conditions under which they are obtained and to determine the crystal structure. This thesis deals in its first two chapters with the production of 6GT in fibre and film forms and the investigation of the validity of 6GT polymorphisms. Chapters 4 and 5 deal with the determination of the unit cells and crystal structure. The correlation of the crystal structure with the physical properties, i.e. mechanical and thermal properties, has been investigated and reported in Chapters 6 and 7. The last part of the thesis deals with the investigation of the morphology of 6GT, carried out using a scanning electron microscope and small-angle X-ray diffraction camera.

CHAPTER TWO

Sample Preparation

and

Preliminary X-Ray Investigations

2.1 INTRODUCTION

Fibres and films are two familiar forms of synthetic polymers that can be produced from the bulk. Their successful production depends on the chemical properties of the bulk polymer and the experimental conditions chosen with relation to the polymer's chemical properties. To produce a continuous filament, the melt viscosity should be within a suitable range; the melt viscosity depends upon the molecular weight and the spinning temperature[19]. Ziabicki[20] reported that polymers having molecular weight ranging between 10,000 and 25,000 can be successfully spun. It was, therefore, important that unless the molecular weight is sufficiently high, the polymer cannot be spun into fibre and consequently drawn.

Dees and Spruiell[21], Abbott and White[22] reported that the spinning conditions (the spinning temperature, take-up velocity and rate of extrusion) affect the structure development of the fibre and the physical properties of various polymers.

This Chapter deals with the history of the bulk polymer, the development of the crystallite orientation and structure in the melt-spun fibres with different take-up velocities and preliminary investigations of as-prepared fibres and films.

2.2 SOURCES OF 6GT POLYMER

The 6GT polymer, used in this work, was obtained from three different sources:

(a) A batch was supplied by Eastman Kodak Ltd. The polymer was prepared according to a procedure that has been outlined by Smith et al[23].

(b) A batch was obtained from M. Gilbert* of the University of Aston. The polymer was prepared according to the procedure described by Gilbert et al[2], which was based on that employed by Smith et al[23].

(c) Several batches were prepared by the Department of Polymer and Fibre Science, UMIST. The polymer was prepared in two stages; in the first stage, hexane-1, 6-diol (130 gm, 1.1 molar) was reacted with dimethyl terephthalate (97.6 gm, 0.5 molar) in the presence of a catalyst solution (0.1 ml of tetra isopropylortho-titanate) to yield dihydroxydiester. The reaction is represented as follows:

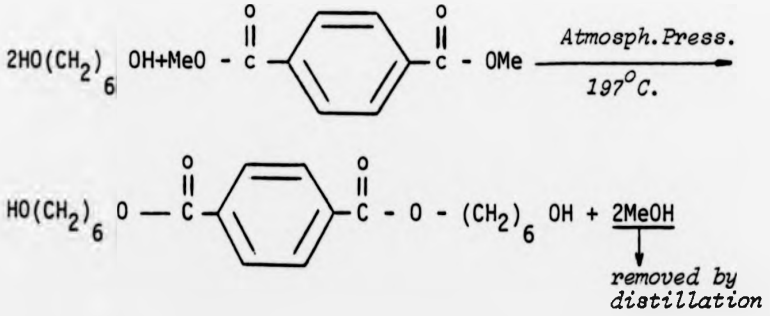

In the second stage, the dihydroxy-diester molecules combine to form a linear polymer chain, with the loss of hexane-1, 6-diol. This was achieved by raising the temperature to 255°C and lowering the pressure to 0.1 mm Hg. The chemical reaction is indicated by the following:

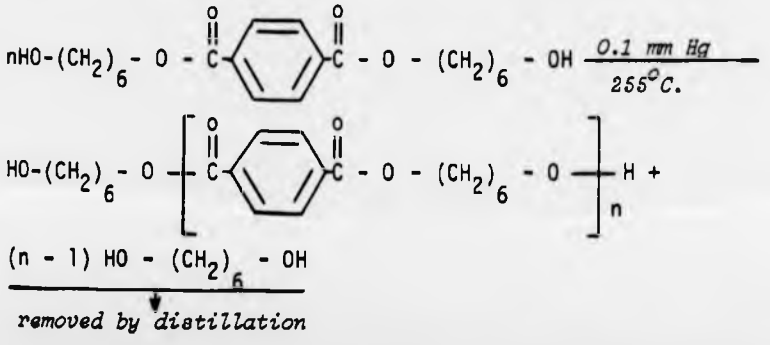

*At present of Loughborough Univereity

The apparatus and the polymerisation procedure have been previously described by Schenk[16] and Ghaffar[17]. The Department of Polymer and Fibre Science has also supplied 6GT polymer in the form of as-spun monofilament fibre with unknown history.

2.3 EXPERIMENTAL

For the purpose of spinning the polymers obtained from the different sources, described in the previous section, the melting point for each polymer was determined by using a Perkin Elmer differential scanning calorimeter (Model 2 DSC-2). Furthermore, the solution viscosity was also determined by the method described next.

2.3.1 Measurement of Solution Viscosity

The measurements of solution viscosity for the different 6GT polymers were performed using an automatic dilution viscometer, immersed in a thermostatically controlled silicon-oil-bath at 25^{o}C (±0.02^{o}C). The solution viscosity was determined by measuring the time required for a fixed volume of solution to flow from one limb of a U-tube into the other, through a capillary. The solvent used in these measurements was chloroform.

2.3.2 Melt-Spinning of Polymer

The polymers used in this work were spun into fibres by using a simplified melt spinning machine capable of dealing with only small batches of polymer (approximately 50 gm). The spinning machine comprised essentially a heated cylinder containing a mixing block, filter and spinneret through which the molten polymer was forced by means of a piston travelling at constant low speed. The temperature of the upper and lower parts of the cylinder was controlled by two separate heaters, so as to

avoid holding the temperature of the polymer at the extrusion temperatures for a long period of time.

The procedure adopted in the spinning of the polymers involved feeding polymer chips (35 gm, dried at 85°C in an evacuated oven for 48 hours) into the cylinder which had been preheated to about 18°C below the equilibrium melting temperature of the polymer. The polymer was held for 15 minutes in the cylinder under pressure, exerted by the piston; the procedure is known as candling. This removed trapped air which, otherwise, would have caused oxidation of the polymer and possible discontinuity in the extruded filament due to the presence of air bubbles.

After candling, a teflon plug was inserted into the cylinder to be above the polymer. The plug's diameter was only marginally smaller than the inner diameter of the cylinder; this prevented molten polymer from flowing back over the piston during extrusion. The temperature of the lower heater was raised to the spinning temperature, which was 10-15°C above the melting temperature. These conditions were maintained for approximately 10 minutes, so as to allow for equilibrium to be established. The polymer was extruded by means of driving the piston at constant low speed. A monofilament was obtained by using a spinneret with a single central hole of 0.5 mm diameter. The extruded monofilament was allowed to fall freely to the ground, a distance of approximately 10 feet; some others were collected with different take-up velocity.

2.3.3 Films Production

In the course of this work, two kinds of films were produced: melt pressed and cast (from solution) films.

(a) Melt-Pressed Films and Sheets

Compression moulded films of 6GT were prepared in the following

manner. A metal frame, made from aluminium sheet 0.3 mm thick and having a rectangular hole in its centre, was used. Four grammes of thin shavings of the polymer were placed inside the rectangular window in the metal frame, which was then sandwiched between two thin metal plates. Each plate was covered from inside with a PET thin film, which effectively prevented the molten polymer from adhering to it. The "sandwich" was placed in a moulding press which has previously been preheated to a temperature of 167±2^{o}C, pressed and held under very slight pressure for two minutes. Then, the pressure was gradually increased at a rate of 2 tons/min. (as indicated on a dial) for a period of about six minutes; at about 12 tons, the pressure was held for two minutes, after which it was released and the sandwich was transferred quickly to an ice/water bath.

The same procedure was also employed in the production of 2mm thick sheets. The experimental conditions were slightly varied; the temperature was fixed at 170^{o}C. The sample was first pressed between the two hot plates for seven minutes, after which a gradually increasing pressure was applied until a pressure of 3-tons was achieved; this pressure was held for 13 minutes.

(b) Cast Films

In order to produce these films, 2 gms of 6GT polymer were dissolved in 50 ml of chloroform. Part of the solution was left to evaporate in air at room temperature, while another was allowed to evaporate inside an oven at 90^{o}C.

The remainder of the solution was used to obtain powder precipitation. The solution was precipitated by methanol in a beaker. The mixture was left standing for 24 hours, after which the contents were filtered. The precipitated powder was finally left to dry at room temperature.

2.4 THE USE OF WIDE-ANGLE X-RAY DIFFRACTION

The structure of the as-spun fibres, prepared films and powder was detected by using X-ray diffraction techniques; wide-angle X-ray diffraction was extensively used. Wide-angle X-ray diffraction photographs were obtained by using a type of camera, described by Elliot[24] and manufactured by G. & D. Searle Ltd. The X-ray target is considered as one focus of the X-ray beam, which is reflected by a gold-surface toroidal mirror at near-grazing incidence bringing the reflected beam to another focus 43 cm away from the first focus. The essential feature of the camera is that X-ray diffraction photographs of good resolution are obtained at comparatively short exposure times. This is achieved by focussing a high intensity, highly monochromatic beam of Ni-filtered Cu K_α X-radiation at the film position. A cylindrical film holder (30 mm radius) was used with the camera which was evacuated to eliminate air-scattering. The fibre sample was mounted with its axis perpendicular to the X-ray beam and being coaxial with the film holder.

2.5 RESULTS

2.5.1 Solution Viscosity

The intrinsic viscosity is defined by the following relation:

$$[\eta] = \left(\frac{\eta_{sp}}{c}\right)_{c=0} = \left(\frac{\ell n\ \eta_r}{c}\right)_{c=0}$$

where $\eta_{sp} = (t-t_0)/t_0$, $\eta_r = t/t_0$, c is the concentration, t is the solution flow time, and t_0 is the solvent flow time.

The measurement of the flow time (Section 2.3.1) was made for the solvent (chloroform) and for solutions of nine different concentrations - ranging between 1.0 gm/dl and about 0.2 gm/dl. The intrinsic viscosity

of the polymer was determined from the linear plots of both the reduced viscosity η_{sp}/c and the inherent viscosity $\ln \eta_r/c$ versus concentration[25]; this was achieved by extrapolation to zero concentration (Figure (2.1)). In this manner, the intrinsic viscosity of the above-mentioned polymers was determined. Using these values, the molecular weight, M, of 6GT polymer was calculated from the empirical equation:

$$[\eta] = K M^a$$

where K and a are constants for a given polymer-solvent system at a given temperature. By using values of intrinsic viscosity and molecular weight of 6GT, reported by Erdogus[18], the molecular weight for the polymers under investigation was determined, which are tabulated together with their intrinsic viscosity below (Table (2.1)).

TABLE (2.1)

Sample	Intrinsic Viscosity dl/gm	Molecular Weight
Department of Polymer and Fibre Science, UMIST, as:		
bulk	0.344	8,950
as-spun fibre	0.528	16,000
M. Gilbert, as bulk	0.474	14,450
Eastman Kodak Ltd.	0.93	44,400

2.5.2 Melt Spinning

The most successful spinning of the different polymers was achieved with that having molecular weight of 44,400; a monofilament was obtained satisfactorily. Gravitationally spun fibres and fibres spun with take-up velocities of 50, 150, 300 and 400 m/min. were collected. Partial

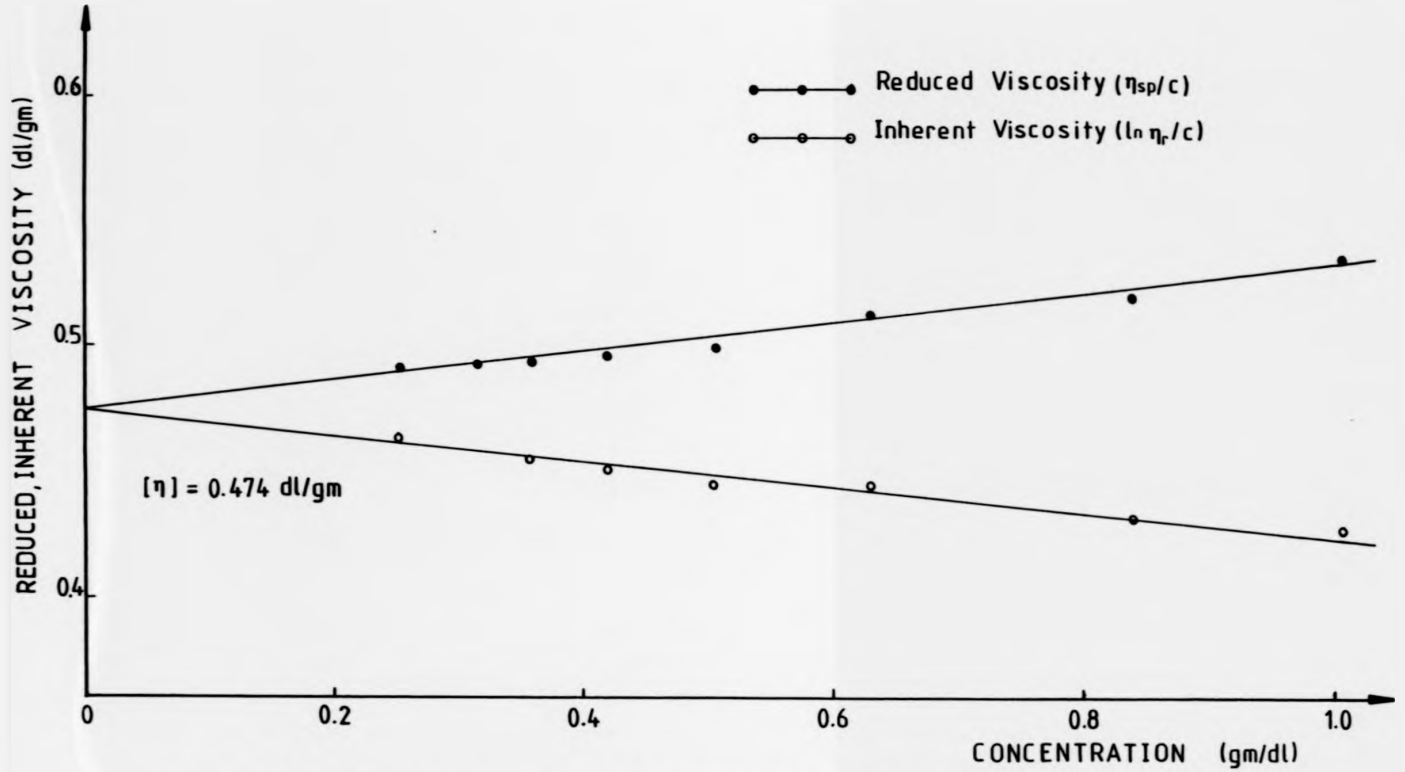

FIG. 2.1 : REDUCED AND INHERENT VISCOSITY VS CONCENTRATION

success was achieved in the spinning of the polymer having molecular weight of 14,450. With this polymer only gravitationally spun filament was collected; however, attempts to collect a long fibre on a bobbin proved unsatisfactory.

The spinning of the polymer having relatively low molecular weight, i.e. 8,950, proved unsuccessful, despite repeated attempts which will be described later. It was found that the polymer either dripped down from the spinneret instead of forming a continuous fibre, or the extruded fibre did not solidify before reaching the ground level. This behaviour was attributed to a rapid extrusion rate which developed as a consequence of the low melt viscosity. The values of the molecular weight of the polymer samples,together with the spinning conditions, are listed below in Table(2.2).

TABLE (2.2)

Molecular Weight	Melting Temperature (°C)	Candling Temperature (°C)	Spinning Temperature (°C)	Orifice Diameter (mm)
8,950	146	127	165	0.5
8,950	146	127	155	0.2
14,450	151	132	168	0.5
44,400	151	132	168	0.5

Next, the investigation of the spun fibres, using wide-angle X-ray diffraction is considered. Plate 1 (a-d) shows the wide-angle X-ray photographs for the gravitationally spun fibres and fibres collected at different take-up velocities respectively; the fibres were spun from polymer having molecular weight 44,400. The plate shows that the

PLATE (1): WAXS photographs of as-prepared 6GT specimens:

(a) gravitationally spun fibre

(b) as-spun with take-up velocity 50 m/min.

(c) " " " " 150 m/min.

(d) " " " " 400 m/min.

(e) gravitationally spun fibre of low molecular weight.

(f) melt-pressed film (quenched in ice/water)

(g) cast film (prepared from solution)

(h) gravitationally spun fibre collected 40 cm below the spinneret

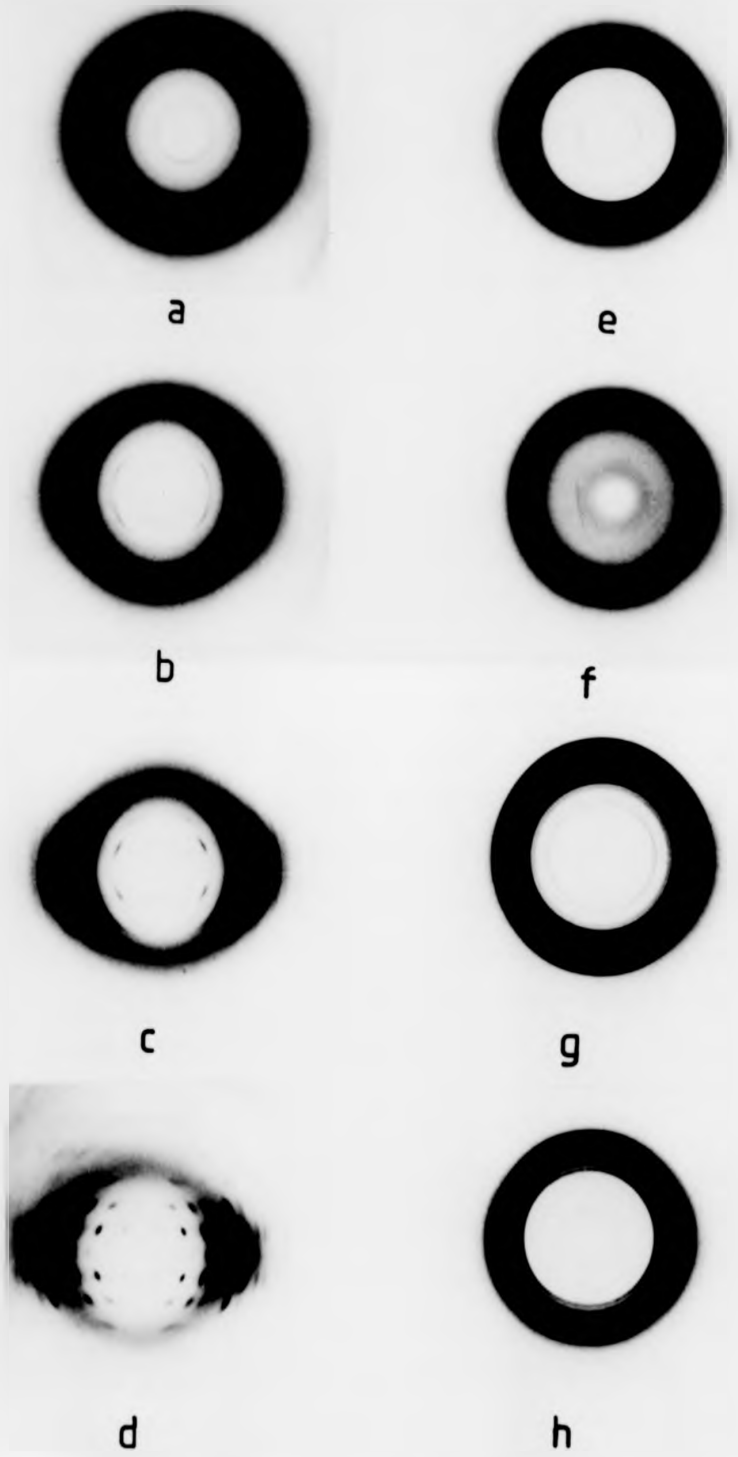

PLATE 1

PLATE (1): WAXS photographs of as-prepared 6GT specimens:

(a) gravitationally spun fibre

(b) as-spun with take-up velocity 50 m/min.

(c) " " " " 150 m/min.

(d) " " " " 400 m/min.

(e) gravitationally spun fibre of low molecular weight.

(f) melt-pressed film (quenched in ice/water)

(g) cast film (prepared from solution)

(h) gravitationally spun fibre collected 40 cm below the spinneret

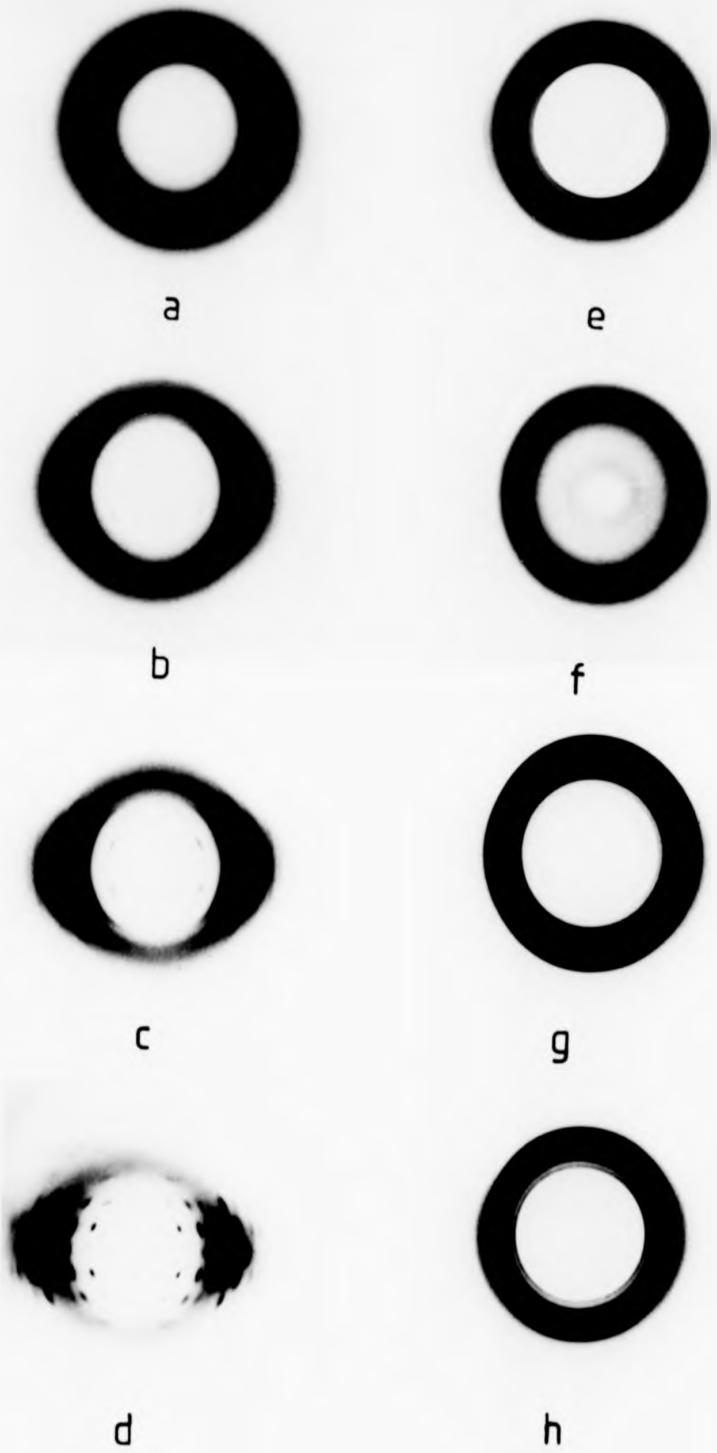

PLATE 1

gravitationally spun fibre developed powder diffraction rings with uniform intensity. The diffraction pattern of the as-spun fibre, collected with take-up velocity 50 m/min.,is shown to take the form of long arcs; the length of these arcs was found to decrease with increasing take-up velocity. The length of the reflections is extremely shortened for the as-spun fibres collected at 400 m/min; these reflections are observed to be intense, elongated diffraction spots arranged in layer lines on the X-ray film.

For more detailed investigation, a close examination of Plate 1(a-d) shows that there are differences between the various patterns other than the length of the diffraction arcs, and these will now be considered. There are changes in the relative intensities of several reflections on different layer lines; these changes are estimated by eye. The first two powder diffraction rings corresponding to the innermost reflections of the first layer line are chosen to illustrate these differences. For gravitationally spun fibre, the first reflection is found to be stronger than the second. With take-up velocity 50 and 150 m/min., the first reflection becomes fainter while the second becomes more intense. Finally, with a take-up velocity of 400 m/min., the first reflection has nearly disappeared while the second has become very well defined and intense.

The wide-angle X-ray diffraction pattern for the gravitationally spun fibres of 6GT polymer, having a molecular weight of 14,450, is identical to that shown in Plate 1(a). The pattern for the fibres having a molecular weight of 8,950 is shown in Plate 1(e), in which slight differences from that in Plate 1(a) appear; the second innermost ring is absent. Also, some of the rings show non-uniformity in intensity, i.e. some rings have high intensity in the meridional and others in the equator.

2.5.3 Films Production

Melt pressed films were produced from the two polymers, having molecular weights of 44,400 and 8,950. The films (thickness of 0.27±0.03 mm) were found to be clear, transparent and ductile. However, when sheets (2mm thick) were produced from the same two polymers, their properties were found to be different. The sheets, produced from the polymer having low molecular weight, were found to be brittle, non-transparent and white in appearance, whereas, those produced from the other polymer were semi-transparent and fairly ductile.

Cast films from the same two polymers were also produced. Opaque thin films were produced from the polymer having high molecular weight, whereas, those produced under the same conditions from solution of polymer having low molecular weight were found to be non-transparent and brittle.

The wide-angle X-ray diffraction photograph for the melt pressed thin film is shown in Plate 1(f)in which a diffuse X-ray diffraction pattern appears. The cast film and the powder were found to have the same X-ray diffraction pattern (Plate 1(g)). The pattern appears as sharp rings with d-spacings different from those for gravitationally spun fibre.

2.6 DISCUSSION

The 6GT polymers from the three different sources were found to have different values of molecular weight (Section 2.5.1). Merz et al[26] have shown that the use of different amounts of catalyst, different times and temperature of preparation and different methods of purification and polymerisation can lead to polymers of different molecular weight.

The difficulties encountered in spinning the 6GT polymer, having relatively low molecular weight were attributed partly to the low melt viscosity. The filament instability has been investigated by White et al[19,27] and Ziabicki[28], who generally explain it according to two mechanisms: capillarity failure and ductile failure. The well known explanation of the filament instabilities is capillarity failure which occurs as a result of the propogation of a disturbance by the surface tension, especially if the liquid possesses low viscosity. As the viscosity increases, the rate of propogation of the disturbance is damped out. Therefore, the break-up of the spin-line for 6GT polymer into droplets was taken as an indication of capillarity failure of low melt viscosity. To overcome it, White et al[19,27] have shown that it can be reduced by decreasing the spinning temperature. They suggested that the melt viscosity increases with decrease of spinning temperature.

Although the difficulty of capillarity failure was overcome by decreasing the spinning temperature, it was found difficult to collect any fibre because it solidified very near to the ground level; this problem was overcome by decreasing the orifice diameter. At this stage, the spun fibre was found to be brittle, which prevented it from being wound up. The brittleness of the fibre was attributed to low molecular weight since fibres of higher molecular weight spun under the same experimental conditions were found to be ductile. Nielsen[29] has reported that for a given polymer, a low molecular weight fraction is usually more crystalline than a high molecular weight fraction.

The results of the wide-angle X-ray diffraction investigations showed that the orientation of the as-spun fibre increases with the take-up velocity, which were in agreement with the results reported individually by Ziabicki et al[30] and Nadella et al[31], who have

found that the crystallite orientation increases with the take-up velocity at constant rate of extrusion and other experimental parameters.

The relative intensities of the reflections in the X-ray patterns were found to vary with different take-up velocities, these variations indicating changes in the crystal structure. The change in the relative intensity can be seen best by comparing the pattern of the gravitationally spun fibre with that collected with take-up velocity 400 m/min.. From Plate 1(a-d), it can be seen that the change in the diffraction pattern occurs gradually with change of take-up velocity. The change in the crystal structure would occur because the stresses imposed on the spin-line have changed. The most effective parameters controlling the spin-line stresses are the tension of the fibre wind up and the extrusion rate. At constant extrusion rate, the tension on the spin-line results as a consequence of the take-up velocity, i.e. the greater the take-up velocity, the greater is the tension along the spin-line which could cause greater crystallite deformation.

White et al[22,32] have investigated the development of fibre structure during melt spinning for polyethylene, polypropylene and polyoxymethylene fibres and have pointed out that an integral part of the problem of structure development during melt spinning is the interaction of rheological factors (stretching of the melt) and non-isothermal effects resulting from the heat transfer from the running filament. Spruiell et al[21] have interpreted the morphological changes according to the mechanism of orientation induced crystallisation proposed by Keller and Machin[33].

The orientation observed with the gravitationally spun fibres of low molecular weight would have been expected to be caused by an increase in stresses on the spin-line, but this is inconsistent with the

results obtained with the gravitationally spun fibre of high molecular weight, in which the spin-line stresses would be expected to be higher[31]. Additional evidence that the spin-line stresses are lower for the low molecular weight material, was found in an experiment in which the gravitationally spun fibre with high molecular weight was collected 40 cm below the spinneret. When comparing the diffraction pattern of this material (Plate 1(h)) with that of the same fibre collected at ground level (Plate 1(a)),their relative intensities are slightly different, but neither shows orientation. The relative intensities of that collected at 40 cm below the spinneret are, however, the same as those of the gravitationally spun fibre of low molecular weight collected at ground level (Plate 1(e)). Because of the smaller weight of the spin-line when fibres are collected 40 cm below the spinneret, the tension in this situation is less than when collected at ground level, confirming that different crystalline structures revealed by the differences in relative intensities in the diffraction patterns are caused by the spin-line tension. The structure of the low molecular weight fibre is consistent with low spin-line stresses. Thus, the orientation of this material is unlikely to be caused by a high spin-line tension.

The orientation which is observed in the low molecular weight material is different in type from that which is developed at high take-up velocities in high molecular weight material, and may be a feature of the very low spin-line stresses which would occur.

The amorphous structure of the pressed films was indicated in their X-ray diffraction pattern by the diffuse scattering appearing in a halo form. However, sheets (2mm thick) did not show the amorphous structure; this could be attributed to a longer time of quenching

which produced crystallisation. Sheets of low molecular weight material were also found to be crystalline but brittle, which suggests that the degree of crystallinity is higher than that in sheets of high molecular weight.

Wide-angle X-ray investigations have shown that the cast films and the powder prepared at room temperature may have different crystal structure from that of spun fibres, as judged from the measurements of d-spacings. On the other hand, the cast films prepared at 90^{o}C have given crystal structure similar to that obtained for the spun fibres collected at 40 cm below the spinneret.

CHAPTER THREE

POLYMORPHISM

OF

POLY (HEXAMETHYLENE TEREPHTHALATE)

3.1 INTRODUCTION

It was concluded in Chapter Two that there is a possibility for 6GT to have more than one kind of crystal structure. Therefore, further investigations have been carried out to assess the different structural changes; these investigations involved different methods of drawing and annealing which will be described in this Chapter.

A parameter of prime importance to drawing is the draw ratio (D.R.), defined as: the ratio of the specimen length after and before drawing. However, the natural draw ratio (N.D.R.) has been defined differently by various workers; in this work, the following definition will be used: the ratio of the cross-sectional area before and after drawing in the neck region, i.e.:

$$N.D.R. = (r_1/r_2)^2$$

where r_1 is the radius of the fibre before drawing and r_2 is the radius of the fibre in the neck region, assuming there are no changes in the volume during drawing.

In drawing fibres, many polymers extend uniformly until their initial length is increased by a few percent where they thin at some point along their length to a smaller cross-section; a neck is formed. On further extension, the neck may stabilise and then the shoulders of the neck travel in opposite directions along the specimen. This phenomenon is known as "cold drawing". This process is highly temperature dependent and has been extensively discussed by several authors[34-38]; at room temperature, some polymers can be readily cold-drawn, but on increasing the temperature, necking may not occur and the specimen will stretch uniformly throughout its length even at

high rates of extension; this type of drawing is known as "hot drawing".

According to Fischer et al[39], drawing usually leads to crystal defects and irregular interfaces between the crystalline and amorphous regions, thus giving diffuse X-ray diffraction patterns. Annealing at low temperature (about 40-60^{o}C below the melting point) leads to an accumulation of these defects, thus, giving rise to clear X-ray diffraction patterns.

When a polymer is subjected to heat treatment, a change in its morphology, physical properties and structure would generally occur after the initial crystallisation; this process is known as annealing. However, these changes not only depend upon the magnitude of the annealing temperature, but also on the length of time and the medium of annealing, as well as the constrained position of the sample under investigation[40].The annealing process usually leads to a growth of the crystalline regions and occasionally to a change in the crystal structure from a less stable to a more stable one[41].

The effect of drawing and annealing on the 6GT polymer will be considered next in more detail.

3.2 EXPERIMENTAL

3.2.1 Drawing

The experimental methods applied to the drawing of 6GT fibres are described in the following sections, which have been considered according to the drawing temperature.

(a) Cold Drawing

An Instron tensile tester (model TM-SM) was used at room temperature in drawing the gravitationally spun fibres and fibres collected

with a take-up velocity of 50 and 400 m/min.. In each experiment, a specimen fibre, 5 cm long, was clamped in the tensile tester. The clamps were provided on the inside with a hard rubber lining so as to minimise slippage and to avoid damaging the fibre specimens. The same draw ratio was obtained at different cross-head speeds.

However, even with careful clamping, slippage of yarns may sometimes occur, especially at high speeds of drawing and high draw ratios. In addition to this, the measurements may be affected by the elastic recovery of the yarns when the applied force is removed. Because of these, the draw ratio cannot be determined accurately from the distance of cross-head travel. Therefore, a quantity called the true draw ratio (T.D.R.) was used and calculated as: the ratio of the cross-sectional area before and after drawing. Thus, the diameter of each fibre was measured before and after drawing, using an optical microscope fitted with a calibrated eye-piece of known magnification (200X and 400X).

(b) Hot Drawing

Hot drawing was carried out on gravitationally spun fibres only. For these experiments, an Instron environmental chamber was used to maintain the required temperature, which can be adjusted thermostatically. The temperature of drawing was adjusted to $85\pm5^{o}C$, and the procedure involved was similar to that employed for cold drawing.

Hot drawing was also performed on another drawing apparatus which consisted essentially of:

(i) Feed and draw rollers around which the fibre was wrapped four times to prevent slippage;

(ii) a thermostatically controlled hot-plate located between the rollers, and

(iii) a bobbin on which the drawn fibre was collected.

The speed of rotation of the draw roller was kept constant, whilst that of the feed roller was altered by means of a gearwheel mechanism. The draw ratio of the fibre was determined from the ratio of speeds of the draw roller and feed roller. The temperature of the hot-plate was set at 90°C.

3.2.2 Annealing

Since the starting polymer materials have undergone different treatments before annealing, i.e. spun with different take-up velocities, drawn with different speeds, temperature and draw ratios; different media and types of annealing were investigated to establish a reliable experimental procedure.

From these studies, it was established that annealing in air offered more reliable results than that in vacuum, and was also found to have less experimental difficulties than that in oil. In forming this conclusion, two relevant aspects were closely studied, i.e. heat transfer and thermal degradation.

The medium in which a polymer is annealed needs to be carefully chosen, because it greatly affects the rate of heat transfer to the material. Halim[42] has investigated the difference between annealing in air and vacuum by observing the behaviour of citric acid crystals mounted on a polypropylene fibre. He concluded that for the same oven thermostat-setting, a vacuum annealed specimen reached a temperature 10-15°C lower than one annealed in air. When two identical samples have been annealed in an oven set at 140°C, one in vacuum,

the other in air, the difference in the relative intensities in their X-ray diffraction patterns showed that the two samples did not reach the same temperature, and that the difference was consistent with that observed by Halim.

Annealing in air, particularly at high temperatures, may lead to thermal degradation of the fibre. Therefore, preliminary experiments using four identical fibres were performed, mainly to discern whether such degradation had occurred. The experiments involved the annealing of fibres in air and vacuum for two and 24 hours. An identical experimental procedure was employed; a fibre was placed on a Teflon sheet and introduced inside a preheated ($140^{o}C$) oven. The four fibres were then exposed to X-ray for the same period of time. The diffraction patterns did not show significant changes, indicating that even if thermal degradation had occurred in air, it had not affected the crystal structure.

Annealing in air was performed inside a cylindrical oven (Heracus), which had been preheated via a thermostat to the required annealing temperature, as recorded by a thermometer of accuracy $\pm 2^{o}C$. The samples were annealed inside the oven for a period of two hours, after which, they were quenched in air at room temperature.

All the samples under investigation in this work were annealed under constant length, because it hinders the disorientation of the crystals relative to the fibre axis[41]. Annealing under tension and under unrestrained conditions were also performed but on selected samples. These different types of annealing are described below.

(I) Annealing under constant length (Taut)

Different fibres were annealed, including gravitationally spun fibres, spun fibres with take-up velocities of 50 and 400 m/min., and

fibres drawn with different draw ratios and at different speeds. A filament was mounted on a sample holder having two vertical support rods. The filament was wound around the support rods with the two ends knotted, keeping the initial length constant. The annealing was carried out over a temperature range extending between 80°C and 160°C, in temperature steps of 10°C; melting was observed to occur at about 160°C.

(II) Annealing under tension (Tensional)

Annealing under this condition was carried out on drawn fibres with draw ratio of 3.5, using a monofilament, and on as-spun fibres collected with take-up velocity 400 m/min., using a bundle of five fibres. The sample was mounted on a frame, with both ends clamped and a 50 gram weight hanging in the middle of the specimen under investigation. The frame was then introduced inside a preheated oven, where the annealing was carried out for two hours at each of three temperatures: 100 , 120 and 140°C.

(III) Annealing under unrestrained conditions (Slack)

This was performed on a filament of fibre spun with a take-up velocity of 400 m/min. and on drawn fibres. The sample was placed on a Teflon sheet inside the oven, where annealing was carried out for two hours at 100 , 120 and 140°C. A Teflon sheet was used to allow the fibre to shrink freely.

3.2.3 Density Measurements

The density measurements were carried out for 6GT as-spun fibres, drawn fibres, pressed and cast films; a density gradient column was used, which was prepared with two solutions, each consisting of carbon tetrachloride and toluene, having densities of 1.20 and

1.32 gm/cm^3 respectively. Insoluble, non-swelling floats (of accurately known density at 23^{o}C) were used to calibrate a 70cm long column, having a density gradient between 1.21 and 1.28 gm/cm^3. A calibration curve was plotted from the measured height of each float and its density.

Different specimens were dropped into the column; the height of the specimens were recorded at different intervals of time from which their density was measured from the calibration curve. The density measurements were checked further by using a density gradient column prepared with solutions of stannic chloride in water.

3.3 RESULTS

3.3.1 Drawing

The drawing conditions, including temperature, speed of drawing and draw ratio of the fibres under investigation, are listed in Table (3.1).

It is seen from Table (3.1) that the natural draw ratio for the gravitationally spun fibres, drawn at room temperature to draw ratio 3.5, increases with increasing speed of drawing. The true draw ratios for samples drawn ultimately to draw ratio 7.5 at cross-head speeds 1 and 100 cm/min. were found to be 5.5 and 5.7 respectively.

It was also observed that in drawing gravitationally spun fibres at room temperature and at low speed of drawing, the fibres were drawn at more than one neck, different from the drawing at high speeds of drawing, where only one neck was observed.

TABLE (3.1)

DRAWING CONDITIONS OF DIFFERENT FIBRE SAMPLES

Sample Designation	Winding Velocity (m/min)	Temperature of Drawing (°C)	Speed of Drawing (cm/min)	Draw Ratio	Natural Draw Ratio
	0				
*G	0				
GC1	0	20	0.5	3.5	3.6
GC2	0	20	1.0	"	3.8
GC3	0	20	5.0	"	4.0
GC4	0	20	25.0	"	4.3
GC5	0	20	50.0	"	4.6
GC6	0	20	100.0	"	4.9
GC7	0	20	1.0	7.5	
GC8	0	20	100.0	"	
GH1	0	85	1.0	4.0	
GH2	0	85	5.0	4.0	
GH3	0	85	100.0	4.0	
GH4	0	85	1.0	8.0	
GH5	0	85	5.0	8.0	
GH6	0	85	100.0	8.0	
**GH7	0	90	240.0	4.0	
**GH8	0	90	240.0	8.0	
+LV	50	20			
LV1	50	20	5	3	
LV2	50	20	100	3	
LV3	50	20	5	5	
LV4	50	20	100	5	
++HV	400				
HV1	400	20	5	2.0	
HV2	400	20	100	2.0	

*G: gravitationally spun fibre

**GH7,GH8: hot-drawn by drawing machine, with T.D.R.= 4.6 and 5.5 respectively.

+LV: as-spun fibre with take-up velocity 50 m/min.

++HV: as-spun fibre with take-up velocity 400 m/min.

When a bundle of six gravitationally spun fibres were clamped in the Instron, with the fibres parallel to each other, it was observed that at high speeds of drawing, e.g. 50 and 100 cm/min., a neck initiated individually in each fibre at the same position and travelled along each fibre with the same speed. At low speeds of drawing, many necks initiated in each fibre at different positions and times and travelled with different speeds. The neck region was observed at high speeds of drawing to be white in colour and shiny; with further drawing and before breaking point was reached, the fibre became opaque. Furthermore, all fibres drawn to high draw ratios were found to turn opaque at all speeds of drawing.

It was observed, during the drawing of cast films in the Instron, that the cast films broke soon after developing a neck. However, it was found possible to draw the cast film by hand to a maximum draw ratio of approximately 2.5.

During hot drawing in the Instron, no neck formation was observed in gravitationally spun fibres, whereas, during hot drawing of the same fibre in the drawing machine, a neck was observed to occur before reaching the hot plate, i.e. the feed roller.

In the wide-angle X-ray diffraction investigations, it was found that drawn fibres yielded very diffuse diffraction patterns, which rendered the detection of the structural changes, associated with the drawing processes, difficult. Therefore, annealing of the drawn fibres was required, if the effect of various drawing conditions on the crystal structure were to be investigated.

3.3.2 Annealing

(I) Annealing of Fibres

The results reported here are for the annealing of various fibres in air at constant length; the history of these fibres before annealing has been listed in Table (3.1). The structural changes at each annealing temperature were investigated by recording their wide-angle X-ray diffraction photographs. These investigations were carried out on all samples and are presented below according to three temperature ranges.

(a) Low Temperature Range (≈80-100°C)

In this range, only the usual changes were observed, i.e. with increasing annealing temperature, the reflections became less diffuse and better resolved. Plate 2(a-d) shows the wide-angle X-ray diffraction photographs of different fibres annealed at 90°C; these fibres include gravitationally spun fibres, as-spun fibres with take-up velocity 50 m/min. and cold drawn fibres with draw ratio 3.5 (T.D.R. = 3.8) and 7.5 (T.D.R. = 5.7).

(b) Intermediate Temperature Range (≈110-135°C)

In this range, different reflections changed in intensity by different amounts - henceforth referred to as relative intensity - and this occurred for several reflections on different layer lines. For example, the wide-angle X-ray diffraction photographs for the annealing at 120°C of fibres having the same origin as those studied in the temperature range (80-100°C) are shown in Plate 2(e-h). These photographs show that some particular reflections became intense, while others became fainter or disappeared.

PLATE (2): WAXS photographs of as-spun and drawn fibres annealed:

at 90°C

(a) gravitationally spun fibre

(b) spun with take-up velocity 50 m/min.

(c) cold drawn fibre (T.D.R.= 3.8)

(d) " " " (T.D.R.= 5.7)

at 120°C

(e) gravitationally spun fibre

(f) spun with take-up velocity 50 m/min.

(g) cold drawn fibre (T.D.R.= 3.8)

(h) " " " (T.D.R.= 5.7)

at 150°C

(j) gravitationally spun fibre

(k) spun with take-up velocity 50 m/min.

(l) cold drawn fibre (T.D.R.= 3.8)

(m) " " " (T.D.R.= 5.7)

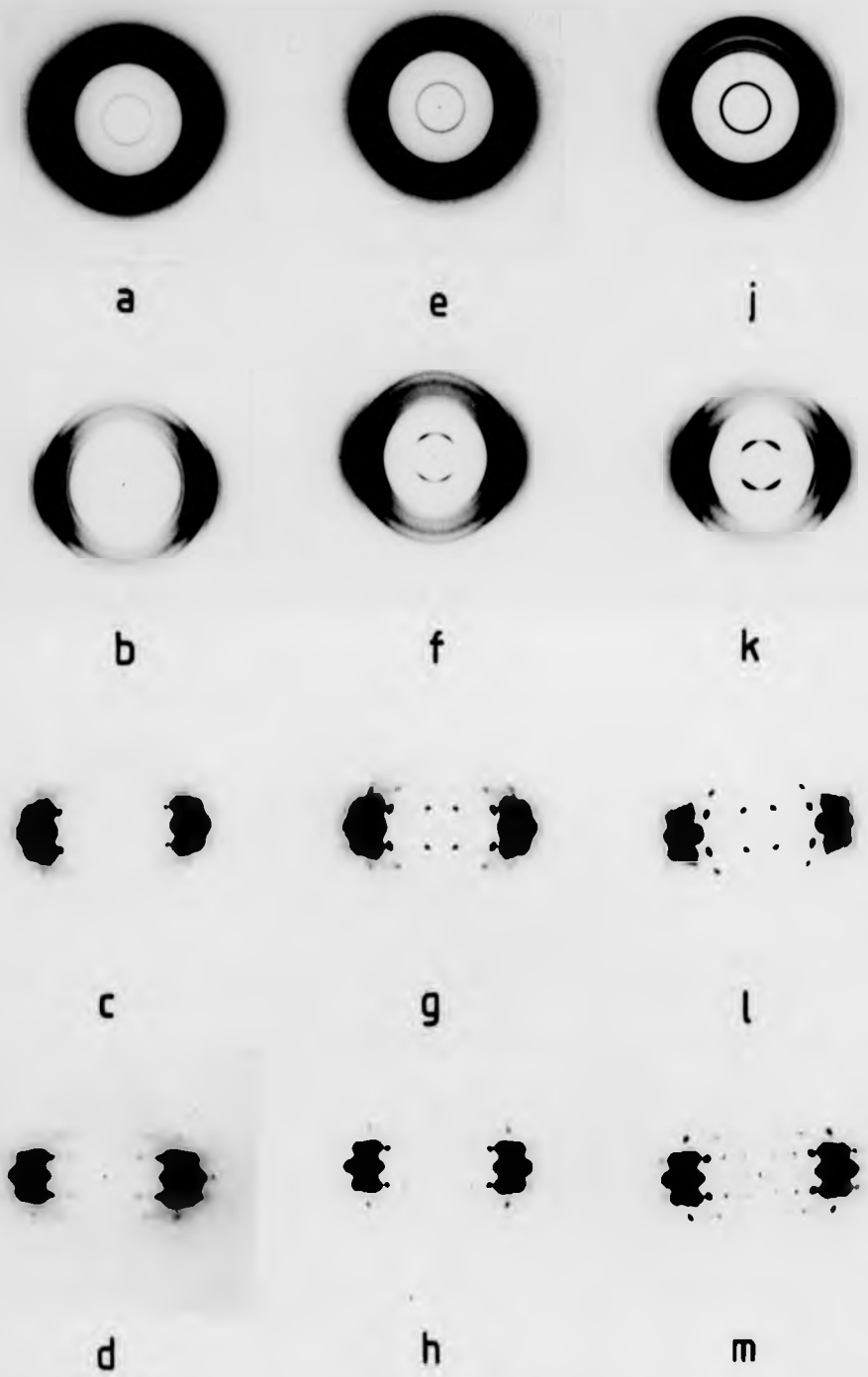

PLATE 2

PLATE (2): WAXS photographs of as-spun and drawn fibres annealed:

at 90°C

(a) gravitationally spun fibre

(b) spun with take-up velocity 50 m/min.

(c) cold drawn fibre (T.D.R.= 3.8)

(d) " " " (T.D.R.= 5.7)

at 120°C

(e) gravitationally spun fibre

(f) spun with take-up velocity 50 m/min.

(g) cold drawn fibre (T.D.R.= 3.8)

(h) " " " (T.D.R.= 5.7)

at 150°C

(j) gravitationally spun fibre

(k) spun with take-up velocity 50 m/min.

(l) cold drawn fibre (T.D.R.= 3.8)

(m) " " " (T.D.R.= 5.7)

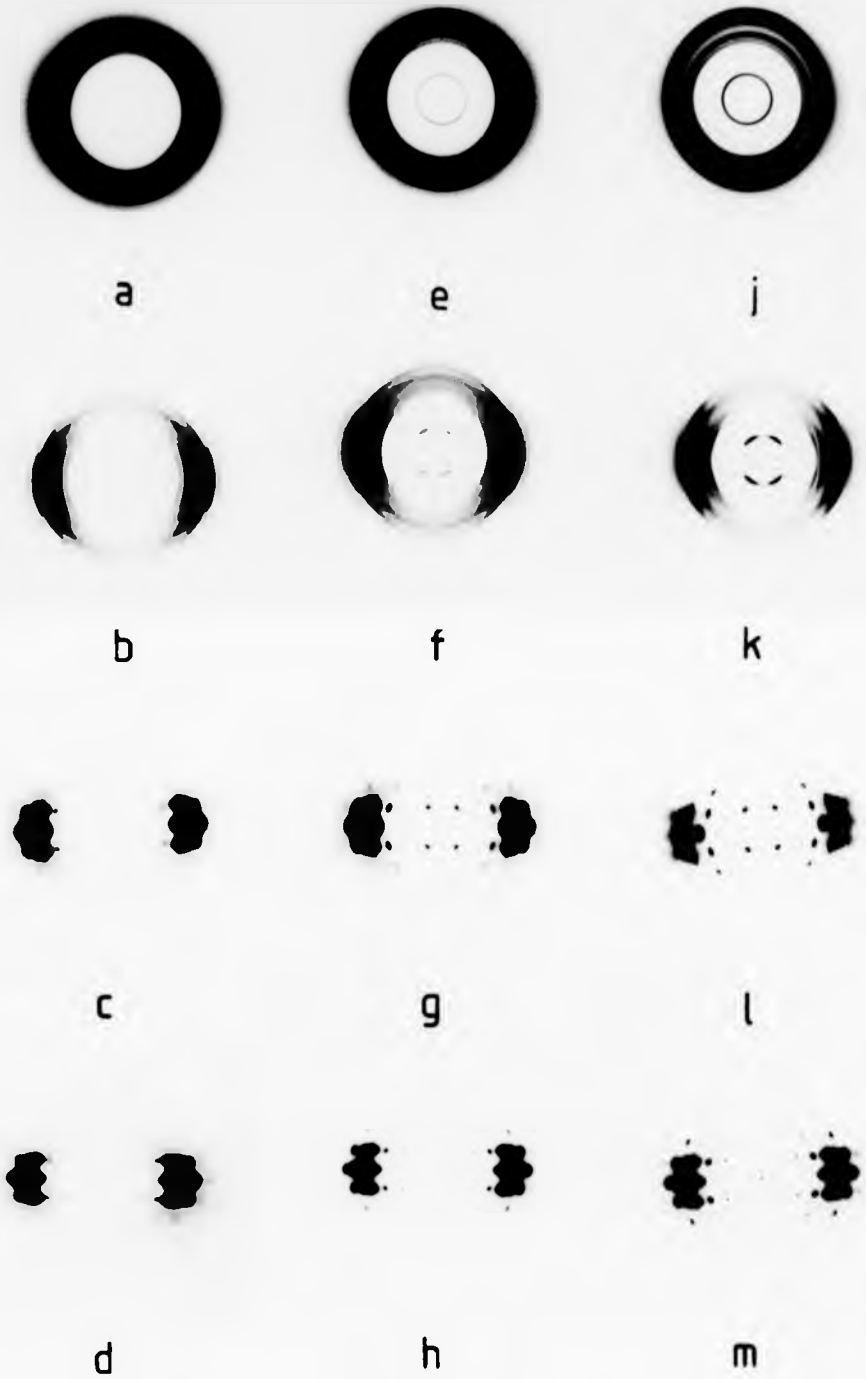

PLATE 2

(c) High Temperature Range (≈140°C - Melting Point)

In this case, the changes in the relative intensities of the X-ray reflections for most fibres were found to increase with increasing annealing temperature and then stablise, i.e. no more changes in the relative intensities were observed up to the melting point. But in the annealing of drawn fibres (T.D.R. = 5.7), the changes in the relative intensity were found to increase with annealing temperature and did not stabilise until complete melting was attained. The annealing temperature, at which these changes stablised, was found to vary with different fibres; with gravitationally spun fibres, the stabilisation was observed at the start of this range, whereas, in the case of as-spun fibres with take-up velocity 50 m/min., the stablisation occurred at a higher annealing temperature, but at a lower temperature than that with drawn fibres (T.D.R. = 3.8). Plate 2(j-m) shows the X-ray diffraction patterns for fibres, having the same origin as those investigated in the two previous ranges, annealed at 150°C.

A close examination of Plate 2 shows that the changes in the relative intensity upon annealing of fibres with low draw ratio are different from those with higher draw ratios. In order to illustrate these differing changes, two samples giving clear X-ray diffraction patterns, even at low annealing temperature, were chosen; hot drawn fibre (T.D.R.=4)and as-spun fibre with take-up velocity 400 m/min. The X-ray diffraction patterns for the hot drawn fibre before and after annealing at 120°C and 150°C are shown in Plate 3(a),(b) and (c), respectively. In Plate 3(b) and (c), it can be seen that the intensities of some reflections, designated by 1, 2, 5 and 8, increase and that of others, i.e. 3, 4, 6, 7, 9 and 10 decrease, and some of the latter

PLATE (3): WAXS photographs of:

hot drawn fibres (T.D.R.= 4) annealed at:

(a) 90°C

(b) 120°C

(c) 150°C

and as-spun fibre with take-up velocity 400 m/min. annealed at:

(d) 90°C

(e) 120°C

(f) 150°C

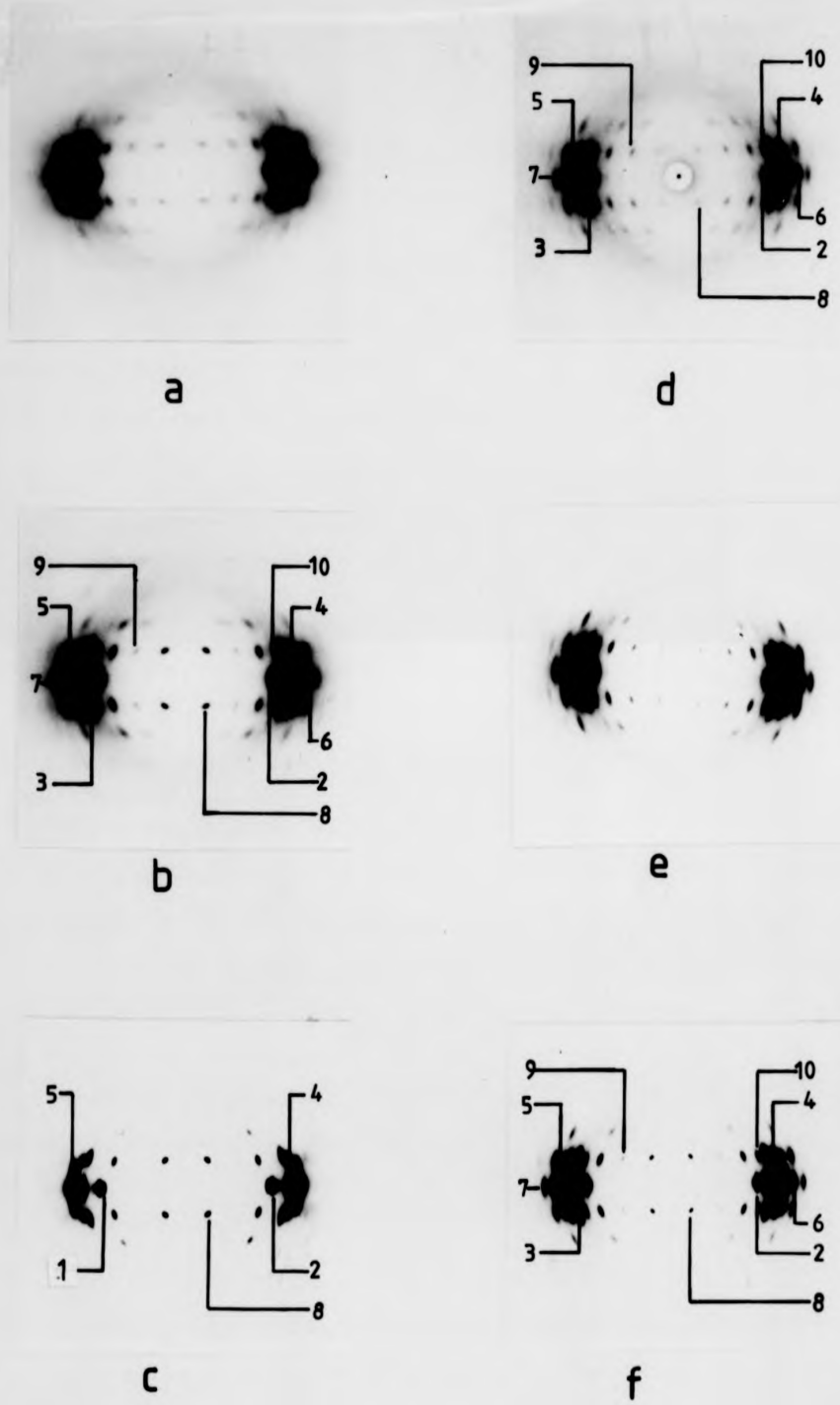

PLATE 3

PLATE (3): WAXS photographs of:

hot drawn fibres (T.D.R.= 4) annealed at:

(a) 90°C

(b) 120°C

(c) 150°C

and as-spun fibre with take-up velocity 400 m/min. annealed at:

(d) 90°C

(e) 120°C

(f) 150°C

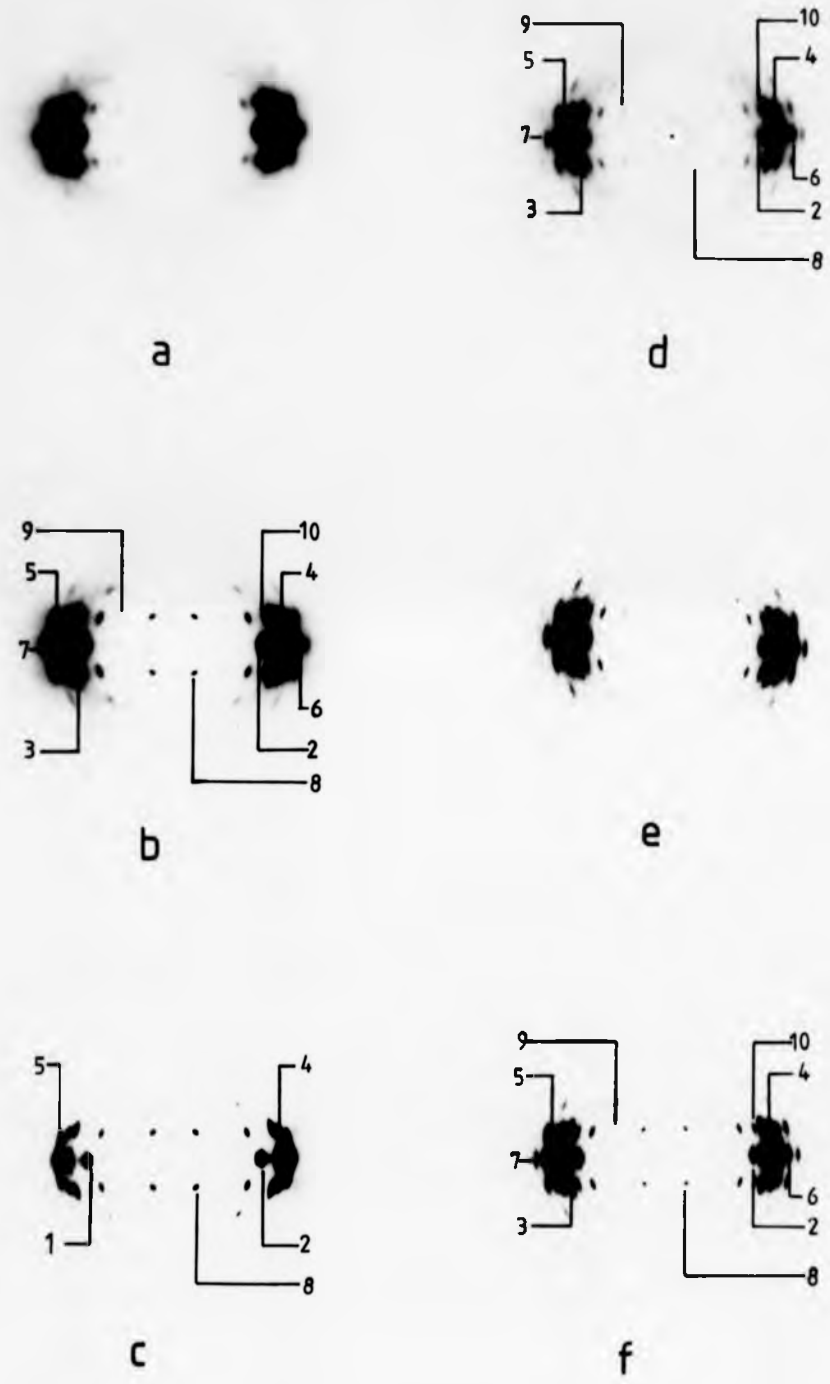

PLATE 3

reflections eventually disappear. The co-ordinates and change in the relative intensities of the reflections in Plate 3(a) and (c), the latter being estimated by eye, are listed in Table (3.2).

The X-ray diffraction patterns for as-spun fibres with take-up velocity 400 m/min. annealed at 90 , 120 and 150°C, are shown in Plate 3(d), (e) and (f) respectively. It is seen that annealing up to 150°C increases the intensities of all the reflections. In particular, the weak reflections, designated by 2, 5 and 8, become more intense relative to the others, while none of the other reflections decay in intensity or disappear. The co-ordinates and the change in relative intensities of the reflections in Plate 3(d) and (f), the latter being estimated by eye, are listed in Table (3.2).

(II) Annealing of Cast Films

The wide-angle X-ray photograph for cast film as-prepared at room temperature was shown in Plate 1(g). The pattern showed sharp powder diffraction rings and was completely different (different d-spacings) from that for a gravitationally spun fibre. The diffraction pattern for drawn film showed too diffuse reflections appearing as long arcs.

The structural changes upon annealing of cast films are presented according to three temperature ranges:

(a) Low Temperature Range (70-90°C)

The reflections on the X-ray diffraction photographs for the as-prepared cast film, showed no significant changes with increasing annealing temperature, while for the drawn cast film, the reflections became less diffuse. The X-ray diffraction patterns for the undrawn and drawn cast films, annealed at 80°C, are shown in Plate 4(a) and (b) respectively.

TABLE (3.2)

Reflection Number	X-Y Co-ordinates		Hot Drawn		Spun with take-up velocity 400 m/min.	
	X (mm)	Y (mm)	Unannealed	Annealed at 150°C	Annealed at 90°C	Annealed at 150°C
1	9.23	0	Diffuse	Medium	-	-
2	9.50	0	Medium	Intense	Very faint	Medium
3	10.30	0	Medium	-	Medium	Medium
4	11.37	0	Very Intense	Intense	Very Intense	Very Intense
5	12.50	0	Very Intense	Very Intense	Medium	Very Intense
6	13.60	0	Medium	Faint	Medium	Medium
7	14.60	0	Medium	Faint	Medium	Medium
8	2.25	3.0	Medium	Very Intense	Faint	Intense
9	5.56	3.0	Medium	Very Faint	Medium	Medium
10	9.65	3.0	Medium	-	Medium	Medium

(b) Intermediate Temperature Range (≈100-120°C)

In this range, it was found that some reflections were becoming fainter. At the same time, some particular weak reflections showed an increase in their intensities with the appearance of new reflections; these changes were found to increase with increasing annealing temperature. The diffraction patterns for the undrawn and drawn cast films, annealed at 110°C, are shown in Plate 4(c) and (d) respectively.

(c) High Temperature Range (130°C - Melting Point)

In this range, the reflections of decaying intensity disappeared while the newly appeared reflections became more intense. These changes were found to stabilise over this range to give a diffraction pattern shown in Plate 4(e) and (f) for the undrawn and drawn cast films respectively, when annealed at 150°C.

The X-Y co-ordinates of the reflections, numbered in Plate 4(b) and (f), and the change in their relative intensities, the latter being estimated by eye, are listed in Table (3.3). In the annealing of the powder sample, the changes appearing in the wide-angle X-ray photographs were observed to be identical to those observed with the undrawn cast film.

3.3.3 Density

The results of the measurement of density for as-spun fibres as a function of winding speed are listed in Table (3.4). The results of density for as-spun fibres, drawn fibres and cast films as a function of temperature are listed in Table (3.5). Table (3.4) shows that the density increases with take-up velocity, while Table (3.5) shows that

PLATE (4): WAXS photographs of cast films:

undrawn annealed at:

(a) 80°C

(c) 110°C

(e) 150°C

drawn annealed at:

(b) 80°C

(d) 110°C

(f) 150°C

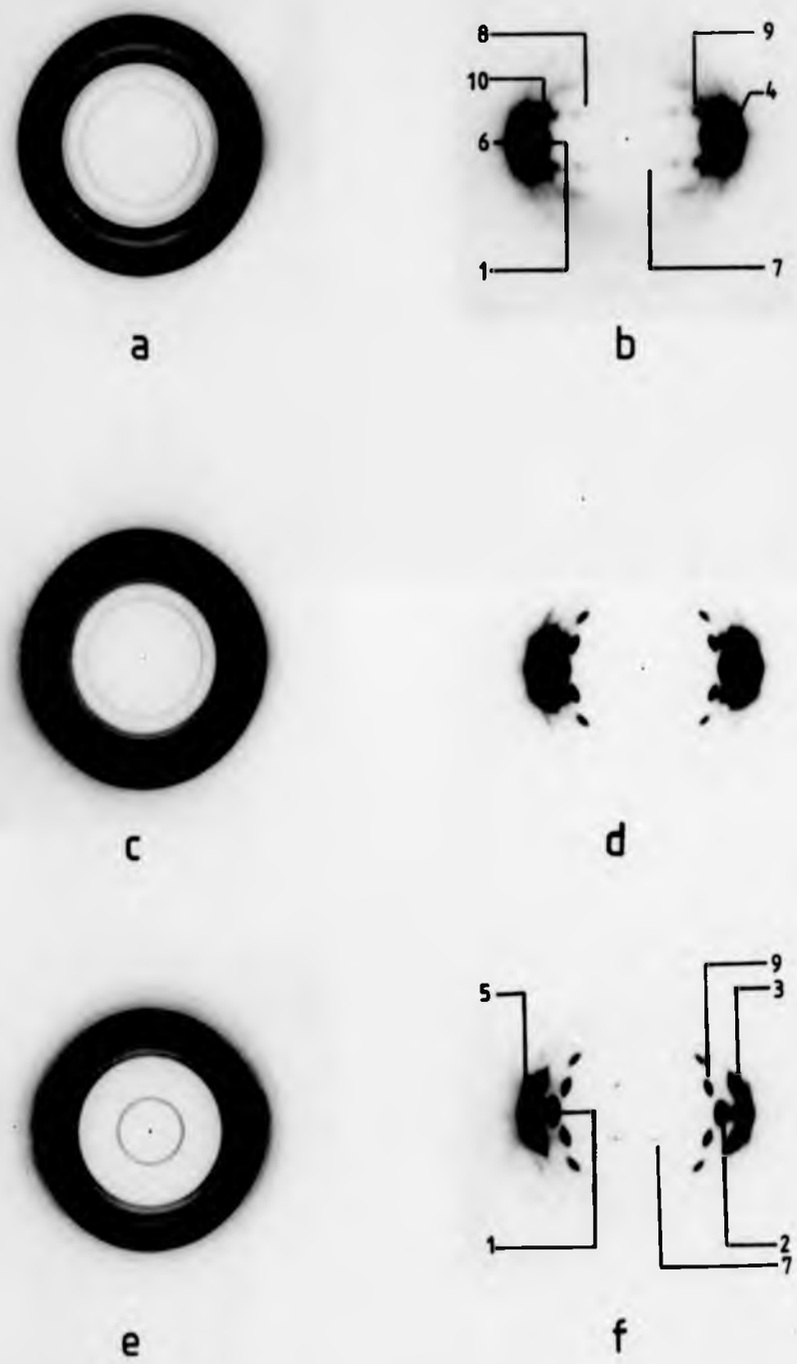

PLATE 4

PLATE (4): WAXS photographs of cast films:

undrawn annealed at:

(a) 80°C

(c) 110°C

(e) 150°C

drawn annealed at:

(b) 80°C

(d) 110°C

(f) 150°C

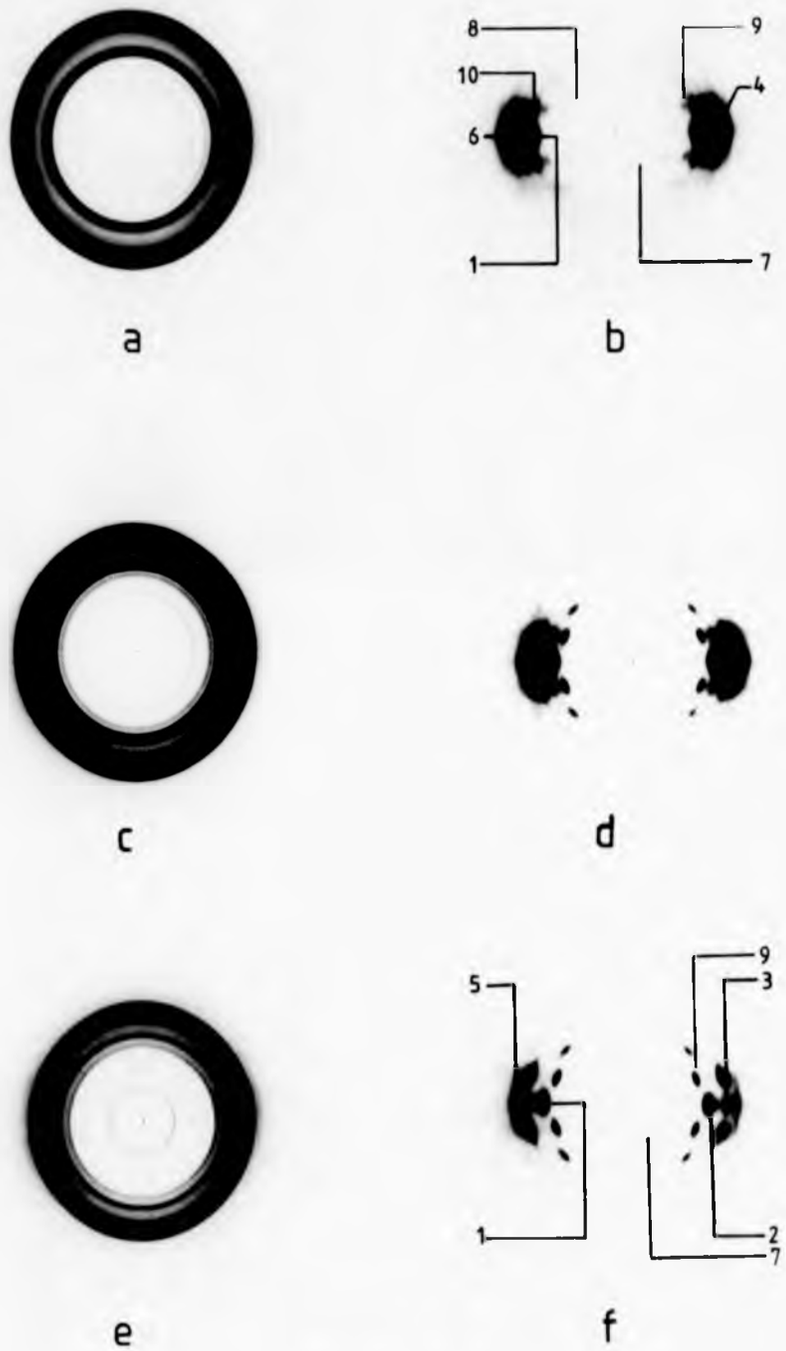

PLATE 4

TABLE (3.3)

Reflection Number	X-Y Co-ordinates		Drawn Cast Film	
	X (mm)	Y (mm)	Annealed at 90°C	Annealed at 150°C
1	9.23	0	Very Intense	Intense
2	9.60	0	-	Intense
3	11.37	0	-	Medium
4	11.70	0	Intense	-
5	12.50	0	-	Intense
6	13.26	0	Intense	-
7	2.25	3.0	Faint	Intense
8	4.54	3.0	Faint	-
9	7.84	3.0	Faint	Very Intense
10	9.35	3.0	Very Intense	-

TABLE (3.4)

The Density of As-Spun Fibres
as a function of Take-up Velocity

Take-up Velocity (m/min.)	Density (gm/cm^3)
0 (Gravitationally spun)	1.236
50	1.236
150	1.238
300	1.242
400	1.242

TABLE (3.5)

The Density of Samples as a function
of Annealing Temperature

Temperature (^oC)	Density (gm/cm^3)			
	*GC_2	+GC_8	**TV = 400	Cast Film
23	1.232	1.232	1.242	1.256
100	1.240	1.241	1.242	
120	1.246	1.242	1.245	1.257
140	1.251	1.246	1.246	1.256

*GC_2: Gravitationally spun fibre drawn at room temperature with T.D.R.= 3.8 (see Table (3.1)).

+GC_8: Gravitationally spun fibre drawn at room temperature with T.D.R.= 5.7 (see Table (3.1))

**TV = 400: As-spun fibre with take-up velocity 400 m/min.

the density for fibres increases with the annealing temperature. On closer examination of Table (3.5), it can be seen that the density of the cast film is higher than that for the fibres and shows no significant changes upon annealing. The density of the as-prepared polymer samples was measured and found to be as follows:-

Chipped as-prepared	1.241 gm/cm^3
Spun fibre collected 40 cm below spinneret	1.237 gm/gm^3
Pressed film (amorphous)	1.226 gm/cm^3
Pressed film annealed at 140^oC	1.251 gm/cm^3

3.4 DISCUSSION

In Chapter Two, the experimental results have indicated a possibility of the occurrence of structural changes with the take-up velocity of the final as-spun fibre. In view of this possibility, further investigations of the structural changes and the factors influencing them were required. In the preceding section of this Chapter, experiments have been described in which the effects of drawing and annealing under different conditions have been studied.

Drawing of unoriented fibres (gravitationally spun) at different temperatures and speeds, and to different draw ratios, would be expected to lead to different morphology but not to cause structural changes. Unfortunately, the X-ray diffraction photographs could not reliably indicate whether structural changes had occurred or not because the patterns were too diffuse. Therefore, annealing the drawn fibres had to be carried out in order to produce clear X-ray diffraction patterns; but, since annealing is accompanied at times by changes in the crystal structure, it is necessary to consider the results in a way which will

show whether the structural changes are due to annealing itself or to the sample treatments prior to annealing or both.

From the results obtained, it was observed that the changes in crystal structure are dependent on the initial state (take-up velocity, draw ratio, speed of drawing and the temperature of drawing), as well as the annealing conditions; but only a limited range of the annealing conditions were considered. The fibre was held at constant length and the effect of annealing temperature was studied.

The changes in crystal structure were found to be highly dependent on the annealing temperature. However, the effects were such that their treatments can be simplified by dividing the entire temperature range into three ranges: low, intermediate and high range, in a manner similar to that described by Loboda-Cackovic et al[43].

All the poorly oriented materials, such as, cold and hot drawn fibres with a low draw ratio and as-spun fibres with low take-up velocity, showed similar behaviour on annealing. The same crystal structure (as shown by the locations and intensities of the reflections on the X-ray diffraction patterns) can be obtained from any of these samples, though it is necessary to anneal different ones to different temperatures to do so. Thus, the pattern for hot drawn fibres annealed at 140°C was the same as that for cold drawn samples annealed at 150°C. The more highly oriented materials, such as, hot and cold drawn fibres with high draw ratios and as-spun fibres with high take-up velocity were also found to behave similarly upon annealing, though different from the poorly oriented ones.

If the diffraction pattern of highly oriented material annealed at high temperature is compared with that of the same material annealed

at low temperature, it is observed that some new reflections have appeared, but that none of those present before and after annealing at low temperature have decayed in intensity. This implies that a new crystal structure develops on annealing this material at high temperature, but that the crystal structure present before and after annealing at low temperature still exists.

If the same comparison is made for poorly oriented material, some reflections have become more intense, but others have decayed in intensity or even disappeared. Thus, in this case, whenever a new crystal structure appears on annealing at high temperature, the crystal structure which had existed before and after annealing at low temperature has been destroyed.

The new reflections which have appeared in the highly oriented material upon annealing at high temperature correspond to those which have become more intense on annealing the poorly oriented material at high temperature. Thus, the new crystal structure appearing with high temperature annealing of highly oriented material, is the same as that which is always present in poorly oriented material but which increases in proportion on annealing at high temperature.

The reflections which have disappeared from the pattern of the poorly oriented material on annealing at high temperature are the same as those present in that of highly oriented material whose intensities do not change with annealing temperature. Thus, the crystal structure destroyed by high temperature annealing of the poorly oriented material is that which exists at all annealing temperatures in the highly oriented one.

From these different changes, it may be deduced that there exist two different crystal structures of 6GT. It is suggested here that the

two crystal structures are to be called α- and β-form; the α-form being exhibited in the highly oriented materials, while β-form develops upon annealing the poorly oriented ones. Drawing and annealing effectively control the proportion of the two forms in the structure. This is illustrated in Table (3.6), where the results of different annealing temperatures of the fibre drawn under different conditions, previously listed in Table (3.1), are summarised. It is seen that the proportion of β-form increases monotonically with the annealing temperature and that of α-form increases with increasing take-up velocity and the draw ratio. It is also seen that the higher the stretching rate, the greater is the proportion of α-form. From Table (3.1), it is seen that the natural draw ratio increases with increasing stretching rate. Therefore, one may conclude that the increase in the proportion of α-form may be the result of an increase in the natural draw ratio.

The increase in the natural draw ratio with the stretching rate has been observed by Marshall and Thompson[35] in their work on PET fibres, using a continuous drawing machine. They proposed that greater adiabatic conditions are produced at higher drawing speeds and, hence, greater natural draw ratio. On the other hand, Allison and Ward[37] investigated the natural draw ratio of PET fibres, using an Instron tensile tester for drawing, and found that it did not vary at low strain rates, i.e. 0.05-5.0 cm/min.. They suggested that the change in the natural draw ratio at higher strain rates may be attributed to void formation. The disagreement between the results reported here and those reported by Allison and Ward, may have emerged as a result of using different polymers, different filament diameter, different pre-orientation or choosing a low draw ratio.

TABLE (3.6)

Effects of Drawing and Annealing on the Proportionality of α- and β-form

Sample Designation*	As-Prepared	Low Temperature Range (~80-100°C)	Intermediate Temperature Range (~110-135°C)	High Temperature Range (~140-150°C)	Melt ≈162°C
G	$\alpha = \beta$	$\alpha \lesssim \beta$	$\alpha \lesssim \beta$	β-form	β-form
LV	$\alpha > \beta$	$\alpha = \beta$	$\alpha \lesssim \beta$	β-form	β-form
HV	α-form	$\alpha >> \beta$	$\alpha \gtrsim \beta$	$\alpha \lesssim \beta$	β-form
GC_{1-4} GH_{1-3}	$\alpha = \beta$	$\alpha = \beta$	$\alpha < \beta$	$\alpha << \beta$	β-form
GC_{5-6} GH_{4-7} LV_{1-2}	diffuse	$\alpha > \beta$	$\alpha \gtrsim \beta$	$\alpha = \beta$	β-form
GC_{7-8}, GH_8 LV_{3-4}, HV_{1-2}	diffuse	$\alpha >> \beta$	$\alpha > \beta$	$\alpha \gtrsim \beta$	β-form

* Sample designations and drawing conditions are listed in Table (3.1).

It was of interest, at this stage, to know whether the increase in the proportion of α-form was caused by the increase in the natural draw ratio or the stretching rate only. To resolve this, gravitationally spun fibres were drawn to a T.D.R. = 5.5 at a speed of 1 cm/min.. The crystal structure of this fibre was found to be the same as that exhibited by fibres of true draw ratio 5, drawn at high speed (100 cm/min.). According to these results, it may be concluded that the crystal structure is affected mainly by the draw ratio rather than the stretching rate, although the draw ratio is not usually expected to change the crystal structure but the morphology.

In order to investigate the behaviour of the two crystal structures (α- and β-form), it is necessary to review some general mechanisms of drawing and annealing of drawn fibres on which the explanations presented here are to be based. Peterlin[44] proposed a molecular model of drawing which accounts for the morphological changes with drawing, i.e. a transformation from the spherulitic structure (or the microspherulitic structure for fibres) to the fibrous structure. At high draw ratios, this structure is accompanied by longitudinal voids along the fibre axis; such voids which render the material opaque are generally assumed to be the cause of the tendency of the fibre to fibrillation. Hay and Keller[45] reported that inhomogeneous deformation (one part of the spherulite or the regions between them are only extended) is associated with voids and crack formation parallel to the drawing direction, turning the fibre to be shiny and white. Accordingly, a fibrillar structure is eventually obtained. The mechanism of inhomogeneous deformation may be applicable here; further investigations by using the scanning electron microscope will be given in Chapter Eight.

Statton[46] in his string model has not excluded some chain folding in an essentially drawn fibre. These chain folds act as nuclei on which, upon annealing such a drawn fibre, melting and recrystallisation to folded chain crystal will be preferred. The chain folding was found by Statton to depend upon the annealing temperature, i.e. the higher the annealing temperature, the more regular is the chain folding introduced into the fibre. Sakaoku and Peterlin[47] studied the effect of annealing on different draw ratios of polyethylene and nylon6 samples. They concluded that the fibre structure tended to become more stable with increasing draw ratio and, hence, offered a better resistance to the changes imposed by annealing.

According to the above mechanisms, it seems reasonable to suggest here that α-form are extended chain crystals and β-form are folded chain crystals. It, therefore, follows that crystallisation from the melt under no stresses should yield β-form. Gravitationally spun fibres from relatively low molecular weight material showed the presence of β-form only. The appearance of α-form together with β-form in the gravitationally spun fibres, having a relatively high molecular weight, may be attributed to the stresses imposed by an appreciably long spinline (10 feet). The gravitationally spun fibres, collected 40 cm below the spinneret were found to have β-form only. The existence of α-form in the as-spun fibres with high take-up velocity can be attributed to melt crystallisation under shear stresses, which may lead to fibrillar habit[48].

Annealing of drawn fibres profoundly affects the presence and also the proportions of the α- and β-form; the results of annealing can be interpreted in terms of melting and recrystallisation process. In the case when α- and β-forms initially existed, annealing was

expected to increase β-form in accordance with the mechanism of chain folding. The decrease in the relative intensities of α-form reflections in the intermediate and high temperature ranges, may be suggested here to be caused by melting and recrystallisation of the small α-form crystals in the intermediate range, and the larger ones in the high temperature range. Recrystallisation is expected to be in a chain folded manner, thus leading to an increase in the proportion of β-form crystals, which if originally existed before annealing, would act as nuclei for more chain folding when annealing is carried out at the intermediate and high temperature ranges.

In the case where only α-form crystals exist before annealing, the appearance of β-form in the intermediate temperature range can be interpreted in terms of crystallisation of molecules that have high molecular mobility. The increase in the relative intensities of β-form reflections with increasing annealing temperature, without any noticeable decrease in the relative intensities of the α-form reflections, can be interpreted by the melting of the small β-form crystals followed by recrystallisation to larger β-form ones.

The appearance of β-form crystals upon annealing of drawn fibres can be explained in terms of epitaxial crystal growth; β-form crystals may grow epitaxially on the surface of α-form crystals. Wunderlich and Melillo[49] showed that chain folded crystals of polyethylene can grow epitaxially on the surface of extended crystals of the same polymer. Within very short periods of time, epitaxial growth may not be available; this is consistent with the absence of β-form crystals in the as-spun fibres with high take-up velocity. In Chapter Eight evidence will be presented which may support this idea.

The results of free annealing at 140^{o}C showed an increase in

β-form crystals when compared with that annealed at a constant length and at the same temperature. On the other hand, annealing under tension introduced more α-form crystals as compared to annealing at a constant length and at the same temperature. It appears that the above-mentioned results are consistent with the mechanism suggested before. The change in the morphology of 6GT with different types of annealing, suggested here, is supported by the mechanism proposed by Statton[46]. According to this mechanism, fibres annealed in a condition where they are free to contract, will have a much greater amount of refolding than those held at constant length. If sufficient tension could be applied during annealing, the refolding would be prevented and an extended chain produced, but tension cannot prevent more refolding, particularly at high annealing temperature close to the melting point. The change in the crystal structure of 6GT seems to be somewhat related to the change in the morphology.

Annealing of Cast Films

The X-ray diffraction pattern for the cast films, as shown in Plate 4(a), is entirely different from that of the β-form. However, upon annealing, the β-form reflections started to appear together with weakening in the relative intensities of the original reflections. This transition continued with increasing annealing temperature, until the β-form reflections finally dominated.

The X-ray diffraction pattern for drawn cast film annealed in the low temperature range, as shown in Plate 4(b), shows that this structure has d-spacings that belong to neither α- nor β-form, as will be seen in Chapter Four. Therefore, it is suggested that this form be called γ-form. Annealing at the intermediate range leads to the

appearance of β-form reflections together with traces belonging to the α-form crystals.

Crystallisation from solution usually occurs in chain folded manner. Therefore, in order to explain the chain folded manner adopted by both crystal forms (β- and γ-form), it may be possible to suggest that γ-form crystals are less stable; upon annealing the γ-form crystals will melt and recrystallise to more stable crystals, i.e. β-form crystals.

So far, in this work, three distinct crystal structure forms have been established. Differences in the experimental conditions under which fibres or cast films have been prepared, are responsible for the development of these structures.

Density

The results of the density measurements for the as-spun fibres listed in Table (3.4) suggest that the crystallinity increases with the take-up velocity. This is in accord with the results of Heuvel and Huisman[50] in their work on PET and Spriuell and White[32] on polypropylene and polyoxymethylene. On the other hand, Abbott and White[22] reported on high density polyethylene that the crystallinity decreases with increasing take-up velocity, attributed to the influence of heat transfer.

Results for the as-spun fibres also suggest that the density of α-form crystals (as-spun fibres with take-up velocity 400 m/min.) is higher than that of β-form crystals (gravitationally spun fibres collected 40 cm below the spinneret).

The increase in the density upon annealing can be interpreted by crystal growth and recrystallisation characteristics of annealing

process. It is seen from Table (3.5) that at room temperature, the density of the drawn fibres (GC_2 and GC_8) is lower that that of as-spun fibres with take-up velocity 400 m/min. (TV = 400), which may be attributed to the deformation of crystalline regions upon drawing. It was established above that the highly oriented materials (TV = 400 and GC_8) have high proportions of α-form, which upon annealing at high temperature become mixed proportions of α- and β-forms. Poorly oriented materials, i.e. GC_2, were found to have a mixture of α- and β-forms, which upon annealing, the proportion of β-form becomes high. The density of the two annealed materials, GC_8 and TV = 400 at 140°C, was the same (1.246 gm/gm^3), which is lower than that of GC_2 (1.251 gm/cm^3). This may suggest that α-form has lower density than β-form. This cannot be conclusively accepted in view of the experimental observations that the density of TV = 400 and GC_8 varied over a wide range for samples of the same history. This was attributed to void and crack formation in the highly drawn fibres, as discussed above. The density values listed in Table (3.5) for these two samples are the highest measured values.

Table (3.5) shows that the density of cast films at room temperature (γ-form) is 1.256 gm/cm^3, and on annealing at 140°C (β-form) the density is shown to have the same value; but, the density of β-form in cast films (140°C) is higher than that of the β-form in fibres GC_2 (140°C). This difference in density may be due to the different methods of crystallisation.

In the case of the cast films, the expected increase in the density upon annealing at 140°C was not observed; this may be attributed to the appearance of β-form, which may, therefore, suggest that β-form has lower density than γ-form.

CHAPTER FOUR

Unit Cell Determination

4.1 INTRODUCTION

X-ray diffraction methods have been extensively used in the investigation of the molecular structure of fibre-forming polymers. Detailed data can only be acquired if the specimen under investigation is crystalline, i.e. if the molecules are arranged in a precise pattern with three-dimensional regularity. However, polymers are not completely crystalline; sometimes only sections of the molecules are arranged with three-dimensional order.

In drawn specimens, the crystallites are oriented with their molecular chain axes parallel to the direction of drawing; then the specimen is said to have uniaxial orientation. In rolled-out sheets, there are both axial and planar orientations, i.e. a particular crystal plane tends to lie in the plane of the sheet[51]. In this case, the specimen is said to have double orientation.

X-ray diffraction patterns, given by oriented specimens, are capable of providing a very complete picture of the structure of the crystalline regions, including information regarding the sterochemical configuration of the molecules and their precise arrangement. At times, the X-ray diffraction photographs of oriented specimens show displacement of the reflections by different amounts from their normal layer line positions, some up and some down. This indicates that the molecular chain axes of the crystals are not parallel to the fibre axis; the crystals are tilted.

4.2 DETERMINATION OF UNIT CELL FROM FIBRE USING SEMICYLINDRICAL FILM

4.2.1 Method of Unit Cell Determination

X-ray diffraction patterns of drawn fibres, taken with the beam perpendicular to the fibre axis, usually take the form of short arcs.

The pattern produced on a cylindrical film for a drawn fibre is similar to that produced when a single crystal is rotated completely around an axis coinciding with the axis of the cylinder. The effect of rotation is produced, since all orientations having the molecular axis parallel to the fibre axis are already present in the specimen.

The method employed for establishing a two-dimensional zero-layer trial lattice was devised by Bunn[52] and extended to three-dimensional form to account for non-zero layers. A device, designed by Buerger for precision photographs was used for measuring the Cartesian co-ordinates, x and y, of all the diffraction spots. In this device, the x-axis was taken along the equator, while the y-axis along the meridian. The measured values of x and y were converted into reciprocal lattice co-ordinates ξ and ζ respectively, using the equations for a cylindrical camera, given by Buerger[53]

$$\xi = [2 - \zeta^2 - 2(1-\zeta^2)^{1/2} \cos \frac{360}{2\pi r} x \,]^{1/2}$$

and $$\zeta = \frac{y}{(y^2+r^2)^{1/2}}$$

where r is the film-specimen distance, being also the radius of the camera (see Section 4.2.2(a)).

(a) Determination of a*, b* and γ* from the construction of Zero-layer Reciprocal Lattice

The construction of the reciprocal lattice is usually started with the zero-layer line (Equator). Intervals of length ${}_0\xi_1$ corresponding to ${}_0\xi$-co-ordinate of the innermost reflection and its multiple orders are marked. The magnitude of the ${}_0\xi$-co-ordinate of the next reflection was known, i.e. ${}_0\xi_2$, but not in direction relative to ${}_0\xi_1$. For graphical representation, a circle of radius ${}_0\xi_2$, centred at point 0

(Figure (4.1)), which denotes the origin of the reciprocal lattice, was drawn; the vector ${}_o\xi_2$ is one radius of this circle. In order to fix the direction of ${}_o\xi_2$ the ${}_o\xi$-co-ordinate of the third reflection was taken as the radius of another circle, whose centre was positioned ${}_o\xi_1$ away from O. The two circles were found to intersect and from their intersections, the directions of ${}_o\xi_2$ and ${}_o\xi_3$ were, thus, determined. With this triangulation procedure, the shape of the reciprocal lattice zero-layer was, therefore, determined (Figure (4.1)). The remaining ${}_o\xi$-values should fit this lattice when centred at the origin O; otherwise, it was necessary to halve the first ${}_o\xi$-value, or the other, and, if necessary, both.

At this stage of the construction, three of the reciprocal cell parameters, i.e. a*, b* and γ*, have been determined. A triclinic system is indicated by the X-ray diffraction photographs when row-line reflections appear without meridional reflections and when γ* is not 90^o. Now, if α* and β* are not equal to 90^o, then the origins of the other layer lines will be offset from the normal to the zero-layer line, passing through its origin. Therefore, in order to establish the values of α*, β* and c*, the magnitude and direction of this offset must be determined.

The magnitude of the offset from the origin of the first layer was determined by letting the smallest value, ${}_1\xi_1$, on the first layer be arbitrarily the (001), and drawing a circle of this radius, centred at the origin of the zero-layer; this is shown by the full circle shown in Figure (4.2). The direction of the offset, at this stage, is still unknown. All other first layer ${}_1\xi$-values were then taken, centering systematically on neighbouring lattice points and drawing arcs to intersect the circle at a common point. It was found that there could be

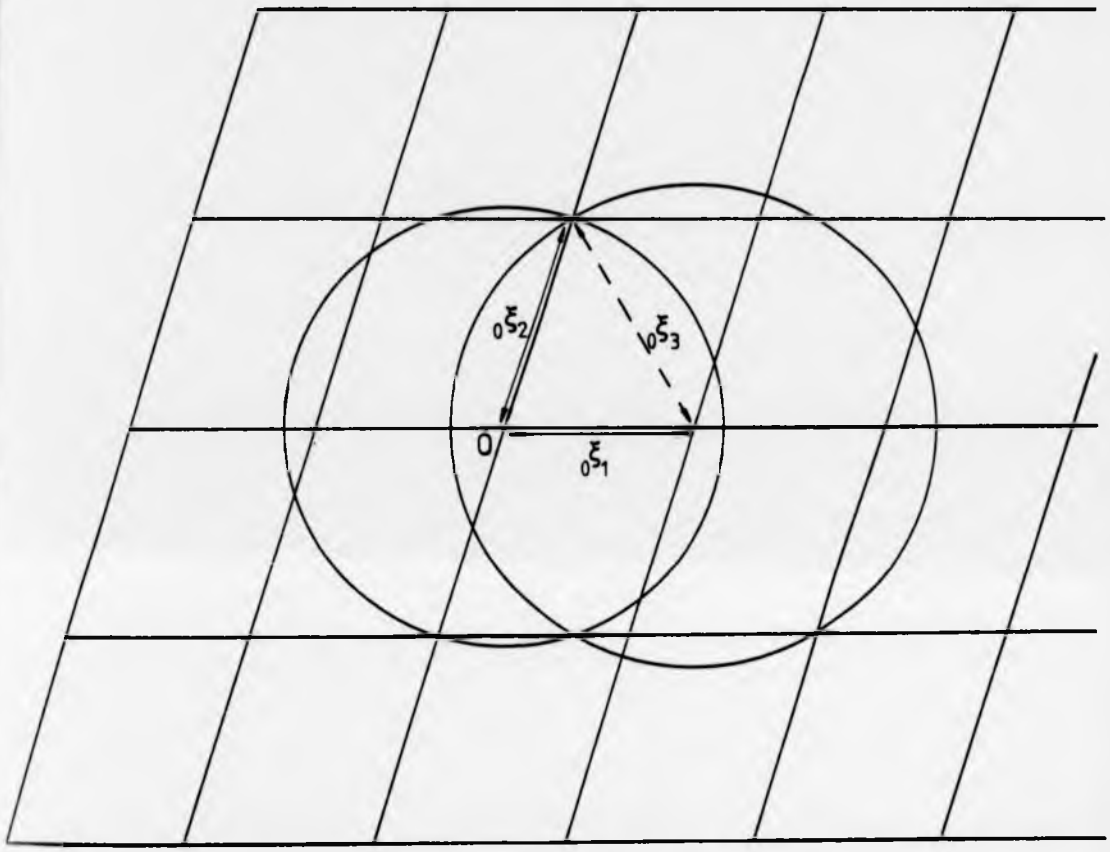

FIG.4.1 : TRIANGULATION PROCEDURE AND ITS EXTENSION TO FORM A LATTICE.

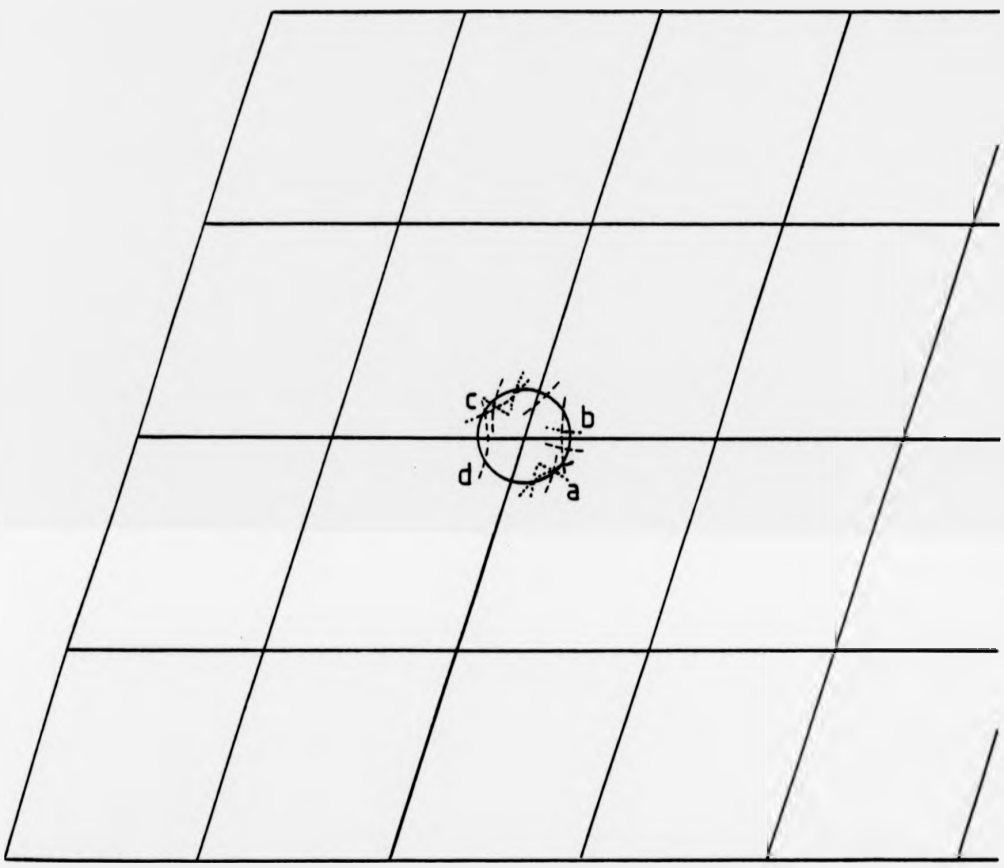

FIG. 4.2 : DIRECTION OF OFFSETTING

FULL CIRCLE : ${}_1\xi_1$

POINTS a, b, c AND d : POSSIBLE ORIGINS DERIVED FROM ${}_1\xi_2$

DOTTED ARCS : ARCS PASS AROUND POINTS a, b AND c FROM ${}_1\xi_3$

DASHED ARCS : ARCS PASS AROUND POINTS a AND c FROM ${}_1\xi_4$

choices of origin when, initially, two or three $_1\xi$-values were tested. The same procedure was employed for the other layers, but each origin being displaced by the same amount as that of the previous one and in the same direction (Figure (4.3)).

(b) Determination of c^*, α^* and β^*

The unit cell reciprocal parameters a^*, b^* and γ^* can be determined directly from the construction of the lattice, but c^*, α^* and β^* must be deduced geometrically. This is done by considering the projection of (001) on to the zero reciprocal layer, as considered in Figure (4.4).

Let

OS = the magnitude of the projection of c^* on to the a^*b^*-plane.

α' = the angle between b^* and OS

β' = the angle between a^* and OS

and $\beta' = \gamma^* + \alpha'$

Then, in the triangle OSP

$$OP = (OS^2 + SP^2)^{1/2} \qquad \text{- - - - - - - - - - - - (1)}$$

Let the angle $OPS = \theta$, then

$$OS = OP \sin\theta \qquad \text{- - - - - - - - - - - - (2)}$$

$$SP = OP \cos\theta \qquad \text{- - - - - - - - - - - - (3)}$$

In the triangle ORP ,

$$OR = OP \cos\alpha^* \qquad \text{- - - - - - - - - - - - (4)}$$

$$PR = OP \sin\alpha^* \qquad \text{- - - - - - - - - - - - (5)}$$

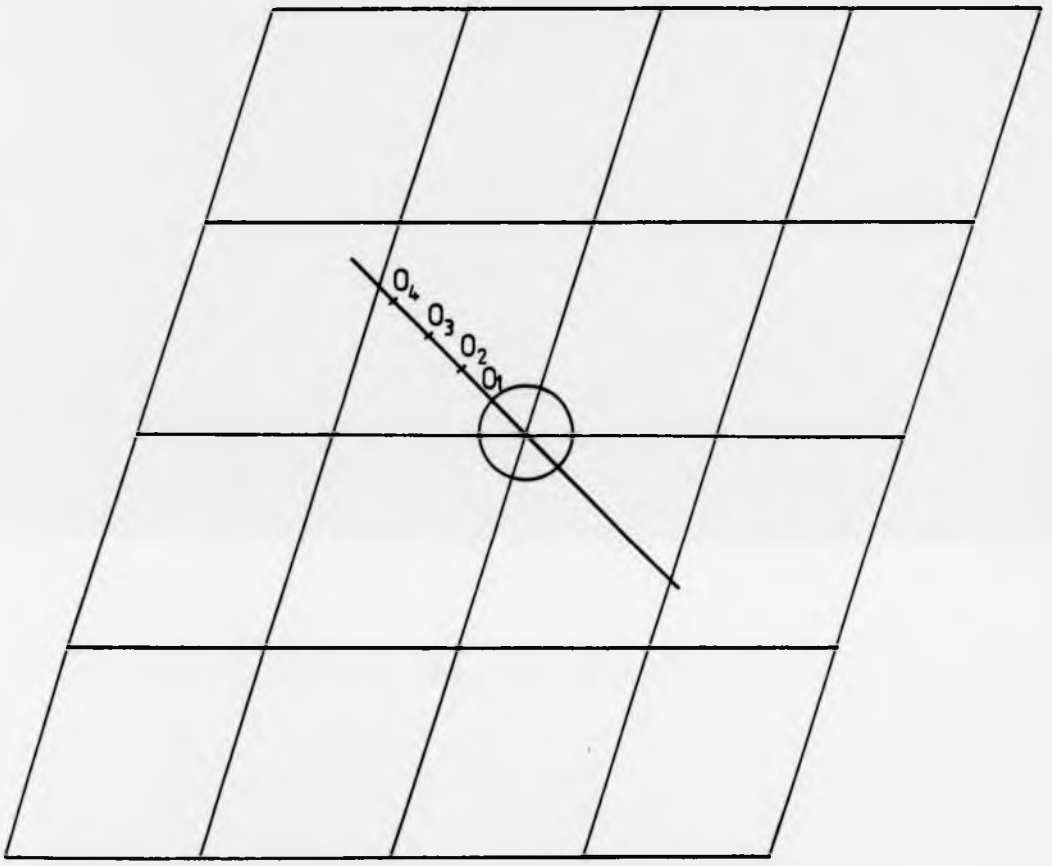

FIG.4.3 : THE RECIPROCAL LATTICE, SHOWING THE ORIGINS OF THE FIRST, SECOND, ETC. LAYERS.

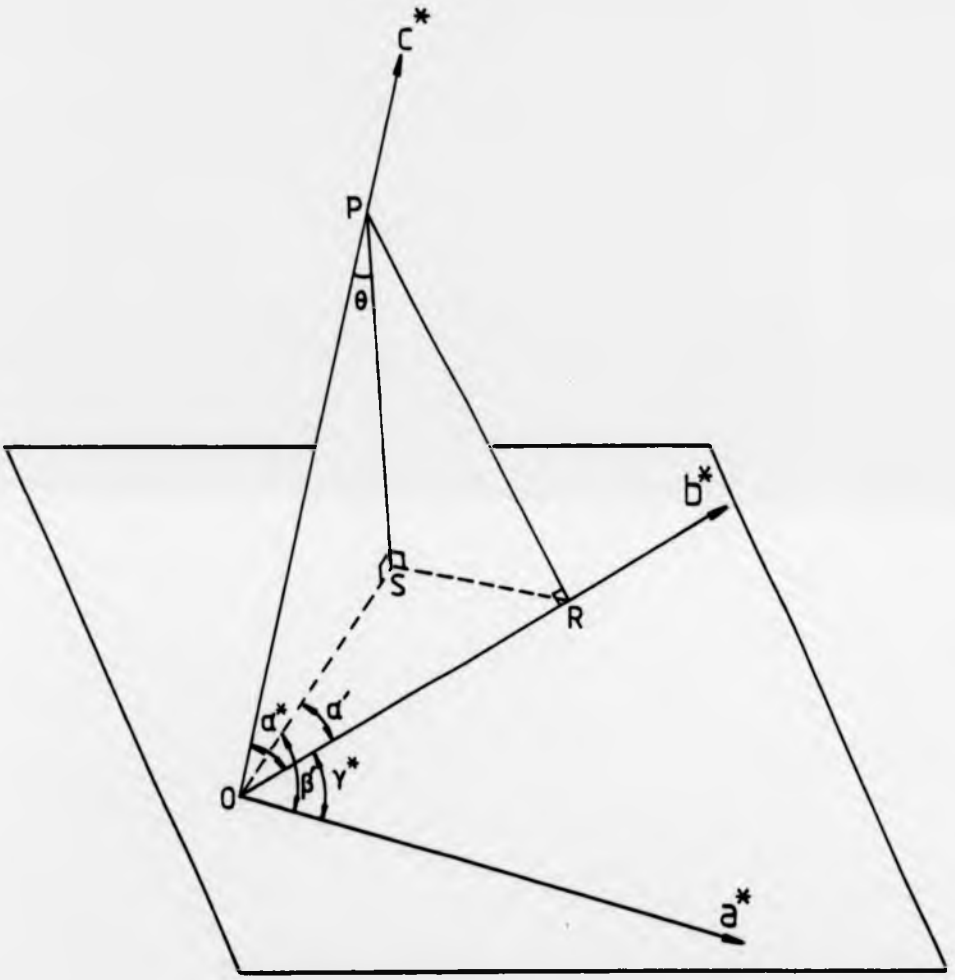

FIG. 4.4 : PROJECTION OF (001) ONTO ZERO LAYER RECIPROCAL LATTICE.

Now in the oblique triangle OSR ,

$$SR^2 = OS^2 + OR^2 - 2\,OS.OR\cos\alpha' \quad \text{- - - - - - - - - (6)}$$

While, in the triangle PSR

$$SR^2 = PR^2 - SP^2 \quad \text{- - - - - - - - - (7)}$$

Substituting eqns. (2-6) in eqn.(7), to get

$$OP^2.\sin^2\theta + OP^2.\cos^2\alpha^* - 2\,OP^2.\sin\theta.\cos\alpha^*.\cos\alpha' = OP^2.\sin^2\alpha^* - OP^2.\cos^2\theta.$$

The equation is simplified with $\sin^2\theta+\cos^2\theta = 1$,

$$\cos^2\alpha^* - 2\sin\theta\cos\alpha^*\cos\alpha' = \sin^2\alpha^* - 1$$

therefore, $\cos\alpha^* = \sin\theta\cos\alpha'$

Similarly,

$$\cos\beta^* = \sin\theta\cos\beta'$$

The parameters α', β', OS and OP are then measured directly from the lattice construction.

Then

$$SP = \zeta_{oo\bar{1}} \quad , \quad OS = \xi_{oo\bar{1}}$$

and $\zeta_{oo\bar{1}}$ and $\xi_{oo\bar{1}}$ are known from the reciprocal co-ordinates.

c^*, which is equal to OP, can be determined from eqn. (1) above. Finally, the values of α^* and β^* can be obtained.

(c) Unit Cell Refinement Procedure

The parameters of the trial unit cell were refined by the least squares method, i.e. the sum of the squares of the distance between the

observed and calculated film co-ordinates of the reflections is minimised. This procedure was realised in a computer program, developed by Hall[54], according to the following steps:-

(1) The reciprocal space co-ordinates for each reflection were calculated from the trial reciprocal unit cell parameters.

(2) If any tilt was present, the reciprocal space co-ordinates were corrected from tilt parameters which included: the angle of tilt (ϕ) (the angle between the fibre axis and the tilted c-axis) and the angle between the tilt line and the a*-axis, known as the azimuthal angle (X). The film co-ordinates were calculated from the reciprocal space co-ordinates.

(3) The observed co-ordinates were matched with the calculated co-ordinates in order to index the observed reflections.

(4) Correction to the trial cell parameters was calculated by a non-linear least-squares procedure to reduce the distance between the observed and calculated locations of the reflections.

(5) The procedure was repeated over several cycles of refinement until a minimum value of the difference between the observed and calculated positions was achieved.

4.2.2 Experimental and Results

(a) Calibration of Film-Specimen Distance

The X-ray diffraction photographs were taken using a Searle camera with a semicylindrical film-holder, as was described in Chapter Two. The film-specimen distance plays an important role in the determination of the unit cell, therefore, it is of importance that

it is set accurately.

This was performed by dusting a fibre with NaCl powder and mounting it in its holder. The X-ray diffraction patterns recorded revealed four powder rings, having an elliptical shape because of using a semicylindrical film. From their major and minor axes and the known d-spacing of the rings, the film-specimen distance was calculated. The average distance from three separate films was calculated and found to be $r = 30.0027$mm with a standard deviation $\sigma^2 = 0.000794$.

(b) Determination of the Unit Cell of α, β and γ-forms

As was mentioned in Chapter Three, there are three polymorphs of 6GT. The major problem in the determination of the unit cell was the uncertainty of whether any diffraction pattern represented a pure state. Some reflections might be there because there was a trace of another polymorph present or might belong to the major phase. Initial attempts used all the reflections on a given photograph; but the resulting unit cells often had a lower density than that of the fibre, contained many chains and for the β-phase did not correctly describe the tilt. Consequently, it was concluded that they were incorrect and that it would be necessary to decide more carefully whether certain reflections should be included or omitted from the determination. Therefore, in order to determine the unit cell for a particular polymorph, the reflections that appear intense in the particular diffraction pattern but are absent or appear weak in those of the other two polymorphs, were used in the construction of the reciprocal unit cell.

I. β-Form

The main objective was to obtain the highest purity of β-form relative to the other two polymorphs in the samples under investigation.

It was concluded, in Chapter Three, that the pure β-form was obtained in gravitationally spun fibres annealed at 150°C (Plate 2(j)); these samples could not be used for the determination of the unit cell because of their disorientation. However, an as-spun fibre with take-up velocity 50 m/min. annealed at 150°C (Plate 2(k)), was found to give an identical diffraction pattern (same relative intensities) but showing some orientation. This was sufficient for the identification of different layer lines but not good enough to locate the reflections accurately. Therefore, the pattern was used as a reference and any reflections in the measured pattern which did not appear in it were assumed to belong to a different phase.

Examples of how these reference patterns were used to deduce the phase causing certain reflections may be seen from Plate (5). Plate 5(a) is a diffraction photograph of two fibres annealed at 150°C, one drawn to draw ratio 3.5 (oriented β-form), the other gravitationally spun fibre (the unoriented β-form referred to above). The innermost equatorial reflection of the oriented fibre (d-spacing = 5.03°A) does not lie on a ring from the unoriented and so it is concluded that this is not a β-form reflection. In Plate 5(b), the ring pattern is from the same material as in Plate 5(a), but this oriented pattern is from a fibre drawn to draw ratio 7.5 annealed at 150°C. This is a mixture of α- and β-forms. Reflections not coinciding with rings were assigned to the α-form. In Plate 5(c) the ring pattern is due to as-prepared cast-film (γ-form), the oriented pattern is the same as in Plate 5(a). The innermost equatorial reflection is now seen to lie on a ring and so is assigned to the γ-form.

For the determination of β-form unit cell, two hot drawn fibres with draw ratios of 4.0 and 3.0, annealed at 150°C under constant length

PLATE (5): WAXS photographs of:

(a) cold drawn fibre (T.D.R.= 3.8) + gravitationally spun fibre — both annealed at 150°C

(b) cold drawn fibre (T.D.R.= 5.7) + gravitationally spun fibre — both annealed at 150°C

(c) cold drawn fibre (T.D.R.= 3.8) annealed at 150°C + as-prepared cast film

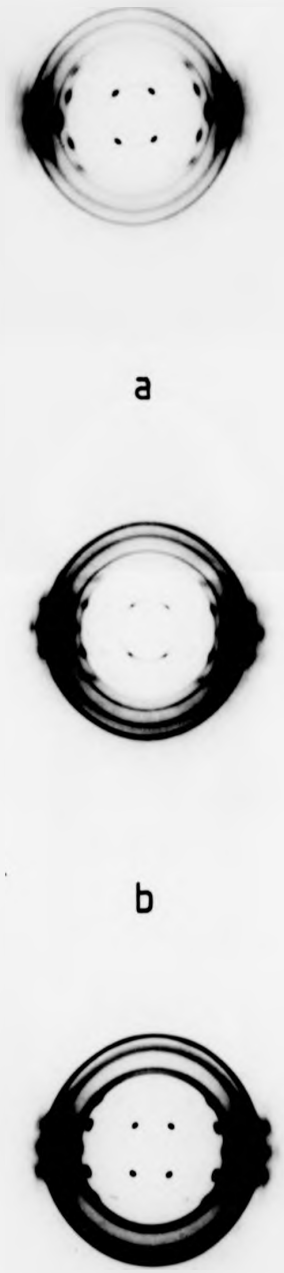

a

b

c

PLATE 5

PLATE (5): WAXS photographs of:

(a) cold drawn fibre (T.D.R.= 3.8) + gravitationally spun fibre — both annealed at 150°C

(b) cold drawn fibre (T.D.R.= 5.7) + gravitationally spun fibre — both annealed at 150°C

(c) cold drawn fibre (T.D.R.= 3.8) annealed at 150°C + as-prepared cast film

a

b

c

PLATE 5

for twelve hours were chosen. The choice of these two fibres was made because the first exhibited good orientation and the second exhibited very narrow line width. The second also had a high proportion of β-form which helped in deciding which reflections belonged to β-form. Since the diameter of the fibre was small, many filaments in a bundle were held parallel in a sample holder. The wide-angle X-ray diffraction patterns for the β-form are shown in Plate 6(a) and (b). The x-y co-ordinates of the diffraction spots on the films were measured for the largest possible number of reflections from photographs of different exposure times, i.e. 1, 2, 6 and 24 hours. The average data are listed in Table (4.1), together with the respective reciprocal co-ordinates. Using some of the reciprocal co-ordinates of the equatorial layer-line, the reciprocal unit cell was constructed, after numerous attempts by the trial and error method to establish a lattice which would fit all the equatorial reflections, as described in Section 4.2.1(a). The reciprocal unit cell was constructed with the following parameters:-

$$_{o}\xi_{1} = 0.32 \text{ r.l.u.} \qquad _{o}\xi_{2} = 0.38 \text{ r.l.u.} \qquad _{o}\xi_{3} = 0.41 \text{ r.l.u.}$$

and the constructed lattice was checked for the remaining $_{o}\xi$-values.

After the construction of the zero-layer lattice, the graphical method for the determination of the magnitude and direction of the offset (Section 4.2.1(b)) was applied for the construction of a three-dimensional lattice. The parameters of the trial reciprocal unit cell were deduced from Figures (4.1 - 4.3). The method, described by Bunn et al[55] and applied by Daubeny et al[7] in their work on 2GT, was used to determine the magnitude of the tilt angle and the direction of tilt between the chain axes and fibre axis. The tilt angle ϕ was

PLATE (6): WAXS photographs of:

hot drawn fibres annealed at 150°C:

(a) T.D.R.= 4

(b) T.D.R.= 3

and samples annealed at 90°C:

(c) as-spun fibre with take-up velocity 400 m/min.

(d) cast film drawn at ≈ 2.5

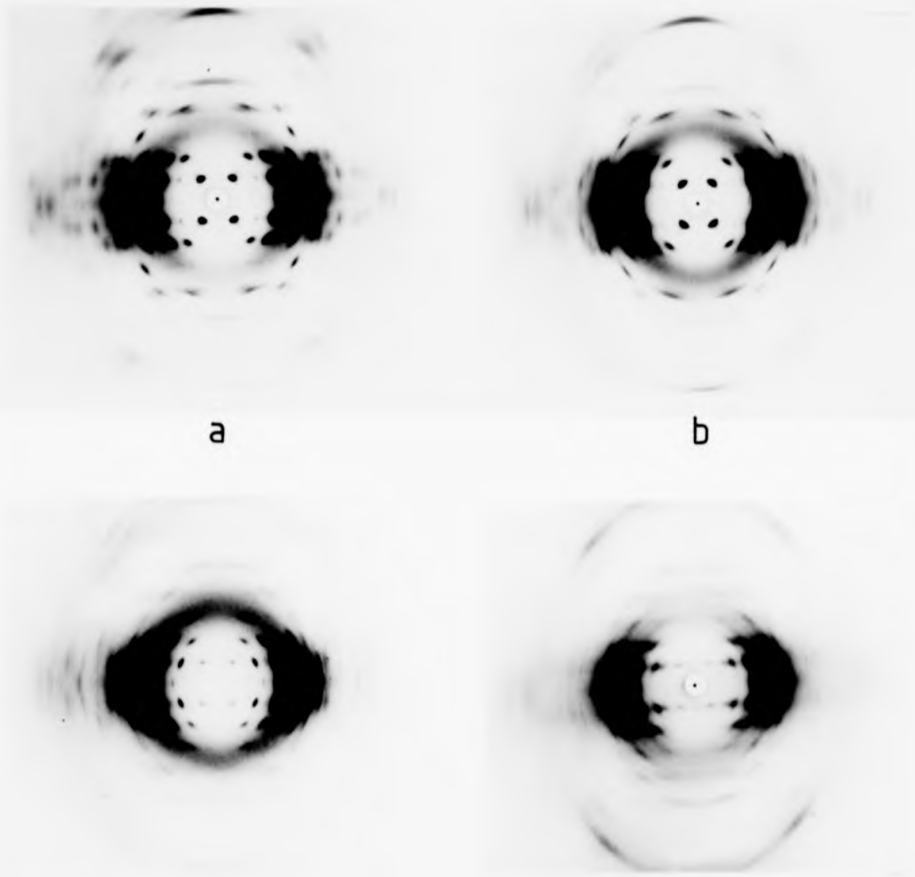

PLATE 6

PLATE (6): WAXS photographs of:

hot drawn fibres annealed at 150°C:

(a) T.D.R.= 4

(b) T.D.R.= 3

and samples annealed at 90°C:

(c) as-spun fibre with take-up velocity 400 m/min.

(d) cast film drawn at ≈ 2.5

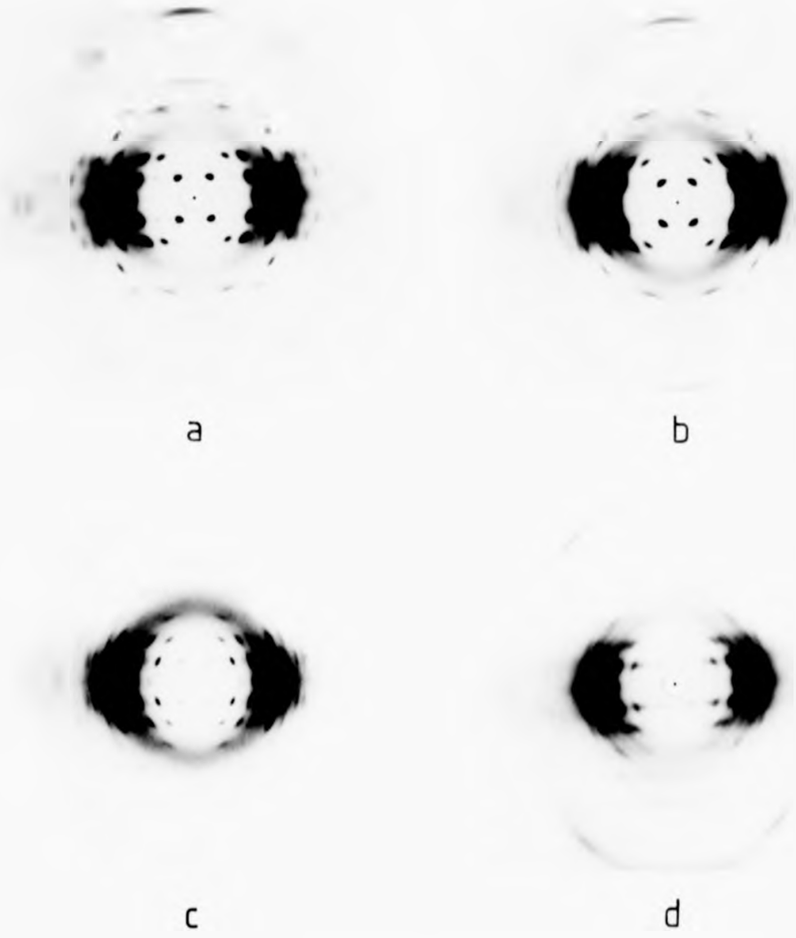

a b

c d

PLATE 6

calculated according to the relation given in Appendix 1, and the method of determination is shown in Figure (4.5); it represents the reciprocal lattice net for c-projection. It was observed that the (hll) reflections were displaced upwards, while the ($\bar{h}$ll) downwards. The magnitude of the tilt was such that the chain axes were, on average, inclined at an angle of 1^{o} to the fibre axis.

The parameters of the trial reciprocal unit cell and the tilt parameters were refined according to the procedure described in Section 4.2.1(c) and found to be

$a^* = 0.380$ r.l.u. $\quad \alpha^* = 116.6^{o}$

$b^* = 0.316$ r.l.u. $\quad \beta^* = 76.7^{o}$

$c^* = 0.122$ r.l.u. $\quad \gamma^* = 71.7^{o}$

The parameters of the real unit cell of β-form were found to be

$a = 4.75\,^{o}\!A \quad \alpha = 55.7^{o}$

$b = 6.23\,^{o}\!A \quad \beta = 116.0^{o}$

$c = 15.68\,^{o}\!A \quad \gamma = 118.8^{o}$

and the volume $V = 326.4\,^{o}\!A^3$.

The density of β-form was measured and found to be 1.251 gm/cm³. The density of the unit cell can be calculated for one monomer from the relation:

$$\mu_{100\%} = \frac{Mm_H}{V}$$

where $\mu_{100\%}$ = the density of 100% crystalline material, i.e. unit cell density,

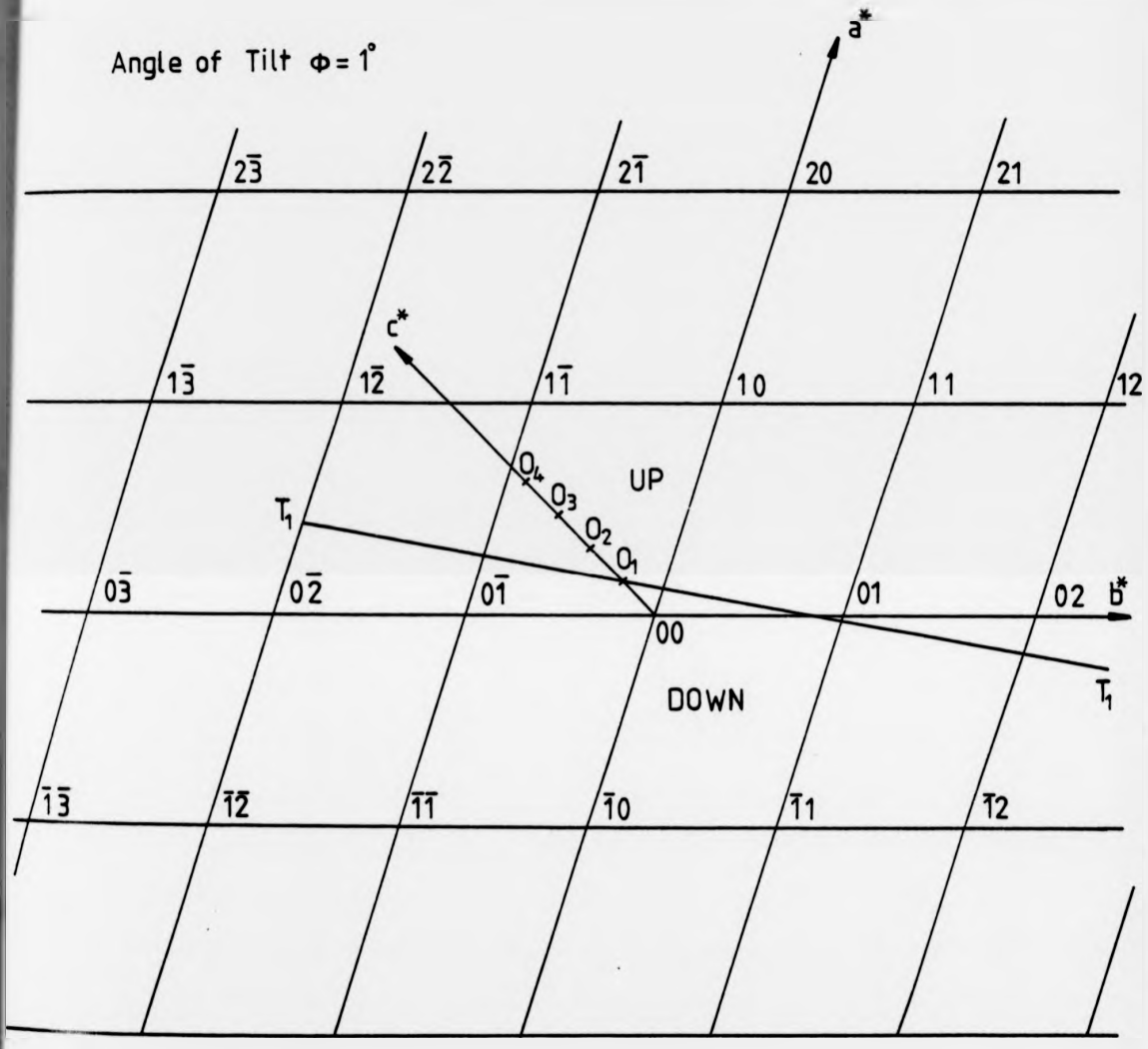

FIG. 4.5 : RECIPROCAL LATTICE NET FOR C-PROJECTION OF β-FORM.

M = the molecular weight of the chemical unit, which is the sum of the atomic weight of the atoms in the monomer, M_{6GT} = 248,

m_H = the mass of hydrogen atom (= 1.66×10^{-24}gm)

and V = the volume of the unit cell

Substituting the relevant values into the relation above, the calculated density of β-form was found to be 1.262 gm/cm^3. A comparison between the observed and calculated co-ordinates and real plane spacings is given in Table (4.2). The mean distance between the observed and calculated position of the reflections was found to be 0.033mm.

II. α-Form

The choice of a representative sample for the α-form proved rather difficult. As was mentioned in Chapter Three, the α-form develops as a consequence of drawing fibres to high draw ratios, which results in diffuseness of patterns. To overcome diffuseness, annealing was required; annealing, however, enhances the development of β-form which can complicate the investigations. It was, therefore, concluded after consideration of these factors that fibres spun with take-up velocity 400 m/min. annealed under constant length at 90^{o}C for two hours, offered the clearest pattern of α-form.

Plate 6(c) shows the wide-angle X-ray diffraction pattern of α-form, using a bundle of parallel fibres. The x-y co-ordinates of the diffraction spots on the film were measured for the largest possible number of reflections from photographs taken at different times of exposure. The data are listed in Table (4.3), together with the

respective reciprocal co-ordinates. The trial and error method was used repeatedly in the construction of a lattice for the equatorial layer line. None of the constructed lattices would fit all of the equatorial reciprocal co-ordinates of α-form, and if one did after halving a* and b*, it was rejected on crystallographic grounds[56]; this will be discussed later in Section (4.4).

One such rejected cell is given here, which will be discussed later. The equatorial layer line of the reciprocal unit cell was constructed, as was described in Section 4.2.1(a), with ${}_o\xi_1$ = 0.17 r.l.u., ${}_o\xi_2$ = 0.23 r.l.u. and ${}_o\xi_3$ = 0.28 r.l.u. In order to fit the remaining ${}_o\xi$-values, ${}_o\xi_2$ had to be halved. The construction of the equatorial layer line is shown in Figure (4.6). The magnitude and direction of the offset was determined according to the same procedure as in β-form. The parameters of the trial reciprocal unit cell were determined and refined by the same procedure as that employed for β-form. The X-ray diffraction pattern for α-form (Plate 6(c)) shows that there was no evidence of crystal tilt with respect to the fibre axis.

The parameters of the reciprocal unit cell were found, after refinement, to be

a^* = 0.170 r.l.u. $\quad \alpha^* = 52.7^o$

b^* = 0.112 r.l.u. $\quad \beta^* = 90.0^o$

c^* = 0.125 r.l.u. $\quad \gamma^* = 90.0^o$

The observed and calculated co-ordinates and real plane spacings are listed in Table (4.4). The mean distance between the observed and calculated position of reflections was found to be 0.021mm. The parameters of the real unit cell of α-form were found to be

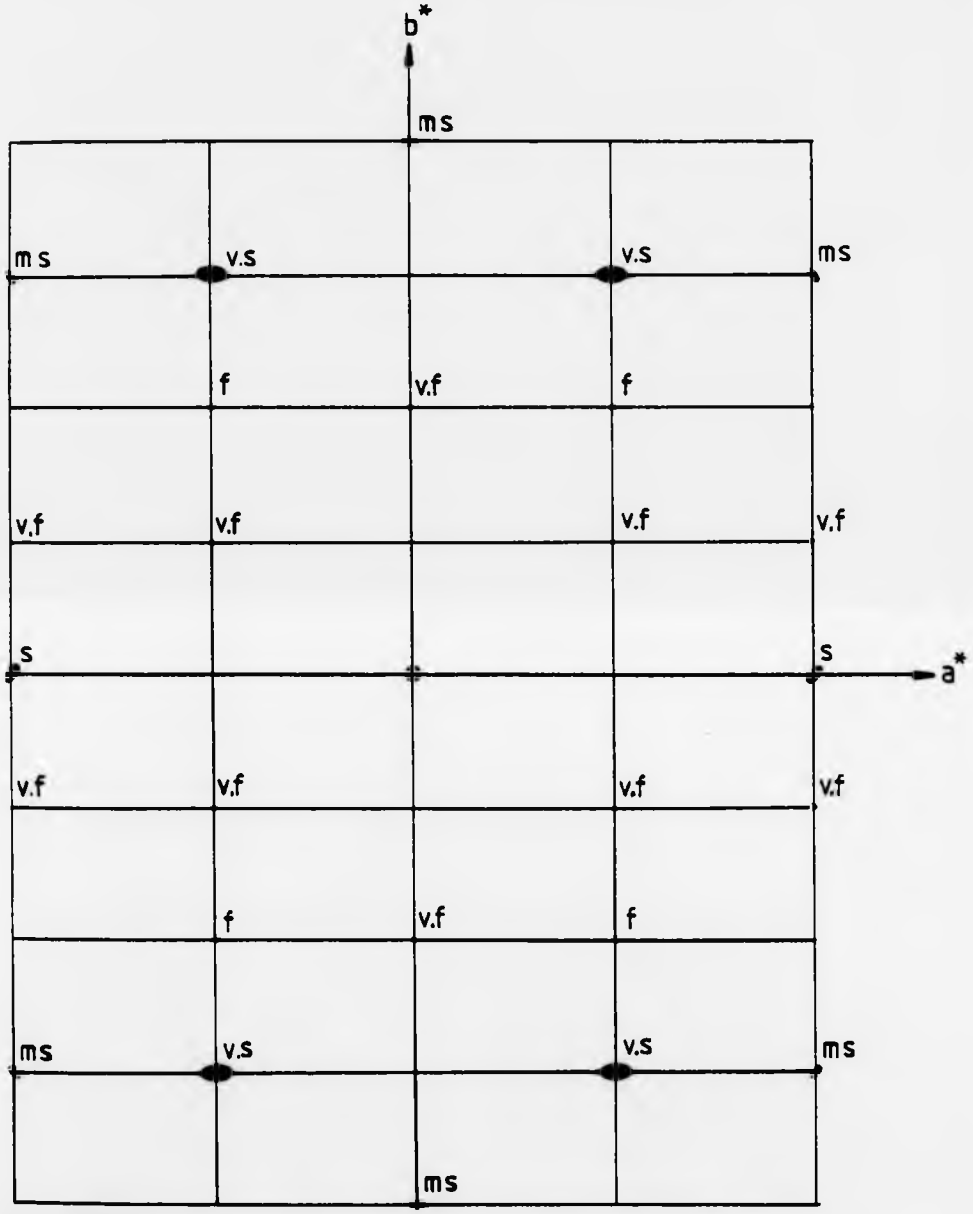

v.s:Very Strong
ms:Medium-to-Strong
s :Strong
f :Faint
v.f:Very Faint

FIG. 4.6 : EQUATORIAL RECIPROCAL LATTICE NET OF THE α-FORM

$a = 9.06\,^{o}A \qquad \alpha = 127.3^{o}$

$b = 17.24\,^{o}A \qquad \beta = 90.0^{o}$

$c = 15.51\,^{o}A \qquad \gamma = 90.0^{o}$

and the volume $V = 1928.19\,^{o}A^{3}$. The measured density and calculated unit cell density were found to be 1.242 gm/cm^3 and 0.214 gm/cm^3 (for one chain per cell) respectively.

III. γ-Form

The preparation of a sample exhibiting good γ-form was restricted to a cast film drawn to draw ratio 2.5, annealed at 90^{o}C for two hours; other possible samples proved unsuitable in view of the difficulties encountered (Chapter Three).

The wide-angle X-ray diffraction pattern of γ-form is shown in Plate 6(d); the x-y co-ordinates of the reflections were measured from photographs taken with different times of exposure. The data obtained are listed in Table (4.5), together with the respective reciprocal co-ordinates.

From the equatorial layer line, only one possible reciprocal unit cell could be constructed; only three strong and well defined reflections, i.e. $_{o}\xi_{1}$ = 0.30 r.l.u., $_{o}\xi_{2}$ = 0.39 r.l.u. and $_{o}\xi_{3}$ = 0.44 r.l.u. could be used. This lattice was checked for the remaining $_{o}\xi$-values of the diffuse and weak reflections. The magnitude and direction of the offset were determined only after halving the $_{o}\xi_{1}$, a condition required to fit the $_{1}\xi$-values. The parameters of the trial reciprocal unit cell were then determined from the reciprocal lattice net and then refined by the same procedure, described in Section 4.2.1(c).

The parameters of the reciprocal unit cell were found, after refinement, to be

$a^* = 0.152$ r.l.u. $\quad \alpha^* = 52.1^o$

$b^* = 0.388$ r.l.u. $\quad \beta^* = 75.1^o$

$c^* = 0.128$ r.l.u. $\quad \gamma^* = 76.8^o$

The observed and calculated co-ordinates and real plane spacings are listed in Table (4.6). The mean distance between the observed and calculated position of reflections is 0.046mm.

The parameters of the real unit cell of γ-form were found to be

$a = 10.56\,^oA$ $\quad \alpha = 126.2^o$

$b = 5.05\,^oA$ $\quad \beta = 98.7^o$

$c = 15.51\,^oA$ $\quad \gamma = 95.2^o$

and the volume $V = 642.35\,^oA^3$.

The measured density and calculated unit cell density were found to be 1.256 gm/cm^3 and 0.641 gm/cm^3 (for one chain per cell) respectively.

4.3 DETERMINATION OF UNIT CELLS FROM DOUBLE-ORIENTATION FILMS, USING THE WEISSENBERG CAMERA

The photographs of doubly-oriented specimens were used to check the unit cells that have been deduced from methods using uniaxial oriented specimens[52]. This check was done because of the assumption made regarding which reflections should be omitted and which should be included, as some other independent confirmation of the cells was desirable. In the diffraction patterns of axially-oriented materials

TABLE (4.1)

LOCATION OF THE DIFFRACTION SPOTS OF β-FORM

(Cartesian and Reciprocal Lattice Co-ordinates)

x(mm)	y(mm)	ξ	ζ
4.84*	0.0	0.1611	0.0
9.65	0.0	0.3203	0.0
11.35	0.0	0.3760	0.0
12.52	0.0	0.4143	0.0
15.80*	0.0	0.5206	0.0
17.90	0.0	0.5878	0.0
19.57	0.0	0.6408	0.0
22.38	0.0	0.7288	0.0
23.50	0.0	0.7634	0.0
24.22*	0.0	0.7855	0.0
25.83	0.0	0.8346	0.0
27.87	0.0	0.8959	0.0
2.28	3.01	0.0759	0.0998
7.98	2.95	0.2646	0.0979
10.73	3.32	0.3547	0.1100
11.48	3.05	0.3794	0.1011
12.52	2.72	0.4134	0.0903
14.45	2.85	0.4759	0.0946
17.77	3.20	0.5820	0.1061
20.55	3.35	0.6696	0.1110
21.55	3.04	0.7012	0.1008
22.36	3.25	0.7260	0.1077
26.93	3.23	0.8653	0.1070
28.38	3.45	0.9081	0.1142
4.46	6.02	0.1484	0.1967
6.97	5.90	0.2304	0.1930
10.78	6.23	0.3542	0.2033
13.95	5.60	0.4572	0.1835
14.80	6.10	0.4838	0.1992
16.23	5.82	0.5298	0.1904
17.42	5.90	0.5674	0.1930
19.87	6.40	0.6434	0.2086
22.20	6.52	0.7152	0.2124
24.13	6.03	0.7753	0.1970
10.91	9.45	0.3562	0.3004
15.18	9.20	0.4914	0.2932
19.05	9.20	0.6120	0.2932
20.00	9.38	0.6409	0.2984
27.70	8.80	0.8736	0.2815

TABLE (4.1) continued

x(mm)	y(mm)	ξ	ζ
4.35	13.22	0.1625	0.4032
6.32	12.70	0.2167	0.3898
9.05	12.80	0.2991	0.3924
10.30	13.10	0.3375	0.4001
17.60	12.65	0.5606	0.3885
20.94	12.87	0.6606	0.3942
23.94	12.50	0.7504	0.3846
7.38	17.20	0.2642	0.4974
11.06	16.83	0.3654	0.4892
12.65	17.20	0.4117	0.4974
15.52	17.33	0.4945	0.5002
16.30	17.45	0.5170	0.5028
23.45	16.53	0.7237	0.4826
25.38	16.53	0.7782	0.4826
13.38	21.40	0.4402	0.5807
15.68	22.44	0.5035	0.5989

* reflections fit the reciprocal unit cell only when b* is halved.

TABLE (4.2)

OBSERVED AND CALCULATED
CARTESIAN CO-ORDINATES AND REAL PLANE SPACINGS
FOR THE β-FORM UNIT CELL

h	k	l	x (mm) obs	y (mm) obs	x (mm) calc	y (mm) calc	d (Å) obs	d (Å) calc
0	1	0	9.65	0.00	9.52	-0.02	4.816	4.882
1	0	0	11.35	0.00	11.48	-0.15	4.102	4.054
1	$\bar{1}$	0	12.52	0.00	12.42	-0.13	3.723	3.753
1	1	0	17.90	0.00	17.25	-0.16	2.624	2.726
1	$\bar{2}$	0	-	-	19.12	-0.11	-	2.462
0	2	0	19.57	0.00	19.29	-0.04	2.408	2.441
2	$\bar{1}$	0	22.38	0.00	22.30	-0.27	2.116	2.124
2	0	0	23.50	0.00	23.42	-0.29	2.020	2.027
2	$\bar{2}$	0	-	-	25.41	-0.25	-	1.877
1	2	0	25.83	0.00	25.81	-0.18	1.848	1.850
1	$\bar{3}$	0	27.87	0.00	28.12	-0.09	1.722	1.708
2	1	0	-	-	28.38	-0.31	-	1.693
0	0	1	2.28	3.01	2.21	2.95	12.297	12.599
0	1	1	7.98	2.95	8.02	2.93	5.467	5.449
$\bar{1}$	1	1	-	-	10.35	3.08	-	4.317
$\bar{1}$	0	1	10.73	3.32	10.81	3.10	4.153	4.148
0	$\bar{1}$	1	11.48	3.05	11.31	2.97	3.929	3.989
1	0	1	12.52	2.72	12.58	2.80	3.645	3.623
1	$\bar{1}$	1	14.45	2.85	14.60	2.82	3.179	3.148
$\bar{1}$	2	1	-	-	16.87	3.06	-	2.741
1	1	1	-	-	17.06	2.78	-	2.718
0	2	1	17.77	3.20	17.67	2.91	2.607	2.627
$\bar{1}$	$\bar{1}$	1	17.77	3.20	17.74	3.12	2.607	2.613
$\bar{2}$	1	1	20.55	3.35	20.66	3.23	2.273	2.263
0	$\bar{2}$	1	-	-	21.14	2.99	-	2.218
1	$\bar{2}$	1	21.55	3.04	21.50	2.84	2.177	2.185
$\bar{2}$	0	1	22.36	3.25	22.63	3.25	2.101	2.078
$\bar{2}$	2	1	-	-	23.23	3.21	-	2.029
2	$\bar{1}$	1	-	-	24.17	2.67	-	1.959
2	0	1	-	-	24.52	2.65	-	1.933
1	2	1	-	-	25.04	2.76	-	1.895
$\bar{1}$	3	1	-	-	25.87	3.04	-	1.836
$\bar{1}$	$\bar{2}$	1	26.93	3.23	26.90	3.14	1.769	1.771
2	$\bar{2}$	1	-	-	27.78	2.69	-	1.721
0	3	1	-	-	27.89	2.89	-	1.715
$\bar{2}$	$\bar{1}$	1	28.38	3.45	28.38	3.26	1.685	1.686
2	1	1	-	-	28.73	2.63	-	1.670
$\bar{2}$	3	1	-	-	29.38	3.19	-	1.634
0	0	2	4.46	6.02	4.43	5.99	6.260	6.299
0	1	2	6.97	5.90	6.92	5.97	5.133	5.130
$\bar{1}$	1	2	-	-	8.39	6.12	-	4.520
$\bar{1}$	0	2	10.78	6.23	10.60	6.14	3.776	3.836
0	$\bar{1}$	2	-	-	13.32	6.01	-	3.222
1	0	2	13.95	5.60	14.01	5.83	3.131	3.099
$\bar{1}$	2	2	14.80	6.10	14.70	6.10	2.948	2.964
0	2	2	16.23	5.82	16.29	5.95	2.740	2.725
1	$\bar{1}$	2	-	-	16.93	5.85	-	2.641

TABLE (4.2) continued

h	k	l	x (mm) obs	y (mm) obs	x (mm) calc	y (mm) calc	d (Å) obs	d (Å) calc
1	1	2	17.42	5.90	17.30	5.81	2.574	2.593
$\bar{1}$	$\bar{1}$	2	-	-	18.63	6.16	-	2.419
$\bar{2}$	1	2	19.87	6.40	19.28	6.29	2.280	2.343
$\bar{2}$	2	2	-	-	21.19	6.26	-	2.158
$\bar{2}$	0	2	22.20	6.52	22.16	6.30	2.067	2.074
0	$\bar{2}$	2	-	-	23.23	6.03	-	1.995
$\bar{1}$	3	2	-	-	23.80	6.08	-	1.951
1	$\bar{2}$	2	24.13	6.03	24.04	5.87	1.928	1.937
1	2	2	-	-	24.59	5.79	-	1.899
0	1	3	-	-	6.37	9.19	-	4.267
$\bar{1}$	1	3	-	-	6.49	9.36	-	4.195
0	0	3	-	-	6.65	9.21	-	4.200
$\bar{1}$	0	3	10.91	9.45	10.88	9.38	3.310	3.325
$\bar{1}$	2	3	-	-	12.55	9.33	-	3.055
0	2	3	15.18	9.20	15.15	9.17	2.695	2.701
0	$\bar{1}$	3	-	-	15.53	9.23	-	2.650
1	0	3	-	-	15.79	9.04	-	2.629
1	1	3	-	-	17.90	9.02	-	2.393
$\bar{2}$	1	3	-	-	18.07	9.52	-	2.354
$\bar{2}$	2	3	19.05	9.20	19.27	9.50	2.273	2.242
1	$\bar{1}$	3	-	-	19.41	9.07	-	2.244
$\bar{1}$	$\bar{1}$	3	20.00	9.38	19.86	9.40	2.182	2.193
$\bar{1}$	3	3	-	-	21.84	9.31	-	2.036
$\bar{2}$	0	3	-	-	22.02	9.55	-	2.017
1	2	3	-	-	24.46	9.00	-	1.861
$\bar{2}$	3	3	-	-	24.98	9.48	-	1.822
0	3	3	-	-	25.16	9.15	-	1.816
0	$\bar{2}$	3	-	-	25.58	9.25	-	1.790
1	$\bar{2}$	3	-	-	26.80	9.09	-	1.724
2	0	3	27.70	8.80	27.69	8.88	1.681	1.680
2	$\bar{1}$	3	-	-	28.71	8.90	-	1.630
$\bar{1}$	1	4	4.35	13.22	4.53	12.93	3.548	3.593
0	1	4	6.32	12.70	6.41	12.73	3.458	3.441
0	0	4	9.05	12.80	8.90	12.76	3.126	3.150
$\bar{1}$	2	4	10.30	13.10	10.26	12.90	2.946	2.974
$\bar{1}$	0	4	-	-	11.57	12.95	-	2.823
0	2	4	-	-	14.22	12.71	-	2.565
$\bar{2}$	1	4	-	-	17.08	13.11	-	2.283
$\bar{2}$	2	4	17.60	12.65	17.38	13.09	2.261	2.260
1	0	4	17.60	12.65	17.80	12.57	2.261	2.248
0	$\bar{1}$	4	-	-	17.91	12.78	-	2.230
1	1	4	-	-	18.85	12.55	-	2.165
$\bar{1}$	3	4	-	-	19.95	12.87	-	2.073
$\bar{1}$	$\bar{1}$	4	20.94	12.87	21.43	12.97	2.005	1.970
1	$\bar{1}$	4	-	-	22.09	12.60	-	1.938
$\bar{2}$	0	4	-	-	22.19	13.13	-	1.918
$\bar{2}$	3	4	-	-	22.89	13.06	-	1.878
0	3	4	23.94	12.50	24.12	12.69	1.829	1.815
1	2	4	-	-	24.66	12.52	-	1.789
$\bar{1}$	1	5	-	-	1.52	17.02	-	3.010
0	1	5	-	-	6.92	16.80	-	2.811
$\bar{1}$	2	5	7.38	17.20	7.44	16.99	2.739	2.757
0	0	5	11.06	16.83	11.15	16.83	2.526	2.520
$\bar{1}$	0	5	12.65	17.20	12.59	17.05	2.389	2.403

TABLE (4.2) continued

h	k	l	x (mm) obs	y (mm) obs	x (mm) calc	y (mm) calc	d (Å) obs	d (Å) calc
0	2	5	-	-	13.46	16.77	-	2.360
$\bar{2}$	2	5	15.52	17.33	15.38	17.21	2.193	2.207
$\bar{2}$	1	5	16.30	17.45	16.23	17.24	2.139	2.152
$\bar{1}$	3	5	-	-	17.99	16.96	-	2.056
1	0	5	-	-	20.06	16.61	-	1.948
1	1	5	-	-	20.13	16.58	-	1.945
0	$\bar{1}$	5	-	-	20.50	16.85	-	1.916
$\bar{2}$	3	5	-	-	20.73	17.18	-	1.895
$\bar{2}$	0	5	-	-	22.68	17.27	-	1.795
0	3	5	23.45	16.53	23.26	16.74	1.773	1.778
$\bar{1}$	$\bar{1}$	5	23.45	16.53	23.32	17.07	1.773	1.768
1	$\bar{1}$	5	25.38	16.53	25.02	16.64	1.684	1.699
1	2	5	25.38	16.53	25.19	16.55	1.684	1.692
$\bar{1}$	2	6	-	-	0.99	21.95	-	2.480
0	1	6	-	-	7.58	21.72	-	2.349
0	2	6	-	-	12.72	21.68	-	2.134
$\bar{2}$	2	6	-	-	12.96	22.23	-	2.097
0	0	6	13.38	21.40	13.40	21.75	2.117	2.100
$\bar{1}$	0	6	13.38	21.40	13.79	22.03	2.117	2.070
$\bar{2}$	1	6	15.68	22.44	15.39	22.27	1.971	1.990
$\bar{1}$	3	6	15.68	22.44	15.73	21.92	1.971	1.988

TABLE (4.3)

LOCATION OF THE DIFFRACTION SPOTS OF α-FORM

(Cartesian and Reciprocal Lattice Co-ordinates)

x(mm)	y(mm)	ξ	ζ
6.13	0.0	0.2038	0.0
6.77	0.0	0.2250	0.0
8.45	0.0	0.2805	0.0
10.30	0.0	0.3414	0.0
10.90	0.0	0.3611	0.0
11.36	0.0	0.3762	0.0
12.54	0.0	0.4147	0.0
13.59	0.0	0.4488	0.0
14.60	0.0	0.4816	0.0
17.90	0.0	0.5875	0.0
18.83	0.0	0.6170	0.0
20.65	0.0	0.6744	0.0
21.23	0.0	0.6925	0.0
23.38	0.0	0.7593	0.0
25.00	0.0	0.8089	0.0
26.35	0.0	0.8498	0.0
2.25	3.02	0.0749	0.1001
5.45	3.02	0.1809	0.1001
7.04	3.02	0.2334	0.1001
8.13	3.02	0.2694	0.1001
9.65	3.02	0.3193	0.1001
10.53	3.02	0.3481	0.1001
11.66	3.02	0.3850	0.1001
13.26	3.02	0.4370	0.1001
15.05	3.02	0.4949	0.1001
15.97	3.02	0.5244	0.1001
16.58	3.02	0.5439	0.1001
17.82	3.02	0.5835	0.1001
19.98	3.02	0.6517	0.1001
21.70	3.02	0.7054	0.1001
22.49	3.02	0.7299	0.1001
24.86	3.02	0.8026	0.1001
26.41	3.02	0.8495	0.1001
27.12	3.02	0.8708	0.1001
3.85	6.10	0.1284	0.1991
6.45	6.10	0.2132	0.1991
8.13	6.10	0.2680	0.1991
11.11	6.10	0.3648	0.1991
12.80	6.10	0.4194	0.1991
15.89	6.10	0.5183	0.1991
17.48	6.10	0.5686	0.1991
19.27	6.10	0.6249	0.1991
21.18	6.10	0.6843	0.1991
21.98	6.10	0.7090	0.1991
24.18	6.10	0.7762	0.1991
26.17	6.10	0.8361	0.1991
28.15	6.10	0.8948	0.1991

TABLE (4.3) continued

x(mm)	y(mm)	ξ	ζ
4.00	9.36	0.1378	0.2977
5.66	9.36	0.1894	0.2977
7.90	9.36	0.2604	0.2977
11.11	9.36	0.3624	0.2977
12.11	9.36	0.3941	0.2977
14.10	9.36	0.4570	0.2977
15.25	9.36	0.4931	0.2977
16.45	9.36	0.5307	0.2977
17.70	9.36	0.5665	0.2977
4.89	13.00	0.1763	0.3974
7.53	13.00	0.2534	0.3974
10.75	13.00	0.3510	0.3974
12.80	13.00	0.4136	0.3974
13.36	13.00	0.4307	0.3974
16.18	13.00	0.5167	0.3974
22.50	13.00	0.7061	0.3974
28.38	13.00	0.8761	0.3974
3.80	17.19	0.1771	0.4969
7.50	17.19	0.2679	0.4969
10.11	17.19	0.3391	0.4969
14.95	17.19	0.4778	0.4969
16.55	17.19	0.5240	0.4969
17.88	17.19	0.5624	0.4969
19.21	17.19	0.6007	0.4969
22.28	17.19	0.6884	0.4969
23.16	17.19	0.7133	0.4969
24.93	17.19	0.7631	0.4969
27.19	17.19	0.8263	0.4969
8.95	22.27	0.3311	0.5958
11.11	22.27	0.3841	0.5958
13.45	22.27	0.4473	0.5958
16.45	22.27	0.5234	0.5958
20.92	22.27	0.6436	0.5958
23.40	22.27	0.7089	0.5958
7.76	29.11	0.3568	0.6961
10.75	29.11	0.4131	0.6961
13.92	29.11	0.4808	0.6961
17.69	29.11	0.5672	0.6961

TABLE (4.4)

OBSERVED AND CALCULATED

CARTESIAN CO-ORDINATES AND REAL PLANE SPACINGS

FOR THE α-FORM UNIT CELL

h	k	l	x (mm) obs	y (mm) obs	x (mm) calc	y (mm) calc	d (Å) obs	d (Å) calc
0	1	0	-	-	3.38	0.00	-	13.713
1	0	0	-	-	5.11	0.00	-	9.064
1	1	0	6.13	0.00	6.13	0.00	7.562	7.562
0	2	0	6.77	0.00	6.76	0.00	6.850	6.856
1	2	0	8.45	0.00	8.49	0.00	5.495	5.468
0	3	0	10.30	0.00	10.17	0.00	4.515	4.571
2	0	0	10.30	0.00	10.26	0.00	4.515	4.532
2	1	0	10.90	0.00	10.81	0.00	4.269	4.303
1	3	0	11.36	0.00	11.41	0.00	4.098	4.081
2	2	0	12.54	0.00	12.33	0.00	3.717	3.781
0	4	0	13.50	0.00	13.62	0.00	3.434	3.428
2	3	0	14.60	0.00	14.52	0.00	3.201	3.218
1	4	0	14.60	0.00	14.57	0.00	3.201	3.206
3	0	0	-	-	15.49	0.00	-	3.021
3	1	0	-	-	15.87	0.00	-	2.951
3	2	0	-	-	16.96	0.00	-	2.765
0	5	0	-	-	17.10	0.00	-	2.743
2	4	0	-	-	17.16	0.00	-	2.734
1	5	0	17.90	0.00	17.89	0.00	2.624	2.625
3	3	0	18.83	0.00	18.66	0.00	2.498	2.521
2	5	0	-	-	20.10	0.00	-	2.346
0	6	0	20.65	0.00	20.65	0.00	2.286	2.285
3	4	0	20.65	0.00	20.83	0.00	2.286	2.267
4	0	0	20.65	0.00	20.84	0.00	2.286	2.266
4	1	0	21.23	0.00	21.13	0.00	2.226	2.236
1	6	0	21.23	0.00	21.33	0.00	2.226	2.216
4	2	0	-	-	22.00	0.00	-	2.152
2	6	0	23.38	0.00	23.25	0.00	2.030	2.041
3	5	0	23.38	0.00	23.37	0.00	2.030	2.031
4	3	0	23.38	0.00	23.38	0.00	2.030	2.030
0	7	0	-	-	24.28	0.00	-	1.959
1	7	0	25.00	0.00	24.87	0.00	1.906	1.915
4	4	0	25.00	0.00	25.21	0.00	1.906	1.890
3	6	0	26.35	0.00	26.21	0.00	1.814	1.823
5	0	0	26.35	0.00	26.37	0.00	1.814	1.813
2	7	0	26.35	0.00	26.60	0.00	1.814	1.798
5	1	0	-	-	26.61	0.00	-	1.797
5	2	0	-	-	27.34	0.00	-	1.753
0	$\bar{1}$	1	-	-	1.10	3.00	-	14.551
0	0	1	2.25	3.02	2.27	3.00	12.330	12.341
0	$\bar{2}$	1	-	-	4.49	3.00	-	8.601
1	$\bar{1}$	1	5.45	3.02	5.24	3.00	7.456	7.694
1	0	1	5.45	3.02	5.61	3.00	7.456	7.305
0	1	1	5.45	3.02	5.67	3.00	7.456	7.246
1	$\bar{2}$	1	7.04	3.02	6.82	3.00	6.069	6.239
1	1	1	-	-	7.65	3.00	-	5.990

contd.

TABLE (4.4) continued

h	k	l	x (mm) obs	y (mm) obs	x (mm) calc	y (mm) calc	d (^{o}A) obs	d (^{o}A) calc
0	$\bar{3}$	1	8.13	3.02	7.89	3.00	5.364	5.509
0	2	1	-	-	9.08	3.00	-	4.870
1	$\bar{3}$	1	9.65	3.02	9.43	3.00	4.607	4.708
2	$\bar{1}$	1	10.53	3.02	10.35	3.00	4.256	4.327
1	2	1	10.53	3.02	10.44	3.00	4.256	4.290
2	0	1	10.53	3.02	10.54	3.00	4.256	4.254
2	$\bar{2}$	1	-	-	11.24	3.00	-	4.010
0	$\bar{4}$	1	-	-	11.32	3.00	-	3.984
2	1	1	11.66	3.02	11.77	3.00	3.875	3.842
1	$\bar{4}$	1	-	-	12.45	3.00	-	3.647
0	3	1	-	-	12.52	3.00	-	3.629
2	$\bar{3}$	1	13.26	3.02	13.01	3.00	3.438	3.500
1	3	1	-	-	13.55	3.00	-	3.369
2	2	1	-	-	13.78	3.00	-	3.318
0	$\bar{5}$	1	15.02	3.02	14.79	3.00	3.053	3.105
2	$\bar{4}$	1	-	-	15.38	3.00	-	2.992
3	$\bar{1}$	1	-	-	15.57	3.00	-	2.958
1	$\bar{5}$	1	-	-	15.68	3.00	-	2.938
3	0	1	-	-	15.70	3.00	-	2.935
0	4	1	15.97	3.02	16.00	3.00	2.887	2.883
3	$\bar{2}$	1	-	-	16.19	3.00	-	2.851
2	3	1	-	-	16.30	3.00	-	2.833
3	1	1	16.58	3.02	16.57	3.00	2.787	2.789
1	4	1	-	-	16.84	3.00	-	2.748
3	$\bar{3}$	1	-	1	17.50	3.00	-	2.649
3	2	1	17.82	3.02	18.09	3.00	2.604	2.567
2	$\bar{5}$	1	-	-	18.14	3.00	-	2.562
0	$\bar{6}$	1	-	-	18.30	3.00	-	2.540
1	$\bar{6}$	1	-	-	19.05	3.00	-	2.445
2	4	1	-	-	19.16	3.00	-	2.433
3	$\bar{4}$	1	-	-	19.37	3.00	-	2.407
0	5	1	-	-	19.54	3.00	-	2.388
3	3	1	19.98	3.02	20.13	3.00	2.338	2.322
1	5	1	-	-	20.25	3.00	-	2.309
4	$\bar{1}$	1	-	-	20.92	3.00	-	2.239
4	0	1	-	-	21.03	3.00	-	2.229
2	$\bar{6}$	1	-	-	21.16	3.00	-	2.215
4	$\bar{2}$	1	-	-	21.41	3.00	-	2.191
3	$\bar{5}$	1	21.70	3.02	21.68	3.00	2.163	2.165
4	1	1	21.70	3.02	21.71	3.00	2.163	2.163
0	$\bar{8}$	1	21.70	3.02	21.89	3.00	2.163	2.147
2	$\bar{5}$	1	-	-	22.26	3.00	-	2.113
4	$\bar{3}$	1	22.49	3.02	22.45	3.00	2.092	2.096
1	$\bar{7}$	1	22.49	3.02	22.53	3.00	2.092	2.089
3	4	1	22.49	3.02	22.57	3.00	2.092	2.086
4	2	1	-	-	22.93	3.00	-	2.055
0	6	1	-	-	23.15	3.00	-	2.037
1	$\bar{6}$	1	-	-	23.76	3.00	-	1.987
4	$\bar{4}$	1	-	-	24.00	3.00	-	1.970
3	$\bar{6}$	1	-	-	24.34	3.00	-	1.944
2	$\bar{7}$	1	-	-	24.39	3.00	-	1.940
4	3	1	24.86	3.02	24.63	3.00	1.906	1.922
3	$\bar{5}$	1	1	1	25.32	3.00	-	1.874
0	$\bar{8}$	1	-	-	25.55	3.00	-	1.858
2	6	1	-	-	25.55	3.00	-	1.858

contd.

TABLE (4.4) continued

h	k	l	x (mm) obs	y (mm) obs	x (mm) calc	y (mm) calc	d (°A) obs	d (°A) calc
4	$\bar{5}$	1	-	-	25.97	3.00	-	1.830
1	$\bar{8}$	1	-	-	26.13	3.00	-	1.820
5	$\bar{1}$	1	26.41	3.02	26.46	3.00	1.802	1.799
5	0	1	26.41	3.02	26.55	3.00	1.802	1.794
4	4	1	-	-	26.74	3.00	-	1.782
0	7	1	-	-	26.85	3.00	-	1.775
5	$\bar{2}$	1	-	-	26.87	3.00	-	1.774
5	1	1	27.12	3.02	27.12	3.00	1.759	1.759
3	$\bar{7}$	1	27.12	3.02	27.27	3.00	1.759	1.750
1	7	1	-	-	27.40	3.00	-	1.742
5	$\bar{3}$	1	-	-	27.75	3.00	-	1.722
2	8	1	-	-	27.80	3.00	-	1.719
0	$\bar{1}$	2	-	-	1.01	6.09	-	7.612
0	$\bar{2}$	2	-	-	2.14	6.09	-	7.612
0	0	2	3.85	6.10	4.55	6.09	6.505	6.171
1	$\bar{1}$	2	-	-	5.26	6.09	-	5.829
1	$\bar{2}$	2	-	-	5.59	6.09	-	5.674
0	$\bar{3}$	2	-	-	5.61	6.09	-	5.665
1	0	2	6.45	6.10	6.89	6.09	5.284	5.101
1	$\bar{3}$	2	-	-	7.64	6.09	-	4.804
0	1	2	8.13	6.10	8.00	6.09	4.617	4.667
0	$\bar{4}$	2	-	-	9.06	6.09	-	4.301
1	1	2	-	-	9.54	6.09	-	4.150
2	$\bar{1}$	2	-	-	10.42	6.09	-	3.894
1	$\bar{4}$	2	-	-	10.45	6.09	-	3.886
2	$\bar{2}$	2	-	-	10.59	6.09	-	3.847
2	0	2	11.11	6.10	11.34	6.09	3.709	3.653
0	2	2	11.11	6.10	11.46	6.09	3.709	3.623
2	$\bar{3}$	2	-	-	11.81	6.09	-	3.539
0	$\bar{5}$	2	-	-	12.53	6.09	-	3.379
1	2	2	12.80	6.10	12.60	6.09	3.320	3.364
2	1	2	-	-	13.14	6.09	-	3.251
1	$\bar{5}$	2	-	-	13.58	6.09	-	3.166
2	$\bar{4}$	2	-	-	13.83	6.09	-	3.120
0	3	2	-	-	14.96	6.09	-	2.922
2	2	2	-	-	15.54	6.09	-	2.830
3	$\bar{1}$	2	15.89	6.10	15.68	6.09	2.776	2.808
1	3	2	15.89	6.10	15.86	6.09	2.776	2.781
0	$\bar{6}$	2	15.89	6.10	16.04	6.09	2.776	2.755
3	0	2	-	-	16.33	6.09	-	2.714
2	$\bar{5}$	2	-	-	16.36	6.09	-	2.709
3	$\bar{3}$	2	-	-	16.67	6.09	-	2.666
1	$\bar{6}$	2	-	-	16.89	6.09	-	2.636
3	1	2	17.48	6.10	17.66	6.09	2.558	2.536
3	$\bar{4}$	2	-	-	18.19	6.09	-	2.472
2	3	2	-	-	18.33	6.09	-	2.456
0	4	2	-	-	18.51	6.09	-	2.435
2	$\bar{6}$	2	19.27	6.10	19.24	6.09	2.350	2.354
1	4	2	19.27	6.10	19.26	6.09	2.350	2.352
3	2	2	-	-	19.56	6.09	-	2.320
0	$\bar{7}$	2	-	-	19.61	6.09	-	2.315
3	$\bar{5}$	2	-	-	20.23	6.09	-	2.252
1	$\bar{7}$	2	-	-	20.33	6.09	-	2.243

contd.

TABLE (4.4) continued

h	k	l	x (mm) obs	y (mm) obs	x (mm) calc	y (mm) calc	d (^{o}A) obs	d (^{o}A) calc
4	$\bar{1}$	2	21.18	6.10	21.08	6.09	2.163	2.172
4	$\bar{2}$	2	21.18	6.10	21.18	6.09	2.163	2.164
2	4	2	21.18	6.10	21.38	6.09	2.163	2.145
4	0	2	-	-	21.59	6.09	-	2.127
4	$\bar{3}$	2	21.98	6.10	21.86	6.09	2.093	2.104
3	3	2	21.98	6.10	21.90	6.09	2.093	2.101
0	5	2	21.98	6.10	22.12	6.09	2.093	2.081
2	$\bar{7}$	2	-	-	22.36	6.09	-	2.062
4	1	2	-	-	22.65	6.09	-	2.039
3	$\bar{6}$	2	-	-	22.69	6.09	-	2.036
1	5	2	-	-	22.78	6.09	-	2.029
4	$\bar{4}$	2	-	-	23.08	6.09	-	2.005
0	8	2	-	-	23.25	6.09	-	1.992
1	$\bar{8}$	2	24.18	6.10	23.88	6.09	1.924	1.945
4	2	2	24.18	6.10	24.22	6.09	1.924	1.921
3	4	2	-	-	24.58	6.09	-	1.896
2	$\bar{5}$	2	-	-	24.65	6.09	-	1.891
4	$\bar{5}$	2	-	-	24.79	6.09	-	1.882
3	$\bar{7}$	2	-	-	25.46	6.09	-	1.838
2	$\bar{8}$	2	-	-	25.69	6.09	-	1.824
0	6	2	-	-	25.83	6.09	-	1.815
4	3	2	26.17	6.10	26.22	6.09	1.793	1.791
1	6	2	26.17	6.10	26.41	6.09	1.793	1.779
5	$\bar{1}$	2	-	-	26.67	6.09	-	1.764
5	$\bar{2}$	2	-	-	26.75	6.09	-	1.759
4	$\bar{6}$	2	-	-	26.91	6.09	-	1.750
0	9	2	-	-	26.98	6.09	-	1.746
5	0	2	-	-	27.09	6.09	-	1.739
5	$\bar{3}$	2	-	-	27.32	6.09	-	1.727
1	$\bar{9}$	2	-	-	27.54	6.09	-	1.714
3	5	2	-	-	27.55	6.09	-	1.714
5	1	2	28.15	6.10	27.99	6.09	1.682	1.690
2	6	2	28.15	6.10	28.09	6.09	1.685	1.682
5	$\bar{4}$	2	28.15	6.10	28.36	6.09	1.671	1.682
3	$\bar{8}$	2	-	-	28.51	6.09	-	1.663
4	4	2	-	-	28.59	6.09	-	1.659
2	$\bar{9}$	2	-	-	29.18	6.09	-	1.629
5	$\bar{2}$	2	-	-	29.34	6.09	-	1.621
4	$\bar{7}$	2	-	-	29.38	6.09	-	1.619
0	$\bar{3}$	3	-	-	3.09	9.38	-	4.850
0	$\bar{1}$	3	4.00	9.36	3.24	9.38	4.700	4.826
1	$\bar{2}$	3	-	-	5.04	9.38	-	4.491
1	$\bar{3}$	3	5.66	9.36	6.08	9.38	4.369	4.277
1	$\bar{1}$	3	5.66	9.36	6.16	9.38	4.369	4.260
0	$\bar{4}$	3	-	-	6.71	9.38	-	4.143
0	0	3	-	-	6.85	9.38	-	4.114
1	$\bar{4}$	3	7.90	9.36	8.52	9.38	3.898	3.768
1	0	3	-	-	8.63	9.38	-	3.746
0	$\bar{5}$	3	-	-	10.25	9.38	-	3.437
0	1	3	-	-	10.39	9.38	-	3.412
2	$\bar{2}$	3	-	-	10.41	9.38	-	3.408
2	$\bar{3}$	3	11.11	9.36	10.96	9.38	3.287	3.311
2	$\bar{1}$	3	11.11	9.36	11.00	9.38	3.287	3.304
1	$\bar{5}$	3	-	-	11.53	9.38	-	3.214

contd.

TABLE (4.4) continued

h	k	l	x (mm) obs	y (mm) obs	x (mm) calc	y (mm) calc	d (^{o}A) obs	d (^{o}A) calc
1	$\bar{1}$	3	-	-	11.66	9.38	-	3.193
2	$\bar{4}$	3	12.11	9.36	12.50	9.38	3.121	3.058
2	0	3	-	-	12.58	9.38	-	3.046
0	$\bar{6}$	3	-	-	13.80	9.38	-	2.867
0	$\bar{2}$	3	14.10	9.36	13.94	9.38	2.827	2.847
2	$\bar{5}$	3	-	-	14.75	9.38	-	2.739
1	$\bar{6}$	3	-	-	14.79	9.38	-	2.734
2	1	3	-	-	14.85	9.38	-	2.726
1	$\bar{2}$	3	15.25	9.36	14.92	9.38	2.676	2.717
3	$\bar{2}$	3	-	-	15.80	9.28	-	2.609
3	$\bar{3}$	3	-	-	16.17	9.38	-	2.565
3	$\bar{1}$	3	16.45	9.36	16.20	9.38	2.534	2.561
3	$\bar{4}$	3	-	-	17.28	9.38	-	2.441
3	0	3	-	-	17.34	9.38	-	2.435
0	$\bar{7}$	3	-	-	17.39	9.38	-	2.430
2	$\bar{6}$	3	17.70	9.36	17.46	9.38	2.399	2.423
0	3	3	17.70	9.36	17.53	9.38	2.399	2.415
2	$\bar{2}$	3	17.70	9.36	17.57	9.38	2.399	2.411
1	$\bar{7}$	3	-	-	18.20	9.38	-	2.347
1	3	3	-	-	18.34	9.38	-	2.334
0	$\bar{4}$	4	-	-	3.81	13.00	-	3.638
1	$\bar{3}$	4	4.89	13.00	4.79	13.00	3.546	3.554
1	$\bar{2}$	4	4.89	13.00	5.27	13.00	3.546	3.509
0	$\bar{1}$	4	-	-	5.38	13.00	-	3.498
1	$\bar{4}$	4	-	-	6.57	13.00	-	3.376
1	$\bar{1}$	4	7.53	13.00	7.59	13.00	3.271	3.263
0	$\bar{5}$	4	7.53	13.00	7.73	13.00	3.271	3.248
0	0	4	-	-	9.17	13.00	-	3.085
1	$\bar{5}$	4	-	-	9.41	13.00	-	3.058
2	$\bar{3}$	4	10.75	13.00	10.45	13.00	2.907	2.940
1	0	4	10.75	13.00	10.63	13.00	2.907	2.921
2	$\bar{2}$	4	10.75	13.00	10.68	13.00	2.907	2.915
2	$\bar{4}$	4	-	-	11.39	13.00	-	2.837
0	$\bar{6}$	4	-	-	11.43	13.00	-	2.832
2	$\bar{1}$	4	-	-	12.02	13.00	-	2.769
1	$\bar{6}$	4	12.80	13.00	12.64	13.00	2.688	2.704
0	1	4	12.80	13.00	12.85	13.00	2.688	2.682
2	$\bar{5}$	4	13.36	13.00	13.26	13.00	2.630	2.640
1	1	4	-	-	13.95	13.00	-	2.572
2	0	4	-	-	14.17	13.00	-	2.550
0	$\bar{7}$	4	-	-	15.11	13.00	-	2.461
2	$\bar{6}$	4	-	-	15.76	13.00	-	2.402
3	$\bar{3}$	4	16.18	13.00	16.01	13.00	2.365	2.380
1	$\bar{7}$	4	16.18	13.00	16.06	13.00	2.365	2.375
3	$\bar{2}$	4	16.18	13.00	16.16	13.00	2.365	2.366
0	2	4	16.18	13.00	16.54	13.00	2.365	2.334
3	$\bar{4}$	4	-	-	16.65	13.00	-	2.324
2	1	4	-	-	16.84	13.00	-	2.308
3	$\bar{1}$	4	-	-	17.10	13.00	-	2.287
4	$\bar{3}$	4	-	-	21.66	13.00	-	1.955
4	$\bar{2}$	4	-	-	21.78	13.00	-	1.947
2	$\bar{8}$	4	-	-	21.85	13.00	-	1.943
4	$\bar{4}$	4	22.50	13.00	22.16	13.00	1.903	1.923
3	$\bar{7}$	4	22.50	13.00	22.41	13.00	1.903	1.908

contd.

TABLE (4.4) continued

h	k	l	x (mm) obs	y (mm) obs	x (mm) calc	y (mm) calc	d (^{o}A) obs	d (^{o}A) calc
4	$\bar{1}$	4	22.50	13.00	22.51	13.00	1.903	1.902
0	$\bar{9}$	4	22.50	13.00	22.60	13.00	1.903	1.897
2	$\bar{3}$	4	-	-	23.13	13.00	-	1.865
4	$\bar{5}$	4	-	-	23.25	13.00	-	1.858
1	$\bar{9}$	4	-	-	23.28	13.00	-	1.856
4	$\bar{2}$	4	-	-	27.84	13.00	-	1.626
5	$\bar{4}$	4	-	-	27.92	13.00	-	1.623
0	$\bar{5}$	4	-	-	27.98	13.00	-	1.620
5	$\bar{1}$	4	28.38	13.00	28.21	13.00	1.602	1.610
3	$\bar{9}$	4	28.38	13.00	28.29	13.00	1.602	1.606
1	$\bar{5}$	4	28.38	13.00	28.57	13.00	1.602	1.594
5	$\bar{5}$	4	-	-	28.84	13.00	-	1.583
2	$\bar{10}$	4	-	-	28.84	13.00	-	1.583
5	0	4	-	-	29.32	13.00	-	1.563
4	$\bar{8}$	4	-	-	29.40	13.00	-	1.560
3	4	4	-	-	29.55	13.00	-	1.554
0	$\bar{2}$	5	-	-	2.52	17.19	-	2.964
1	$\bar{3}$	5	3.80	17.19	3.70	17.19	2.922	2.962
0	$\bar{5}$	5	3.80	17.19	4.11	17.19	2.922	2.910
1	$\bar{4}$	5	3.80	17.19	4.15	17.19	2.922	2.909
1	$\bar{2}$	5	-	-	6.04	17.19	-	2.817
1	$\bar{5}$	5	-	-	6.86	17.19	-	2.771
0	$\bar{1}$	5	7.50	17.19	7.46	17.19	2.733	2.735
0	$\bar{6}$	5	-	-	8.57	17.19	-	2.665
1	$\bar{1}$	5	-	-	9.28	17.19	-	2.619
1	$\bar{6}$	5	10.11	17.19	10.19	17.19	2.563	2.557
2	$\bar{3}$	5	10.11	17.19	10.24	17.19	2.563	2.554
2	$\bar{4}$	5	10.11	17.19	10.41	17.19	2.563	2.542
2	$\bar{2}$	5	-	-	11.31	17.19	-	2.481
0	0	5	-	-	11.50	17.19	-	2.468
2	$\bar{5}$	5	-	-	11.78	17.19	-	2.449
0	$\bar{7}$	5	-	-	12.55	17.19	-	2.397
1	0	5	-	-	12.77	17.19	-	2.381
2	$\bar{1}$	5	-	-	13.36	17.19	-	2.342
1	$\bar{7}$	5	-	-	13.73	17.19	-	2.317
2	$\bar{6}$	5	-	-	14.02	17.19	-	2.297
0	1	5	14.95	17.19	15.40	17.19	2.236	2.207
2	0	5	16.55	17.19	16.02	17.19	2.135	2.168
3	$\bar{3}$	5	16.55	17.19	16.13	17.19	2.135	2.161
3	$\bar{4}$	5	16.55	17.19	16.24	17.19	2.135	2.154
1	1	5	16.55	17.19	16.39	17.19	2.135	2.145
0	$\bar{9}$	5	16.55	17.19	16.44	17.19	2.135	2.141
2	$\bar{7}$	5	16.55	17.19	16.81	17.19	2.135	2.119
3	$\bar{2}$	5	16.55	17.19	16.85	17.19	2.135	2.116
3	$\bar{5}$	5	16.55	17.19	17.18	17.19	2.135	2.096
1	$\bar{8}$	5	-	-	17.38	17.19	-	2.084
3	$\bar{1}$	5	17.88	17.19	18.33	17.19	2.054	2.028
3	$\bar{6}$	5	19.21	17.19	18.83	17.19	1.977	1.999
2	1	5	19.21	17.19	19.09	17.19	1.977	1.984
0	2	5	19.21	17.19	19.30	17.19	1.977	1.972
2	$\bar{8}$	5	-	-	19.96	17.19	-	1.936
1	2	5	-	-	20.12	17.19	-	1.927
0	$\bar{9}$	5	-	-	20.35	17.19	-	1.915
3	0	5	-	-	20.41	17.19	-	1.911

contd.

TABLE (4.4) continued

h	k	l	x (mm) obs	y (mm) obs	x (mm) calc	y (mm) calc	d (°A) obs	d (°A) calc
3	$\bar{7}$	5	-	-	21.06	17.19	-	1.878
1	$\bar{9}$	5	-	-	21.13	17.19	-	1.874
4	$\bar{3}$	5	22.28	17.19	22.04	17.19	1.816	1.828
4	$\bar{4}$	5	22.28	17.19	22.12	17.19	1.816	1.823
2	$\bar{2}$	5	22.28	17.19	22.43	17.19	1.816	1.809
4	$\bar{2}$	5	22.28	17.19	22.60	17.19	1.816	1.800
4	$\bar{5}$	5	23.16	17.19	22.85	17.19	1.773	1.788
3	1	5	23.16	17.19	22.97	17.19	1.773	1.782
0	3	5	23.16	17.19	23.24	17.19	1.773	1.769
2	$\bar{9}$	5	23.16	17.19	23.36	17.19	1.773	1.764
3	$\bar{8}$	5	-	-	23.72	17.19	-	1.747
4	$\bar{1}$	5	-	-	23.77	17.19	-	1.745
1	3	5	-	-	23.95	17.19	-	1.737
4	$\bar{6}$	5	-	-	24.17	17.19	-	1.726
0	$\bar{10}$	5	-	-	24.31	17.19	-	1.720
1	$\bar{10}$	5	24.93	17.19	24.99	17.19	1.693	1.690
4	0	5	24.93	17.19	25.48	17.19	1.693	1.669
3	2	5	-	-	25.90	17.19	-	1.652
2	3	5	-	-	25.98	17.19	-	1.648
4	$\bar{7}$	5	-	-	26.02	17.19	-	1.647
3	$\bar{9}$	5	27.19	17.19	26.74	17.19	1.599	1.618
2	$\bar{10}$	5	27.19	17.19	26.97	17.19	1.599	1.608
0	4	5	27.19	17.19	27.27	17.19	1.599	1.596
4	1	5	27.19	17.19	27.66	17.19	1.599	1.581
1	4	5	-	-	27.90	17.19	-	1.572
5	$\bar{3}$	5	-	-	28.12	17.19	-	1.564
5	$\bar{4}$	5	-	-	28.19	17.19	-	1.561
5	$\bar{8}$	5	-	-	28.32	17.19	-	1.556
1	$\bar{5}$	6	-	-	1.37	22.30	-	2.449
1	$\bar{3}$	6	-	-	2.03	22.30	-	2.443
0	$\bar{6}$	6	-	-	3.29	22.30	-	2.425
0	$\bar{2}$	6	-	-	3.92	22.30	-	2.413
1	$\bar{6}$	6	-	-	6.59	22.30	-	2.343
1	$\bar{2}$	6	-	-	6.93	22.30	-	2.332
0	$\bar{7}$	6	8.95	22.27	9.02	22.30	2.262	2.258
2	$\bar{4}$	6	8.95	22.27	9.32	22.30	2.262	2.246
0	$\bar{1}$	6	8.95	22.27	9.39	22.30	2.262	2.243
2	$\bar{5}$	6	-	-	10.01	22.30	-	2.218
2	$\bar{3}$	6	-	-	10.12	22.30	-	2.214
1	$\bar{7}$	6	11.11	22.27	10.69	22.30	2.175	2.191
1	$\bar{1}$	6	11.11	22.27	11.01	22.30	2.175	2.178
2	$\bar{6}$	6	-	-	11.94	22.30	-	2.138
2	$\bar{2}$	6	-	-	12.13	22.30	-	2.130
0	$\bar{8}$	6	13.45	22.27	13.49	22.30	2.074	2.072
0	0	6	13.45	22.27	13.83	22.30	2.074	2.057
2	$\bar{7}$	6	-	-	14.66	22.30	-	2.021
1	$\bar{8}$	6	-	-	14.68	22.30	-	2.020
2	$\bar{1}$	6	-	-	14.89	22.30	-	2.010
1	0	6	-	-	15.00	22.30	-	2.006
3	$\bar{4}$	6	16.45	22.27	15.95	22.30	1.944	1.964
3	$\bar{5}$	6	16.45	22.27	16.38	22.30	1.944	1.946
3	$\bar{3}$	6	16.45	22.27	16.45	22.30	1.944	1.943
3	$\bar{6}$	6	-	-	17.66	22.30	-	1.891
0	$\bar{9}$	6	-	-	17.73	22.30	-	1.881

Contd.

TABLE (4.4) continued

h	k	l	x (mm) obs	y (mm) obs	x (mm) calc	y (mm) calc	d (°A) obs	d (°A) calc
3	$\bar{2}$	6	-	-	17.80	22.30	-	1.886
1	$\bar{9}$	6	-	-	18.68	22.30	-	1.849
1	$\bar{1}$	6	-	-	19.00	22.30	-	1.835
3	$\bar{7}$	6	-	-	19.66	22.30	-	1.809
3	$\bar{1}$	6	-	-	19.84	22.30	-	1.801
2	$\bar{9}$	6	20.92	22.27	21.31	22.30	1.759	1.743
2	1	6	-	-	21.59	22.30	-	1.732
0	10	6	-	-	21.94	22.30	-	1.719
3	$\bar{8}$	6	-	-	22.21	22.30	-	1.709
0	$\bar{2}$	6	-	-	22.28	22.30	-	1.706
4	$\bar{4}$	6	-	-	22.33	22.30	-	1.704
3	0	6	-	-	22.43	22.30	-	1.700
4	$\bar{5}$	6	-	-	22.65	22.30	-	1.692
4	$\bar{3}$	6	-	-	22.70	22.30	-	1.690
1	$\bar{10}$	6	-	-	22.74	22.30	-	1.689
1	$\bar{2}$	6	23.40	22.27	23.07	22.30	1.665	1.677
4	$\bar{6}$	6	23.40	22.27	23.64	23.30	1.665	1.656
4	$\bar{2}$	6	23.40	22.27	23.74	22.30	1.665	1.652
2	$\bar{10}$	6	-	-	25.01	22.30	-	1.607
3	$\bar{9}$	6	-	-	25.18	22.30	-	1.601
4	$\bar{7}$	6	-	-	25.24	22.30	-	1.599
2	$\bar{2}$	6	-	-	25.32	22.30	-	1.597
4	$\bar{1}$	6	-	-	25.39	22.30	-	1.594
3	1	6	-	-	25.43	22.30	-	1.593
0	$\bar{2}$	7	-	-	4.14	29.07	-	2.030
1	$\bar{7}$	7	-	-	4.44	29.07	-	2.026
2	$\bar{5}$	7	7.76	29.11	6.86	29.07	1.971	1.989
1	$\bar{2}$	7	7.76	29.11	7.33	29.07	1.971	1.981
2	$\bar{4}$	7	7.76	29.11	7.34	29.07	1.971	1.980
0	$\bar{8}$	7	7.76	29.11	8.50	29.07	1.971	1.957
2	$\bar{6}$	7	7.76	29.11	8.51	29.07	1.971	1.957
2	$\bar{3}$	7	-	-	9.64	29.07	-	1.932
1	$\bar{8}$	7	10.75	29.11	10.45	29.07	1.905	1.913
0	$\bar{1}$	7	10.75	29.11	10.97	29.07	1.905	1.900
2	$\bar{7}$	7	10.75	29.11	11.41	29.07	1.905	1.889
1	$\bar{1}$	7	-	-	12.55	29.07	-	1.860
2	$\bar{2}$	7	-	-	12.84	29.07	-	1.852
0	$\bar{9}$	7	13.92	29.11	13.98	29.07	1.822	1.822
2	$\bar{8}$	7	-	-	14.88	29.07	-	1.797
1	$\bar{9}$	7	-	-	15.27	29.07	-	1.786
3	$\bar{5}$	7	-	-	15.28	29.07	-	1.786
3	$\bar{4}$	7	-	-	15.51	29.07	-	1.779
0	0	7	-	-	16.09	29.07	-	1.763
3	$\bar{6}$	7	-	-	16.11	29.07	-	1.762
2	$\bar{1}$	7	-	-	16.46	29.07	-	1.752
3	$\bar{3}$	7	-	-	16.76	29.07	-	1.744
1	0	7	17.69	29.11	17.23	29.07	1.717	1.731
3	$\bar{7}$	7	17.69	29.11	17.87	29.07	1.717	1.713
2	$\bar{9}$	7	-	-	18.66	29.07	-	1.690
0	$\bar{10}$	7	-	-	18.85	29.07	-	1.685
3	$\bar{2}$	7	-	-	18.85	29.07	-	1.685
1	$\bar{10}$	7	-	-	19.85	29.07	-	1.656
2	0	7	-	-	20.33	29.07	-	1.643
3	$\bar{8}$	7	-	-	20.35	29.07	-	1.643
0	1	7	-	-	20.86	29.07	-	1.628

TABLE (4.5)

LOCATION OF THE DIFFRACTION SPOTS OF γ-FORM

(Cartesian and Reciprocal Lattice Co-ordinates)

x(mm)	y(mm)	ξ	ζ
9.23	0.0	0.3064	0.0
11.70	0.0	0.3875	0.0
13.26	0.0	0.4384	0.0
23.82	0.0	0.7732	0.0
24.82	0.0	0.8039	0.0
27.19	0.0	0.8756	0.0
28.59	0.0	0.9173	0.0
2.25	3.02	0.0750	0.1002
4.54	3.02	0.1509	0.1002
5.52	3.02	0.1833	0.1002
7.84	3.02	0.2600	0.1002
9.35	3.02	0.3096	0.1002
10.44	3.02	0.3454	0.1002
11.53	3.02	0.3810	0.1002
12.13	3.02	0.4006	0.1002
16.81	3.02	0.5516	0.1002
18.14	3.02	0.5940	0.1002
19.86	3.02	0.6483	0.1002
21.34	3.02	0.6946	0.1002
22.50	3.02	0.7307	0.1002
4.40	6.12	0.1464	0.1999
5.75	6.12	0.1905	0.1999
7.02	6.12	0.2320	0.1999
10.89	6.12	0.3579	0.1999
12.16	6.12	0.3990	0.1999
4.25	9.37	0.1456	0.2981
8.32	9.37	0.2739	0.2981
11.18	9.37	0.3648	0.2981
14.30	9.37	0.4535	0.2981
16.99	9.37	0.5478	0.2981
5.24	12.97	0.1862	0.3968
8.42	12.97	0.2803	0.3968
10.14	12.97	0.3326	0.3968
3.85	16.72	0.1742	0.4868
7.51	16.72	0.2654	0.4868
14.30	16.72	0.4590	0.4868

TABLE (4.6)

OBSERVED AND CALCULATED

CARTESIAN CO-ORDINATES AND REAL PLANE SPACINGS

FOR THE γ-FORM UNIT CELL

h	k	l	x (mm) obs	y (mm) obs	x (mm) calc	y (mm) calc	d (°A) obs	d (°A) calc
1	0	0	-	-	4.56	0.00	-	10.162
2	$\bar{0}$	0	9.23	0.00	9.14	0.00	5.033	5.081
1	$\bar{1}$	0	11.70	0.00	11.58	0.00	3.980	4.021
0	1	0	11.70	0.00	11.73	0.00	3.980	3.969
2	$\bar{1}$	0	13.26	0.00	13.16	0.00	3.518	3.545
1	1	0	-	-	13.56	0.00	-	3.441
3	$\bar{0}$	0	-	-	13.78	0.00	-	3.387
3	$\bar{1}$	0	-	-	16.00	0.00	-	2.927
2	1	0	-	-	16.56	0.00	-	2.830
4	$\bar{0}$	0	-	-	18.51	0.00	-	2.540
4	$\bar{1}$	0	-	-	19.61	0.00	-	2.403
3	1	0	-	-	20.26	0.00	-	2.328
1	$\bar{2}$	0	-	-	23.30	0.00	-	2.037
5	$\bar{0}$	0	-	-	23.36	0.00	-	2.032
2	$\bar{2}$	0	23.82	0.00	23.62	0.00	1.995	2.011
5	$\bar{1}$	0	23.82	0.00	23.71	0.00	1.995	2.004
0	2	0	23.82	0.00	23.95	0.00	1.995	1.985
4	1	0	-	-	24.43	0.00	-	1.948
3	$\bar{2}$	0	24.82	0.00	24.90	0.00	1.919	1.913
1	2	0	-	-	25.52	0.00	-	1.869
4	$\bar{2}$	0	27.19	0.00	27.01	0.00	1.762	1.772
2	2	0	-	-	27.89	0.00	-	1.720
6	$\bar{1}$	0	-	-	28.18	0.00	-	1.704
6	0	0	28.59	0.00	28.37	0.00	1.681	1.694
5	1	0	-	-	28.96	0.00	-	1.662
$\bar{2}$	$\bar{0}$	1	7.84	3.02	8.46	3.00	5.537	5.183
0	$\bar{1}$	1	9.35	3.02	9.38	3.00	4.740	4.731
1	$\bar{1}$	1	-	-	9.67	3.00	-	4.601
2	0	1	10.44	3.02	10.40	3.00	4.289	4.305
$\bar{1}$	$\bar{1}$	1	11.53	3.02	11.17	3.00	3.915	4.033
2	$\bar{1}$	1	12.13	3.02	11.91	3.00	3.736	3.802
$\bar{3}$	0	1	-	-	13.00	3.00	-	3.504
$\bar{1}$	1	1	-	-	13.72	3.00	-	3.331
0	1	1	-	-	14.19	3.00	-	3.228
$\bar{2}$	$\bar{1}$	1	-	-	14.32	3.00	-	3.200
$\bar{2}$	1	1	-	-	14.78	3.00	-	3.150
3	$\bar{0}$	1	-	-	15.00	3.00	-	3.063
3	$\bar{1}$	1	-	-	15.29	3.00	-	3.009
1	1	1	-	-	16.06	3.00	-	2.873
$\bar{3}$	1	1	16.81	3.02	17.12	3.00	2.751	2.705
$\bar{4}$	0	1	-	-	17.67	3.00	-	2.626
$\bar{3}$	$\bar{1}$	1	18.14	3.02	18.19	3.00	2.561	2.555
2	1	1	-	-	18.96	3.00	-	2.457
4	$\bar{1}$	1	-	-	19.29	3.00	-	2.417
4	0	1	19.86	3.02	19.72	3.00	2.351	2.367
$\bar{4}$	1	1	-	-	20.33	3.00	-	2.301

contd.

TABLE (4.6) continued

h	k	l	x (mm) obs	y (mm) obs	x (mm) calc	y (mm) calc	d (°A) obs	d (°A) calc
1	$\bar{2}$	1	-	-	20.99	3.00	-	2.232
0	$\bar{2}$	1	21.34	3.02	21.47	3.00	2.198	2.185
2	$\bar{2}$	1	21.34	3.02	21.58	3.00	2.198	2.175
$\bar{5}$	0	1	22.50	3.02	22.47	3.00	2.091	2.094
$\bar{4}$	$\bar{1}$	1	22.50	3.02	22.48	3.00	2.091	2.094
3	1	1	22.50	3.02	22.55	3.00	2.091	2.087
$\bar{1}$	$\bar{2}$	1	-	-	22.97	3.00	-	2.052
3	$\bar{2}$	1	-	-	23.16	3.00	-	2.036
0	0	2	4.40	6.12	4.81	6.09	6.225	6.044
$\bar{1}$	0	2	5.75	6.12	5.10	6.09	5.586	5.903
0	$\bar{1}$	2	7.02	6.12	7.07	6.09	5.037	5.026
1	0	2	-	-	7.93	6.09	-	4.692
1	$\bar{1}$	2	-	-	8.06	6.09	-	4.646
$\bar{2}$	0	2	-	-	8.47	6.09	-	4.500
$\bar{1}$	$\bar{1}$	2	-	-	8.83	6.09	-	4.376
2	$\bar{1}$	2	10.89	6.12	11.09	6.09	3.763	3.715
2	0	2	12.16	6.12	12.09	6.09	3.457	3.474
$\bar{2}$	$\bar{1}$	2	12.16	6.12	12.22	6.09	3.457	3.446
$\bar{3}$	0	2	-	-	12.69	6.09	-	3.344
0	$\bar{1}$	3	4.25	9.37	4.71	9.38	4.649	4.556
$\bar{1}$	$\bar{1}$	3	-	-	6.42	9.38	-	4.202
$\bar{1}$	0	3	-	-	6.79	9.38	-	4.126
1	$\bar{1}$	3	-	-	6.85	9.38	-	4.113
0	0	3	-	-	7.25	9.38	-	4.029
$\bar{2}$	0	3	8.32	9.37	9.14	9.38	3.810	3.646
1	0	3	-	-	10.16	9.38	-	3.454
$\bar{2}$	$\bar{1}$	3	-	-	10.22	9.38	-	3.441
2	$\bar{1}$	3	11.18	9.37	10.76	9.38	3.274	3.344
$\bar{3}$	0	3	-	-	12.88	9.38	-	3.000
2	0	3	14.30	9.37	14.11	9.38	2.799	2.824
$\bar{3}$	$\bar{1}$	3	14.30	9.37	14.61	9.38	2.799	2.756
3	$\bar{1}$	3	-	-	15.20	9.38	-	2.682
1	$\bar{2}$	3	16.99	9.37	16.83	9.38	2.473	2.490
0	$\bar{2}$	3	16.99	9.37	16.86	9.38	2.473	2.487
$\bar{4}$	0	3	16.99	9.37	17.18	9.38	2.473	2.452
2	$\bar{2}$	3	-	-	18.12	9.38	-	2.355
$\bar{1}$	$\bar{2}$	3	-	-	18.20	9.38	-	2.347
3	0	3	-	-	18.52	9.38	-	2.316
$\bar{1}$	1	3	-	-	18.61	9.38	-	2.308
0	$\bar{1}$	4	-	-	1.57	13.01	-	3.767
$\bar{1}$	$\bar{1}$	4	-	-	3.53	13.01	-	3.658
1	$\bar{1}$	4	5.24	12.97	6.15	13.01	3.519	3.418
$\bar{2}$	$\bar{1}$	4	8.42	12.97	8.25	13.01	3.175	3.188
$\bar{1}$	0	4	8.42	12.97	8.82	13.01	3.175	3.124
0	0	4	10.14	12.97	9.72	13.01	2.979	3.022
$\bar{2}$	0	4	10.14	12.97	10.34	13.01	2.979	2.952
2	$\bar{1}$	4	-	-	10.93	13.01	-	2.886
1	0	4	-	-	12.55	13.01	-	2.712

contd.

TABLE (4.6) continued

h	k	l	x (mm) obs	y (mm) obs	x (mm) calc	y (mm) calc	d (^{o}A) obs	d (^{o}A) calc
1	$\bar{1}$	5	-	-	5.97	17.20	-	2.820
$\bar{2}$	$\bar{1}$	5	-	-	6.02	17.20	-	2.817
$\bar{1}$	0	5	-	-	11.01	17.20	-	2.501
2	$\bar{1}$	5	-	-	11.51	17.20	-	2.466
$\bar{3}$	$\bar{1}$	5	-	-	11.56	17.20	-	2.463
$\bar{2}$	0	5	-	-	11.91	17.20	-	2.440
0	$\bar{2}$	5	-	-	11.98	17.20	-	2.435
0	0	5	-	-	12.23	17.20	-	2.417

there is only information about the lattice plane a reciprocal lattice point lies in and its distance from the origin of that plane. Directional information is lost. With doubly-oriented sheet, the diffraction patterns retain this information and diffraction patterns similar to the oscillation patterns of single crystals can be obtained. Therefore, the standard single crystal methods can be used, provided the orientation is sufficiently good.

In these investigations, a Weissenberg camera was used. The equatorial Weissenberg photographs can be made by the normal beam method[57], in which the axis of rotation of the crystal is normal to the incident X-ray beam. The upper layer line Weissenberg photograph can be made by the equi-inclination method[57], in which the axis of rotation of the specimen is inclined at an angle to the incident X-ray beam. For each upper level photograph, two instrument settings should be determined.

(a) The inclination angle μ, given by

$$\mu = \sin^{-1} \frac{\zeta}{2}$$

where ζ-value can be calculated from the film co-ordinates, as was shown in Section 4.2.1.

(b) The layer line screen setting S

The displacement of the screen can be calculated from the relation given by

$$S = r_s \tan \mu$$

where r_s is the radius of the screen.

4.3.1 Experimental

(a) Preparation of Double-Orientation Films

Melt pressed sheets of unoriented specimens (4x2x0.2 cm), as prepared in Chapter Two, were subjected to cold rolling, resulting in a substantial thickness reduction. The rolling device comprised a pair of rollers, seven inches in diameter, driven at the same speed with an adjustable gap between them. At the start, the gap between the two rollers was set to 2mm. The gap then decreased every time the sample passed between them, until a limit gap was reached beyond which the specimens started shattering. Two different roller speeds were used, 4 and 40 ft./min.

The specimens were annealed at fixed length at 140°C for two hours. The wide-angle X-ray diffraction patterns of the annealed rolled sheet were recorded with two directions of the incident X-ray beam; perpendicular to the rolled surface and parallel to the rolled surface but perpendicular to the machine direction. Another doubly-oriented specimen was prepared from a section of melt pressed thin films of unoriented specimen (see Chapter Two), having a thickness 0.3±0.03 mm. and width of 5 mm. The section was cold-drawn on a tensile testing machine with cross-head speed of 100 cm/min. to a draw ratio of 4. The specimen was annealed under fixed length at 140°C for two hours. The wide-angle X-ray diffraction pattern for this drawn specimen was recorded with the same two directions of the incident X-ray beam, as were used with the rolled sheets described above.

(b) Weissenberg Photographs

The rolled specimen was trimmed to a slice of 0.5x0.5x10mm, to

facilitate taking a Weissenberg photograph. The specimen was aligned in a Weissenberg goniometer head with the long dimension (rolling direction) in the axis of rotation, and in such a way that the primary X-ray beam was found to be perpendicular to the rolling plane of the specimen when the oscillation angle indicated 134^{o}.

For an equatorial Weissenberg photograph, the layer-line screen was adjusted to select the equatorial layer only. The correct positioning of the screen was checked by an exposure for one hour, where the incident X-ray beam was perpendicular to the rolling plane of the specimen, which was held stationary. The film cassette was then displaced and the specimen rotated through 90^{o}, before taking another X-ray photograph on the same film for a period of one hour. After selecting the equator correctly by the screen, the specimen was made to oscillate through an angle of about 205^{o} with simultaneous translational movement of the film cassette. Photographs were taken for different times of exposure, i.e. 24, 48 and 100 hours.

For the upper layer line Weissenberg photographs, the incident X-ray beam was adjusted to be inclined at an angle of 2.9^{o} to the axis of rotation of the specimen. The layer line screen was displaced by 1.4 mm for the first layer line. The correct positioning of the screen was checked in the same manner as that for the equator. The film cassette was moved through a distance equal to the displacement of the screen and in the same direction. The oscillation of the specimen was performed under exactly the same conditions as those for the equatorial Weissenberg photograph. For the second layer line, an inclination angle 5.8^{o} was used and the layer line screen and film cassette were displaced by 2.8 mm. The positioning of the screen, the oscillation of the specimen and the Weissenberg photograph were carried out under the same conditions as those for the equatorial and

the first layer line.

The other doubly-oriented specimen, melt-pressed and drawn by the Instron at speed of 100 cm/min., was also used in these studies; the specimen was 0.14 mm thick. From this specimen, two samples were trimmed to a slice 0.28x0.14x12 mm. The two samples were then joined together at the two ends by epoxy resin, ensuring there was no air gap in between; this provided a specimen having dimensions of 0.28x0.28x12 mm. The same procedure employed in taking Weissenberg photographs described above was used.

4.3.2 Results

The X-ray diffraction patterns for the cold-drawn sheets were very diffuse and poorly defined. The wide-angle X-ray diffraction patterns for the rolled sheet, annealed at 140°C, were shown in Plate 7(a) and (b) for the incident X-ray beam being perpendicular to the rolled surface, and for being parallel to the rolled surface but perpendicular to the machine direction respectively. It was found that the doubly-oriented specimens with rolling speeds of 4 and 40 ft./min. have the same diffraction pattern with the indication of having high proportions of β-form. Plate 7(c) and (d) show the wide-angle X-ray diffraction patterns for the pressed film, drawn by the Instron and annealed at 140°C, with the incident X-ray beam being perpendicular to the surface of the film and when parallel to the surface of the film but perpendicular to the drawing direction respectively. The diffraction patterns were found to indicate some proportion of α-form.

Plate 8(a) shows the equatorial oscillation photograph for the rolled sheet, with the specimen oscillating through 205° simultaneously with a translational movement of the film cassette through 102 mm.

PLATE (7): WAXS photographs of:

rolled sheet annealed at 140°C when:

(a) the X-ray beam is perpendicular to the rolled surface

(b) " " " " parallel " " " " but perpendicular to the rolling direction

drawn pressed film annealed at 140°C when:

(c) the X-ray beam is perpendicular to film surface

(d) " " " " parallel " " " but perpendicular to drawing direction

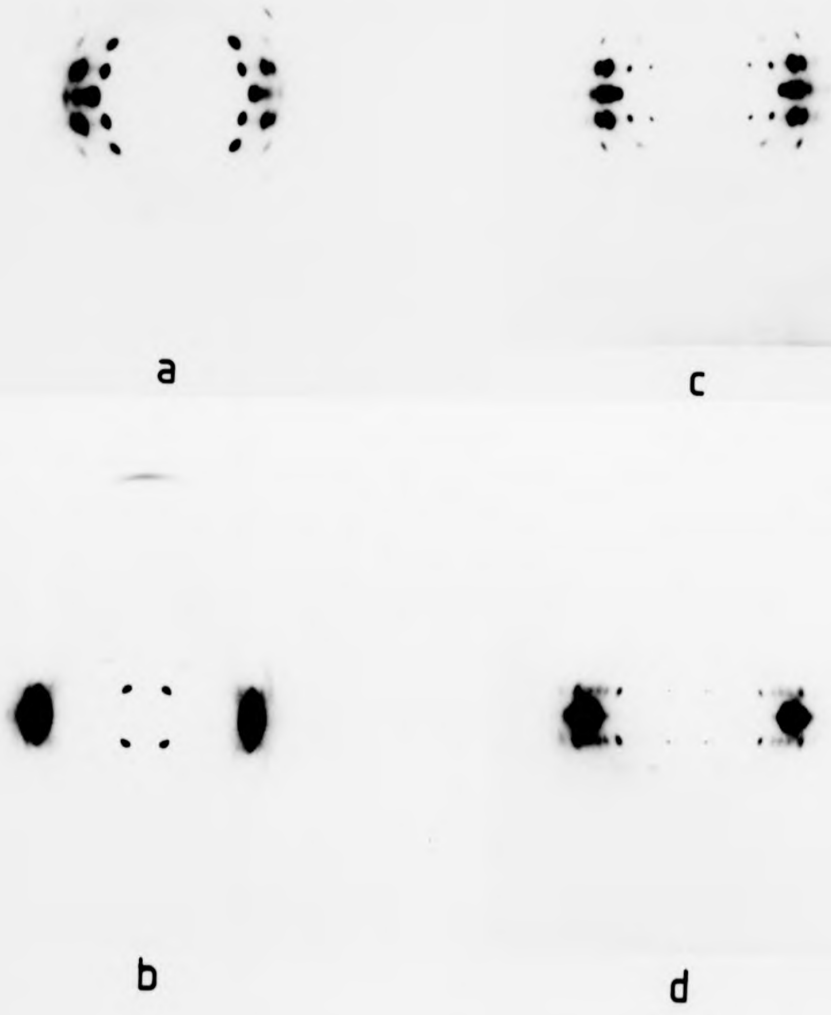

PLATE 7

PLATE (7): WAXS photographs of:

rolled sheet annealed at 140°C when:

(a) the X-ray beam is perpendicular to the rolled surface

(b) " " " " parallel " " " " but perpendicular to the rolling direction

drawn pressed film annealed at 140°C when:

(c) the X-ray beam is perpendicular to film surface

(d) " " " " parallel " " " but perpendicular to drawing direction

PLATE 7

PLATE (8): Weissenberg oscillation photographs for:

rolled sheet

(a) equatorial layer line (hk0)

(b) first layer line (hk1)

(c) second layer line (hk2)

drawn pressed film

(d) equatorial layer line (hk0)

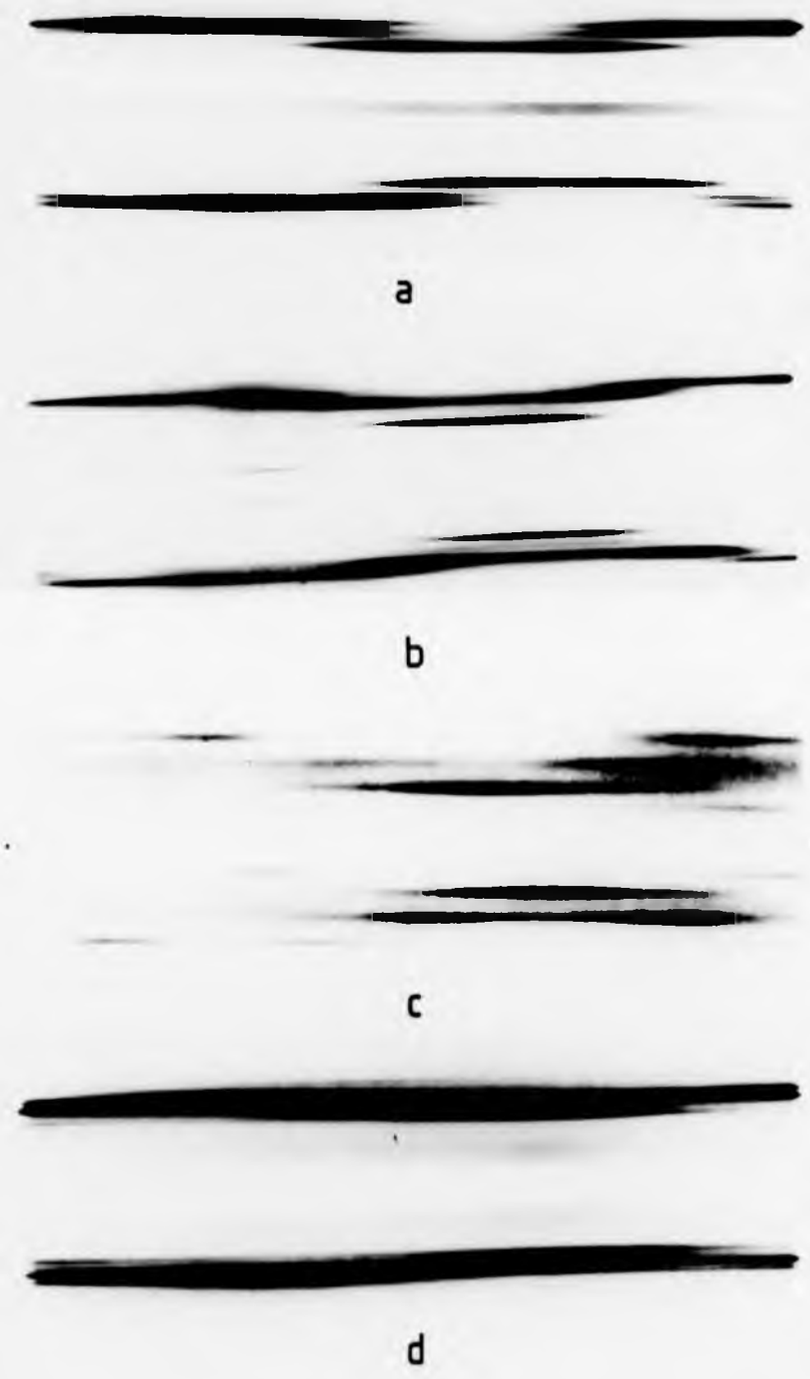

PLATE 8

PLATE (8): Weissenberg oscillation photographs for:

rolled sheet

(a) equatorial layer line (hk0)

(b) first layer line (hk1)

(c) second layer line (hk2)

drawn pressed film

(d) equatorial layer line (hk0)

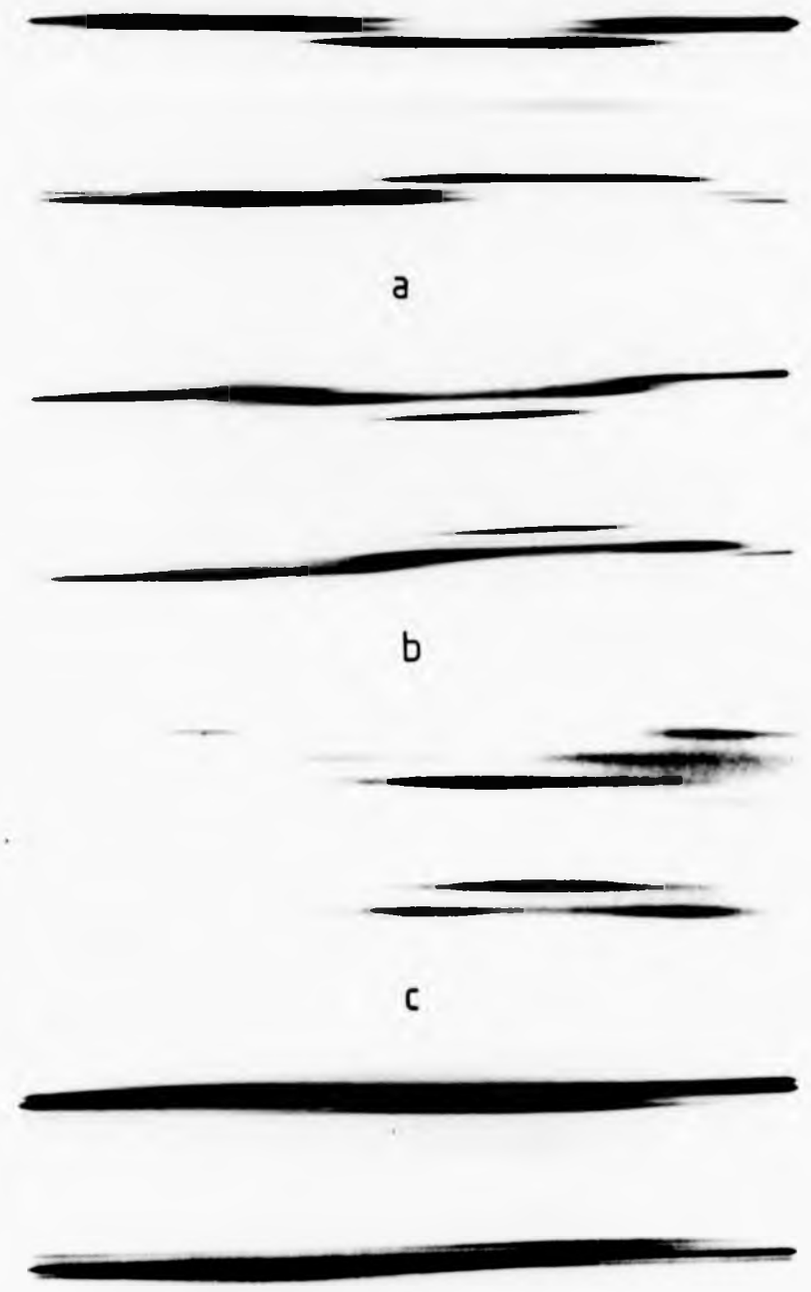

PLATE 8

The oscillation angle, as indicated on the camera, varied between 5^{o} and 210^{o} as the specimen oscillated. When this angle was 134^{o}, the X-ray beam was perpendicular to the rolled surface; when it was 45^{o}, the beam was parallel to the rolled surface but perpendicular to the rolling direction. In this photograph, the b*-axis is shown to be inclined by 70^{o} to the normal to the rolling plane and perpendicular to the direction of rolling (c-axis), all reflections being symmetrical about the b*-direction. This is attributed to the possibility of a twinning effect in the plane of rolling; Mencik[10] has also observed twinning in his work on biaxial 4GT films.

The reflections in these diffraction patterns appeared in the shape of streaks; the position of maximum intensity in the streak was taken as an indication of the position of the reciprocal lattice points. The reciprocal lattice co-ordinates for each streak was measured by means of a Wooster Chart, which were then marked on paper, as is shown in Figure (4.7). The constructed zero-layer reciprocal lattice of β-form, shown in Figure (4.1), was overlaid on Figure (4.7) such that the zero positions were made to coincide with each other. The constructed reciprocal lattice (Figure (4.1)) was then rotated around the zero position in such a way that the marked positions coincided with most of the reflections. It was found that most of these marked reflections coincided with the constructed reciprocal lattice of the β-form (Figure (4.8)). The remainder of those reflections, when overlaid on the constructed reciprocal lattice of the α-form (Figure (4.6)), were found to coincide with them, as shown in Figure (4.9).

Plate 8(b) shows the first layer line Weissenberg oscillation photograph for the same specimen as above. The marked positions of the reciprocal lattice, following the same procedure as that for the

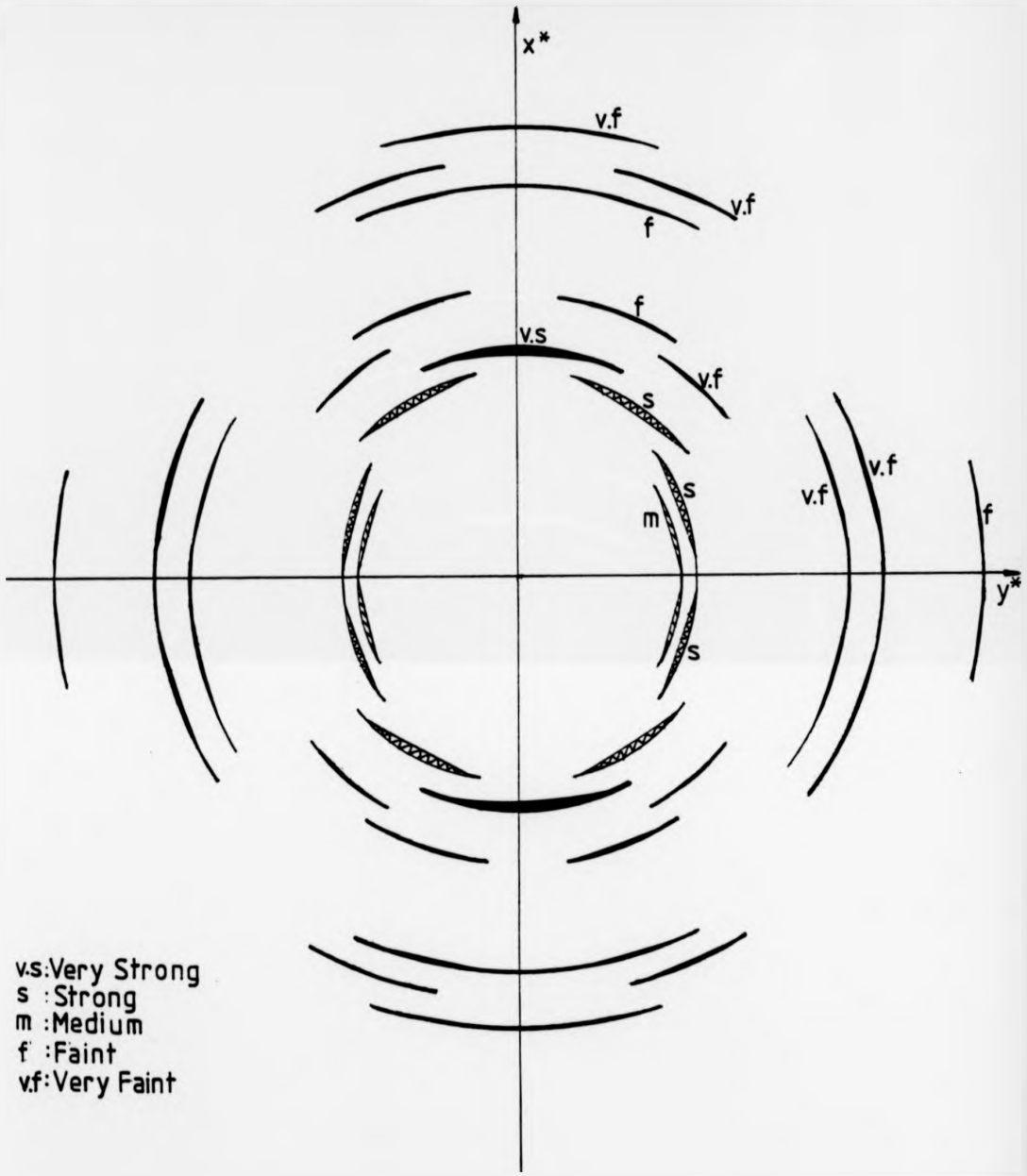

FIG. 4.7 EQUATORIAL RECIPROCAL LATTICE FOR DOUBLY-ORIENTED SHEET

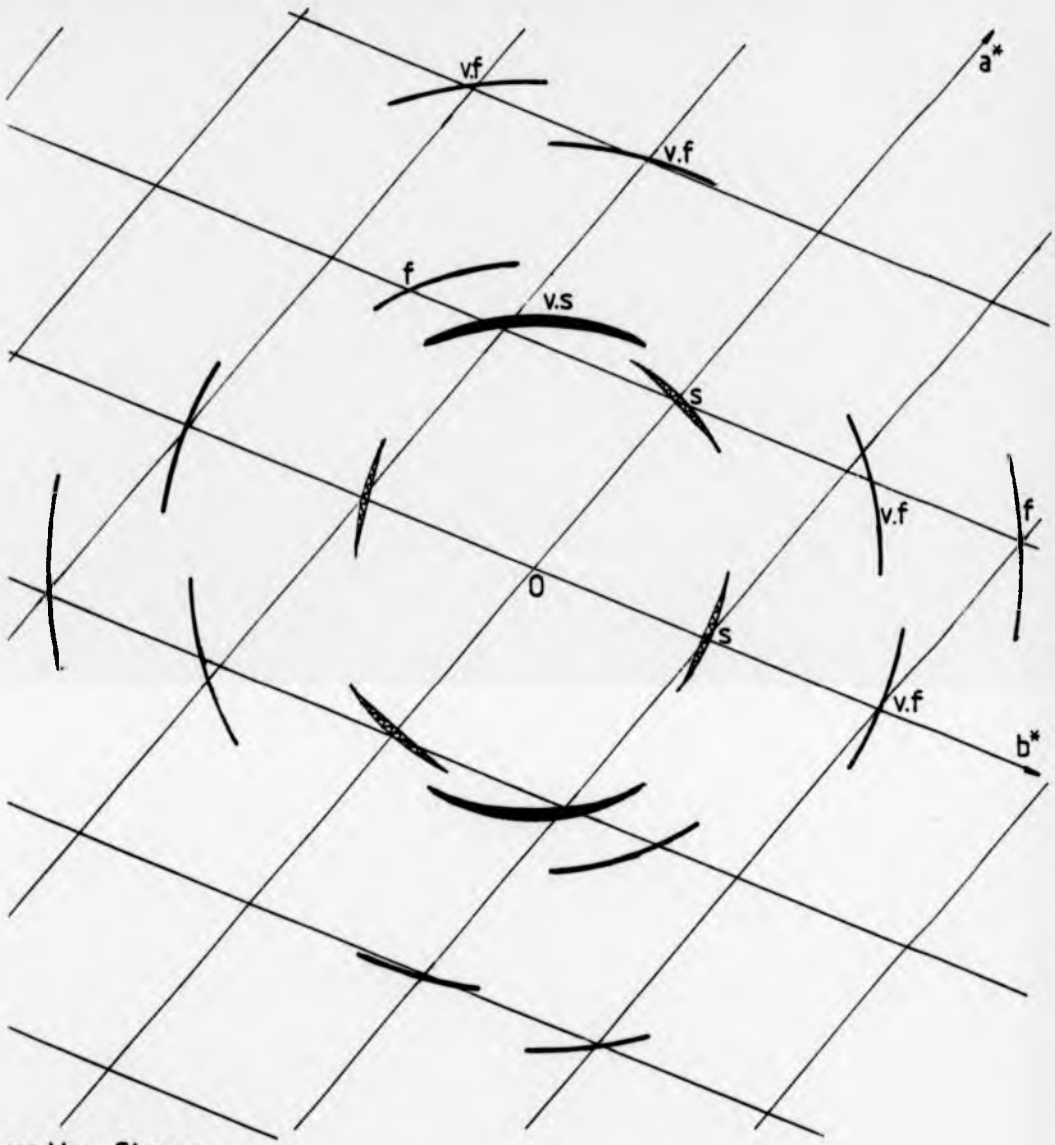

vs: Very Strong
s : Strong
f : Faint
vf: Very Faint

FIG. 4.8 : EQUATORIAL RECIPROCAL LATTICE NET FOR THE DOUBLY-ORIENTED SHEET OF THE β-FORM

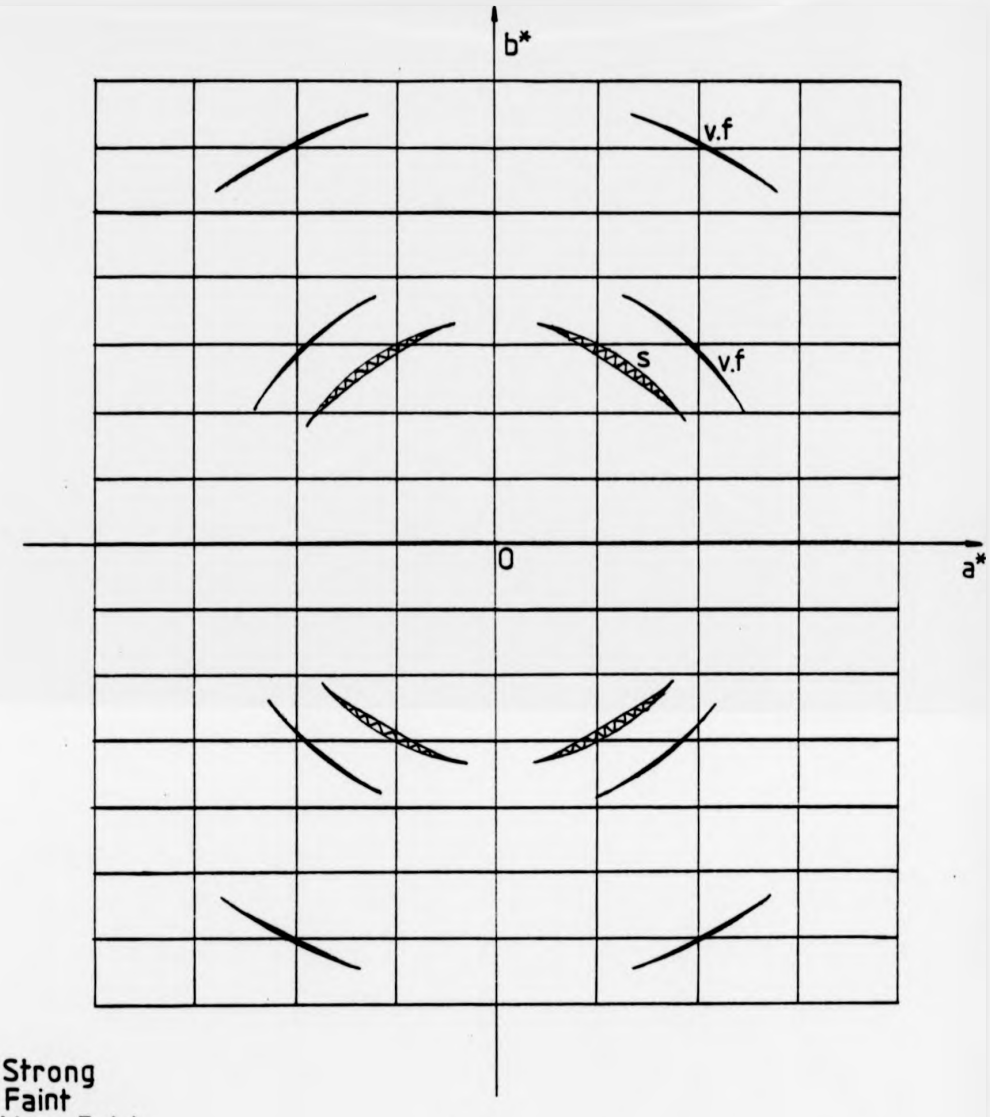

s ; Strong
f : Faint
v.f: Very Faint

FIG. 4.9 : EQUATORIAL RECIPROCAL LATTICE NET OF THE α-FORM FOR THE DOUBLY-ORIENTED SHEET

equator, are shown in Figure (4.10). The zero-position in Figure (4.1) was placed over one of the positions marked (001) in such a way that a* and b* retained the same direction as in the equatorial layer line, i.e. y*-axis (see Figure (4.8)) makes an angle of 22^{o} with the b*-axis. The resultant overlay is shown in Figure (4.11). The offset was found to be 0.075 r.l.u. making an angle 135^{o} with b*.

The second layer line of the Weissenberg oscillation photograph and the marked positions of the reciprocal lattice for the same specimen as above are shown in Plate 8(c) and Figure (4.12) respectively. The zero position of Figure (4.1) was placed over the position marked (002) while retaining the same direction of a* and b* mentioned above; the resultant overlay is shown in Figure (4.13).

The Weissenberg equatorial oscillation photograph for the cold drawn thin films showed very long streaks, as shown in Plate 8(d). The marked positions for the reciprocal lattice, as measured by Wooster Chart at the centre of the streaks are shown in Figure (4.14) and the overlay of the marked positions with the α-form constructed reciprocal lattice (Figure (4.6)) is shown in Figure (4.15).

4.4 DISCUSSION

The unit cell determination for the three polymorphs in 6GT, i.e. α-, β- and γ-forms, was found rather difficult because of the difficulty in producing a clear X-ray photograph for an oriented specimen of a pure polymorph.

From the investigation of the purity of the β-form from different specimens, a reflection of d-spacing 5.03 Å, which was seen in the equator of all the patterns (Plate 6(a) and (b)) did not appear to

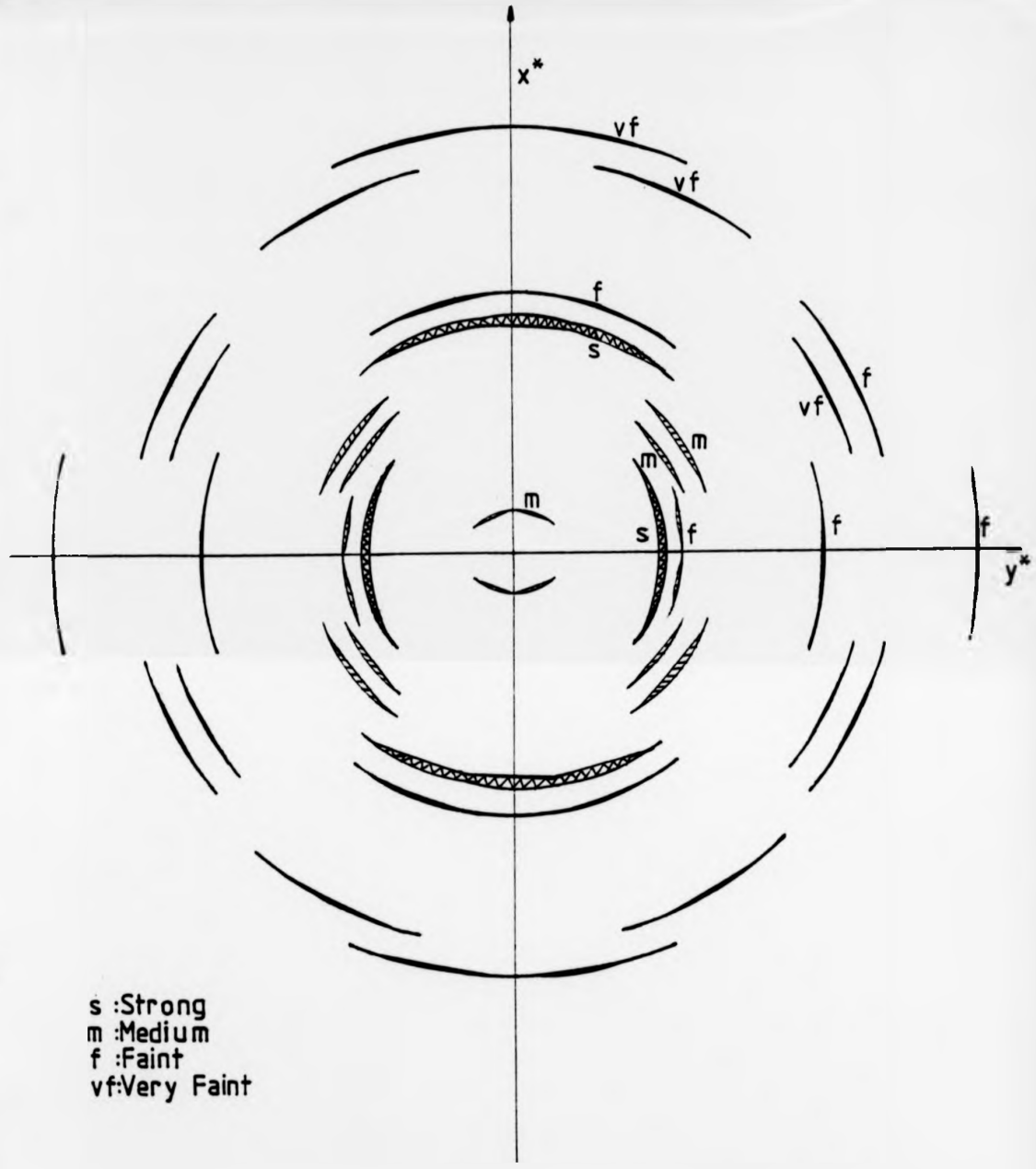

FIG. 4.10: FIRST LAYER LINE RECPROCAL LATTICE FOR THE DOUBLY-ORIENTED SHEET

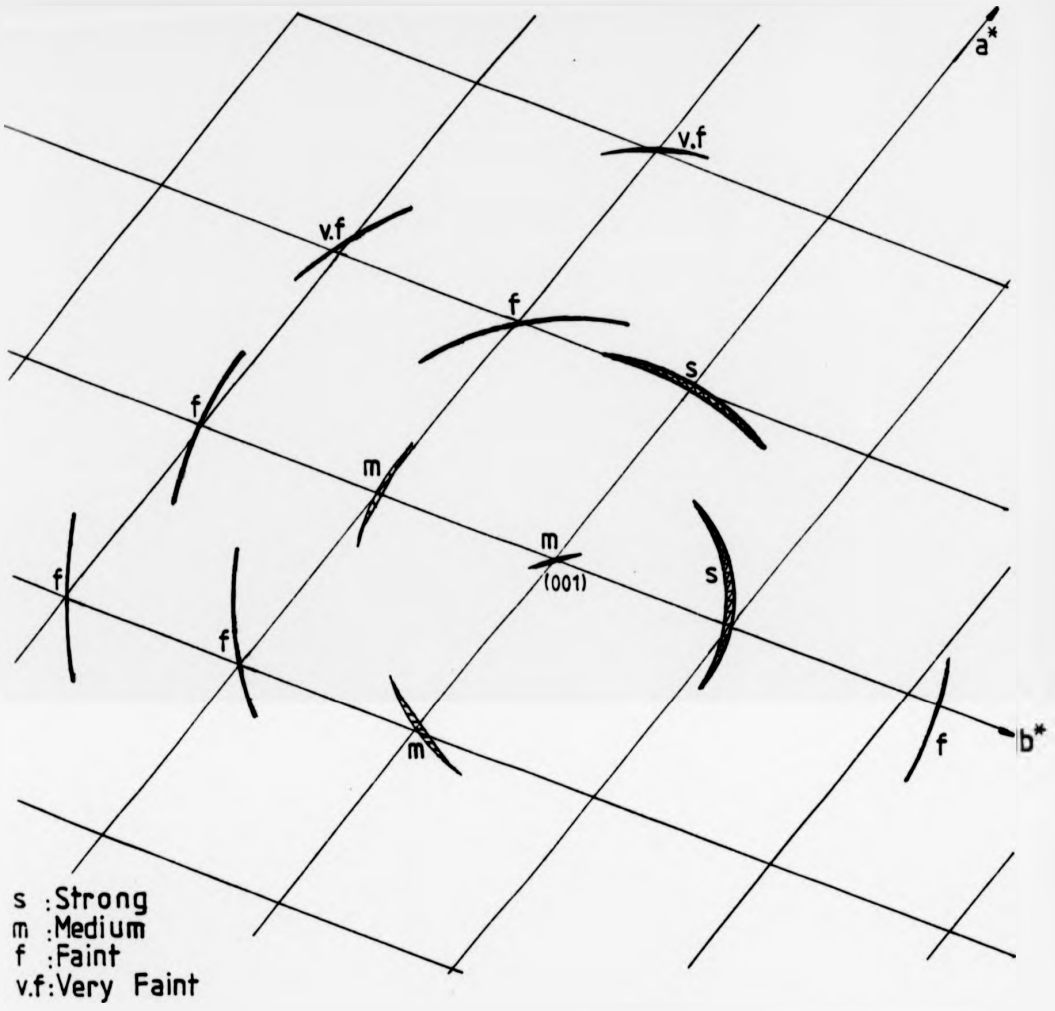

FIG. 4.11 : FIRST LAYER LINE RECIPROCAL LATTICE NET FOR THE DOUBLY-ORIENTED SHEET OF THE β-FORM.

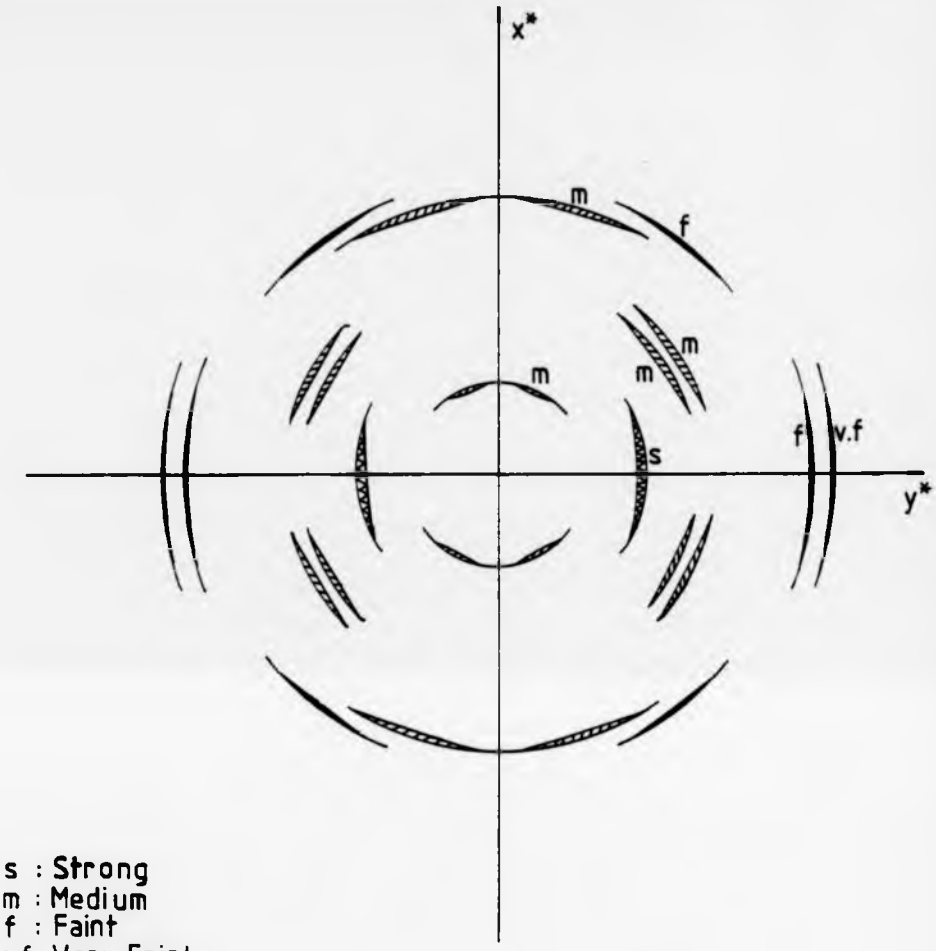

s : Strong
m : Medium
f : Faint
v.f: Very Faint

FIG. 4.12 : SECOND LAYER LINE RECIPROCAL LATTICE FOR THE DOUBLY-ORIENTED SHEET

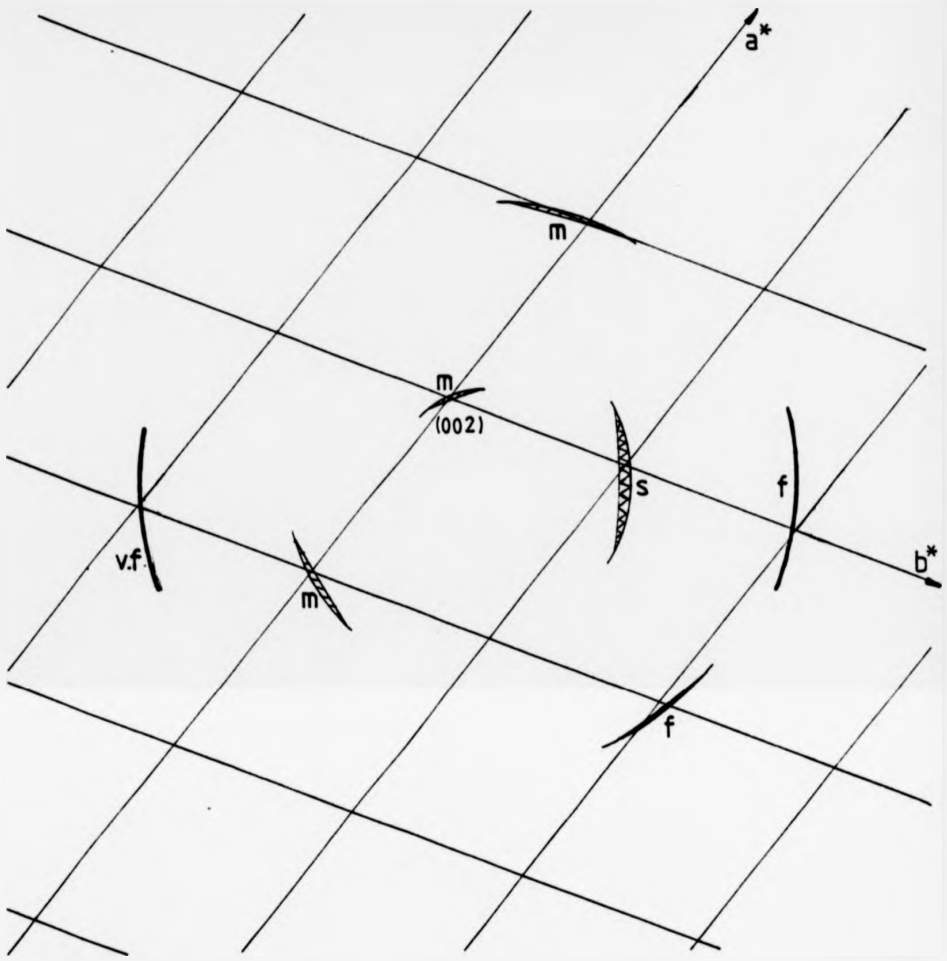

s : Strong
m : Medium
f : Faint
v.f: Very Faint

FIG. 4.13 SECOND LAYER LINE RECIPROCAL LATTICE NET FOR THE DOUBLY ORIENTED SHEET OF THE β-FORM

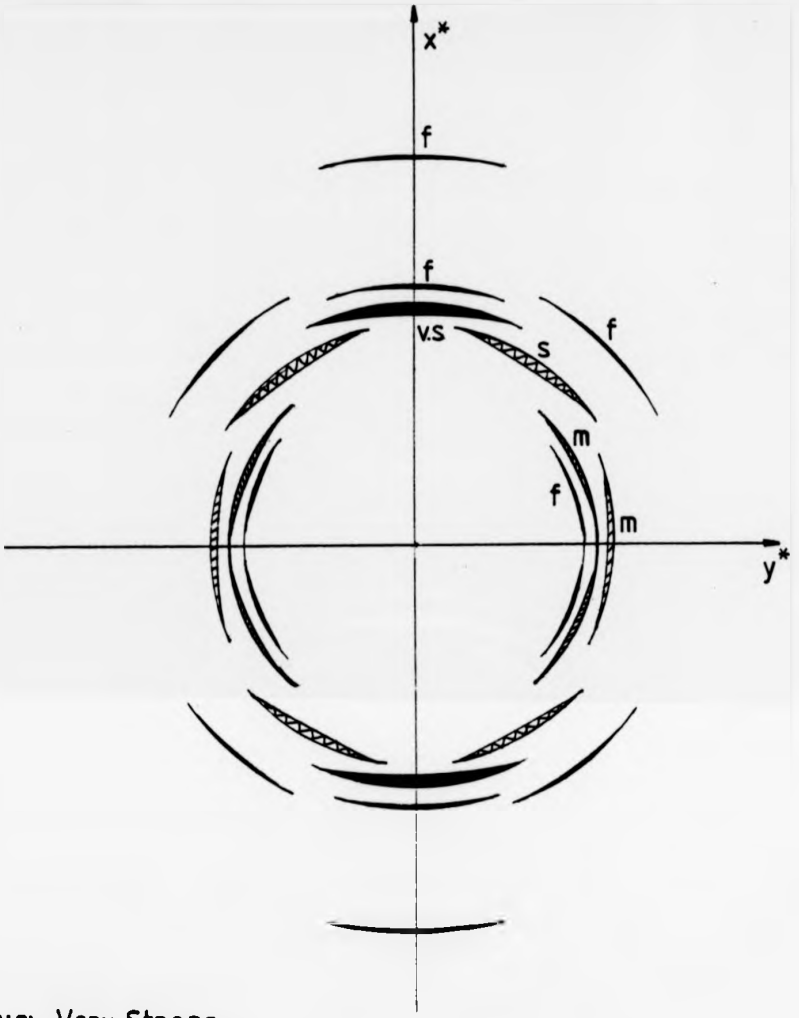

v.s: Very Strong
s : Strong
m : Medium
f : Faint

FIG. 4.14 : EQUATORIAL RECIPROCAL LATTICE FOR THE DOUBLY-ORIENTED PRESSED FILM

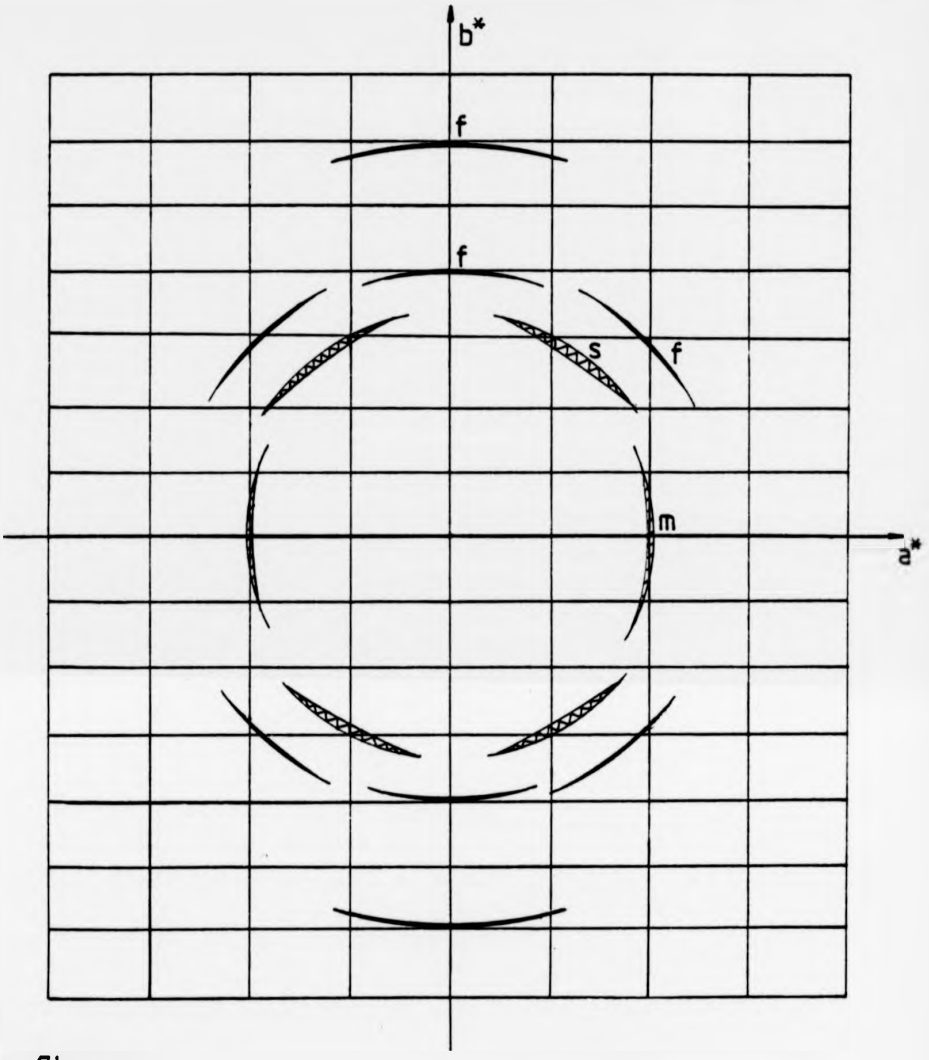

s : Strong
m : Medium
f : Faint

FIG. 4.15 : EQUATORIAL RECIPROCAL LATTICE NET OF THE α-FORM FOR THE DOUBLY - ORIENTED PRESSED FILM.

belong to this form; this reflection was attributed to γ-form polymorph, as shown in Section 4.2.2(b). Some reflections in the higher layer lines of the diffraction pattern of β-form material agreed poorly with their positions predicted from the unit cell (see Table (4.2). Their locations seemed to be sensitive to changes in the proportions of the other forms and could not be accurately determined.

Three remaining reflections would only fit the reciprocal lattice if b* was halved. This doubles the unit cell size and requires there to be two independent chains per cell. Since the reflections were few and faint, this means the chains must differ only slightly. Therefore, it was thought that progress in structure determination would best be made by ignoring them in the first instance. If there were genuinely two chains per cell, a structure would then be obtained with a cell half the true size, containing only one chain in the average of the two conformations. On the other hand, their appearance might be caused by some form of defect structure leading to a superlattice.

The β-form was observed to exhibit tilt which appears to be a feature common to the GT series, i.e. 2-[7], 3-[8], 4-[11,12] and 5GT[14]. After refining the trial unit cell, the tilt was found to be 0.75^{o} which satisfactorily explained the displacement of the reflection. The mean distance between the observed and calculated position of the reflections, including the previously mentioned badly fitting reflections, was found to be 0.033 mm, which is less than the accuracy of measuring the location of the reflections.

From the measured (1.251 gm/cm^3) and calculated unit cell (1.262 gm/cm^3) densities of β-form, the number of monomers per unit cell was calculated, using the relation

$$n \approx \frac{\mu_m}{\mu_{100\%}}$$

where μ_m is the measured density, and found to be only one.

It is usually expected that the measured density is less than that calculated from the unit cell, because of imperfections of the crystals, i.e. presence of amorphous regions. However, the difference between them was found to be small; the measured density may have been influenced by possible presence of α- and γ-forms in the samples under investigation.

The only reflections on the Weissenberg photographs which did not fit the constructed lattice could be accounted for by the other polymorphs. The agreement was also checked for the first and second layer lines. The offset was found to make an angle 135^{o} with the b*-axis, which is in good agreement with the value measured from the cylindrical camera, i.e. 135^{o}.

It was, therefore, concluded that the β-form crystal is triclinic with an identity period of one chain (15.68 Å) and one monomer per unit cell. The lattice parameters were found to be

a = 4.75 Å	$\alpha = 55.7^{o}$
b = 6.23 Å	$\beta = 116.0^{o}$
c = 15.68 Å	$\gamma = 118.8^{o}$

The unit cell determined for the α-form was found to fit most of the reflections well. The few fitting badly (see Table (4.4)) appeared to change position when the proportion of other polymorphs changed. After the refinement of the unit cell, the mean distance between the observed and calculated position of the reflections,

including the badly fitting reflections mentioned above, was found to be 0.021 mm. The parameters of the reciprocal unit cell were found to be

$a^* = 0.170$ r.l.u. $\quad \alpha^* = 52.7^0$

$b^* = 0.112$ r.l.u. $\quad \beta^* = 90.0^0$

$c^* = 0.125$ r.l.u. $\quad \gamma^* = 90.0^0$

Two other pieces of evidence confirm this unit cell. The first evidence was the Weissenberg photographs (Section 4.3.2) in which the reflections appeared as long streaks. Although these made the desired accuracy of measurements unattainable, they were found to fit the reciprocal unit cell well. The other evidence is an electron diffraction pattern of hk0-plane of a single crystal of 6GT. Brisse[58] has obtained crystals giving two different patterns, one of which is shown in Plate 9(a) and gives the following parameters:

$a^* = 0.171$ r.l.u.

$b^* = 0.112$ r.l.u.

and $\gamma = 90.0^0$

These parameters are in close agreement with those obtained above for the α-form. The parameters from Brisse's other pattern will be discussed later.

The unit cell reported here was found to be monoclinic with a calculated density of 0.214 gm/cm^3. The measured density was found to be 1.242 gm/cm^3. From the ratio $\mu_m/\mu_{100\%}$, the number of monomers per unit cell was found to be six. With a monoclinic cell, this would mean that either three or six of them must be independent, i.e. no symmetry relation between them. This is extremely unlikely.

This unit cell was found to fit all the evidence well and confirmed further by the powerful evidence of the electron diffractogram. A possible suggestion may be that the true unit cell contains two chains and that the additional reflections come from some form of disordering.

The X-ray diffraction pattern for cast films (Plate 6(d)) has a reflection (d-spacing = 5.03 Å), and this was attributed to γ-form, as was described in Section 4.2.2(b).

The mean distance between the observed and calculated position of reflections, after the refinements of the constructed reciprocal unit cell, was found to be 0.046mm, which is considered as reasonable. This value is higher than either of those found for the α- and β-forms, which was expected because of the low accuracy of measurements due to the diffuseness of the reflections. The parameters of the reciprocal unit cell, after refinement, were found to be

$a^* = 0.152$ r.l.u. $\quad \alpha^* = 52.1^\circ$

$b^* = 0.388$ r.l.u. $\quad \beta^* = 75.1^\circ$

$c^* = 0.128$ r.l.u. $\quad \gamma^* = 76.8^\circ$

The reciprocal lattice parameters of Brisse's other electron diffractogram of single crystal, shown in Plate 9(b), are as follows:

$a^* = 0.308$ r.l.u.

$b^* = 0.392$ r.l.u.

and $\gamma^* = 76.2^\circ$

These parameters appear to be in close agreement with those of γ-form except that a* has been halved.

PLATE (9): Electron diffraction pattern of (hk0) plane of single crystal of 6GT:

(a) rectangular hk0 section (α-form)

(b) oplique hk0 section (γ-form)

(after Brisse)

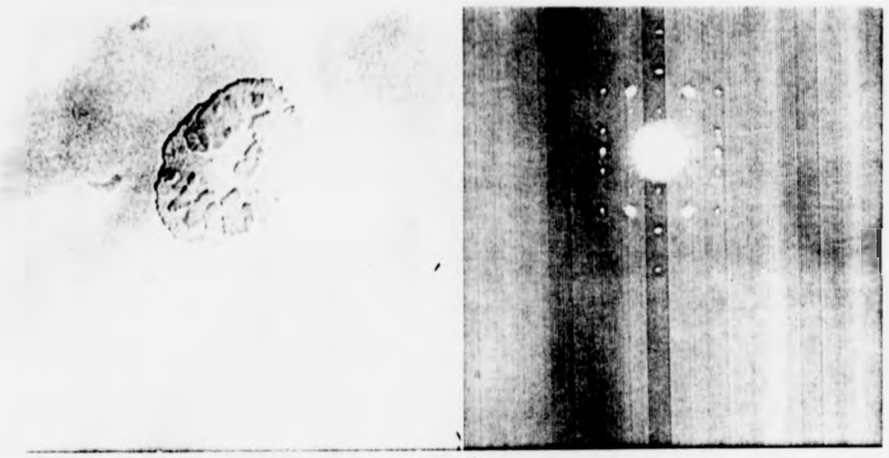

PLATE 9a 6GT rectangular hk0 section

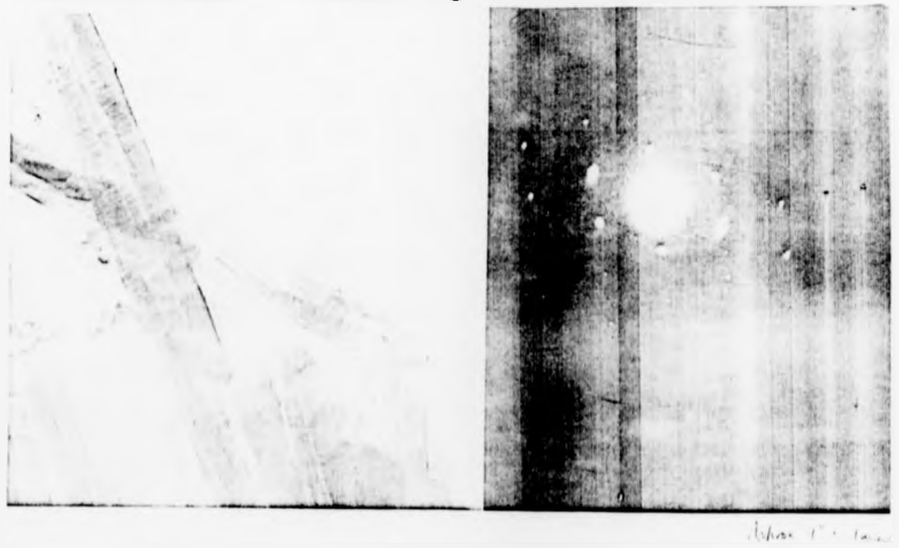

PLATE 9b 6GT oblique hk0 section

PLATE (9): Electron diffraction pattern of (hk0) plane of single crystal of 6GT:

(a) rectangular hk0 section (α-form)

(b) oplique hk0 section (γ-form)

(after Brisse)

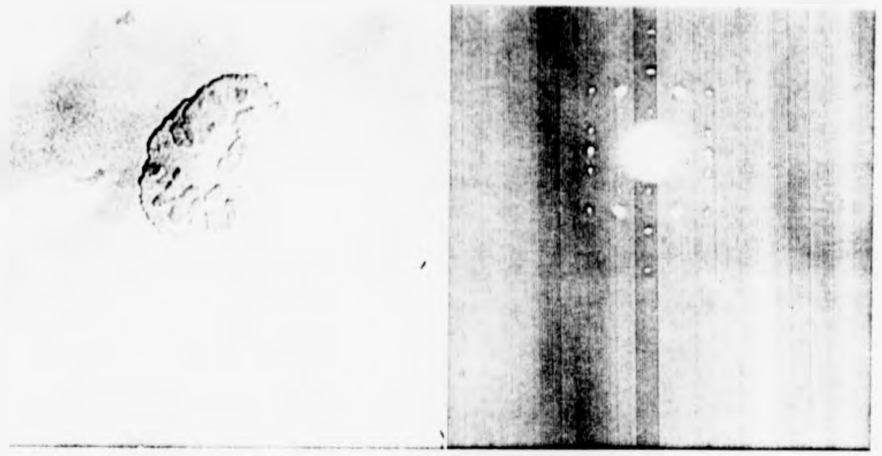

PLATE 9a 6GT rectangular hk0 section

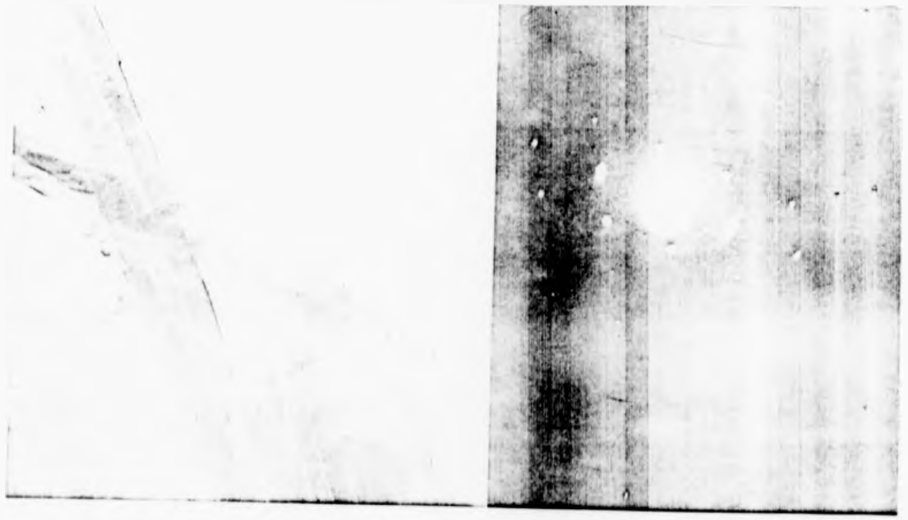

PLATE 9b 6GT oblique hk0 section

The unit cell, after refinement, was found to be triclinic with a calculated density of 0.641 gm/cm^3. From the ratio of the measured (1.256 gm/cm^3) and calculated densities, the number of monomers per unit cell was found to be two. In conclusion, the unit cell for the γ-form is triclinic with identity period of one chain (15.51 ^{o}A) having two monomers per unit cell.

The three lattices proposed above will account for all the spots on the diffraction patterns which have been recorded, except for three which require b* of the β-form reciprocal unit cell to be halved. It is, however, necessary to assume that all of the materials are mixtures of polymorphs, though in varying proportions, so that in determining a unit cell from any one pattern, certain reflections may be omitted. This is risky and could easily lead to misleading results. However, the diffractograms of Brisse, which give independent confirmation of two of the lattices, are strong evidence that in this case, the procedure has not been misapplied.

The unit cell parameters for the α-,β- and γ-forms and the two unit cells previously reported by Bateman et al[4] and Joly et al[15] are listed in Table (4.7). Bateman's and Joly's unit cells appear to have been constructed from measurements on samples having a mixture of, at least, two polymorphs. It was found that neither of the two unit cells would fit all observed reflections of any of the materials described above. Also, the calculated density of Bateman's unit cell (1.144 gm/cm^3) was lower than the measured density of the samples quenched from the melt (1.226 gm/cm^3).

TABLE (4.7)

UNIT CELL PARAMETERS

Parameter	α-Form	β-Form	γ-Form	Bateman[4]	Joly[15]
a (A)	9.06	4.75	10.56	4.57	4.99
b (A)	17.24	6.23	5.05	6.10	4.76
c (A)	15.51	15.68	15.51	15.40	15.40
α(degree)	127.3	55.70	126.2	105.50	119.80
β(degree)	90.0	116.0	98.7	98.50	97.80
γ(degree)	90.0	118.8	95.3	114.50	95.20
V ($\AA^3$)	1928	326	642	360	309

CHAPTER FIVE

Crystal Structure of β-Form

5.1 INTRODUCTION

The structural analysis of high polymers is complex; it is complicated particularly by imperfect crystallite orientation, the small total number of diffraction spots, the large number of overlapping reflections and the appearance of high and variable background intensity of scattered radiation. The analysis of the crystal structure is performed according to a procedure which involves the following:

(a) The determination of the unit cell and space group.

(b) The measurement of the integrated intensity of each observed reflection.

(c) Assuming values of bond parameters.

(d) Proposing a molecular model.

(e) Refining the model against the intensity data.

In this Chapter, a description of the structural analysis of the β-form of 6GT, whose unit cell was established in the previous Chapter, is given.

5.2 INTENSITY MEASUREMENT

The factor of primary importance for the intensity measurements is that the X-ray diffraction photographs must be obtained with maximum contrast. This ensures optimum diffraction intensity which is compatible with optimum peak-to-background intensity ratio. In order to achieve this, it is deemed essential to minimise the contributions of background intensity due to unwanted scattering, which is associated with the X-ray source or the sample; the former could be minimised by the alignment and evacuation of the X-ray camera used. The X-ray camera

used in this work was, therefore, aligned to give highly monochromatic Ni-filtered Cu K_α X-ray beam. The alignment was judged by the X-ray diffraction photograph for NaCl powder, when it appeared as very sharp intense rings.

Another prerequisite of these measurements is the choice of the specimen under investigation; the specimen should possess high crystallinity, good orientation and be free from the other polymorphs of 6GT. The preparation of a 6GT specimen having these properties proved rather difficult, as was described in Chapter Four; all the materials were a mixture of polymorphs.

The preparation of a fibre with a high proportion of β-form required drawing with low draw ratio. However, the X-ray diffraction pattern for such fibre exhibited long arcs, indicative of poor orientation, which are unsuitable for intensity measurements. Unfortunately, the improvement of orientation brought about the appearance of a high proportion of α-form; this proportion could be reduced by annealing at high temperatures but does not remove it completely. Consequently, it was thought preferable to prepare samples with good orientation (T.D.R. = 4) annealed at 150°C for 12 hours, then cooled slowly (10°C/hr.) to room temperature. The sample was prepared as a bundle of five filaments, clamped in the sample holder with the filaments parallel to each other.

A set of eight X-ray diffraction photographs was made using different times of exposure, i.e. 15 minutes-32 hours; in each case, the time of exposure was double the previous one. This procedure ensured bringing out the strong reflections with the short exposure times and the weak ones with the longer exposure times. The complete set of photographs was then developed in freshly prepared developer and fixer.

Throughout the exposures, the current through the X-ray tube and voltage across it were kept steady.

5.2.1 Measurement of Intensity of X-ray Diffraction Spots

A method to obtain the integrated intensities from X-ray diffraction photographs of polymeric fibres has been developed by Hall and Pass[59]. In this method, the intensity is measured by producing contour maps of optical density using a digital microdensitometer and a "photowrite" from which the total intensity is obtained by integrating round the contour lines. This method has been extended by Neisser[60], so that instead of manual integration round contour lines, the intensity is determined directly by computer, and the recent method was used in the present work.

The X-ray diffraction photographs for 6GT were scanned using an Optronix "Photoscan" digital microdensitometer at the S.R.C. Daresbury Laboratories. The area scanned on each film measured 60 x 60 mm^2, thus producing 600 x 600 (x-y) data points per film. The data were then stored on magnetic tape, and from which contour maps were created; from these maps the location of the centre was measured and the area of the individual reflections was estimated. These and the digitized intensity data were used as input data to a computer program designed for the calculation of the integrated intensities. The program performs the calculation of the integrated intensity according to the following steps:

1. The selected field of the reflection is corrected for the Lorentz polarisation factor on a point-by-point basis.

2. A correction is introduced to account for background intensity for each diffraction spot.

3. For the purpose of computing the integrated intensity of a given spot, the program assumes that the shape of this spot could be approximated by an ellipse. Accordingly, the location of the peak value is found. At this stage, a fraction of the peak intensity is computed by multiplying this peak value by one of a certain set of numbers ranging between 0.1 and 0.8, which could assume values in increments of 0.1 only. The set comprised four such numbers which were determined by the user depending on the nature of the spot; for intense, well-defined spot low values were used, whereas, for weak and diffuse ones, high values were used. The program then proceeded to locate all data points whose values were greater than or equal to this fraction and these locations were subsequently employed in the determination of an ellipse. The procedure was repeated using a smaller fraction of the peak intensity and increasing ellipse size until the largest satisfactory ellipse was fitted. Criteria wereavailable to indicate if the reflection was merging into another one and, if so, the fitting procedure was stopped. In this case, the final ellipse was scaled up by a predetermined scheme to a true representation of the reflection boundary. All the data points lying within the boundary of this ellipse were then summed to give the integrated intensity.

5.2.2. Separation of Intensity Contributions by α and β-Forms

It was mentioned above that a sample with good orientation was chosen for the intensity measurements of the β-form. However, the wide-angle X-ray diffraction pattern for this sample showed the co-existence of a small proportion of α-form crystals with the dominant β-form ones. The reflections from the α-form crystals which directly interfere with the intensity measurement of the β-form should be considered. Attempts were, therefore, made to separate the intensity contribution by the α-form reflections from that by the β-form in the

X-ray diffraction pattern under investigation by adopting the following procedure:

The integrated intensity of a reflection belonging to the α-form (d = 7.46 Å) appearing on the first layer line of the X-ray diffraction pattern under investigation, was measured. The integrated intensity of the same reflection appearing in the X-ray diffraction pattern of a dominant α-form sample, taken with equal exposure time, was measured. A ratio of the latter integrated intensity to the former was calculated; it was used in calculating the integrated intensity of the β-form reflection considered as being affected by an intensity contribution by an overlapping α-form reflection. The intensity contribution by the α-form reflection was calculated by multiplying this ratio by the measured integrated intensity of the overlapping reflections in the X-ray diffraction pattern under investigation. Finally, the integrated intensity of the β-form reflection was calculated by subtracting the integrated intensity contribution by the α-form from the measured integrated intensity of the overlapping reflections.

5.3 DETERMINATION OF CHAIN CONFORMATION

It was shown in Chapter Four that the identity period was 15.68 Å and, by comparing it with the chemical repeat unit 16.1 Å, one monomer per crystallographic repeat was, therefore, found. Comparison of the density calculated from the unit cell with the measured value, then showed that there was one molecular chain per cell. This monomer unit is shown in Figure (5.1), which also defines the symbols used in specifying particular bonds and angles.

The values of bond lengths and angles were assumed to be the same as those in comparable low molecular weight compounds. The values

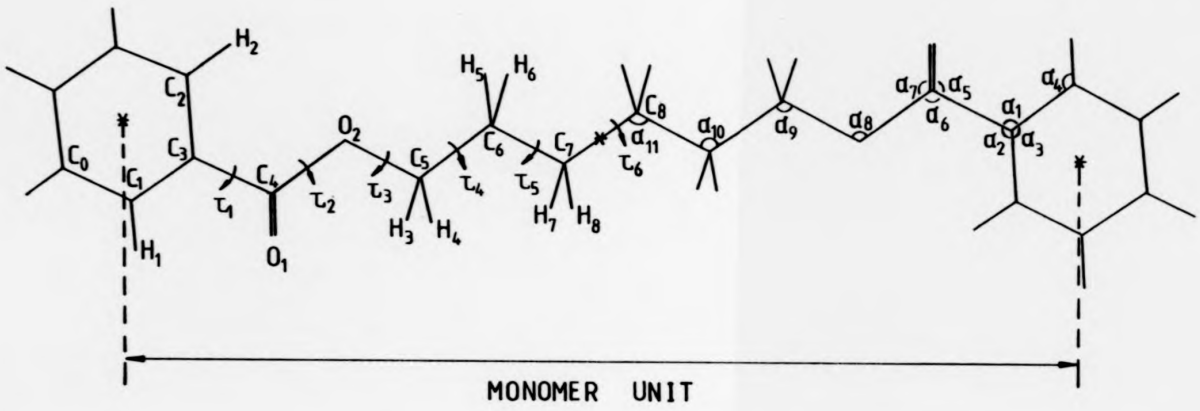

FIG. 5.1 : MONOMER OF 6GT. *Centre of Symmetry.

assumed are shown in Table (5.1), and were chosen by using as guides the studies of Perez and Brisse[61] in their structural analysis of (hexa-methylene glycol dibenzoate) and of Hall and Pass[11] in their determination of the structure of 4GT.

5.4 THE MOLECULAR MODEL

For the work of Perez and Brisse[61,62] on oligomers of glycol terephthalate polymers, and from the structural determinations of 2GT[7] and 4GT[11,12], it seemed reasonable to assume that the chain conformation would be centro-symmetric. Thus, since bond lengths and angles are fixed, the only degrees of freedom available to the system are the chain conformation angles τ_1 to τ_5, as shown in Figure (5.1) (from the assumption of centro-symmetry $\tau_6 = 180^o$) and the angles which define the inclination of the molecules within the unit cell. The definition of τ and the way it is measured will be given later. The terephthaloyl unit has always been found in all similar structures to be within a few degrees of planarity and so in the initial model τ_1 was made to be 0.0. Similarly, τ_2 has been found to be always close to 180^o in similar compounds and was also fixed at this value. It was seen in Chapter Four that the crystallographic repeat length (15.68 Å) is slightly shorter than the calculated fully extended length (16.10 Å); this suggests that τ_3, τ_4 and τ_5 should not vary much from 180^o.

Another model was built by using the same values of $\tau_1 - \tau_6$ as those reported by Perez et al[61] on their work on the crystal structure of hexamethylene glycol dibenzoate. The results of the τ's for these two models after refinement - described in the next section - were found to be the same. Structural investigations of the constructed models

TABLE (5.1)

Values assumed for Bond Lengths and Angles

Bond	Length ($\mathring{A}$)
C_0-C_1	1.38
C_1-C_3	1.37
C_2-C_3	1.38
H_1-C_1	1.00
H_2-C_2	0.98
C_4-C_3	1.48
O_1-C_4	1.20
O_2-C_4	1.33
C_5-O_2	1.45
H_3-C_5	0.97
C_6-C_5	1.49
C_7-C_6	1.52
C_8-C_7	1.50
	Angle(deg)
α_1	118
α_2	123
α_3	119
α_4	120
α_5	124
α_6	113
α_7	123
α_8	116
α_9	108
α_{10}	112
α_{11}	113

were carried out using a computer program, which will be described in detail next.

5.5 THE LINKED ATOMS LEAST SQUARES COMPUTER PROGRAM, LALS

The program LALS has been designed essentially to overcome the problems arising in the determination of crystal structure using intensity data collected from fibre X-ray diffraction photographs. This method was developed by Arnott et al[63]. It has been described and analysed by them and involves the refinement of the positional and conformational chain parameters of a model system so as to minimise the sum of the squares of the differences between the observed and calculated structure factors. Before refining the model against the X-ray intensity data, two additional refinements could also be performed:

(a) Elastication refinement

The initial model parameters might not meet the constraints of symmetry and chain repeat length. It is then possible to adjust these parameters by small amounts from the initial input values in an attempt to meet the constraints. This can be controlled by choosing a suitable input weighting scheme.

(b) Contact refinement

This refinement is employed to minimise the sum of the squares of the differences between the separation of the centres of a pair of atoms and the sum of their Van der Waals radii for all pairs whose separation is smaller than this sum.

For computation purposes, a model of the chain is built by successively adding atoms, starting at H_1 and proceeding to C_9 (Fig.(5.1)).

Suppose the atom C_5 has been reached and C_6 is about to be laid down; its position will be determined by three parameters, the bond length C_5-C_6, the bond angle α_3 and the conformation angle τ_3. The method by which τ_3 is measured may be understood by reference to Figure (5.2). In this figure, the section of the chain C_4-O_2-C_5-C_6 is held so that O_2-C_5 (the bond about which τ_3 is being measured) is normal to the plane of the diagram with C_4-O_2 (the section already built) above the plane of the diagram and C_5-C_6 (the section about to be built) below. τ_3 is then measured; it is positive if measured clockwise and negative if anticlockwise.

When the chain conformation has been fixed, the molecule still has to be placed in the unit cell. Its location is determined by the fact that the centre of the benzene ring (C_1-C_2-C_3) lies at the cell origin and the chain axis coincides with the c-axis but the relation of the chain about its axis is still undetermined.

In LALS the orientation of the molecule is controlled by the three Eulerian angles (ϕ's). To bring the molecule into its correct orientation, it is rotated by ϕ_x about x, followed by a rotation ϕ_y about y and then by ϕ_z about z. The rotation is anticlockwise looking in the negative direction along an axis. ϕ_x and ϕ_y will be fixed by the requirement that the chain axis coincides with the c-axis and ϕ_z controls the rotation of the chain about its axis.

5.6 RESULTS

5.6.1 Refinement of the Model

The first stage of the refinement involved elastication, as described above, to produce a model to meet the crystallographic requirements. The bond angles and lengths were kept constant at the

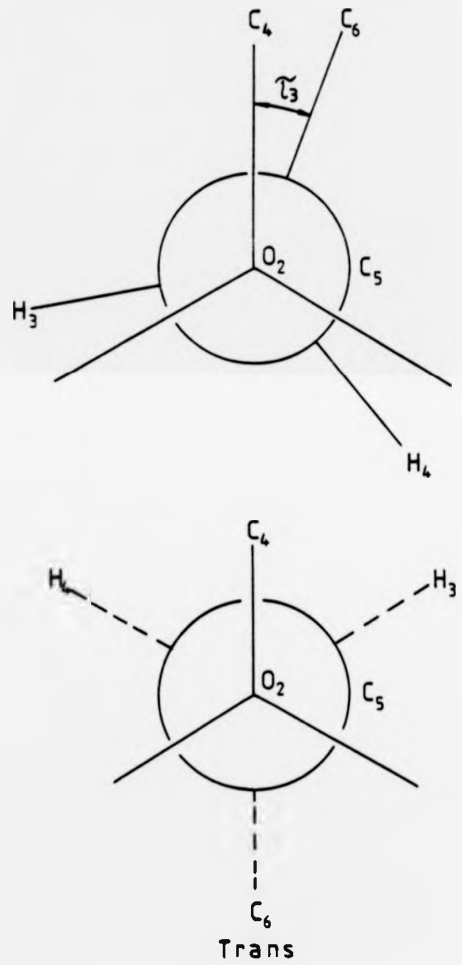

FIG. 5.2 : CONVENTION FOR MEASURING THE CONFORMATION ANGLE τ.

values listed in Table (5.1). The terephthaloyl parts of the chain were kept planar, i.e. τ_1 was fixed at 0.0^0. τ_2 was similarly restricted, and for centro-symmetry τ_6 had to be left at 180^0. The parameters allowed to vary were the conformation angles τ_3, τ_4 and τ_5 and the Eularian angles ϕ_x and ϕ_y. Since ϕ_z is the rotation of the chain about its axis, it was kept fixed during this procedure. These τ's were allowed to move only by 3^0 each cycle as the molecule was adjusted to meet the necessary constraints; this was facilitated by means of a weighting scheme within the program which could be controlled with the input data. At the end of this refinement, the two models were found to have the same values of τ's.

It was found that a model centrosymmetric about the points marked in Figure (5.1) (the central bond along the chain C_7-C_8 and also the centre of each benzene ring) could be built to meet the required crystallographic repeat length. The τ's values at the end of this stage are listed in column 1 of Table (5.2).

5.6.2 Refinement of the Model against the X-ray Intensity Data

The parameters, defining the chain conformation of the model given in column 1 of Table (5.2), were refined against the X-ray intensity data to minimise the quantity $|F_o-F_c|$. These values were weighted according to the Cruickshank weighting scheme, using the following formula:

$$W = 1.0/(A+BF_o+CF_o^2)$$

where W is the weighting factor for each reflection and is determined by the observed structure factor, F_o. A, B and C are constants chosen such that the very intense reflections have low weighting and the weak ones have high weighting. This scheme, then, ensures that the

TABLE (5.2)

Parameters defining Chain Conformation

	1	2	3
τ_1 (deg)	-2.(9)	12.(4)	13.(1)
τ_2 (deg)	-176.(1)	-169.(7)	-146.(1)
τ_3 (deg)	171.(4)	-177.(9)	-148.(2)
τ_4 (deg)	-177.(8)	-167.(2)	-171.(1)
τ_5 (deg)	178.(9)	-154.(2)	171.(4)
τ_6 (deg)	180.(0)	180.(0)	180.(0)
θ (deg)	-18.(0)	-39.(7)	-29.(4)
ϕ (deg)	28.(9)	28.(4)	27.(6)
ψ (deg)	95.(4)	87.(2)	88.(6)
R		20.6	28.2

refinements are not biased towards the strong reflections only.

In the first stage of the refinement, performed on observed reflections only, the bond lengths and angles were kept constant at the values given in Table (5.1). Meanwhile, τ_1-τ_5 and the Eulerian angles ϕ_x, ϕ_y and ϕ_z were allowed to vary without restrictions; the values at the end of this stage are given in column 2 of Table (5.2). The residual factor is given by:

$$\sum R = \frac{\sum |F_o - F_c|}{\sum F_o}$$

Reflections on the same layer line with similar d-spacings were treated in the refinement as belonging to a composite group.

In Table (5.2), three parameters (θ, ϕ and ψ) are given in addition to those already defined. Only θ is essential to locate the chain; it is the angle about the c-axis through which the molecule must be rotated to bring the normal to the benzene ring (C_1-C_2-C_3) from the (010) plane to its correct position and it is positive if this rotation is anticlockwise looking in the negative c-direction. ϕ and ψ are not essential to defining the structure but help in visualising the orientation of the terephthaloyl residue. ϕ is the angle between the bond C_3-C_4 and the c-axis; ψ is the angle the normal to the benzene rings (C_1-C_2-C_3) makes with the c-axis.

Unobserved reflections were then included in the refinement at threshold intensity and only omitted if the calculated value was less than this threshold. Attempts were made to calculate the threshold intensity by adopting the following procedure:

A map of the intensity distribution in the region where the reflection was expected to appear was produced by printing the intensity

values from the microdensitometer scan of this region. This was large enough to include a nearby observed reflection. The ratio of the highest intensity value in the expected position of the unobserved reflection to the highest in the observed was then calculated. The threshold intensity was then taken as that of the observed reflection multiplied by this ratio.

The calculated threshold intensity was found to vary considerably as a consequence of a variation in the background from one region to another. In some instances, the unobserved reflections were found to exist in the intensity distribution map; therefore, such reflections were included in the calculations as observed reflections. The refined values of the conformational parameters are listed in column 3 of Table (5.2). The residual factor, R-factor = 28.2, was calculated on observed reflections only.

The fractional atomic co-ordinates calculated from the parameters listed in column 3 of Table (5.2) are listed in Table (5.3).
A comparison between the observed and calculated structure factors for β-form is given in Table (5.4). The chain conformation and packing within the unit cell are illustrated in Figures (5.3)-(5.5).

5.7 DISCUSSION

The shape of the terphthaloyl residue defined by τ_1, is near to planar conformation, as seen in column 3 of Table (5.2). Daubeney et al[7] have found that in 2GT the carbonyl unit was about 10^o out of the plane of the benzene ring. Deviations from planarity of 10^o-20^o might not be surprising, although for 3-[8], 4-[13], and α-5GT[14] it was found to be about 10^o. τ_2 is usually close to 180^o in similar structures; the deviation here (τ_2 = -146^o) is larger than those found

TABLE (5.3)

Fractional Atomic Co-ordinates

Atom	x	y	z
C_1	-0.251	-0.246	0.030
C_2	0.150	0.139	0.060
C_3	-0.101	-0.106	0.090
H_1	-0.433	-0.424	0.052
H_2	0.258	0.239	0.103
C_4	-0.217	-0.228	0.187
O_1	-0.393	-0.460	0.225
O_2	-0.107	-0.054	0.226
C_5	-0.040	-0.173	0.341
H_3	-0.181	-0.361	0.368
H_4	0.211	-0.167	0.374
C_6	-0.107	-0.010	0.367
H_5	0.014	0.191	0.328
H_6	-0.325	-0.037	0.348
C_7	0.008	-0.093	0.486
H_7	-0.134	-0.282	0.525
H_8	0.250	-0.088	0.512
C_8	-0.008	0.093	0.514

TABLE (5.4)

Observed and Calculated d-Spacings

and Structure Factors

Indices	d_{calc}(Å)	d_{obs}(Å)	F_{calc}	F_{obs}
0 1 0	4.88	4.82	81	93
1 0 0	4.05	4.10	84	87
1 $\bar{1}$ 0	3.75	3.72	168	238
1 1 0	2.72	2.62	21	15
1 $\bar{2}$ 0	2.46	-	23	(9)*
0 2 0	2.44	2.41	17	13
2 $\bar{1}$ 0	2.12	2.12	39	19
2 0 0	2.03	2.02	6	11
2 $\bar{2}$ 0	1.88	-	64	48
1 2 0	1.85	1.85	15	37
1 $\bar{3}$ 0	1.71	1.72	6	11
2 1 0	1.69	-	9	(9)*
0 0 1	12.60	12.30	16	23
0 1 1	5.45	5.47	30	57
$\bar{1}$ 1 1	4.32	-	34	28
$\bar{1}$ 0 1	4.15	4.15	63	92
0 $\bar{1}$ 1	3.99	3.93	47	69
1 0 1	3.62	3.65	31	26
1 $\bar{1}$ 1	3.15	3.18	20	22
$\bar{1}$ 2 1	2.74	-	21	(14)*
1 1 1	2.72	-	8	(14)*
0 2 1)	2.63)	2.607	42	45
$\bar{1}$ $\bar{1}$ 1)	2.61)			
$\bar{2}$ 1 1	2.26	2.27	35	32
0 $\bar{2}$ 1	2.22	-	25	21
1 $\bar{2}$ 1	2.19	2.18	4	24
$\bar{2}$ 0 1	2.08	2.10	31	27
$\bar{2}$ 2 1	2.03	-	29	(18)*
2 $\bar{1}$ 1	1.96	-	21	(14)*
2 0 1	1.93	-	8	(11)*
1 2 1	1.90	-	10	(7)*
$\bar{1}$ 3 1	1.84	-	1	(7)*
$\bar{1}$ $\bar{2}$ 1	1.77	1.77	37	32
2 $\bar{2}$ 1	1.72	-	16	(9)*
0 3 1	1.72	-	4	(9)*
$\bar{2}$ $\bar{1}$ 1	1.69	1.69	36	36
2 1 1	1.67	-	10	(9)*
$\bar{2}$ 3 1	1.63	-	6	(9)*
0 0 2	6.30	6.26	8	18
0 1 2	5.13	5.13	20	33
$\bar{1}$ 1 2	4.52	-	8	(6)*
$\bar{1}$ 0 2	3.84	3.78	6	12
0 $\bar{1}$ 2	3.22	-	11	(6)*
1 0 2	3.10	3.13	19	22

TABLE (5.4) contd.

Indices	d_{calc} (Å)	d_{obs} (Å)	F_{calc}	F_{obs}
$\bar{1}$ 2 2	2.96	2.95	20	20
0 2 2	2.73	2.74	28	27
1 $\bar{1}$ 2	2.64	-	8	(6)*
1 1 2	2.59	2.57	24	25
$\bar{1}$ $\bar{1}$ 2	2.42	-	2	(3)*
$\bar{2}$ 1 2	2.34	2.28	6	10
$\bar{2}$ 2 2	2.16	-	2	(6)*
$\bar{2}$ 0 2	2.07	2.07	2	9
0 $\bar{2}$ 2	2.00	-	12	(6)*
$\bar{1}$ 3 2	1.95	-	16	(6)*
1 $\bar{2}$ 2	1.94	1.93	2	9
1 2 2	1.90	-	3	(6)*
0 1 3	4.27	-	3	(6)*
$\bar{1}$ 1 3	4.20	-	7	(6)*
0 0 3	4.20	-	0	(6)*
$\bar{1}$ 0 3	3.33	3.31	23	34
$\bar{1}$ 2 3	3.06	-	4	(10)*
0 2 3	2.70	2.70	12	31
0 $\bar{1}$ 3	2.65	-	10	(10)*
1 0 3	2.63	-	8	(10)*
1 1 3	2.39	-	4	(10)*
$\bar{2}$ 1 3	2.35	-	19	(10)*
$\bar{2}$ 2 3	2.24	2.27	11	17
1 $\bar{1}$ 3	2.24	-	4	(10)*
$\bar{1}$ $\bar{1}$ 3	2.19	2.18	11	14
$\bar{1}$ 3 3	2.04	-	13	(9)*
$\bar{2}$ 0 3	2.02	-	5	(9)*
1 2 3	1.86	-	12	(9)*
$\bar{2}$ 3 3	1.82	-	6	(9)*
0 3 3	1.82	-	8	(9)*
0 $\bar{2}$ 3	1.79	-	9	(9)*
1 $\bar{2}$ 3	1.72	-	2	(6)*
2 0 3	1.68	1.68	1	11
2 $\bar{1}$ 3	1.63	-	12	(6)*
$\bar{1}$ 1 4	3.59	3.55	24	25
0 1 4	3.44	3.46	20	19
0 0 4	3.15	3.13	18	20
$\bar{1}$ 2 4	2.97	2.95	10	16
$\bar{1}$ 0 4	2.82	-	4	(6)*
0 2 4	2.57	-	7	(6)*
$\bar{2}$ 1 4	2.28	-	14	(6)*
$\bar{2}$ 2 4)	2.26)	2.26	27	36
1 0 4)	2.25)			
0 $\bar{1}$ 4	2.23	2	2	(6)*
1 1 4	2.17	-	6	(6)*
$\bar{1}$ 3 4	2.07	-	1	(6)*
$\bar{1}$ $\bar{1}$ 4	1.97	2.00	5	11
1 $\bar{1}$ 4	1.94	-	13	(6)*
$\bar{2}$ 0 4	1.92	-	1	(6)*
$\bar{2}$ 3 4	1.88	-	2	(6)*
0 3 4	1.82	1.83	11	21
1 2 4	1.79	-	4	(6)*

TABLE (5.4) contd.

Indices	d_{calc} (Å)	d_{obs} (Å)	F_{calc}	F_{obs}
$\bar{1}$ 1 5	3.01	-	16	(9)*
0 1 5	2.81	-	17	(9)*
$\bar{1}$ 2 5	2.76	2.74	6	11
0 0 5	2.52	2.53	13	10
$\bar{1}$ 0 5	2.40	2.39	18.	26
0 2 5	2.36	-	4	(9)*
$\bar{2}$ 2 5	2.21	2.19	18	18
$\bar{2}$ 1 5	2.15	2.14	18	20
$\bar{1}$ 3 5	2.06	-	17	(9)*
1 0 5	1.95	-	9	(9)*
1 1 5	1.94	-	18	(6)*
0 $\bar{1}$ 5	1.92	-	7	(6)*
$\bar{2}$ 3 5	1.90	-	1	(6)*
$\bar{2}$ 0 5	1.80	-	1	(6)*
0 3 5)	1.78)	1.77	20	18
$\bar{1}$ $\bar{1}$ 5)	1.77)			
1 $\bar{1}$ 5)	1.70)	1.68	22	12
1 2 5)	1.69)			
$\bar{1}$ 2 6	2.48	-	11	(10)*
0 1 6	2.35	-	24	(10)*
0 2 6	2.13	-	22	(18)*
$\bar{2}$ 2 6	2.10	-	20	(18)*
0 0 6)	2.10)	2.12	16	48
$\bar{1}$ 0 6)	2.07)			
$\bar{2}$ 1 6)	1.99)	1.97	51	58
$\bar{1}$ 3 6)	1.99)			

*Brackets indicate reflection is unobserved.

Value within brackets is threshold of observation in vicinity of the reflection.

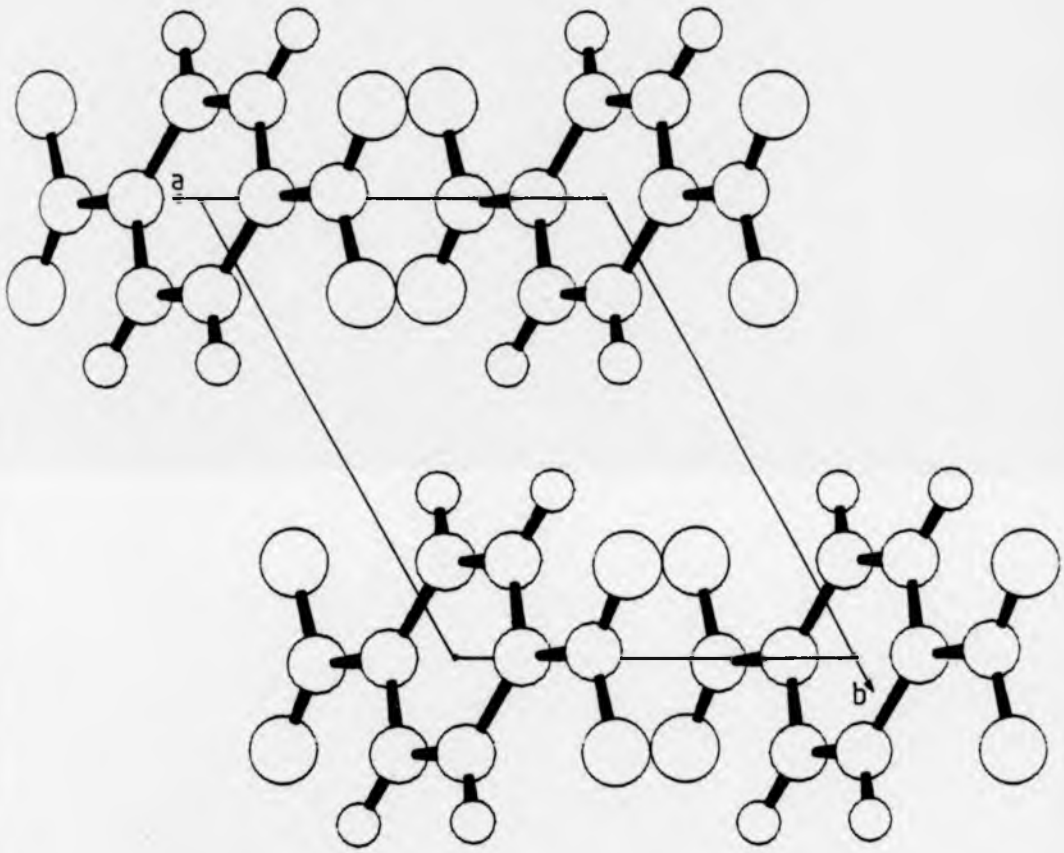

FIG. 5.3 : PROJECTION ON TO a-b PLANE

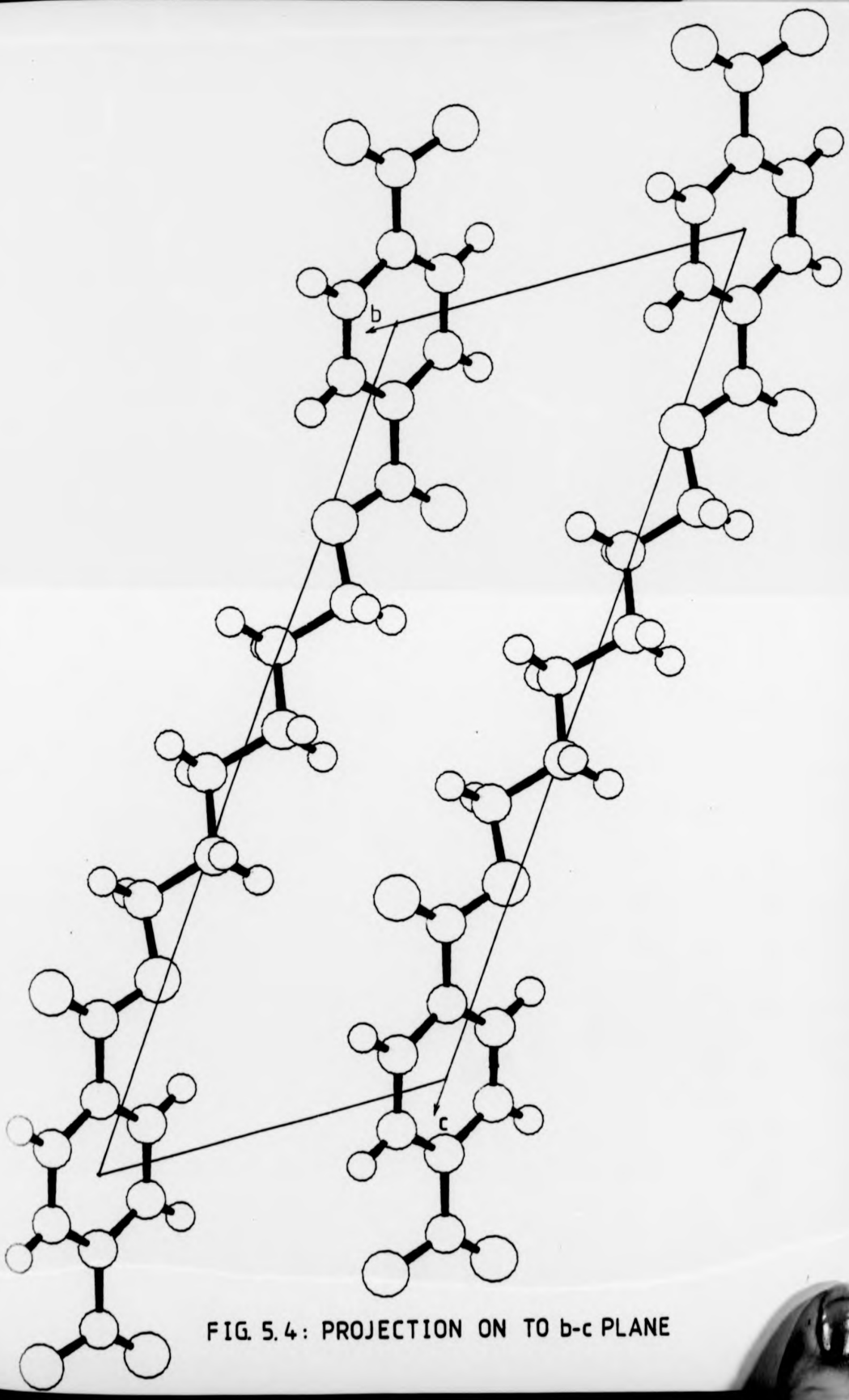

FIG. 5.4: PROJECTION ON TO b-c PLANE

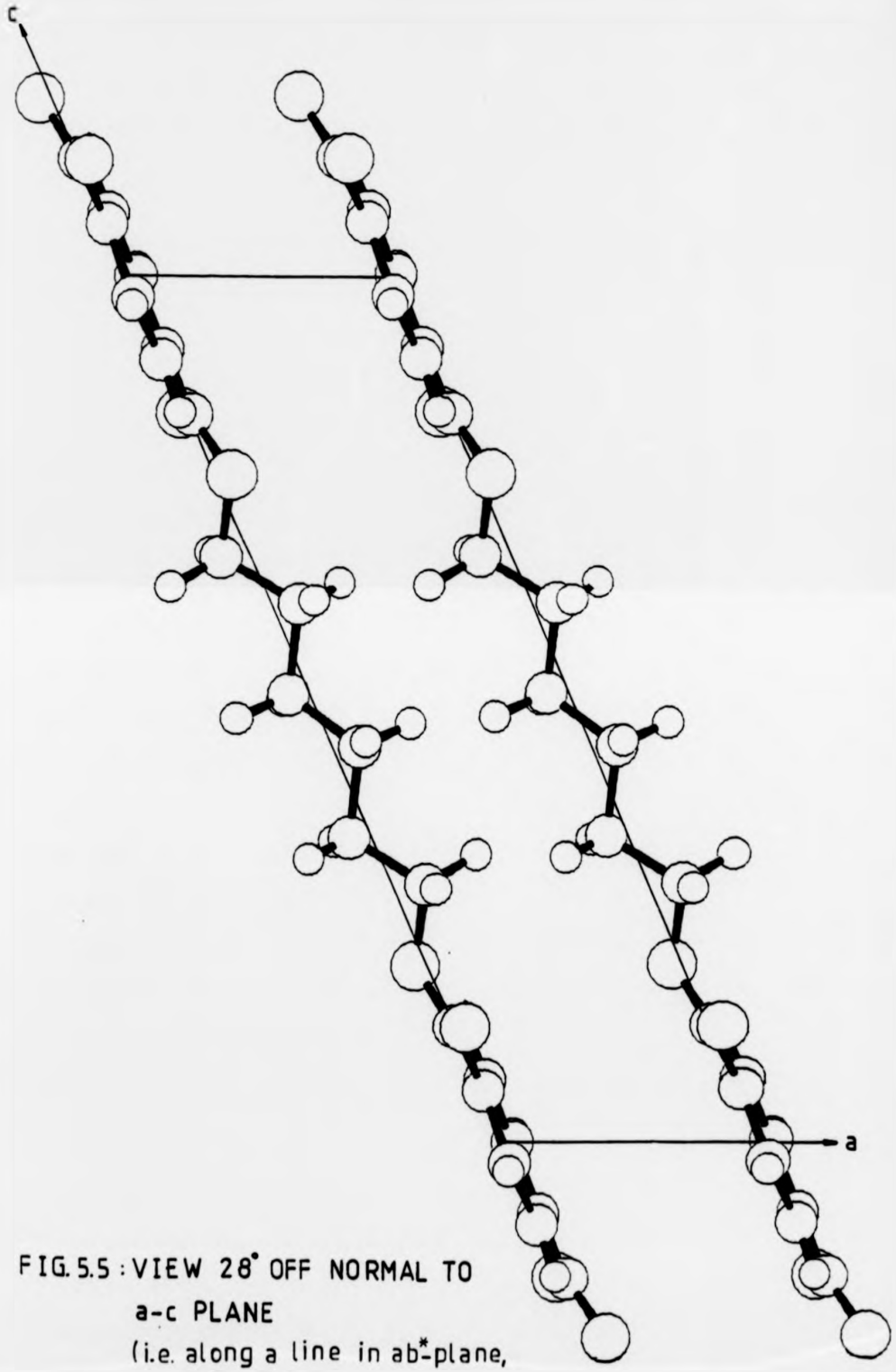

FIG. 5.5 : VIEW 28° OFF NORMAL TO
a-c PLANE
(i.e. along a line in ab^*-plane,
28° to b^*)

in other materials. The value of τ_3 varies widely in different compounds: for 6GT, τ_3 was found to be -148^0. τ_4 and τ_5 were found to be near to a planar conformation; both were 171^0.

The deviation from the planarity for the τ_2 and τ_3 values, after introducing the unobserved reflections, was observed to be high. The value of τ_3, similar to that given above, has been found in other materials[13], but the deviation of τ_2 from 180^0 is unusually large. These values may have been affected by the calculated integrated intensities, since the value of the residual factor on observed reflections only(28.2%) is higher than that for the other members of the series having similar structure.

The measurement of the integrated intensities was undoubtedly affected by the intensity contributed by the other polymorphs, i.e. α- and γ-form. The integrated intensities were measured using the computer method because it appeared to offer the best available and most convenient method. However, at the time it was used the computer program was in a state of development, and in the course of its application to this material, several weaknesses were discovered. Some of these have been corrected in later versions of the program but these became available too late to use in the present investigations. The principal difficulties were as follows:

In the intensity measurement, the ratios of the integrated intensities of the same spot on films taken with different exposure times were found incompatible with the times of exposure. These discrepancies were attributed to the corrections introduced into these measurements. In this work each point was corrected by the LP factor before background correction was made. It has later been found that this leads to a poor background correction.

In higher layer lines, weak reflections were banana shaped and the ellipse fitting routine could not handle these, particularly where there was high background or overlap with another layer line. The integrated intensity of these reflections was measured by adopting the same procedure used in measuring the threshold intensity (Section 5.6.2).

It can be seen from Table (5.4) that the structure factor for the observed reflections is higher than the calculated one, particularly for the weak reflections, which may be attributed to the presence of small proportion of α-form crystals in the sample under study. It appears that the ratio, calculated in Section 5.2.2, may have not been satisfactory for all reflections, as it may vary from one reflection to another.

CHAPTER SIX

Mechanical Properties

6.1 INTRODUCTION

It has been concluded in Chapter Four that 6GT has three polymorphic forms, i.e. α-, β- and γ-form. The proportions of these forms have been found to depend upon the procedure of production, i.e. melt-crystallisation under no stresses (β-form), melt-crystallisation under imposed stresses (α-form), and crystallisation from solution (γ-form). Furthermore, the proportions of these forms have also been found to depend upon the draw ratio and the annealing temperature.

Thus, the mechanical properties in this work were carried out mainly to investigate if the proportion of the various polymorphs will affect the mechanical properties. In this Chapter, three types of tests will be presented: stress-strain behaviour for as-spun fibres with different take-up velocities, stress-strain behaviour of treated fibres (drawn with different speed of drawing to different draw ratios) and elastic recovery. The shrinkage of these fibres will also be presented, in an attempt to relate this to the elastic recovery. Finally, the results will be discussed and also compared with other GT's.

6.2 EXPERIMENTAL

6.2.1 Tensile Measurements

The mechanical properties of the melt-spun and drawn fibres were measured at room temperature using an Instron tensile tester. In each test, the load-elongation curves were obtained for 10 samples each having an initial fibre length of 5 cm. A typical experimental load-elongation curve for the as-spun fibre with take-up velocity 50m/min. is shown in Figure (6.1), on which the yield load (Y), drawing load (D), the load at break (LB), and the extension at break (EB) are indicated. The values

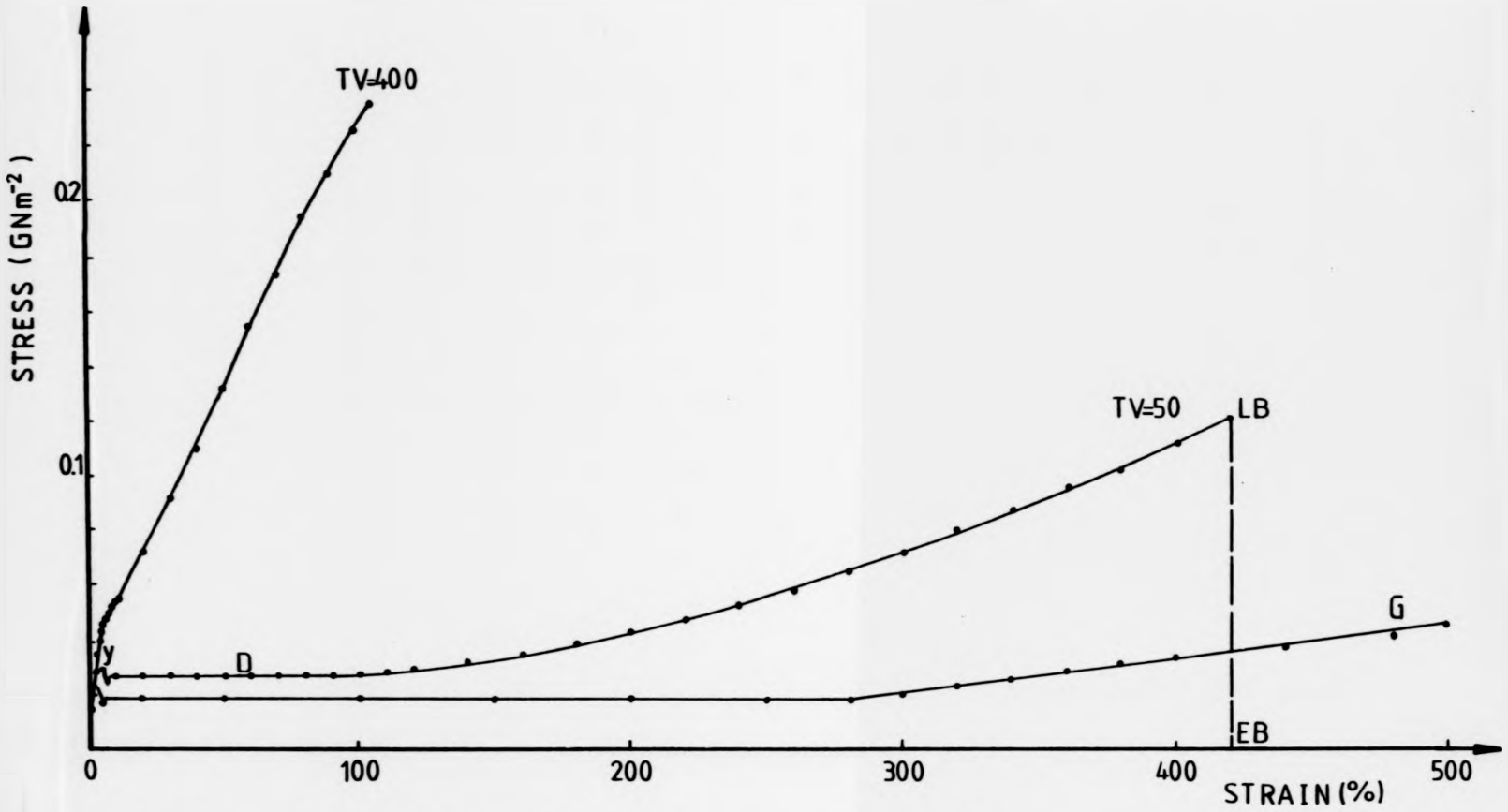

FIG. 6.1 STRESS-STRAIN CURVES FOR MELT-SPUN FIBRES

on the load-axis were expressed as load divided by the original cross-sectional area, and those on the elongation-axis as percent strain. The cross-sectional area of each fibre was determined separately using a microscope fitted with a calibrated eyepiece. Before testing, all samples were stored for several days in a standard atmosphere of 20°C temperature and 60% relative humidity.

6.2.2 Recovery Measurements

Two types of recovery were investigated in this work: total and immediate recovery. A recovery test and the appropriate terms are shown in Figure (6.2). The procedure employed involved extending a fibre in an Instron tensile tester to a chosen strain (at cross-head speed of 1 cm/min.). At the required strain, the fibre was held for two minutes after which the cross-head speeds were reversed in direction until reaching their original positions. The fibre was held for five minutes - under no strain - and then re-extended.

The "immediate recovery" is defined as the strain recovered after the first two minutes of stress relaxation, and the "total recovery" as the strain recovered after two minutes at constant strain, followed by the return of the cross-head speed and a waiting period of five minutes.

6.2.3 Shrinkage Measurements

The shrinkage investigations were performed on as-spun and drawn fibres with different draw ratios. These experiments were carried out using mineral oil of boiling point 265°C, and hot air as annealing media. The oil was preheated and held thermostatically at the required annealing temperature. A single fibre specimen 10 cm long, was clamped at both ends and hung freely immersed in the oil for two minutes. After annealing, the specimen was quenched in water at room temperature, washed in acetone and dried before measuring the final length.

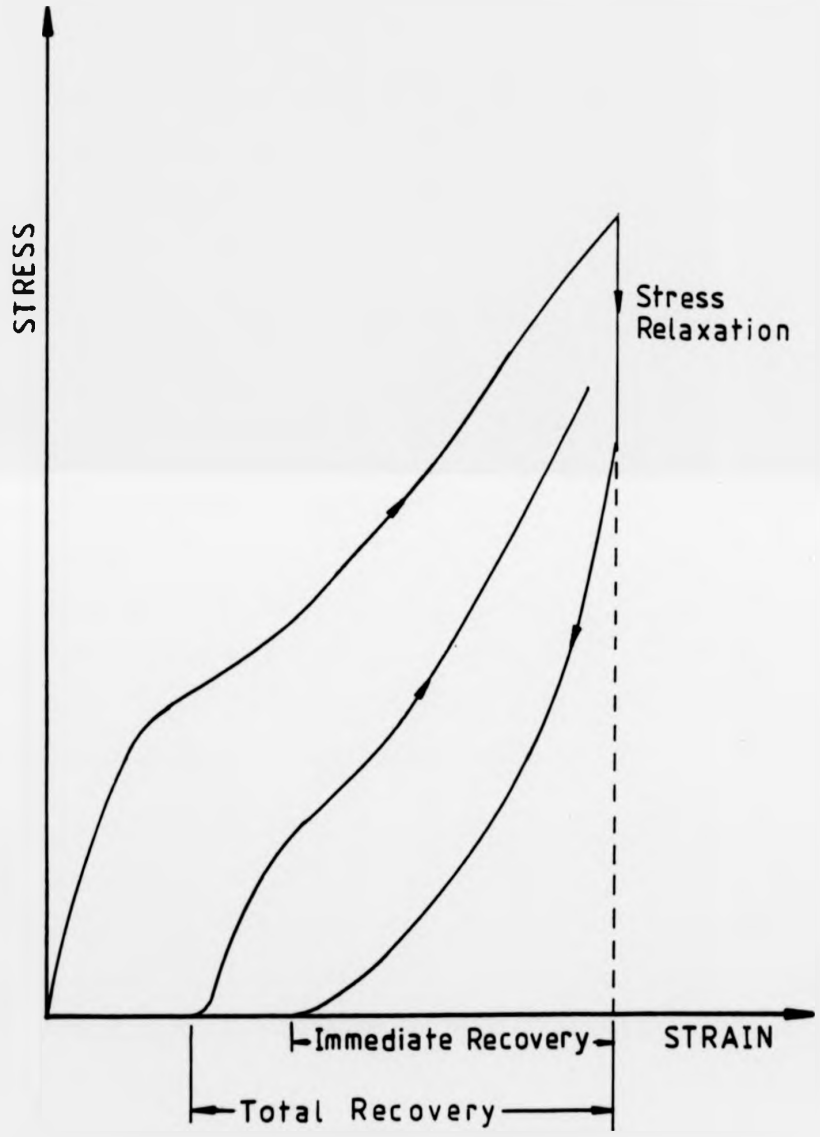

FIG. 6·2 : THE RECOVRY CYCLE AND DEFINITION OF TERMS.

Shrinkage in hot air was carried out using an oven. At any one annealing temperature, one filament of fibre, 10 cm long, was clamped at both ends in a sample holder in a relaxed position and introduced into the oven. In these experiments, it was observed that soon after introducing the sample holder into the oven, a drop of 15-25^{o}C in the oven's temperature was recorded. The required annealing temperature was found to re-establish its value after 15-25 minutes. Annealing was then carried out for a further one hour.

6.3 RESULTS

6.3.1 Stress-Strain Behaviour for As-Spun Fibres

The results from the load-extension curves for the gravitationally spun fibres tested at different rates of extension are shown in Table (6.1), in which the yield stress, drawing stress and fibre strength are shown to increase with increasing extension rate in the range 1-25 cm/min. However, at 50 and 100 cm/min., the values of all these parameters are found to be lower than that at 25 cm/min.

Figure (6.1) shows the stress (force/original cross-sectional area) strain ($\Delta L/L$)% curves for as-spun fibres; gravitationally spun and spun with take-up velocity 50 and 400 m/min. In general, the properties of yield stress and tensile strength were shown to increase with the take-up velocity while elongation at break decreased. In addition, it can be observed in Figure (6.1) that the gravitationally spun fibre (G) and the as-spun with take-up velocity 50 m/min. (TV=50) exhibited a yield drop and necking formation, while the fibre spun with take-up velocity 400 m/min. (TV=400) exhibited no neck.

TABLE (6.1)

The Effect of Rate of Extension

on Stress-Strain Behaviour

Extension rate cm/min.	Yield Stress $Nm^{-2}x10^7$	Drawing Stress $Nm^{-2}x10^7$	Stress at Break $Nm^{-2}x10^7$	Extension at Break cm.
1	1.938	1.770	8.309	32.8
5	2.157	1.854	8.393	32.6
10	2.622	1.989	9.101	32.1
25	3.034	2.022	10.173	34.5
50	2.373	1.618	8.831	33.0
100	2.245	1.820	9.627	33.4

6.3.2 Stress-Strain Behaviour of Drawn Fibres

In order to investigate the stress-strain behaviour of drawn fibres, gravitationally spun fibres drawn with different drawing conditions (A, B and C) are listed in Table (6.2). The proportion of crystal structure in these samples before and after the stress-strain test is also given.

TABLE (6.2)

Sample Designation	Speed of Drawing cm/min.	Draw Ratio	True Draw Ratio	Annealing Temperature after Drawing	Crystal Structure before test	Crystal Structure after test
A	1	3.5	3.8	-	$\alpha=\beta$	α
B	100	3.5	4.9	-	$\alpha>\beta$	α
C	100	7.5	5.7	-	α	α
D	1	3.5	3.8	140	$\alpha<<\beta$	$\alpha>>\beta$
E	100	3.5	4.9	140	$\alpha=\beta$	$\alpha>>\beta$

The stress-strain curves for samples A, B and C are shown in Figure (6.3). It can be seen that different draw ratios affect the property level, i.e. tenacity and breaking extension as well as the shape of the curve.

In order to investigate the effect of heat treatment on the stress-strain behaviour, two samples A and B were annealed at constant length for two hours. These samples are designated by D and E, as shown in Table (6.2). The stress-strain curves for these two samples are shown in Figure (6.4).

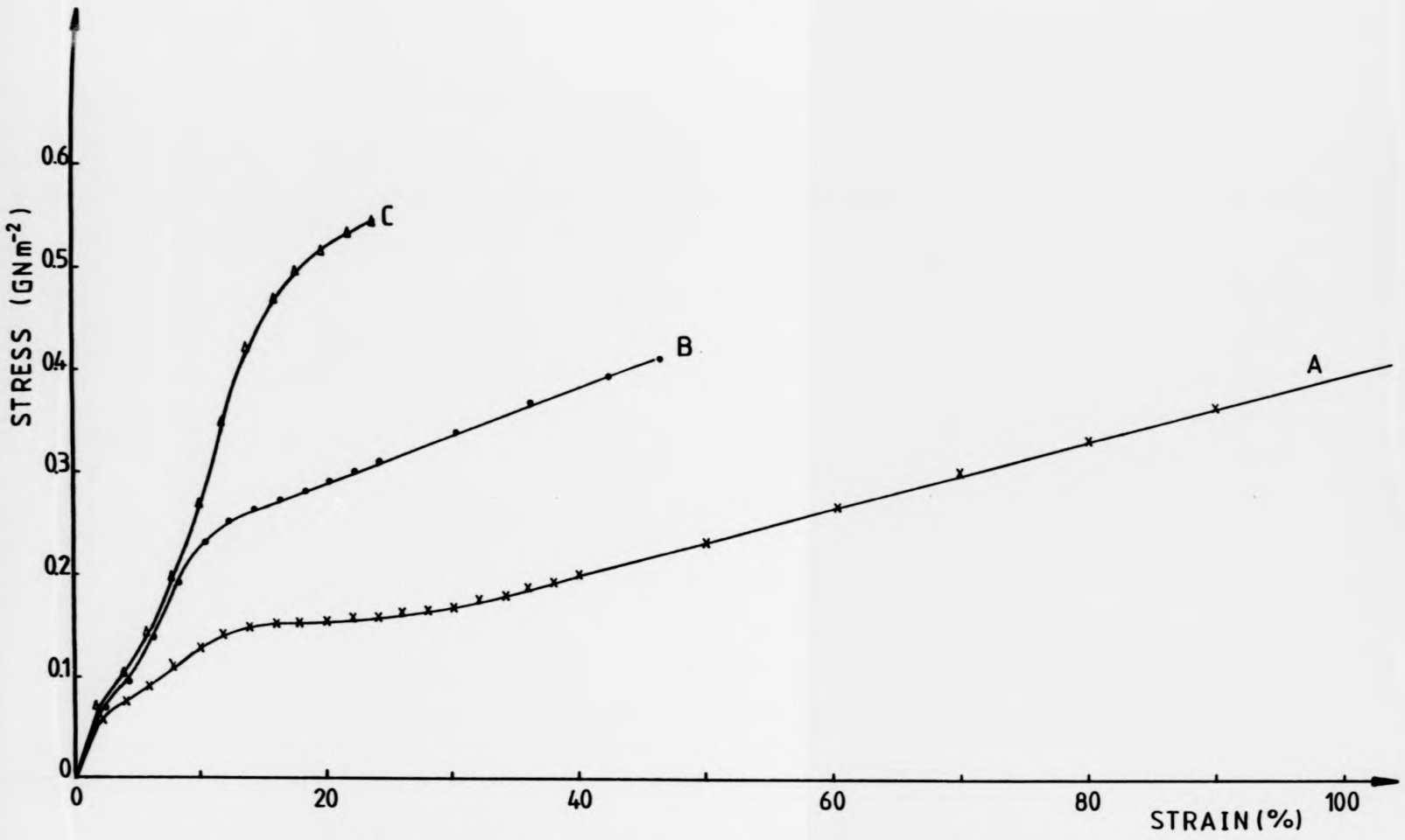

FIG. 6.3 : STRESS-STRAIN CURVES FOR DRAWN FIBRES

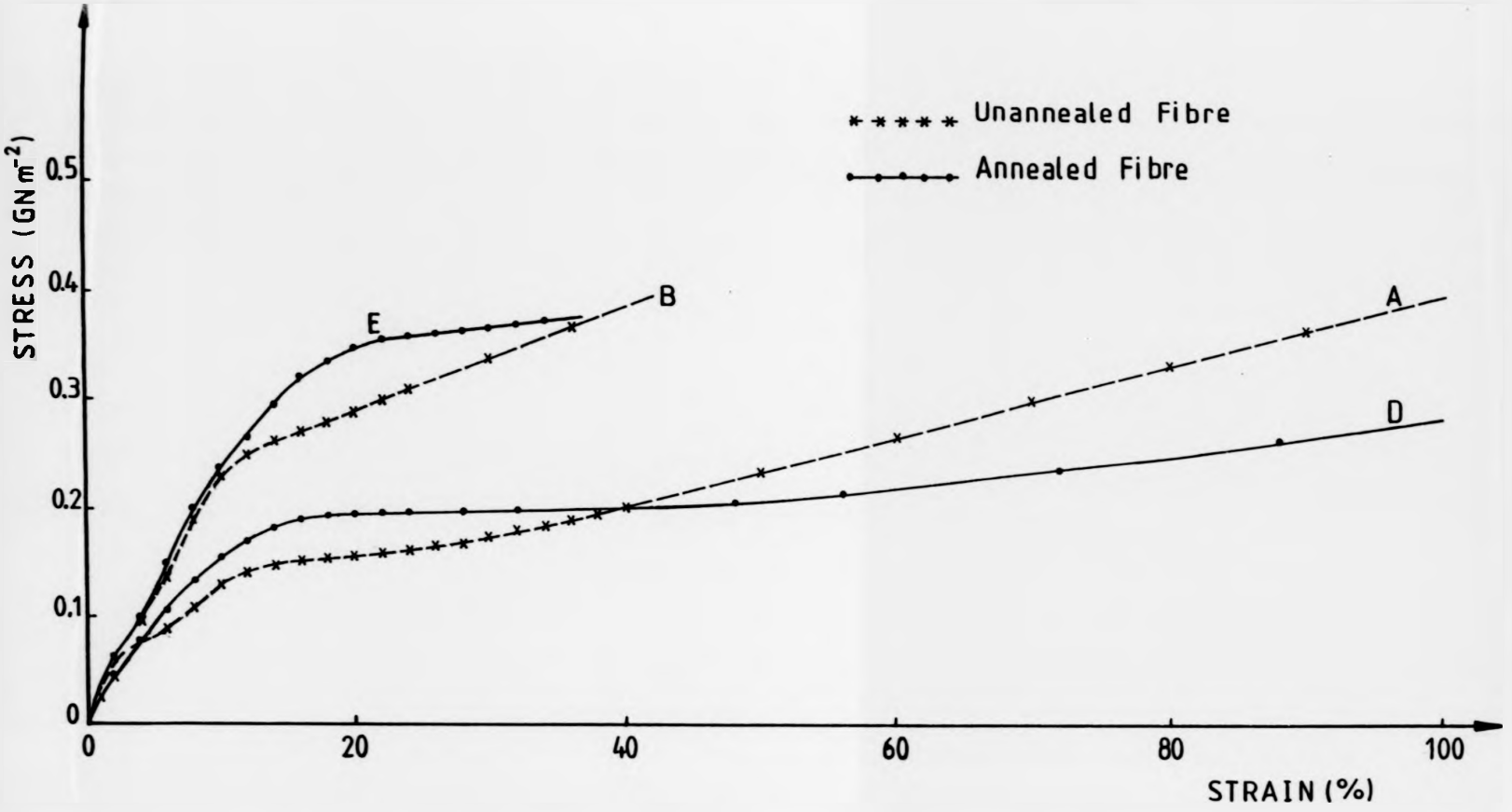

FIG. 6.4 THE EFFECT OF ANNEALING ON THE STRESS-STRAIN CURVES OF THE DRAWN FIBRES.

6.3.3 Recovery Results

The total recovery percentage was determined by using the following relation:

$$\text{Total recovery \%} = \frac{\text{total recovery}}{\text{extension}} \times 100$$

The total recovery % versus strain % were plotted for samples A, B and C and also the immediate recovery for samples A and B, as shown in Figure (6.5). This figure shows that the total recovery % decreases with increasing applied strain % and the total recovery for the samples of low draw ratio are lower than that of high draw ratio (A<B<C). On the other hand, the immediate recovery is shown to increase with the applied strain, and the samples of low draw ratios exhibit lower immediate recovery.

The effect of heat treatment on total recovery can be seen in Figure (6.6) where sample D exhibited much higher recovery than that of unannealed sample (A) and also higher than both B and E.

6.3.4 Shrinkage

The shrinkage "S" was calculated from the following formula:

$$S = \frac{l_o - l}{l_o}$$

where l_o and l are the initial and final fibre length respectively. Shrinkage percentage for samples A, B, C and as-spun fibres with take-up velocity 400 m/min. (TV=400) is plotted versus the annealing temperature of the oil bath, as shown in Figure 6.7(a). This figure shows that the shrinkage increases with the annealing temperature. However, for all samples, shrinkage increases slightly up to 120°C, above which a high increase was observed. It also shows that the drawn fibres shrank more

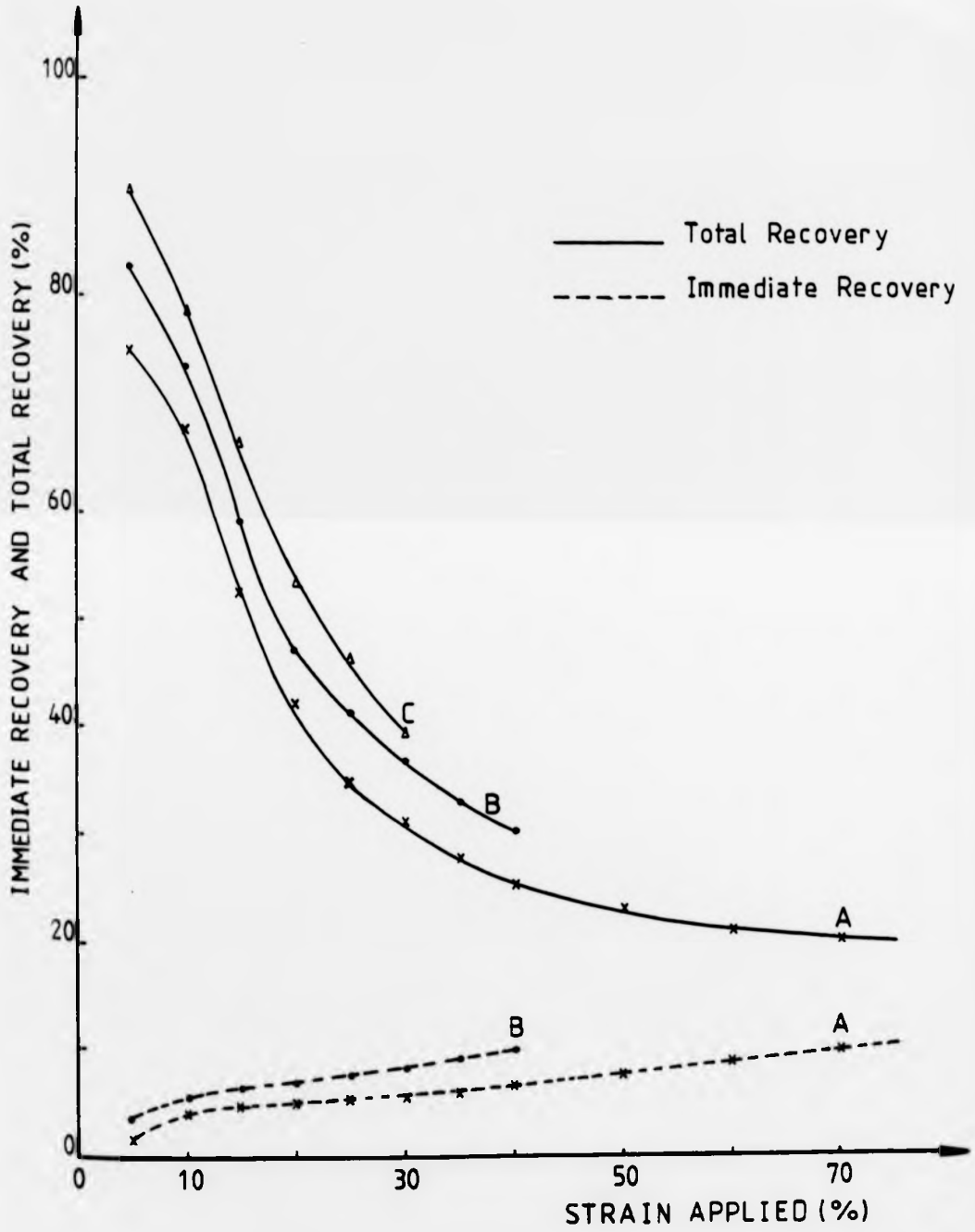

FIG. 6.5 : TOTAL RECOVERIES AND IMMEDIATE RECOVERIES OF THE FIBRES VS. APPLIED STRAIN.

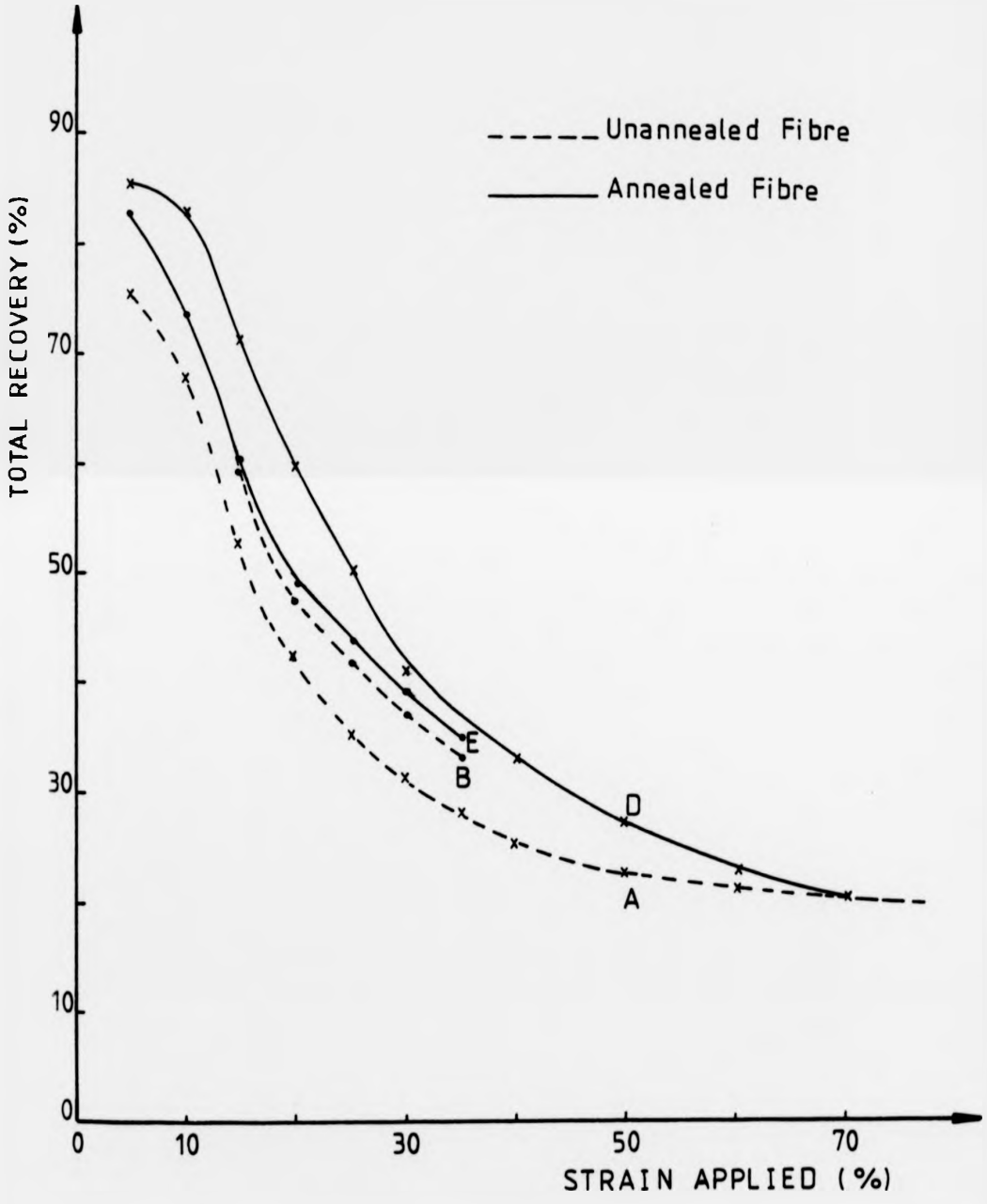

FIG. 6.6 : THE EFFECT OF ANNEALING ON THE TOTAL RECOVERIES OF THE DRAWN FIBRES VS. APPLIED STRAIN.

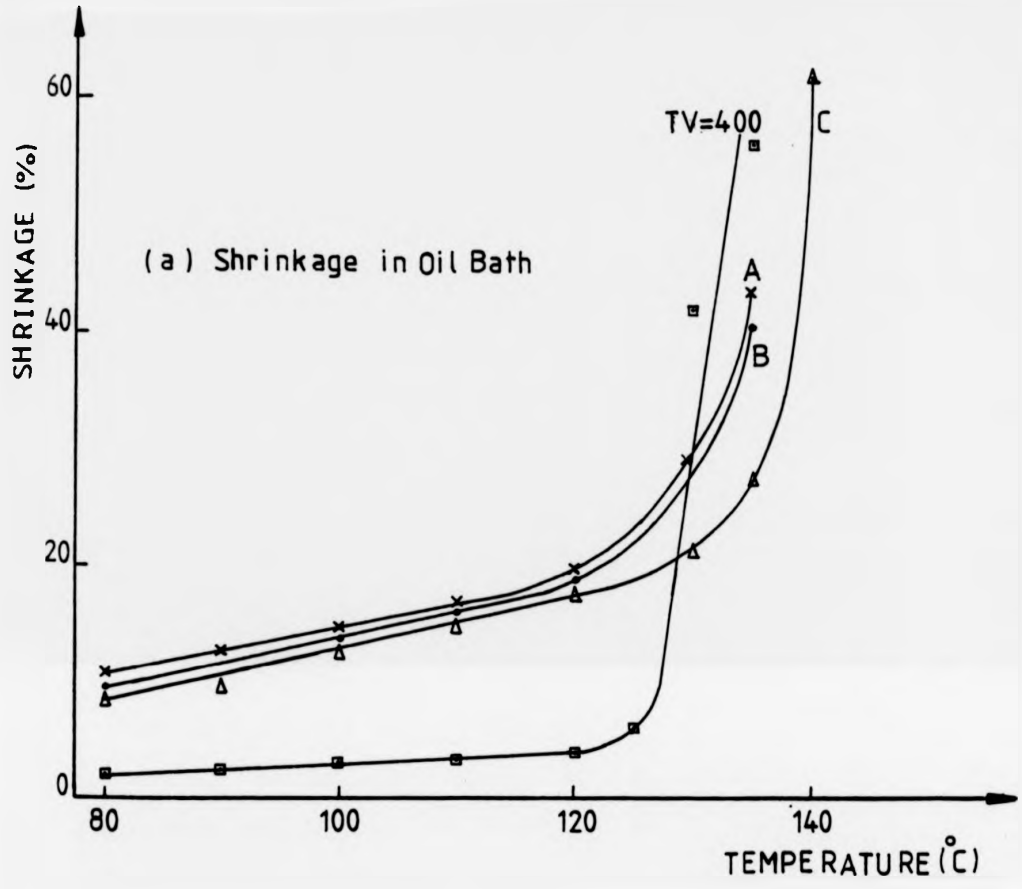

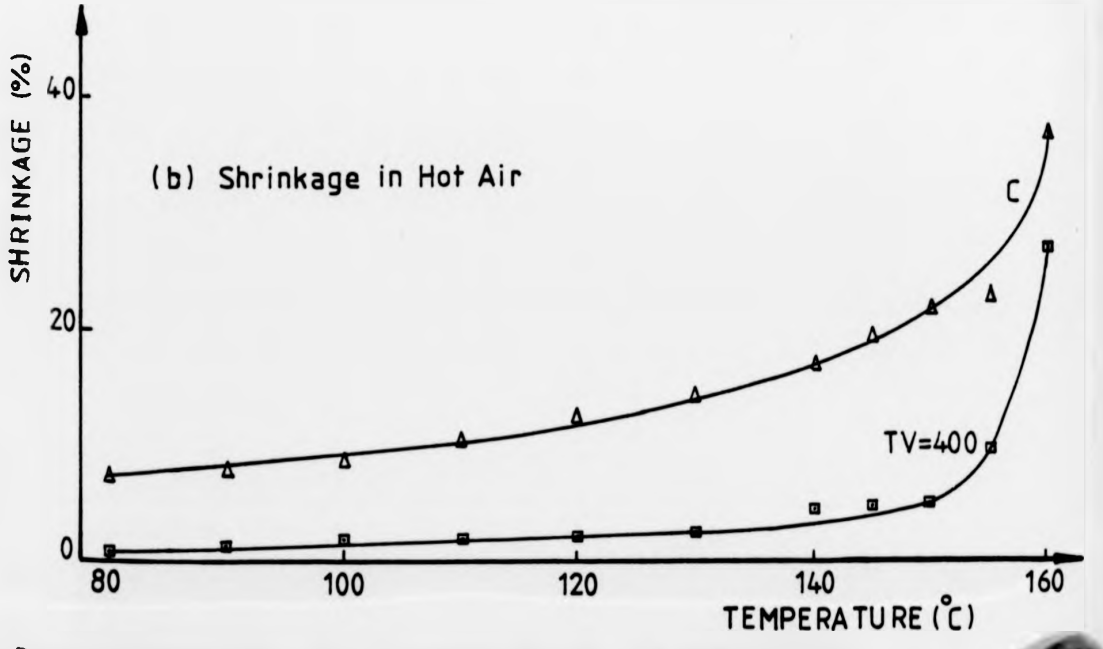

FIG 6.7: SHRINKAGE AS A FUNCTION OF TEMPERATURE

than the as-spun ones. Of particular interest, shrinkage is shown to decrease with the increase in the draw ratio.

The results of annealing in hot air also showed that shrinkage increases with the annealing temperature, as shown in Figure 6.7(b). This figure also shows that the drawn fibres shrank more than the as-spun ones when both annealed at a particular temperature. It can be seen that annealing in oil resulted in more shrinkage than annealing in hot air for the same sample at the same temperature.

6.4 DISCUSSION

The results of the stress-strain curves for the gravitationally spun fibres at different rates of extension (Table (6.1)) show a fall in the yield and drawing stresses at cross-head speeds between 25 and 50 cm/min. Similar observations on 6GT were reported by Schenk[16] where he attributed this fall to slippage of the yarn in the clamps. But in this work, it has been observed that slippage only occurs when the neck shoulder reaches the clamps at high extension. Therefore, it cannot affect the yield and the drawing stresses.

A fall in the drawing stress has been observed by Allison and Ward[37] in their work on 2GT and Peters et al[64] in their work on 4GT at extension rate 1 and 5 cm/min. respectively. Both results were interpreted on the basis that the generated heat cannot be conducted quickly away from the neck region and the process approaches an adiabatic state.

The results in this work could be explained on the same basis, the difference in the rate of extension at which the decrease in the drawing load starts being a characteristic of a polymer. On the other hand,

the wide-angle X-ray diffraction pattern of 6GT shows that the α-form proportion increases markedly at extension rates above 25 cm/min. and this might contribute to the change in behaviour.

In Figure (6.1), the shape of the stress-strain curves is seen to be affected by the preorientation caused by the take-up velocity of the as-spun fibres. The extension of as-spun fibres with low take-up velocity exhibits a yield point and a neck, while the extension of as-spun fibres with high take-up velocity shows no neck formation; the latter may be because fibres have been already drawn. Figure (6.1) also shows that the yield and the breaking stresses increase with the take-up velocity. Similar observations were reported by White et al[32] in their work on as-spun fibres of polyethylene and polypropylene. They reported that the increase in the yield stress and tensile strength was attributed to the increase in the number of the tie molecules and in the molecular orientation with the take-up velocity.

The main difficulty in comparing properties of fibres having different draw ratios and consequently different crystal structures, is to know whether the changes in the properties in question are caused by the difference in crystal structures. Ward et al[6], in their work on 2GT, 3GT and 4GT,have reported that draw ratios affect the property level only, i.e. tenacity and breaking extension but not the shape of the curves. With this in mind, the three stress-strain curves shown in Figure (6.3) (curves A, B and C), may be discussed here for the three different draw ratios and, consequently, different crystal structures (see Table (6.2)). The curves A, B and C have a primary yield at about 2.5% strain, followed by a plateau. In curve C, the plateau (2.5-8% strain), is followed by strain-hardening and ultimately reaching failure at 24% strain. In curves A and B, the plateau (2.5-10% strain)

is followed by another yield point at about 12% strain. The second yield point in curve B is followed by strain-hardening till failure (46% strain). In curve A, the second yield point (12% strain) is followed by a wide plateau region (13-26% strain) and strain-hardening ultimately reaching failure point at 100% strain.

Investigations into the mechanical properties of drawn samples of 4GT[6] and 5GT[65] have shown that the stress-strain curves for these polymers behaved in a manner dependent on the changes of the crystal structure with tension. For drawn fibres of 4GT[6], the stress-strain curve showed a pronounced plateau region between 4% and about 12% strain, over which the X-ray diffraction pattern showed a transformation of the material from the contracted α-form to the extended β-form at 14% strain. In the case of 5GT[65], the stress-strain curves for the contracted α-form showed a plateau region between 20% and 40% strain which was consistent with the structural transformation of the contracted α-form to the extended β-form. In the case of 2GT and 3GT where the molecular conformations are extended and contracted respectively, no structural changes in both samples have been reported. Where the drawn samples of 2GT[6] showed no plateau in the stress-strain curve, nevertheless, a plateau was observed in stress-strain curve of 3GT[6]. The plateau in this case was attributed to the deformation in the crystalline and noncrystalline regions being appreciably different, i.e. inhomogeneous deformation.

The stress-strain behaviour shown in Figure (6.3) can be explained in the following manner; fibres B and C have high proportion of α-form which on further extension no detectable change in the X-ray diffraction pattern was observed. This may suggest that the plateau following the first yield point may be a characteristic of α-form. Fibre A initially has more β-form than B and C, and then transforms to α-form during the

experiment. Therefore, the second plateau, observed for sample A and not for B and C, is related to this transformation. The transformation from β- to α-form should involve a crystal deformation of β-form being chain folded crystals to extended chain crystals (α-form), since both crystals have fully extended chain repeat lengths (see Chapter Four).

Further indications of features of the stress-strain curve which might be attributed to a particular crystal form are seen in Figure (6.4). Sample D is predominantly β-form (see Table (6.2)), and the primary yield and plateau are missing from it. The yield point at about 12% strain is followed by a wide plateau (16-46% strain), and strain-hardening region (46-104% strain). This wide plateau is related to a β/α transition; this transition was detected by the wide-angle X-ray diffraction.

Sample E has a structure in which both α- and β-form exist before the test; the primary yield point and plateau in curve E can still be seen. The disappearance of this plateau in curve D may thus be attributed to the near disappearance of α-form upon annealing.

The total recovery of samples A, B and C, and also the immediate recovery of samples A and B versus the applied strain, are shown in Figure (6.5). As expected, the higher the draw ratio, the higher are the total and immediate recovery. For sample A, at strain level greater than 12%, the total recovery falls rapidly up to 30% strain. This may be attributed to that in this region, the β/α transition takes place irreversibly. Above 30% strains, the total recovery decreases slightly up to 90%. Such a transition is not found in sample C, thus giving a curve with different shape than A. The shape of curve B is somewhat similar to that of A; this may be due to the presence of a small proportion of β-form crystals.

Referring to Figure (6.6) in which each point represents a separate experiment, fibre A will have undergone an α-yield before recovery from strains greater than 2.5%, whereas, fibre D will not (see Figure (6.4)). Therefore, at all strains greater than a few percent, this irrecoverable deformation will have taken place in A but not in D and so fibre D will have superior recovery. However, the proportion of β-form crystals in D is greater than in A, so when the β/α transition commences at strains of about 15%, the recovery of D falls more rapidly relative to that of A. The two curves converge towards each other at high strains, this is particularly noticeable at strains greater than 30%, where, from Figure (6.4) the yielding is continuing for D but has stopped for A.

Samples B and E both have α-form present, and both yield at about 2.5%, hence, recoveries at small strains are similar. However, the poorer recovery of fibre B at strains about 15% can be attributed to its lower yielding relative to E, where the yield in this region is accompanied by β/α transition which might occur in E more than in B.

The shrinkage of fibres in air (Figure 6.7(b)) is found to be less than that in oil (Figure 6.7(a)), which may be due to the rate of heat transfer in the two media, being higher in oil than in air. The shrinkage in air may have also been affected by the drop in the oven's temperature on introducing the fibre inside and the time taken by the oven to regain its initial temperature. During this time, the fibre is subjected to pre-annealing; fibres that have been heat treated previously at a particular temperature will shrink less, when annealing proceeds to a higher temperature, than those directly annealed at this higher temperature[40].

It can be seen in Figure 6.7(a) that the shrinkage is decreasing

with increasing draw ratio. However, shrinkage is considered as the reverse process of drawing, thus one would have to expect that the higher the draw ratio, the higher is the shrinkage. It has been reported[41] that in oriented fibres, the amorphous regions are highly ordered and are held under stresses higher than in the undeformed material. Annealing at low temperature is mainly related to stress relief in the amorphous region; therefore, fibres with high draw ratios exhibit higher shrinkage. Annealing in the high temperature regions results in maximum shrinkage which is attributed to melting processes. The results of 6GT fibres (Figure 6.7(a)) may be explained as follows:

The initial structure of fibre A is of α- and β-forms, whereas, α-form is dominant in fibre B, and fibre C has α-form structure. As it has been stated in Section (3.4), upon annealing, a transition from α- to β-form would occur in fibres with α-β mixture. Since shrinkage is accompanied by chain folding[66], therefore, the greater shrinkage in sample A can be attributed to transformation of α-form (extended chain crystals) to the β-form (folded chain crystals). On the other hand, since α-form remains constant upon annealing sample C, the appearance of β-form is not attributed to the α/β transition (see Section 3.4). Such appearance is caused by crystallisation of the mobile molecules in the amorphous region. Accordingly, it is thus possible that the lower shrinkage in sample C may be affected by the presence of α-form crystals over all temperature ranges up to complete melting. This explanation is seen to fit in with the results obtained for sample B in which the α-form is dominant and, hence, giving rise to a shrinkage magnitude between those of A and C.

The lower shrinkage magnitude in the case of the as-spun fibre with take-up velocity 400 m/min.(TV=400) could be explained in terms of entropy of the amorphous region which is already higher than that in the drawn ones[40].

CHAPTER SEVEN

THERMAL STUDIES

(Melting Behaviour)

7.1 INTRODUCTION

Gilbert[2] and Schenk[16] have both observed multiple melting endotherms in 6GT, and in view of the discovery of its polymorphic form in this work, it might be possible to associate these peaks with melting of the various polymorphs. However, multiple melting endotherms are commonly observed in many polymers of which only one crystal structure exists, and so they may be unrelated to the polymorphism of this material. An investigation is described below which attempts to distinguish between these possibilities.

7.2 EXPERIMENTAL METHODS

The measurements of melting temperature were carried out with a Perkin-Elmer differential scanning calorimeter (DSC-2). Detailed descriptions of the theory and operating principles of a differential scanning calorimeter are given in the literature[67].

Throughout the DSC work, samples were encapsulated in aluminium sample pans and placed in the sample holder. An empty aluminium pan of the same weight as that used with the sample, was used as a reference and placed in the reference holder. Each holder has its own heater and temperature sensor. With the DSC-2 instrument, argon at a flow rate of 200 cc/min. was used as a purge gas.

Initially, the melting temperatures of the polymer were determined with approximately 10 mgm of the following polymer samples:

(a) Chips of 6GT polymer in the as-prepared state.

(b) Cast films prepared at room temperature (Section 2.3.3).

(c) Low crystallinity (melt-pressed) films of 6GT polymer (Section 2.3.3).

(d) As-spun fibre with take-up velocity 400 m/min.

(e) Pressed film drawn to D.R.= 5 with cross-head speed of 100 cm/min.

(f) Pressed film hot drawn to D.R.= 3.

(g) Cast film annealed at 120°C in an oven for 2 hours.

(h) Cast film annealed at 140°C in an oven for 2 hours.

(j) Pressed film annealed at 120°C in an oven for 2 hours.

(k) Pressed film annealed at 140°C in an oven for 2 hours.

Each sample was scanned from ambient temperature (47°C) for the instrument at a rate of 10°C/min. This heating rate was chosen to achieve good resolution of the melting endotherm. Some experiments were performed in which 10 mgm of the polymer sample was melted at 170°C in the instrument, and held for five minutes. These conditions were chosen to ensure that all previous thermal history was destroyed. The sample was then cooled in the instrument at a rate of 320°C/min. to a preset crystallisation temperature and allowed to remain at it for five minutes. The scanning was then started from the crystallisation temperature at a heating rate of 10°C/min. This procedure was repeated several times, corresponding each time to a different crystallisation temperature.

In further experiments, different rates of heating, i.e. 5, 10, 20 and 40°C/min. were used with samples crystallised at 117°C. Also, different rates of cooling were investigated; in these experiments a 10 mgm sample was melted at 170°C and held in the instrument for five minutes. The instrument was then cooled at a preset cooling rate to ambient temperature for the instrument and held, at least, for five minutes to attain thermal equilibrium (indicated by the instrument). In each case, scanning was started from ambient temperature at a heating rate of 10°C/min.

Another set of experiments was performed in which the samples were annealed in the DSC-2. This involved holding the film in the instrument below the melting point for different periods of time and scanning from the annealing temperature at a rate of $10^{o}C$/min. The melting temperatures were taken to be the peaks minima of the endotherm.

7.3 RESULTS

The thermogram for the chips is shown in Figure (7.1) from which three melting endotherms are seen. The temperature of these are called T_1, T_2 and T_3. The peak height of the endotherm, and the temperature at which it occurs are defined as I, II and III. The melting temperatures of the samples listed in the previous section are given in Table (7.1), and it is seen that not all of them show three melting points. Where this occurs, the results of the experiments, shown in Figure (7.2), which will be discussed later, were used to identify the endotherms.

In general, peak (I) is present, even at low crystallisation temperature, with its height remaining constant at small values; it disappears at high crystallisation temperature ($120^{o}C$). Peak (II) is present, even when the crystallisation temperature is room temperature with its height and temperature remaining constant until reaching a definite crystallisation temperature ($110^{o}C$); the peak height and temperature then increase with crystallisation temperature. With further increase in crystallisation temperature, peak (II) becomes the largest peak present and continues increasing in size and temperature until it is the only peak present for material crystallised at $127^{o}C$. Peak (III) is observed at the same temperature irrespective of the crystallisation temperature. The peak height is large at low crystallisation temperature (T_c), but at some value of T_c, at which peak (II) begins to increase in height, the height of peak (III) decreases.

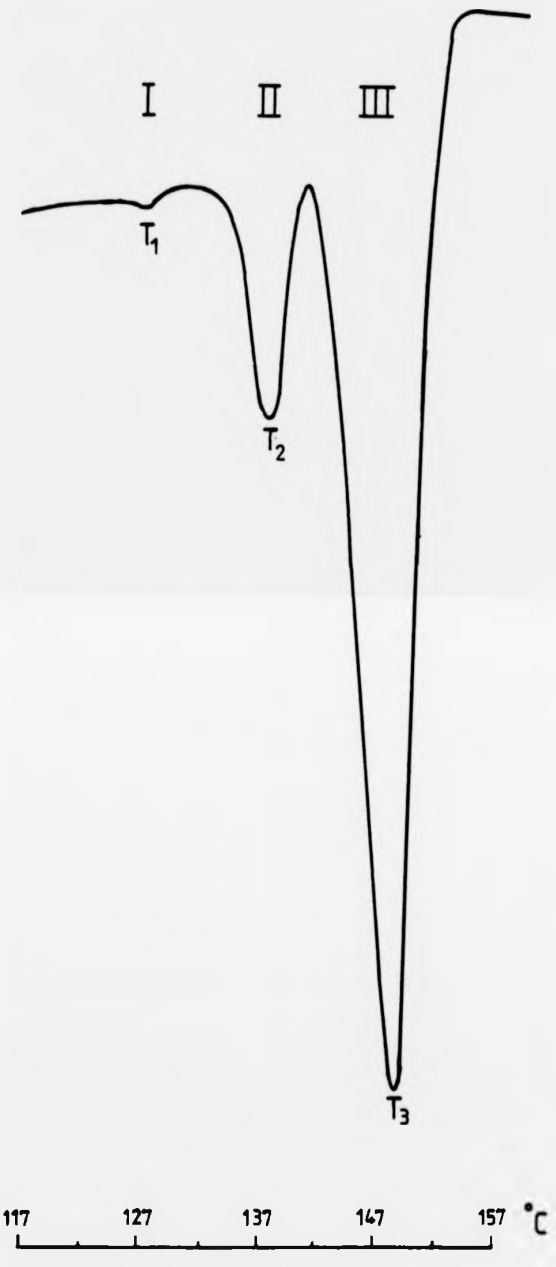

FIG. 7.1 : TYPICAL MULTIPLE-MELTING ENDOTHERMS OF 6GT.

TABLE (7.1)

Melting Temperatures of the As-Prepared Polymers

Sample	Melting Temperature (^{o}C)
(a) Chips (as-prepared)	T_1 = 127.5 T_2 = 138.0 T_3 = 149.2
(b) Cast film	T_1 = 125.4 T_2 = 150.0
(c) Low crystallinity melt-pressed film	T_3 = 146.5
(d) As-spun fibre with take-up velocity 400 m/min.	T_3 = 147.3
(e) Pressed film drawn (D.R.= 5) with cross-head speed 100 cm/min.	T_3 = 150.5
(f) Pressed film hot drawn (D.R.= 3)	T_3 = 148.7

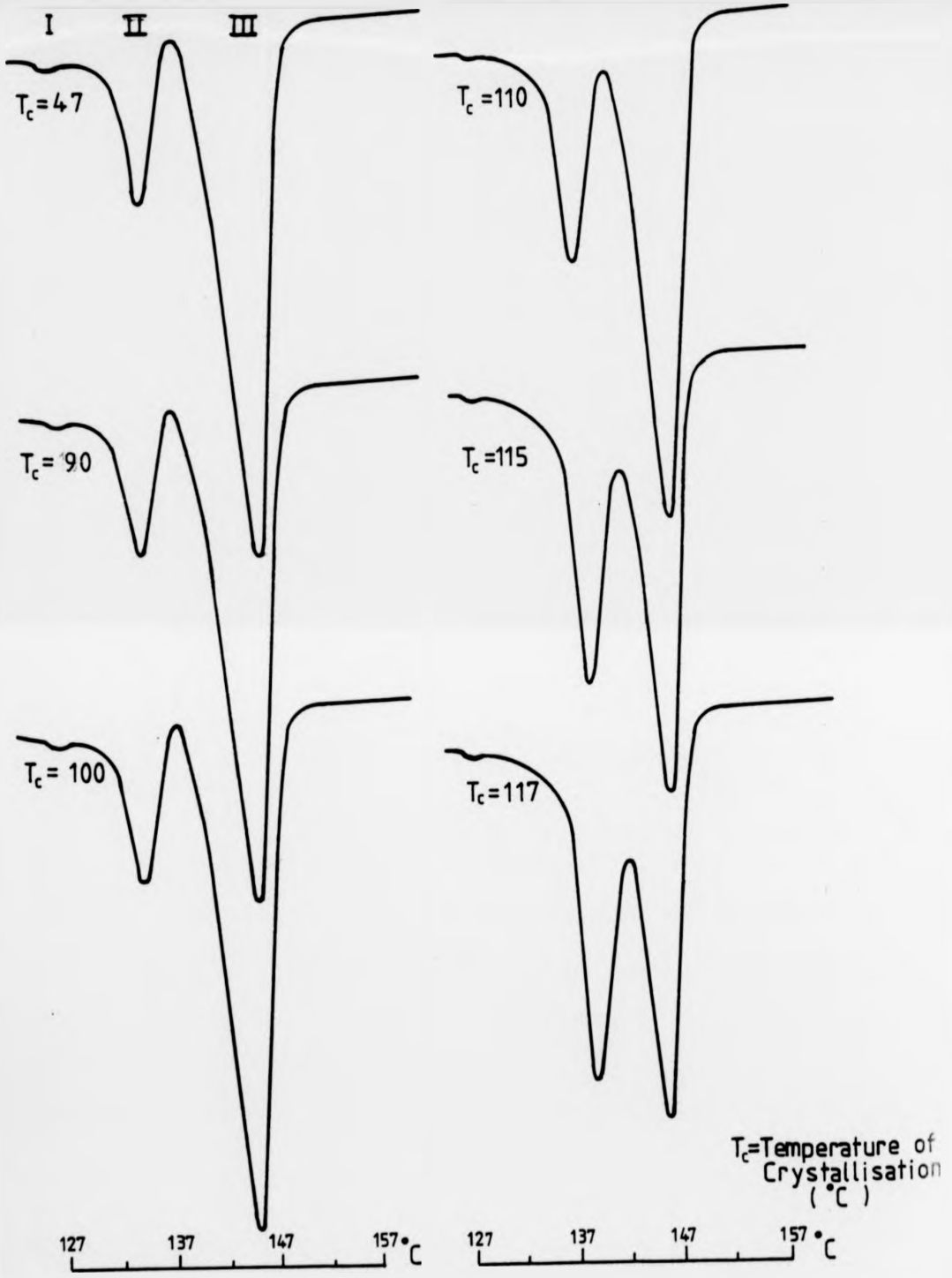

FIG. 7.2 : MELTING ENDOTHERMS OF 6GT AS A FUNCTION OF CRYSTALLISATION TEMPERATURE.

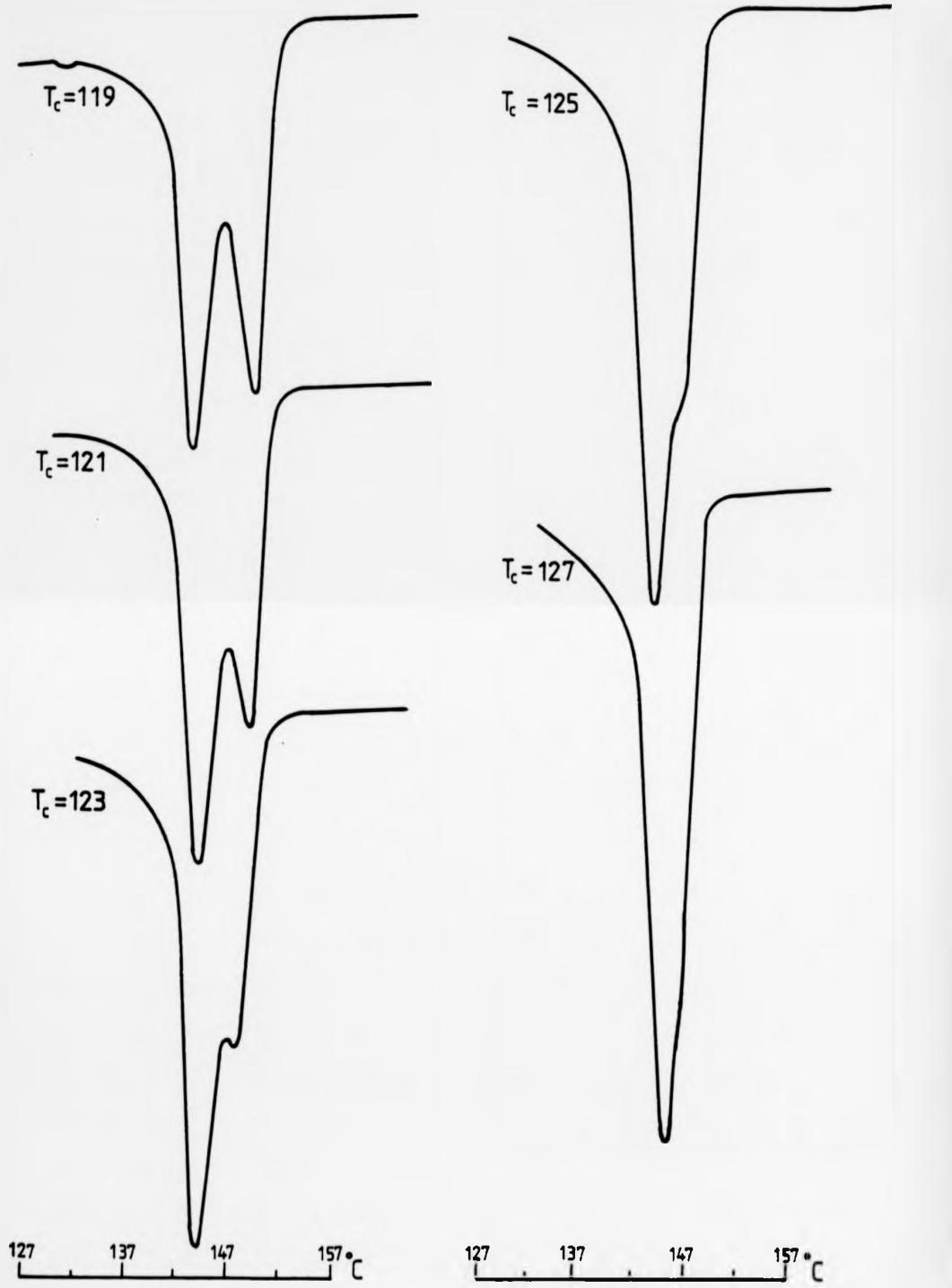

Cont. FIG. 7.2

Figure (7.3) shows the effect of cooling rate, during the crystallisation process at room temperature, on the melting endotherms (peaks I, II and III). When the cooling rate decreases, peak II increases in temperature and height while peak III occurs at the same temperature but decreased in height. Figure (7.4) shows the effect of rate of heating during the remelting process on the three peaks I, II and III. When the rate of heating increases, peak II increases in temperature and height, while peak III occurs at the same temperature but increased in height. Peaks II and III tend to merge together at a high rate of heating.

The effect of annealing on the endotherms is shown in Figure (7.5) for drawn films annealed in the DSC-2 at 125°C for ½, 1 and 2 hours, and scanned from this temperature. The unannealed sample has only one peak at 150.5°C. The sample annealed for half an hour has a peak at 153°C and a shoulder; the shoulder becomes more pronounced with annealing for one hour. Annealing the sample for two hours causes two peaks merging together at 152.2°C and 153.3°C.

The DSC test for rapidly quenched melt-pressed film (sample c) shows peak III only. Annealing the amorphous film (sample j) for two hours in an oven at 120°C causes peak II at 128°C and peak III at 148°C. After annealing the amorphous film at 140°C for two hours in an oven (sample k), the DSC test shows one wide endotherm (peak III) (see Figure (7.6)). The test for cast film shows peak I appearing at 125.4°C and peak III at 150°C (sample b). Annealing the cast film in an oven for two hours at 120°C (sample g), the test shows peak I at 125.5°C, peak II at 128°C and peak III at 151°C. Annealing cast film at 140°C for two hours in the oven (sample h), the test shows peak III appearing at 152°C with a shoulder around 148°C, as is shown in Figure (7.7).

FIG. 7.3 : EFFECT OF COOLING RATE ON MELTING ENDOTHERMS.

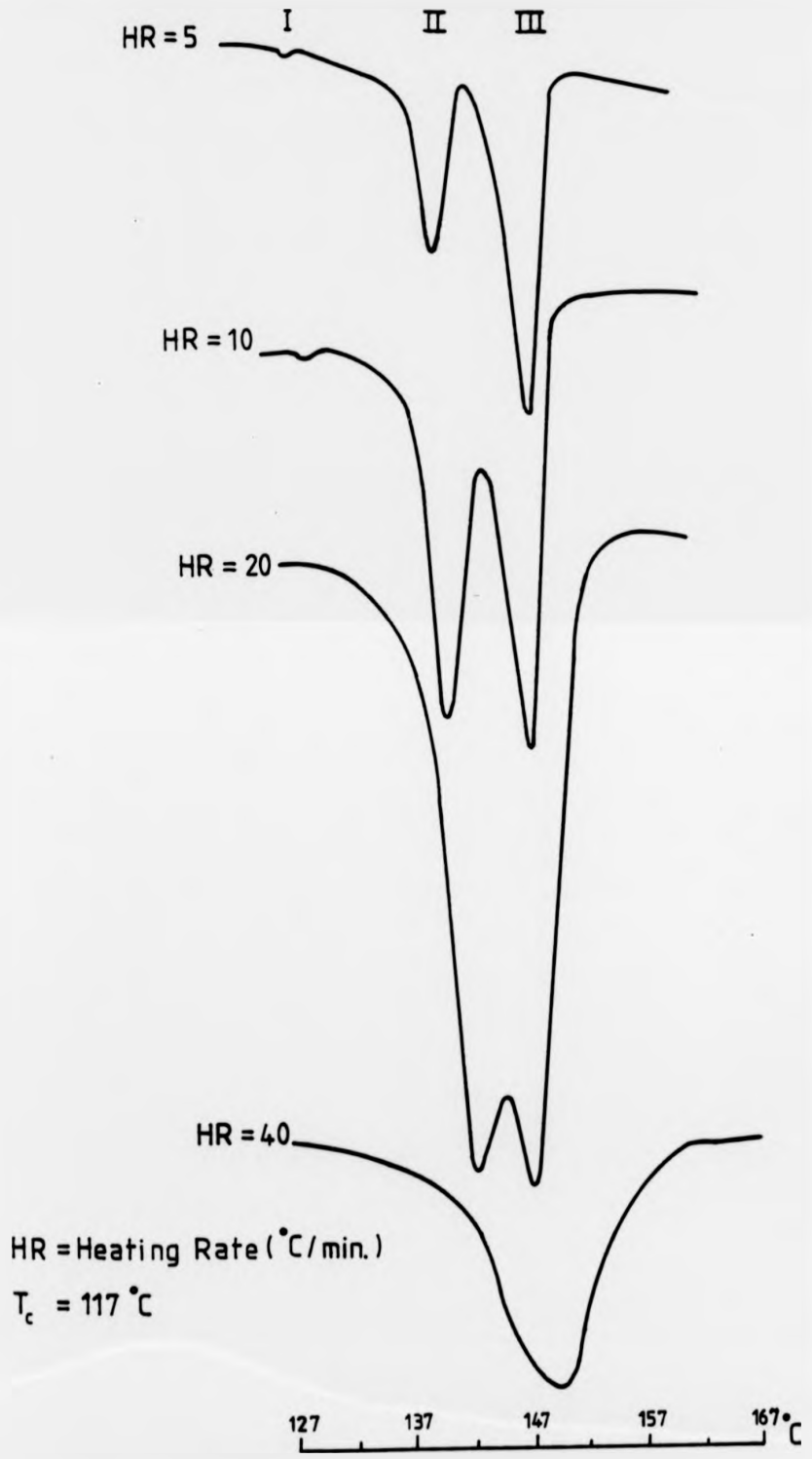

FIG. 7.4 : EFFECT OF HEATING RATE ON MELTING ENDOTHERMS.

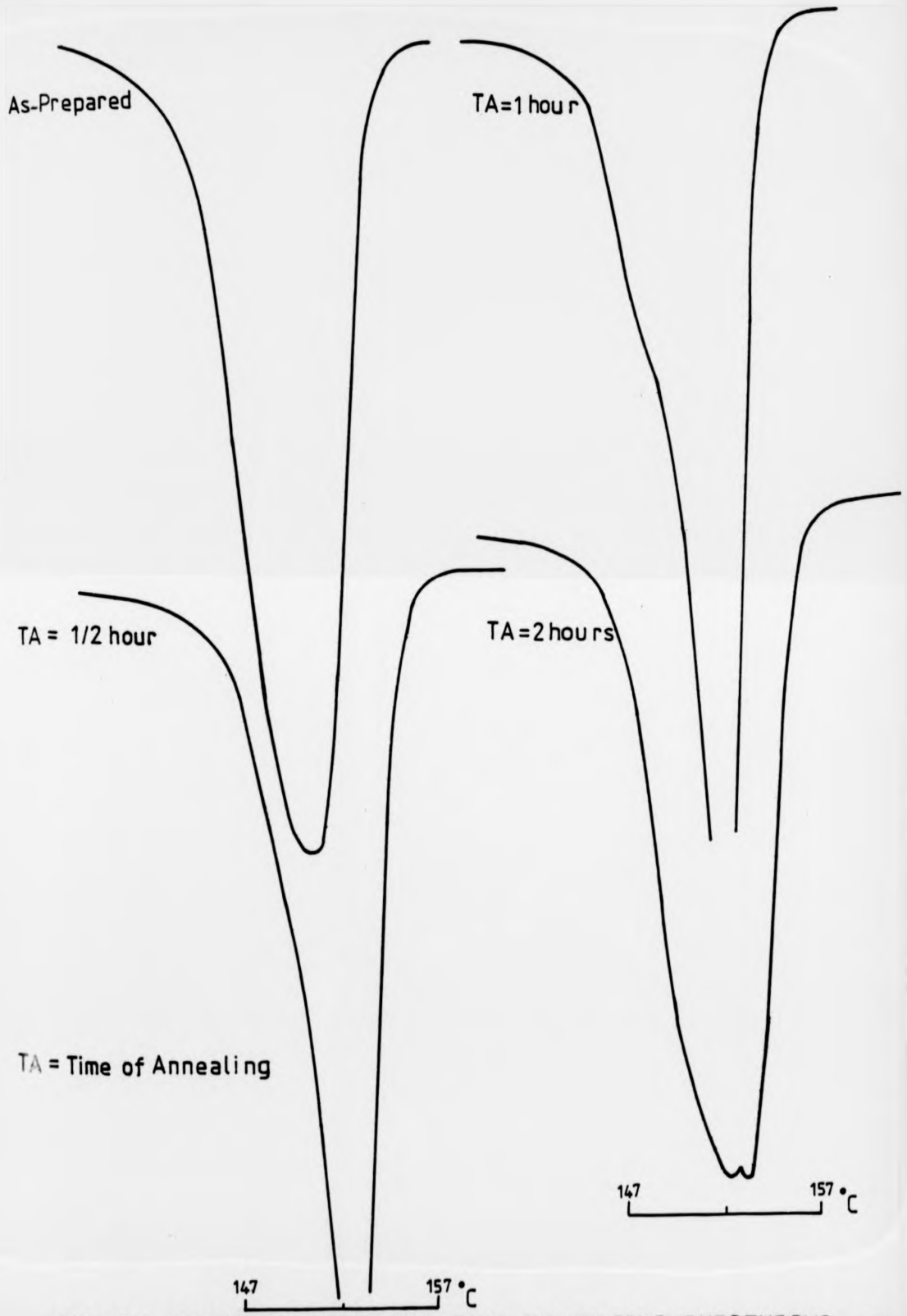

FIG. 7.5 : EFFECT OF ANNEALING TIME ON MELTING ENDOTHERMS FOR DRAWN FIBRES.

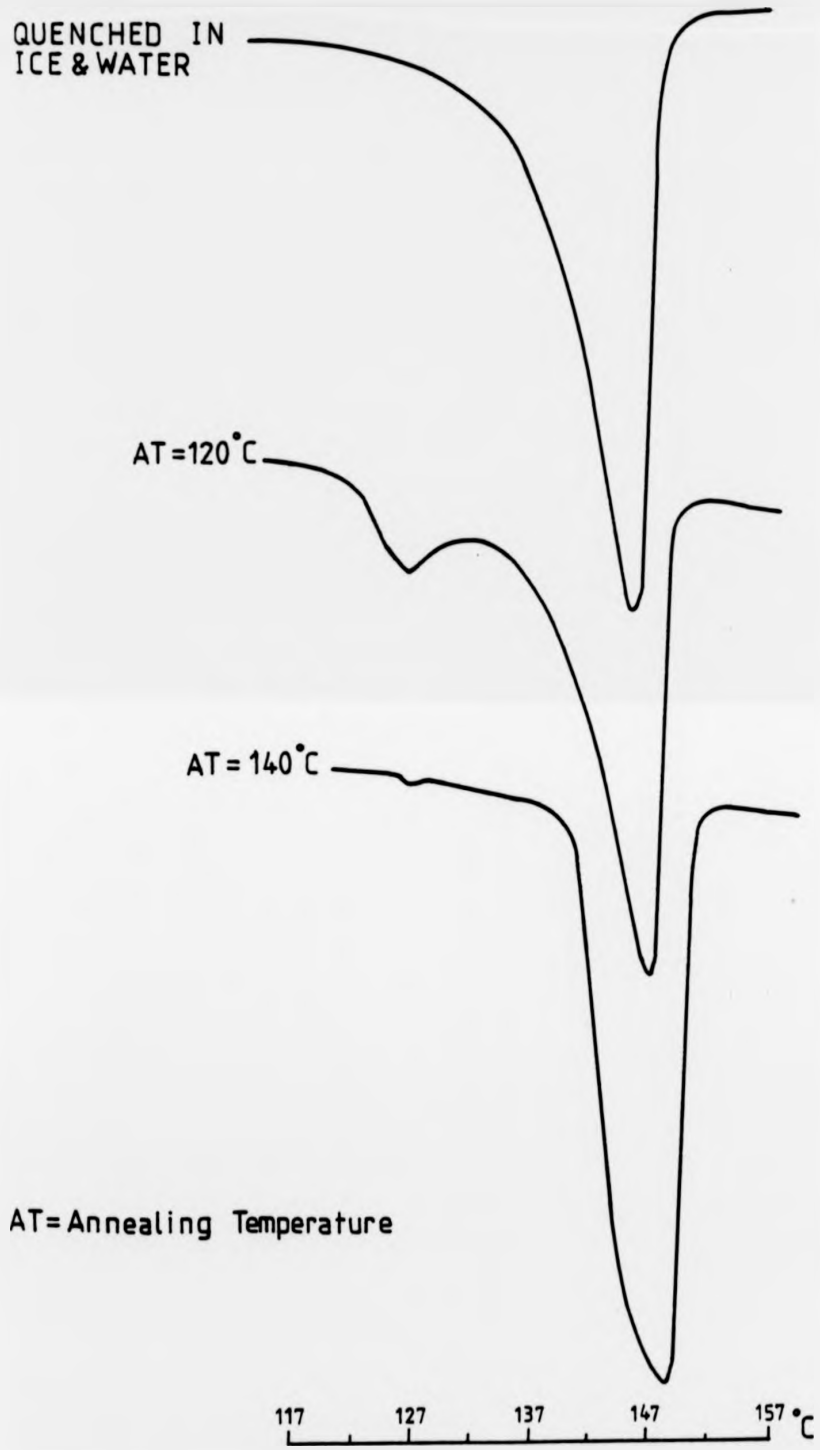

FIG. 7.6: EFFECT OF ANNEALING TEMPERATURE ON MELTING ENDOTHERMS FOR THE MELT-PRESSED FILMS

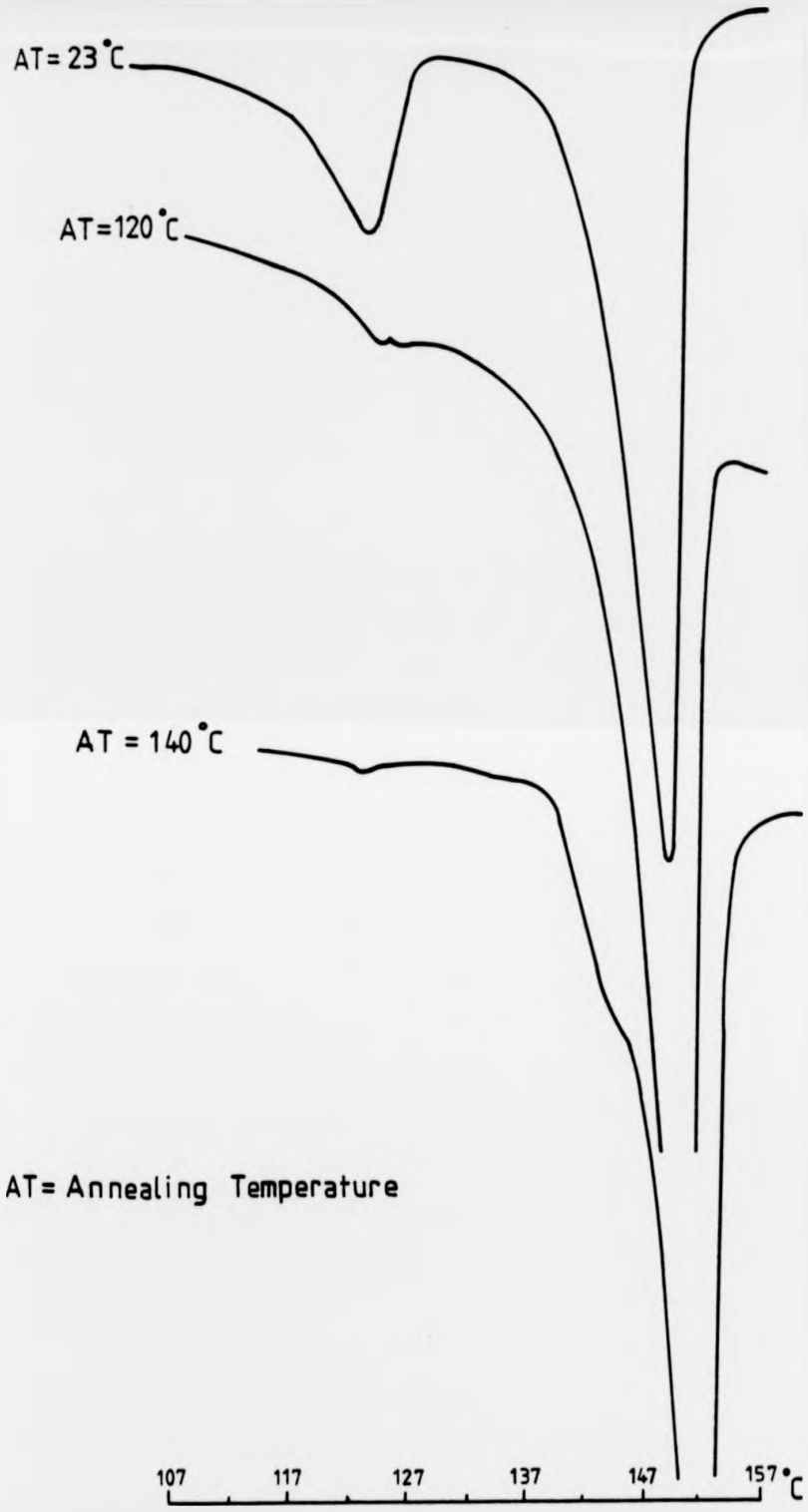

FIG.7.7: EFFECT OF ANNEALING TEMPERATURE ON MELTING ENDOTHERMS FOR THE CAST FILM

7.4 DISCUSSION

In these studies, the major problem is to determine whether the three melting endotherms shown in Figure (7.1), are due to the existence of different crystal structures or to a general phenomenon in polymers, or both. For this purpose, the behaviour of each peak is discussed in relation to the changes in crystal structure, as recorded by X-ray diffraction.

Peak (I): When a sample is crystallised from the melt, its endotherm for peak I is unaffected by crystallisation temperature (Figure 7.2), and is always small. For an as-prepared cast film (Figure 7.7), the peak is of greater height but occurs at the same temperature. On annealing the cast film at 120°C (in oven), the height reduces but the temperature stays the same; this is accompanied by peak II appearing at 128°C. Annealing the cast film at 140°C results in peak I becoming very small and peak II increasing in height and temperature and merging with peak III. This behaviour appears to be compatible with that recorded in the X-ray diffraction investigations of the cast film. It has been shown that cast films give γ-form. Upon annealing at 120°C, the reflections indicate a decay in γ-form and the appearance of β-form. Upon annealing at 140°C, γ-form completely disappears, leaving β-form only. On this basis, it is therefore concluded that peak I is due to the melting of γ-form crystals.

Peak II: This peak always appears in the thermograms for the samples crystallised from the melt, even at low crystallisation temperatures, i.e. room temperature. It is found to remain constant in height and temperature until 110°C, when its height and temperature start increasing (Figure (7.2)). For both pressed and cast films annealed at

120°C, peak II appears at 128°C in the thermogram. Upon annealing at 140°C, the peak increases in height and temperature and merges with peak III (Figures (7.6) and (7.7)). The appearance and behaviour of peak II is consistent with the appearance and behaviour of β-form upon crystallisation and annealing, as recorded in the X-ray diffraction studies. It was mentioned in Chapter Three that crystallisation from the melt under no stresses gives rise to β-form crystals (chain folded crystals). The proportion of this form was found to increase with the annealing temperature. Accordingly, it is concluded that peak II is due to the melting of β-form crystals. The behaviour of peak II appears to be consistent with that predicted by Hoffman and Weeks[68], in which the peak arises from the melting of relatively high molecular weight chain folded lamellae. An increase in the crystallisation temperature (T_c) leads to an increase in the lamellar thickness and, hence, the height and temperature of the peak.

Peak III: Peaks I and II have been identified with γ- and β-forms respectively, so it seems likely that peak III belongs to α-form. However, peaks such as II and III commonly occur in polymers, so the third peak may be unrelated to the polymorphism.

The double melting endotherms, the high and low melting points, is a general feature for polymers; in this work, they are referred to as peaks III and II respectively. Different theories have been proposed to account for their appearance and behaviour as a function of temperature and time of annealing. Of these explanations, two may be considered as being applicable to the results in this work.

Bell and Dumbleton[69,70] reported, in their work on nylon6.6, that the appearance of the double melting peaks is due to the existence of two or more distinct morphological forms (extended and folded chains); but, Roberts[71] and Sweet et al[72] have, in general, renounced this hypothesis

for the case of annealed PET, on the ground that there are changes in the relative areas of the two endotherms when DSC heating rate is changed. As the heating rate is increased, the higher temperature endotherm (peak III) becomes smaller and the lower temperature endotherm (peak II) becomes larger by approximately the same amount. This is taken to mean that the high temperature endotherm is due to partial melting at low temperature and recrystallisation of initial small and imperfect crystals during heating in the DSC instrument.

The possibility of recrystallisation was initially proposed by Jaffe and Wunderlich[73]. This theory appears to be the most acceptable one; it has been employed by many workers to explain the behaviour of multiple melting endotherms of 2GT[71,72] and 4GT[74]. However, it does not offer explanation of all the observations with 6GT; peak III increases in height with increasing rate of heating during remelting (Figure (7.4)). The theory also does not explain the appearance of only one endotherm (Peak III) for the oriented specimen of 6GT (spun with take-up velocity 400 m/min. and drawn films) which is the same endotherm as that for the low crystalline specimen. The X-ray diffraction pattern for the as-spun fibre provides good indication that the sample is very well crystalline and oriented (α-form), as was shown in Plate 1(d), and for the drawn films shows a diffuse pattern but also belonging to α-form.

The annealing of highly oriented samples in the DSC at 125^{o}C for ½ and 1-hour, leads to an asymmetric endotherm (peak III) and annealing for 2-hours leads to two peaks of the same height merging together (Figure (7.5)). The X-ray diffraction pattern for annealed samples of high draw ratio shows the appearance of β-form without any reduction in α-form (see Chapter Three). From the above results, a more likely suggestion is that the high endotherm (peak III) in the highly drawn

samples is due to the melting of chain extended crystals (α-form) and the low endotherm (peak II) due to the melting of chain folded crystals (β-form).

CHAPTER EIGHT

Morphological Studies

Small-Angle X-Ray Diffraction

and

Scanning Electron Microscopy Techniques

8.1 INTRODUCTION

Having discovered the polymorphism of 6GT in which three distinct crystal structures have been found, and in view of the drawing and annealing results presented in the previous chapters, attempts have been made to investigate the crystal morphology characteristic of each crystal form. In this study, small-angle X-ray scattering and scanning electron microscopy have been used.

The X-rays are scattered by fluctuations in electron density; the angle through which they are scattered depends on the linear scale of these fluctuations. Thus, fluctuations caused by the atomic arrangement within the unit cell scatter X-rays through angles of several degrees, whereas, fluctuations on the scale of 100 Å or more scatter them by less than a degree[75]. Generally, two types of small-angle X-ray diffraction patterns are exhibited by polymers: diffuse scattering and discrete diffractions. The former has been interpreted in terms of voids or microvoids, whereas, the latter indicates periodicity in electron density[76].

The structural model normally used to explain this periodicity is that the crystallites are folded chain lamellae stacked on top of each other and separated by disordered material. The long period is the thickness of a lamella plus that of the layer of disordered material and can be calculated from the scattering angle using Bragg's equation, $\lambda = 2\ d \sin\theta$. Variations in the intensity and position of these reflections have been explained in terms of the chain folded structure.

Investigations of the fibre surface and the internal structure of 6GT were also made using scanning electron microscope. The great depth of focus and variable field of view make this technique very useful in the study of polymer morphology. The principles and advantages of this

technique are described in the literature[77].

8.2 EXPERIMENTAL METHODS

Throughout this work, the small-angle X-ray photographs were obtained using a camera (Rigaku-Denki) fitted with two pinholes, 0.3 and 0.2 mm diameter, to collimate the X-ray beam. The sample-film distance was adjusted to 30.0 cm. A suitable thickness of the sample under investigation was chosen to obtain the X-ray scattering of sufficient intensity to give a satisfactorily explosed film in over 24-hours, unless otherwise stated. The investigations were performed on the following samples, both before and after annealing:

(1) Gravitationally spun fibres, in which the crystal structure is a mixture of α and β-forms.

(2) As-spun fibres with take-up velocity 400 m/min., in which the crystal structure is dominant α-form.

(3) Hot-drawn fibres (T.D.R.= 4), in which the crystal structure has equal proportions of α and β-forms.

(4) Cold-drawn fibres (T.D.R.= 5.7), in which the crystal structure is α-form.

These samples were specifically chosen to relate the morphological changes, if any, to the crystal structure, and also to investigate the effect of drawing and annealing on the crystal morphology. Annealing was performed in air at different temperatures for 2-hours with the fibres held at constant length.

Surface and internal studies were also performed using a scanning electron microscope (International Scientific Instrument - TV Mini SEM).

The accelerating voltage used was 10kV; a magnification between 20 and 20,000 could be achieved with a resolution of 500 Å. The procedure adopted in these studies was as follows:

(a) A sample holder was covered by a thin layer of double adhesive tape. The samples under investigation were then carefully mounted, as recommended by Sparrow[78] to avoid the faults which may distort the image.

(b) The samples were coated, using SEM Coating Unit (Polaron Equipment Ltd.), by gold to improve the electrical conductivity.

(c) The sample holder was then introduced into the scanning electron microscope, where an image can be magnified and seen on a TV screen. The reproducibility of the results obtained was checked by scanning five individual samples in each test.

8.3 RESULTS

8.3.1 Small-Angle X-Ray Scattering

The results obtained will be presented for samples as-prepared and as-annealed at two temperature ranges; intermediate range (annealed up to 120°C) and high range (annealed up to 150°C). The small-angle X-ray photographs for the chosen samples at these temperatures are shown in Plate 10(a-m).

(a) As-Prepared Samples

The diffraction pattern for the gravitationally spun fibres (exposed for 45-hours), shown in Plate 10(a) exhibits a diffuse broad-ring pattern, showing maxima on the meridian together with a small streak on the equator. For the as-spun fibres with take-up velocity 400 m/min.

this diffuse pattern disappears; instead, two discrete points showing maxima on the meridian develop (Plate 10(b)). The equatorial streak exhibited in the pattern for this sample is longer than that for the gravitationally spun fibres. The pattern for the hot drawn fibres (T.D.R.=4)shows two discrete horizontal reflections of uniform intensity (Plate 10(c)). The highly drawn fibres did not exhibit any diffraction, except for a long streak on the equator, even with a 100-hour exposure time, as shown in Plate 10(d).

(b) Annealing at the Intermediate Temperature Range (110-135^{o}C)

Over this range, the intensity of the reflections for all the samples under investigation was found to increase relative to those of the as-prepared fibres, as shown in Plate 10(e-h). A result of particular interest at this range is the development of weak four-point in the diffraction pattern of the cold drawn fibres, shown in Plate 10(h).

(c) Annealing at the High Temperature Range (140^{o}C - Melting Point)

In comparing the results obtained over this temperature range with those over the intermediate temperature range, a considerable increase in the intensity of the small-angle X-ray reflections can be clearly seen for the gravitationally spun fibres (Plate 10(j)) and for the hot drawn fibres (Plate 10(l)). However, such an increase of intensity is not observed in the patterns for the as-spun fibres with take-up velocity 400 m/min. and the cold drawn fibres, as shown in Plate 10(k) and (m) respectively.

The long period of each sample under investigation was calculated, using Bragg's law $\lambda = 2\ d \sin\theta$; the change in the long period for each sample at various annealing temperatures is shown in Table (8.1). From

this diffuse pattern disappears; instead, two discrete points showing maxima on the meridian develop (Plate 10(b)). The equatorial streak exhibited in the pattern for this sample is longer than that for the gravitationally spun fibres. The pattern for the hot drawn fibres (T.D.R.=4)shows two discrete horizontal reflections of uniform intensity (Plate 10(c)). The highly drawn fibres did not exhibit any diffraction, except for a long streak on the equator, even with a 100-hour exposure time, as shown in Plate 10(d).

(b) Annealing at the Intermediate Temperature Range (110-135^{o}C)

Over this range, the intensity of the reflections for all the samples under investigation was found to increase relative to those of the as-prepared fibres, as shown in Plate 10(e-h). A result of particular interest at this range is the development of weak four-point in the diffraction pattern of the cold drawn fibres, shown in Plate 10(h).

(c) Annealing at the High Temperature Range (140^{o}C - Melting Point)

In comparing the results obtained over this temperature range with those over the intermediate temperature range, a considerable increase in the intensity of the small-angle X-ray reflections can be clearly seen for the gravitationally spun fibres (Plate 10(j)) and for the hot drawn fibres (Plate 10(l)). However, such an increase of intensity is not observed in the patterns for the as-spun fibres with take-up velocity 400 m/min. and the cold drawn fibres, as shown in Plate 10(k) and (m) respectively.

The long period of each sample under investigation was calculated, using Bragg's law $\lambda = 2\ d \sin\theta$; the change in the long period for each sample at various annealing temperatures is shown in Table (8.1). From

PLATE (10): SAXS photographs of:

as-prepared:

(a) gravitationally spun fibre

(b) as-spun with take-up velocity 400 m/min.

(c) hot drawn (T.D.R.= 4)

(d) cold drawn (T.D.R.= 5.7)

annealed at 120°C:

(e) gravitationally spun fibre

(f) as-spun with take-up velocity 400 m/min.

(g) hot drawn (T.D.R.= 4)

(h) cold drawn (T.D.R.= 5.7)

annealed at 150°C:

(j) gravitationally spun fibre

(k) as-spun with take-up velocity 400 m/min.

(l) hot drawn (T.D.R.= 4)

(m) cold drawn (T.D.R.= 5.7)

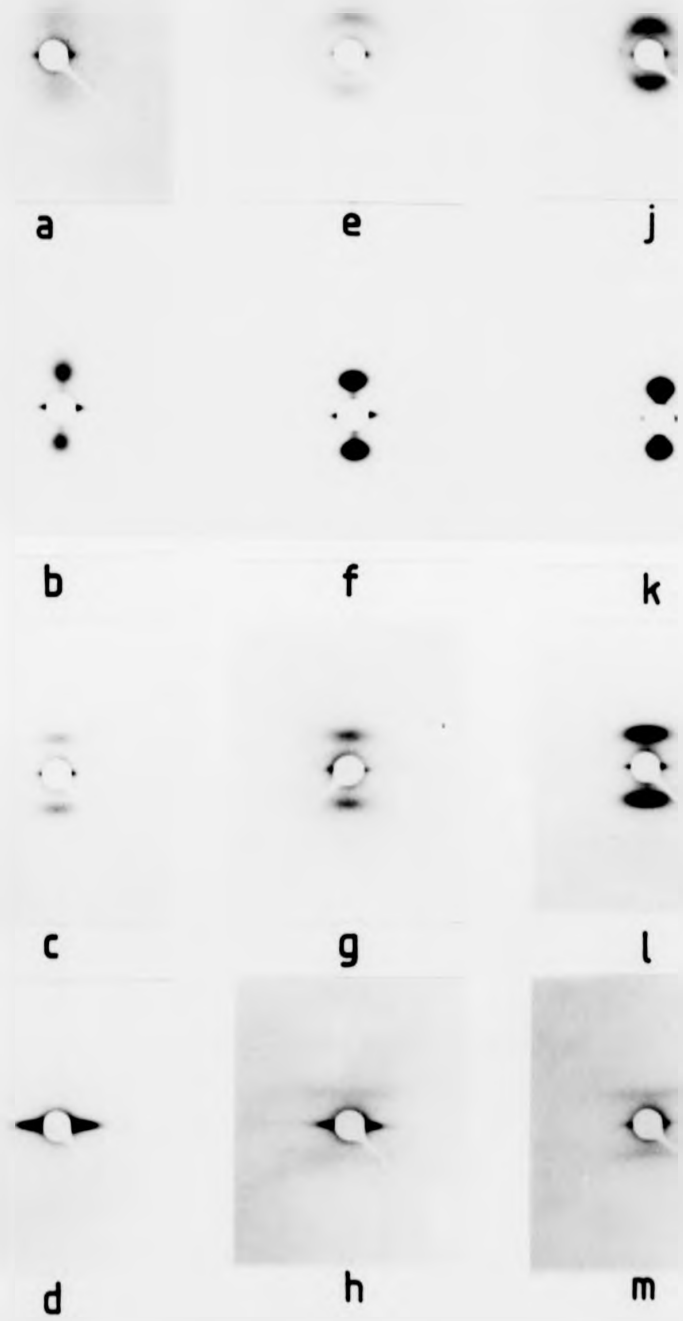

PLATE 10

PLATE (10): SAXS photographs of:

as-prepared:

(a) gravitationally spun fibre

(b) as-spun with take-up velocity 400 m/min.

(c) hot drawn (T.D.R.= 4)

(d) cold drawn (T.D.R.= 5.7)

annealed at 120°C:

(e) gravitationally spun fibre

(f) as-spun with take-up velocity 400 m/min.

(g) hot drawn (T.D.R.= 4)

(h) cold drawn (T.D.R.= 5.7)

annealed at 150°C:

(j) gravitationally spun fibre

(k) as-spun with take-up velocity 400 m/min.

(l) hot drawn (T.D.R.= 4)

(m) cold drawn (T.D.R.= 5.7)

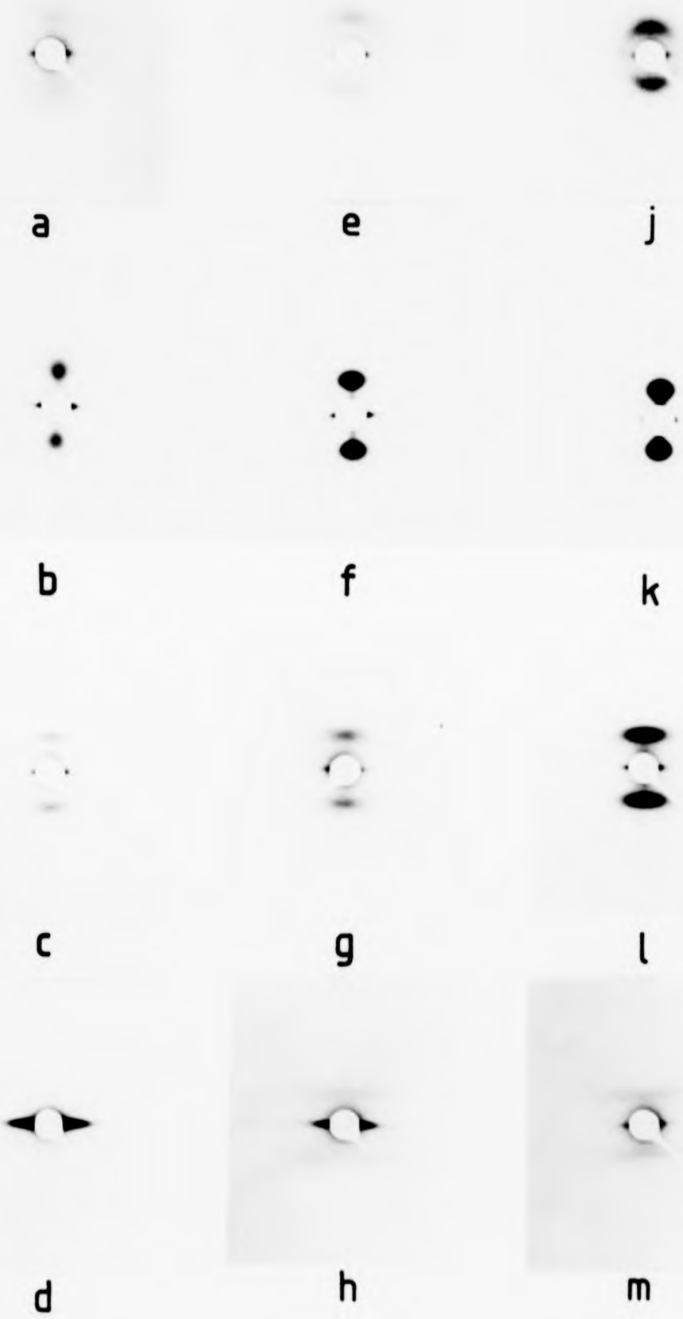

PLATE 10

TABLE (8.1)

Effect of Annealing Temperature on the Long Period

Annealing Temperature (^{o}C)	Long Period ($\mathring{A}$)			
	Gravitationally Spun Fibre	As-Spun Take-up Velocity 400 m/min.	Hot Drawn Fibre (T.D.R.= 4)	Cold Drawn Fibre (T.D.R.=5.7)
Room Temperature	-	150	154	-
100	135	150	151	-
120	146	152	154	167
140	160	160	156	172
150	182	178	161	178
160	-	-	169	180

this table, it can be seen that the long period for all samples increases with the annealing temperature, and that is greater for the cold drawn fibres at each annealing temperature than for the hot drawn. The long period of the as-spun fibres with take-up velocity 400 m/min. is greater than that of the gravitationally spun fibres. Upon annealing, the increase in the long period of the gravitationally spun fibres is found to be greater than that of as-spun fibres with take-up velocity 400 m/min.

8.3.2 Scanning Electron Microscopy

(a) Surface Studies

The scanning electron micrographs of the gravitationally spun, hot drawn (T.D.R.= 4) and cold drawn (T.D.R.= 5) fibres are shown in Plate 11(a-c). It can be seen that the surfaces of the gravitationally spun unannealed and hot drawn fibres annealed at 140^{o}C are smooth, whereas, for the cold drawn fibres annealed at 120^{o}C, a striated surface is seen. Plate 11(d-f) shows the scanning electron micrographs of these samples, after etching in chloroform which is a strong solvent for 6GT; it attacks the surface very rapidly. Therefore, etching was carried out by treating the samples for two seconds. It can be seen that the solvent has attacked the surface of the gravitationally spun fibre throughout, while the etching of hot drawn fibres shows that some regions have been affected more than others. Etching of cold drawn annealed fibres resulted in the development of a more pronounced striated surface.

Etched surfaces of cold and hot drawn films were also examined under the scanning electron microscope and are shown in Plate 12(a) and (b) respectively. The areas enclosed by the etch marks on the surface of the hot drawn films are oval, elongated in the drawing direction,

PLATE (11): Scanning electron micrographs of longitudinal surface of 6GT fibre:

(a) gravitationally spun fibre

(b) hot drawn fibre (T.D.R.= 4)

(c) cold drawn fibre (T.D.R.= 5)

(d) etched surface of gravitationally spun fibre

(e) " " " hot drawn fibre

(f) " " " cold " "

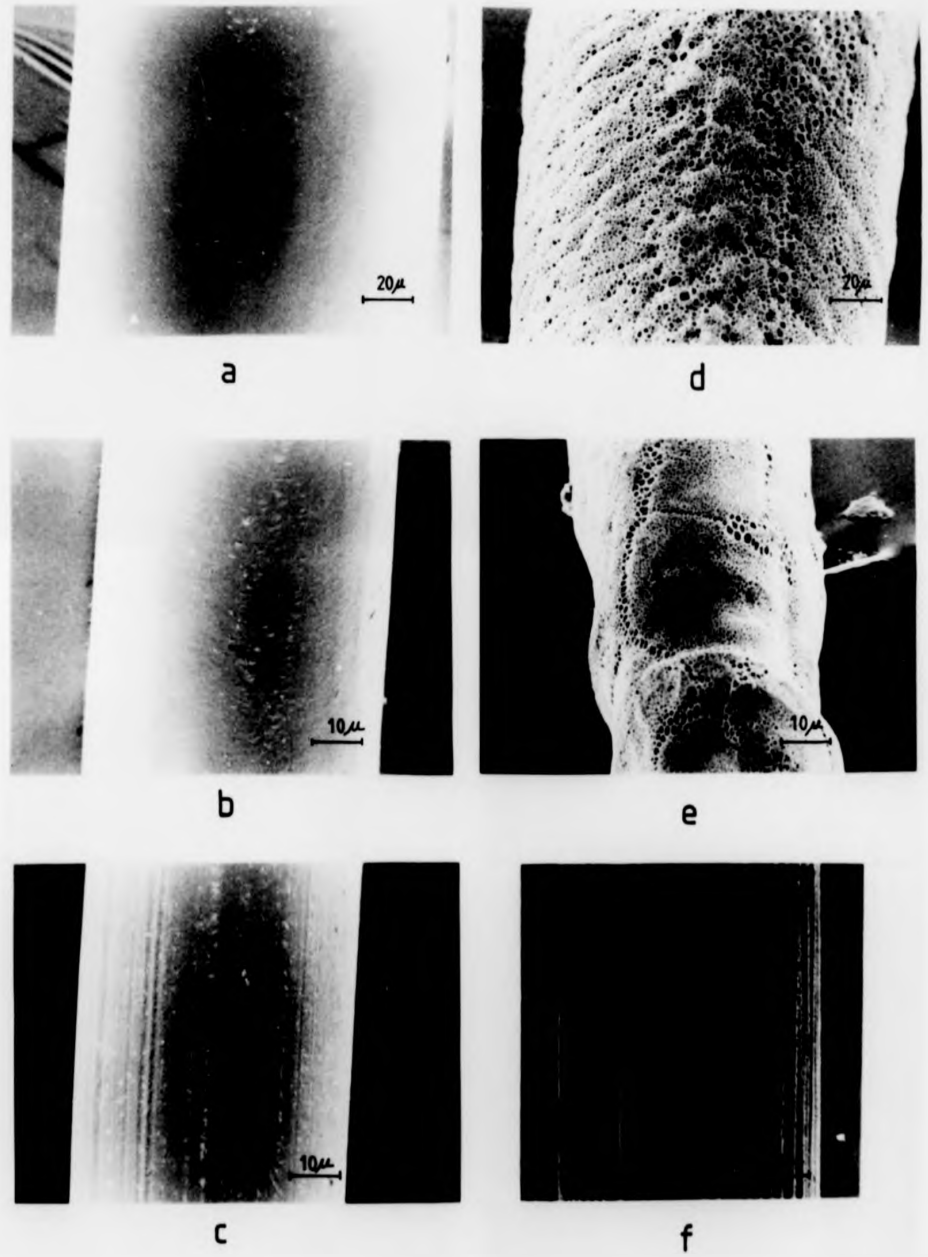

PLATE 11

PLATE (11): Scanning electron micrographs of longitudinal surface of 6GT fibre:

(a) gravitationally spun fibre

(b) hot drawn fibre (T.D.R.= 4)

(c) cold drawn fibre (T.D.R.= 5)

(d) etched surface of gravitationally spun fibre

(e) " " " hot drawn fibre

(f) " " " cold " "

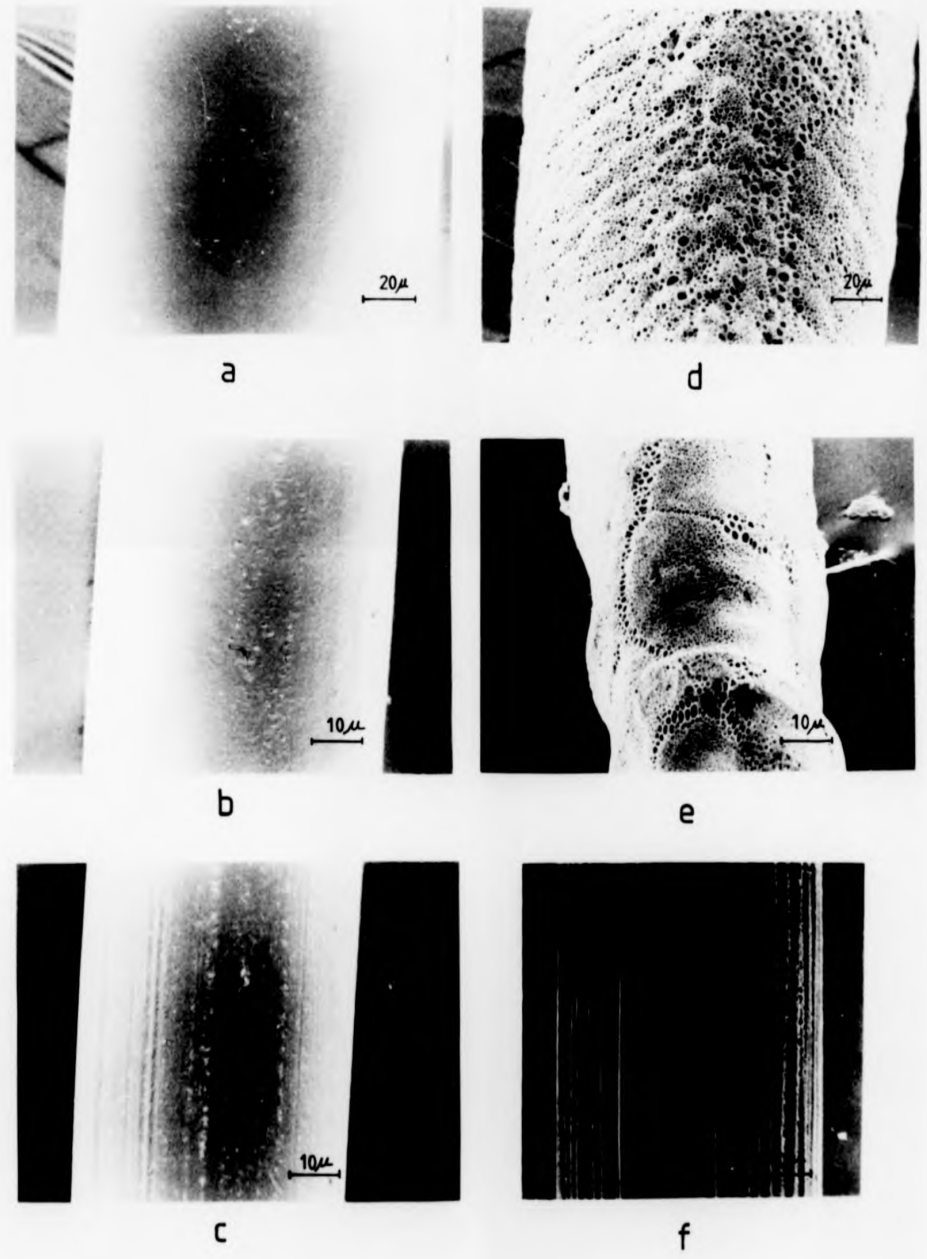

PLATE 11

PLATE (12): Scanning electron micrographs of:

etched films:

(a) cold drawn

(b) hot drawn

peeled fibres showing the internal structure of:

(c) as-spun with take-up velocity 400 m/min.

(d) as (c) magnified (10,000X)

(e,f) cold drawn fibre

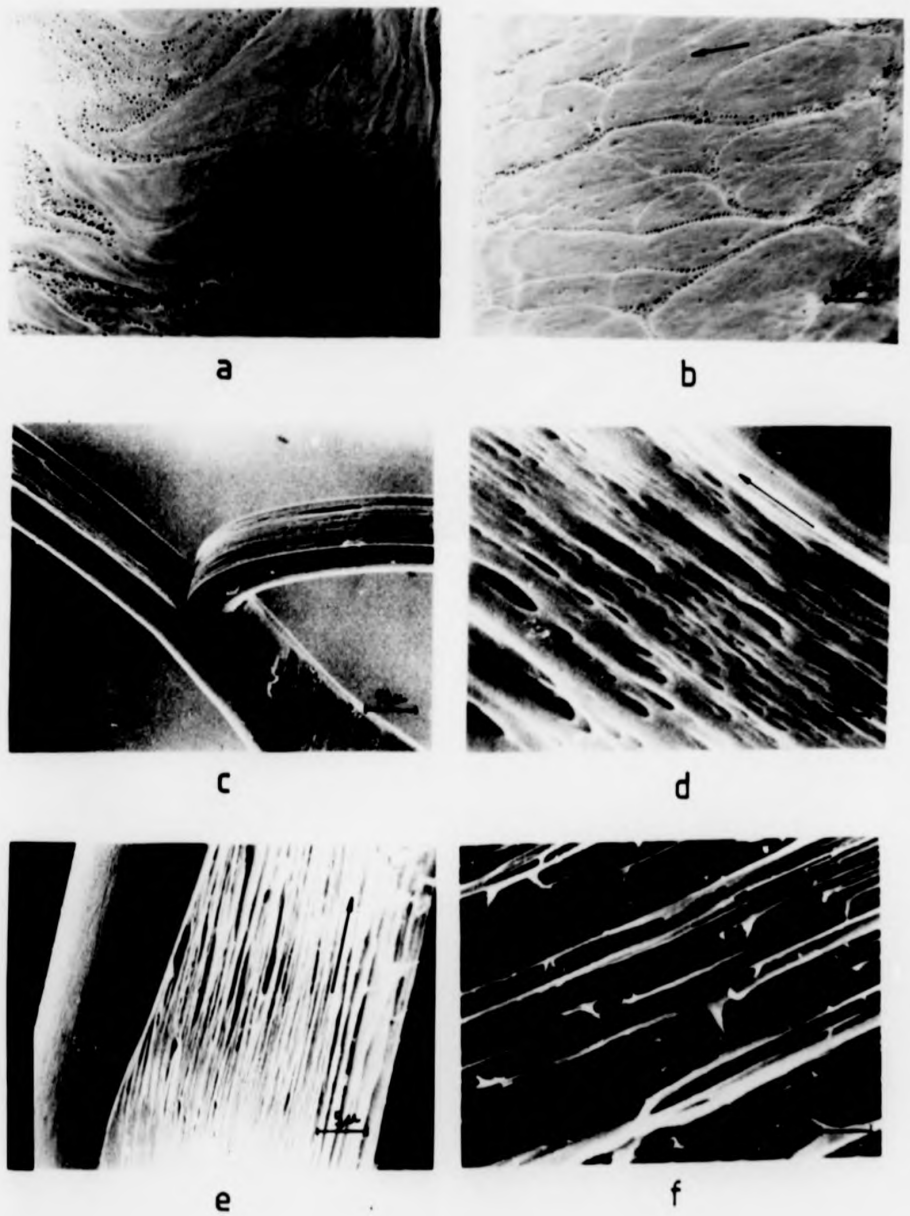

PLATE 12

PLATE (12): Scanning electron micrographs of:

etched films:

(a) cold drawn

(b) hot drawn

peeled fibres showing the internal structure of:

(c) as-spun with take-up velocity 400 m/min.

(d) as (c) magnified (10,000X)

(e,f) cold drawn fibre

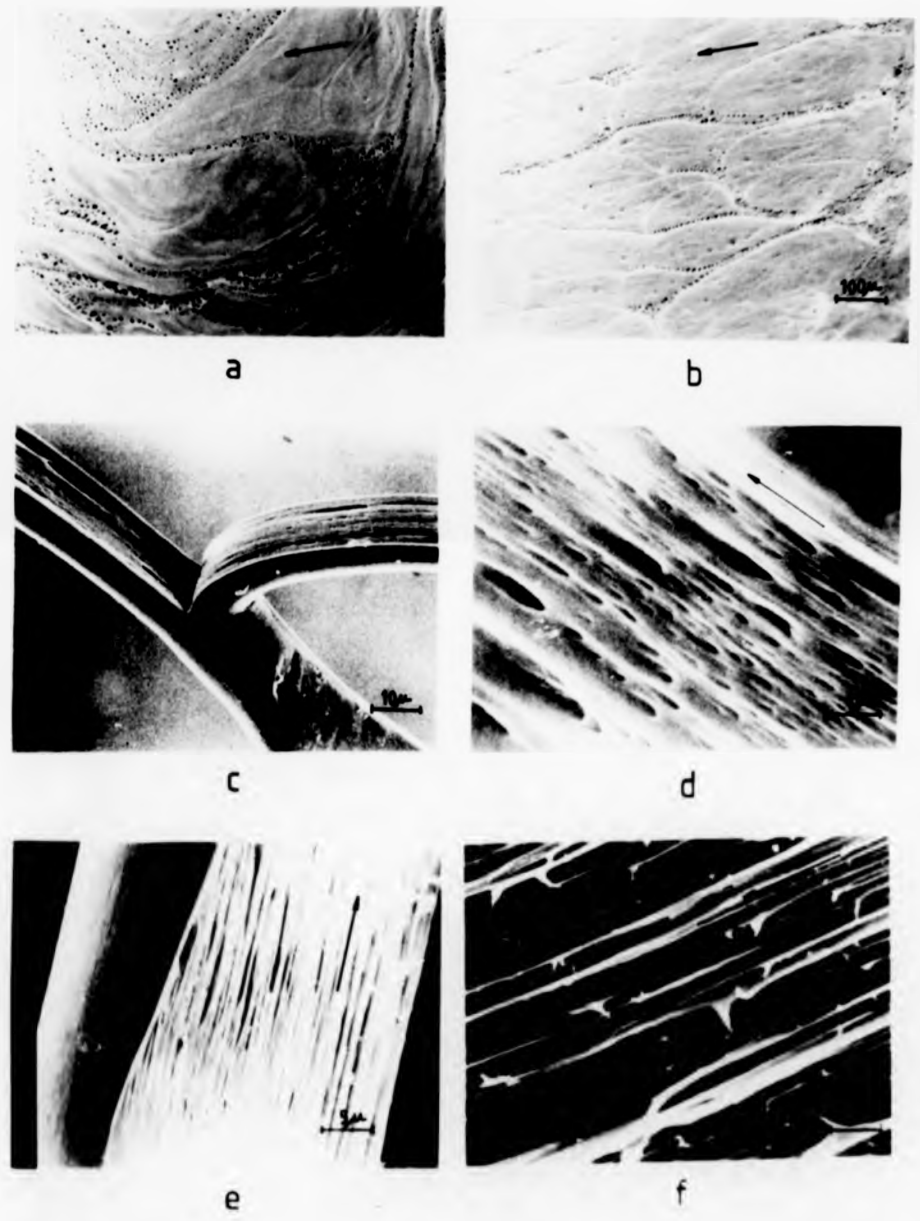

PLATE 12

whereas, in the case of the cold drawn films, these areas are of no particular shape.

(b) Internal Studies

In these studies, fibres were peeled according to the method recommended by Scott[79]. Since peeling at room temperature may disrupt the molecular arrangement and fibre structure, in these studies it was carried out under liquid nitrogen.

A peeled as-spun fibre with take-up velocity 400 m/min. is shown in Plate 12(c), in which longitudinal voids along the fibre axis can be seen; Plate 12(d) shows a region of this sample at a higher magnification and these voids in the internal structure can be clearly seen. The internal structure of the cold drawn fibres is found to be of fibrillar nature, as shown in Plate 12(e-f).

8.4 DISCUSSION

In the previous chapters, it was suggested that the structural changes in 6GT occur as a result of morphological changes. In these investigations, a small angle X-ray technique was, therefore, used to find a relationship between these structural and morphological changes. The results from this technique will be discussed and analysed in relation with those from the wide-angle X-ray technique discussed in previous chapters.

The diffuse, small-angle X-ray diffraction broad-ring pattern exhibited by the unannealed gravitationally spun fibres indicates the presence of unoriented, stacked, and irregular lamellae. These might be part of a spherulitic structure[76]. The intensity maximum on the meridian may be attributed to some degree of molecular orientation

taking place. When as-spun fibres with take-up velocity 400 m/min. were investigated, the broad diffuse ring pattern was found to have disappeared and the pattern shows two distinct diffuse reflections with intensity maxima on the meridian. This is consistent with an increase in the c-axis orientation parallel to the fibre axis with increasing take-up velocity, as shown in Plate 1(a) and (d).

The small-angle X-ray diffraction pattern exhibited by the hot drawn fibres, shown in Plate 10(c), may be explained by lamellae of narrow breadth , their surface being perpendicular to the fibre axis[80]. The cold drawn fibres with high draw ratio, on the other hand, exhibited only an equatorial streak which may be attributed to void formation or microvoids along the fibre axis. The absence of the distinct reflections on the meridian, for this sample, may suggest that the structure is of fibrillar nature, with fibrils running along the fibre axis[76].

If the meridional maxima are caused by the electron density difference between the amorphous and crystalline regions, then one would expect that upon annealing, the intensity will increase. Thus, upon annealing the samples under investigation at 120°C, the intensity of the small-angle reflections increased. The appearance of the weak four point pattern with the cold drawn fibres annealed at 120°C, indicates that the lamellar face must be at a 38° angle to the chain axis. On the other hand, the wide-angle X-ray diffraction pattern for this sample indicates an orientation of the molecular chain parallel to the fibre axis.

However, when annealing was performed at higher temperatures (150°C), the increase in the intensity of the reflections was pronounced in both gravitationally spun and hot drawn fibres, whereas, such an

increase was not observed for the as-spun fibres with take-up velocity 400 m/min. or for the cold drawn fibres. These results can be interpreted and related to 6GT polymorphism, discussed in Chapter Three. The explanation given below will be based on the following points reported in the previous chapters:

(1) The α-form crystals are assumed to be extended chain crystals, whereas, the β-form crystals are chain folded ones.

(2) The proportion of α-form crystals increases with the draw ratio, whereas, that of the β-form crystals increases with the annealing temperature.

(3) The increase in the proportion of β-form upon annealing may take place by either an irreversible transformation from α- to β (melting and recrystallisation) or by epitaxial crystallisation of molecules or segments of molecules in the amorphous region on the surface of the α-form crystals in which case the proportion of α-form crystals does not change. Furthermore, with both mechanisms, i.e. melting and crystallisation on the one hand and the epitaxial growth on the other, each depends on the initial fibre structure before annealing; the former mechanism dominates when the initial structure has approximately equal proportions of both crystal forms, whereas, the latter dominates when the initial structure is α-form.

Thus, the morphological changes observed in the small-angle X-ray photographs can be interpreted in terms of the crystal structure as follows:

If the discrete reflections on the meridian are caused by the presence of the β-form (chain folded) crystals, then one would expect

such reflections to be exhibited by the gravitationally spun and hot drawn fibres, but not by the as-spun fibres with take-up velocity 400 m/min. and the cold drawn ones in both of which the crystal structure is α-form. In view of the results obtained and shown in Plate 10(a-d), the above argument seems valid except for the as-spun fibres with take-up velocity 400 m/min., in which two distinct reflections on the meridian can be clearly seen. These could be produced if some molecular chains were irregularly and loosely folded, hence giving rise to an irregular periodicity which could cause large, diffuse diffraction spots. The chain conformation in the folds is β, other crystalline material is fibrillar and in the α-form. Ziabicki[81] has reported that even the largest possible take-up velocity is not high enough to complete the unfolding. Such folding can be overcome by drawing and, hence, the cold drawn fibres (T.D.R.= 5.7) did not show meridional reflections.

The intensity of the meridional reflections in the gravitationally spun and hot drawn fibres increased after annealing at 120°C (Plate 10 (e,g)). This would mean that more chain folding had occurred. Such an increase may be caused by the crystallisation of the mobile molecules in the amorphous region in a chain folded manner. This is consistent with the wide-angle X-ray results; at this temperature the proportion of β-form increased.

In the case of as-spun fibres with take-up velocity 400 m/min. (Plate 10(f)), the increase in the intensity of the meridional reflections after annealing at 120°C could be explained by refolding of the loosely irregular folded chains. This may also be accompanied by the crystallisation of the mobile molecules in the amorphous region in a chain folded manner. This is also consistent with the wide-angle

X-ray results which show an increase in the β-form on annealing at 120°C.

The appearance of the weak four points in the small-angle X-ray diffraction pattern upon annealing the cold drawn fibres at 120°C (Plate 10(h)) may be caused by the crystallisation of the mobile molecules in the amorphous region in a chain folded manner growing epitaxially on the extended chain crystals. This fits in with the wide-angle X-ray results which show appearance of small proportion of β-form at this temperature.

The considerable increase in the intensity of the meridional reflections upon annealing the gravitationally spun and hot drawn fibres at 150°C (Plate 10(j) and (l)), can be attributed to the melting of α-form crystals and recrystallisation to β-form. The presence of β-form crystals in the initial structure may act as nuclei for more chain folding to occur. The wide-angle X-ray results, in this temperature range, also indicated a considerable increase in the proportion of β-form in these fibres associated with a similar decrease in that of α-form. The considerable increase in the intensity of the meridional reflections after annealing at 150°C was not found for the as-spun fibres with take-up velocity 400 m/min. (Plate 10(k)). However, for this fibre, the wide-angle X-ray studies showed an increase in the proportion of β-form without any noticeable decrease in that of α-form. This could be attributed to the β-form crystals refolding, increasing their thickness and thereby increasing the long period.

In the case of the cold drawn fibres annealed at 150°C (Plate 10 (m)), the insignificant increase in the intensity of the four-point reflections indicates that the chain folding is restricted. This is consistent with the results obtained from the wide-angle X-ray studies

in which the increase of β-form upon annealing is not associated with the decrease in the proportion of α-form. As expected, the long period characteristic of each fibre increases with the annealing temperature. This may be caused by an increase in crystal thickness. In the case of the cold drawn fibres, the long period changes little. If the β-form crystals have grown epitaxially on the α-form, they would thicken (i.e. the proportion of β-form would increase) without change of long period.

Further morphological studies were carried out using the scanning electron microscope; the cold drawn fibres of α-form structure showed a striated surface which may be an indication of fibrillar structure. This surface topology was not found with the gravitationally spun and hot drawn fibres, whose surfaces are smooth and where the crystal structure of these fibres is of approximately equal proportions of α- and β-forms.

Etching of 6GT fibres may show that the surface of the hot drawn fibres could be spherulitic. The etched surfaces of hot and cold drawn films also show the spherulitic structure. The deformation can be seen to be inhomogeneous[45] (see Section 3.4) for the cold drawn films, whereas, it is homogeneous for the hot drawn.

The internal studies of the as-spun fibres with take-up velocity 400 m/min. showed longitudinal voids in the fibre structure, thus, confirming the small-angle X-ray results in which the equatorial streak exhibited by these fibres is more pronounced than that exhibited by the gravitationally spun fibre. The internal structure of the cold drawn fibres also supports the small-angle X-ray results, i.e. the structure is fibrillar with fibrils running along the fibre axis.

In conclusion, the morphology and polymorphisms of 6GT are interdependent; the evidence from small-angle X-ray scattering and electron microscopy supports the assumption that α-form crystals are extended chain but the β-form are folded.

CHAPTER NINE

CONCLUSION

AND

FUTURE WORK

9.1 CONCLUSIONS

From the experimental results obtained in the course of this work, the following conclusions may be drawn:

(1) Successful spinning of 6GT fibres with different take-up velocities can be achieved with suitably chosen spinning parameters. The wide-angle X-ray investigations reveal a change in the crystal structure with the take-up velocity. Furthermore, the increase in the take-up velocity improves the molecular orientation. A different crystal structure is also found in cast films prepared from solution. Thus, the crystal structure of 6GT is dependent on the crystallisation conditions.

(2) The wide-angle X-ray studies of drawn and annealed samples confirm the existence of more than one crystal structure. Three distinct crystal structures have been identified; it is suggested they are to be called α, β and γ-form. The first two crystal structures are characteristic of melt-spun fibres, whereas, the γ-form is characteristic of cast films prepared from solution.

The α-form crystals are dominant in the highly drawn fibres and in the as-spun with high take-up velocity. The β-form crystals exist in the as-spun fibres with low take-up velocity and also in fibres with low draw ratios; it dominates on annealing.

(3) The unit cell of each of the three forms have been determined and are given in Table (9.1). The β and γ-forms are triclinic, each with an identity period of one chain. The β-form has one monomer per unit cell, whereas, the γ has two. The unit cell of the α-form is monoclinic with an identity period of one chain and with six monomers per unit cell. However, it is unlikely that there are so many independent monomers, and

TABLE (9.1)

Unit Cell Parameters

Parameters	α-form	β-form	γ-form
a (^{o}A)	9.06	4.75	10.56
b (^{o}A)	17.24	6.23	5.05
c (^{o}A)	15.51	15.68	15.51
α (degree)	127.3	55.7	126.2
β (degree)	90.0	116.0	98.7
γ (degree)	90.0	118.8	95.3

it is suggested that the true unit cell contains two only, the additional reflections being caused by some kind of systematic disordering.

In comparing the identity period of these three forms with the chemical repeat unit, the molecular conformation for each form is found to be fully extended, its length being extended 98% of that of the chemical repeat. Thus, the molecular conformation is all trans.

The crystal structure determination is complicated by the difficulties encountered in preparing a sample that is very well crystalline, highly oriented and free from other polymorphs. With such limitations present, the crystal structure of β-form is determined and found to be satisfactory.

(4) Since the molecular conformation of the three crystal forms is fully extended, and in view of the drawing and annealing results, the structural changes seem to be a morphological feature. It is suggested that the α-form is an extended chain crystal and the β-form is a chain folded one. This suggestion explains the existence of different proportions of α and β-form and the transition between them as a result of drawing and annealing. The α-form proportion increases with the draw ratio and dominates at high draw ratios, with the β- to -α transition being irreversible. The proportion of β-form increases with the annealing temperature; depending on the initial structure, this increase may either be due to α- to -β transition resulting from melting of α-form crystals followed by recrystallisation to β-form or that the mobile molecules in the amorphous region crystallise epitaxially on the surface of the α-form crystals.

The γ-form is the least stable polymorph and it is suggested to be of chain folded crystals. The γ- to -β transition occurs upon annealing in the intermediate temperature range, i.e. 110-135^{o}C.

Three melting points of 6GT have been detected, using the DSC technique, at 125, 148 and 153^{o}C, corresponding to the three polymorphs γ, β and α respectively.

9.2 SUGGESTIONS FOR FUTURE WORK

Further investigations would be of interest, particularly spinning with take-up velocities higher than 400 m/min. to produce fibres of α-form structure having better orientation and investigating further structural changes, if any. The crystal structure determination of the α and γ-forms from single crystal specimens would be valuable. Finally, the purity of β-form from γ-form could be investigated by wide-angle X-ray studies on samples while being annealed at a temperature in the intermediate temperature range, particularly at 125^{o}C.

APPENDIX I

The calculation of tilt can be understood with reference to the figure below, which shows the reciprocal lattice point above the equator. The height of any point above the equator (as measured from the X-ray film) is given by

$$\zeta_n = Z_n \cos \phi - X \sin \phi$$

where Z_n is the untilted height of the reciprocal lattice layer, ϕ is the angle of tilt and X is the measured distance in the diagram of the point from the tilt line.

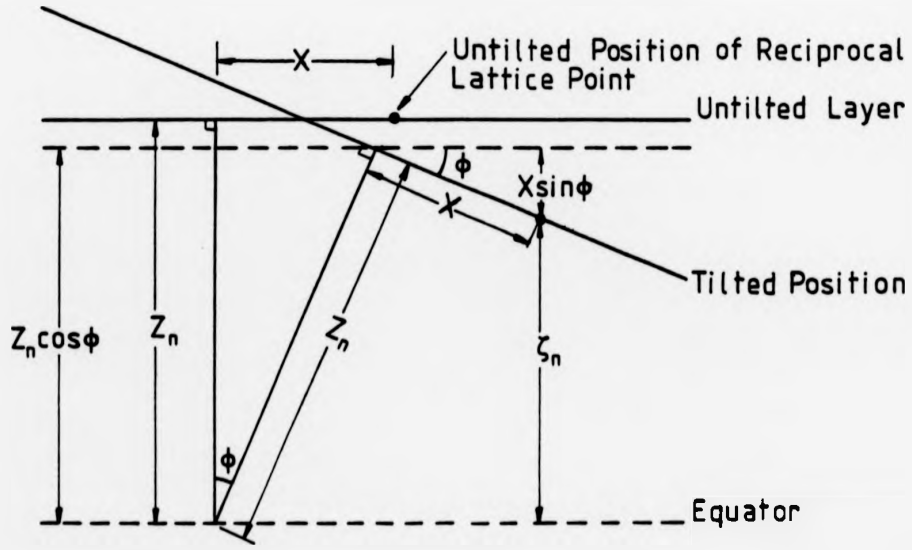

REFERENCES

(1) I. GOODMAN — Angew.Chem., 74, 606 (1962)

(2) M. GILBERT and F. J. HYBART — Polymer, 13, 327 (1972)

(3) G. FARROW, J. McINTOSH and I. M. WARD — Makromol.Chem., 38, 147 (1960)

(4) J. BATEMAN, R. E. RICHARDS, G. FARROW and I. M. WARD — Polymer, 1, 63 (1960)

(5) R. JAKEWAYS, I. M. WARD, M. A. WILDING, I. H. HALL, I. J. DESBOROUGH and M. G. PASS — J.Polym.Sci.,(Polym.Phys.Edn.), 13, 799 (1975)

(6) I. M. WARD, M. A. WILDING and H. BRODY — J.Polym.Sci.,(Polym.Phys.Edn.), 14, 263 (1976)

(7) R. de P. DAUBENY, C. W. BUNN and C. J. BROWN — Proc.Roy.Soc.(A),226, 531 (1954)

(8) I. J. DESBOROUGH, I. H. HALL and J. Z. NEISSER — Polymer, 20, 545 (1979)

(9) S. POULIN-DANDURAND, S. PEREZ, J. F. REVOL and F. BRISSE — Polymer, 20, 419 (1979)

(10) Z. MENCIK — J.Polym.Sci.,(Polym.Phys.,Ed.), 13, 2173 (1975)

(11) I. H. HALL and M. G. PASS — Polymer, 17, 807 (1976)

(12) M. YOKOUCHI, V. SAKAKIBARA, Y. CHATANI, H. TADOKORO, M. TANAKA and R. YODA — Macromolecules, 9, 268, (1976)

(13) I. H. HALL and I. J. DESBOROUGH — Polymer, 18, 825 (1977)

(14) I. H. HALL and N. N. RAMMO — J.Polym.Sci.,(Phys.Ed.), 16, 2189 (1978)

(15) A. M. JOLY, G. NEMOZ, A. DOUILLARD and G. VALLET — Die Makromol.Chem.,176, 479 (1975)

(16) V. T. J. SCHENK — Ph.D. Thesis, UMIST (1970)

(17) A. GHAFFAR — Ph.D. Thesis, UMIST (1971)

(18) M. M. ERDOGUS — Ph.D. Thesis, UMIST (1970)

(19) J. L. WHITE — J.Appl.Polym.Sci.,(Appl.Polym.Symp.) 33, 31 (1978)

(20)	A. ZIABICKI	"Man Made Fibre" p.169, Vol. 1, edited by H.F. Mark, S.M. Atlas and E. Cernia. Interscience Publishers (1967)
(21)	J. R. DEES and J. E. SPRUIELL	J.Appl.Polym.Sci.,18, 1053 (1974)
(22)	L. E. ABBOTT and J. L. WHITE	J.Appl.Polym.Sci.(Appl.Polym.Symp.), 20, 247 (1973)
(23)	J. G. SMITH, C. J. KIBLER and B. J. SUBLETT	J.Polym.Sci.,Part A-1, 4, 1851 (1966)
(24)	A. ELLIOTT	J.Sci.Instrum., 42, 312, (1965)
(25)	P. J. FLORY	"Principles of Polymer Chemistry", Chapter 9; Cornell University Press (1953)
(26)	E. H. MERZ, L. E. NIELSEN and R. BUCHDAHL	Ind.Eng.Chem.,43, 1396 (1951)
(27)	J. L. WHITE and Y. IDE	J.Appl.Polym.Sci.(Appl.Polym.Symp.), 27, 61 (1975)
(28)	A. ZIABICKI	"Man Made Fibres", p.13, Vol.1, edited by H.F. Mark, S.M. Atlas and E. Cernia. Interscience Publishers (1967)
(29)	L. E. NEILSEN	"Mechanical Properties of Polymer" pp.39, Reinhold (1962)
(30)	A. ZIABICKI and K. KEDZIERSKA	J.Appl.Polym.Sci., 6, 111 (1962)
(31)	H. NADELLA, H. M. HENSON, J. E. SPRUIELL and J. L. WHITE	J. Appl.Polym.Sci., 21, 3003 (1977)
(32)	J. E. SPRUIELL and J. L. WHITE	J.Appl.Polym.Sci.(Appl.Polym.Symp.), 27, 121 (1975)
(33)	A. KELLER and M. J. MACHIN	J.Macromol.Sci. Phys.B-1, 1, 41 (1967)
(34)	P. I. VINCENT	Polymer, 1, 7 (1960)
(35)	I. MARSHALL and A. B. THOMPSON	Proc.Roy.Soc. R-2, 221, 541 (1954)
(36)	Y. S. LAZURKIN	J.Polym.Sci., 30, 595 (1958)
(37)	S. W. ALLISON and I. M. WARD	Brit.J.Appl.Phys., 18, 1151, (1967)
(38)	D. C. HOOKWAY	J.Text.Inst.(Proc.), 49, 292 (1958)
(39)	E. W. FISHER, H. GODDAR and W. PIESCZEK	J.Polym.Sci., Part-C, (Polym.Symp.), 32, 149 (1971)

(40) A. B. THOMPSON — "Fibre Structure" Chapter 14, edited by J.W.S. Hearle and R.H. Peters. Butterworth & Co. Publishers (1963)

(41) B. WUNDERLICH — "Macromolecular Physics" Chapter 7, Vol.2, Academic Press, New York (1976)

(42) N. A. HALIM — Ph.D. Thesis, UMIST (1980)

(43) G.S.Y. YEH, R. HOSEMANN, J. LOBODA-CACKOVIC and H. CACKOVIC — Polymer, 17, 309 (1976)

(44) A. PETERLIN — J.Mater.Sci., 6, 490 (1971)

(45) I. L. HAY and A. KELLER — Kolloid, Z.Z.Polymer, 204, 43 (1965)

(46) W. O. STATTON — J.Polym.Sci.,Part-C,(Polym.Symp.), 32, 219 (1971)

(47) K. SAKAOKU and A. PETERLIN — J.Macromol.Sci.Phys., B-1, 1, 103 (1967)

(48) B. WUNDERLICH — "Macromolecular Physics" Chapter 4, Vol.1, Academic Press, New York, (1973)

(49) B. WUNDERLICH and L. MELILLO — Makromol.Chem., 118, 250 (1968)

(50) H. M. HEUVEL and R. HUISMAN — J.Appl.Polym.Sci., 22, 2229 (1978)

(51) C. W. BUNN — "X-Ray Diffraction by Polycrystalline Materials", pp.358-365, edited by H.S. Peiser, H.P. Rooksby and A.J.C. Wilson. Chapman and Hall Ltd. (1960)

(52) C. W. BUNN — "Chemical Crystallography", Chapter 6, Oxford University Press (1961)

(53) M. J. BUERGER — "X-Ray Crystallography", Chapter 8. Wiley, New York (1958)

(54) I. H. HALL — Private communication

(55) C. W. BUNN, H. S. PEISER and A. TURNER-JONES — J.Sci.Instrum., 21, 10 (1944)

(56) "International Tables for X-Ray Crystallography", Vol. I , The Kynoch Press (1952)

(57) M. J. BUERGER — "X-Ray Crystallography", Chapter 12, Wiley, New York (1958)

(58) F. BRISSE — Private communication

(59) I. H. HALL, M. G. PASS — J.Appl.Cryst., 8, 60 (1975)

(60) J. Z. NEISSER — Ph.D. Thesis, UMIST (1980)

(61) S. PEREZ and F. BRISSE — Acta Cryst., B-33 (1977)

(62) S. PEREZ and F. BRISSE — Acta Cryst., B-32, 470 (1976)

(63) S. ARNOTT and A. WONACOTT — Polymer, 7, 157 (1966)

(64) W. MARRS, R. H. PETERS and R. H. STILL — J.Appl.Polym.Sci., 23, 1094 (1979)

(65) N. N. RAMMO — Ph.D. Thesis, UMIST (1977)

(66) P. F. DISMORE and W. O. STATTON — J.Polym.Sci., Part-C, 13, 133 (1966)

(67) P. E. SLADE and L. T. JENKINS — "Thermal Analysis", Vol.1 Arnold (1966)

(68) J. D. HOFFMAN and J. J. WEEKS — J.Res.Natl.Bur.Stand., 66A, 13 (1962)

(69) J. P. BELL, P. E. SLADE and J. H. DUMBLETON — J.Polym.Sci., A-2, 6, 1773 (1968)

(70) J. P. BELL and J. H. DUMBLETON — J.Polym.Sci., A-2, 7, 1033 (1969)

(71) R. C. ROBERTS — J.Polym.Sci.,(B), 8, 381 (1970)

(72) G. E. SWEET and J. P. BELL — J.Polym.Sci.,(A-2), 10, 1273 (1972)

(73) M. JAFFE and B. WUNDERLICH — Kolloid. Z.Z.Polym., 216/217, 203 (1967)

(74) W. MARRS, R. H. PETERS and R. H. STILL — J.Appl.Polym.Sci., 25, 1077 (1979)

(75) P. H. GEIL — "Polymer Single Crystals", Chapter 1, Interscience Publishers (1963)

(76) W. O. STATTON — "Newer Methods of Polymer Characterisation", Chapter 6, edited by K. E. Bacon, Interscience Publishers (1964)

(77) J. E. CASTLE — "The Use of the Scanning Electron Microscope", Chapter 3, edited by Hearle, Sparrow and Cross. Pergamon Press Ltd. (1972)

(78) J. T. SPARROW — "The Use of the Scanning Electron Microscope", Chapter 7, edited by Hearle, Sparrow and Cross. Pergamon Press Ltd. (1972)

(79) R. G. SCOTT — ASTM Bull No. 257, 121 (1959)

(80) M. KAKUDO and N. KASAI — "X-Ray Diffraction by Polymers" Modansha Ltd., Tokyo, Japan (1972)

(81) A. ZIABICKI and K. KEDZIERSKA — J.Appl.Polym.Sci., 6, 361 (1962)